Dissertation

submitted to the

Combined Faculty of Natural Sciences and Mathematics

of Heidelberg University, Germany

for the degree of

Doctor of Natural Sciences

Put forward by

Alexander Felski

Born in: Duisburg, Germany

Oral examination: 20th October 2021

Problems in $\mathcal{PT}$-symmetric Quantum Field Theory

Towards Renormalization of the D-Dimensional
$\phi^2(i\phi)^\varepsilon$ Quantum Field Theory

and

Non-Hermitian Extensions of the
Nambu–Jona-Lasinio Model

Abstract

Two problems of $\mathcal{PT}$-symmetric quantum field theory are discussed: In the first part, the D-dimensional quantum field theory with the self-interaction $\phi^2(i\phi)^\varepsilon$ is analyzed. Techniques introduced previously in a first-order study of the perturbative nonlinearity expansion in ε, [1], are generalized for the application at higher orders and used to determine the expansion coefficients of the ground-state energy density, the p-point Green's functions, and the effective mass of the theory. The perturbative renormalization of the two-dimensional model is discussed to second order in the nonlinearity expansion and the behavior is contrasted with that in a coupling-constant expansion through a multiple-scale analysis. In the second part, the $3+1$ dimensional Nambu–Jona-Lasinio model is modified by $\mathcal{PT}$-symmetric and anti-$\mathcal{PT}$-symmetric non-Hermitian bilinears to analyze the role of $\mathcal{PT}$ symmetry in fermionic quantum field theory. The generated masses of the fermion as well as the scalar and pseudoscalar mesons are obtained. The study is supplemented by an analysis of the fermion mass in the similarly modified $1+1$ dimensional chiral Gross-Neveu model.

Abstract

Diese Arbeit diskutiert zwei Probleme der $\mathcal{PT}$-symmetrischen Quantenfeldtheorie: Der erste Teil beschreibt die Analyse der bosonischen Quantenfeldtheorie mit der Wechselwirkung $\phi^2(i\phi)^\varepsilon$ in D Dimensionen durch eine Störungsentwicklung in dem Nichtlinearitätsparameter ε. Diese in [1] etablierte Methodik wird für die Analyse über die erste Ordnung hinaus verallgemeinert und zur Berechnung der Grundzustandsenergiedichte, der p-Punkt Greenschen Funktionen und der effektiven Masse genutzt. Darüber hinaus wird die perturbative Renormierung in zwei Dimensionen zu zweiter Ordnung in der ε-Entwicklung beschrieben und mit der Störungsentwicklung in der Kopplungskonstanten verglichen. Der zweite Teil beschreibt die Erweiterung des $3+1$ dimensionalen Nambu–Jona-Lasinio Modells durch nicht-hermitesche Bilinearterme, sowohl $\mathcal{PT}$-symmetrische als auch nicht-$\mathcal{PT}$-symmetrische, um den Einfluss der $\mathcal{PT}$ Symmetrie in fermionischen Quantenfeldtheorien zu analysieren. Die generierten Massen der Fermionen, sowie der skalaren und pseudoskalaren Mesonen, werden bestimmt. Diese Studie wird durch die Berechnung der Fermionenmasse in dem vergleichbaren $1+1$ dimensionalen chiralen Gross-Neveu Modell ergänzt.

Contents

List of Figures

General Introduction

The Hermiticity of physical observables is one of the Dirac–von Neumann axioms of quantum physics. Applied to the Hamiltonian, it ensures the spectral reality and thus the probability-conserving time evolution of a model. But while Hermiticity is certainly a sufficient assumption to guarantee these properties, it is not a necessary requirement for the existence of real eigenvalues. This observation lies at the center of $\mathcal{PT}$-symmetric theories.

$\mathcal{PT}$ theory is the study of systems that are symmetric under combined parity reflection $\mathcal{P}$ and time reversal $\mathcal{T}$:

$$\mathcal{P}: \ x \to -x, \qquad \mathcal{T}: \ t \to -t \quad \text{and} \quad i \to -i.$$

Since time reversal is an antilinear operation, it also acts as complex conjugation.

In a $\mathcal{PT}$-symmetric system, that is when the Hamiltonian commutes with the symmetry operator $[H, \mathcal{PT}] = 0$, in which all eigenstates of the Hamiltonian are also eigenstates of the $\mathcal{PT}$ operator, all eigenvalues are real: Under multiplication with $\mathcal{PT}$, and making use of the commutation relation with H, the eigenvalue equation $H\psi = E\psi$ takes the form $E\psi = E^*\psi$. Generally, $\mathcal{PT}$ symmetry is said to be realized in an *unbroken* phase when a spectrum of real eigenvalues is obtained. Notably, the existence of such a phase is independent of the Hermiticity of the model, opening up a large class of non-Hermitian systems to be considered as physical models.

On the other hand, due to the antilinearity of the time-reversal operator $\mathcal{T}$, the eigenstates ψ of the Hamiltonian are not necessarily all eigenstates of the $\mathcal{PT}$ operator as well. This commonly results in complex eigenvalues appearing in conjugate pairs. $\mathcal{PT}$ symmetry is then said to be realized in a *broken* regime.

1

The existence of broken and unbroken symmetry regions, as well as the transition between these phases, distinguishes non-Hermitian $\mathcal{PT}$-symmetric systems intrinsically from regular Hermitian models and has led to the active study of a wide variety of $\mathcal{PT}$ theories.

Experimental applications of $\mathcal{PT}$-symmetric models range from classical mechanical examples, such as driven coupled pendula [2], over a by now large number of implementations in optical [3–7], acoustical [8–10], and microwave systems [11, 12], to electronics [13, 14], superconductivity [15, 16], and atomic physics [17]. Besides the development of the mathematical foundations of $\mathcal{PT}$ theory, an even wider variety of systems is the subject of theoretical discussions: An overview over these topics can be found for example in [18, 19] or the proceedings of the conference series on "Pseudo-Hermitian Hamiltonians in Quantum Physics" [20].

This thesis discusses two problems in $\mathcal{PT}$-symmetric quantum field theory: The first part presents an analysis of the D-dimensional theory with the self-interaction $\phi^2(i\phi)^\varepsilon$. It builds upon a previous study, [1], in which new techniques were introduced, that allowed the discussion of this system through a perturbative expansion in the nonlinearity parameter ε. Here, these techniques are generalized for the analysis beyond first order and the general coefficient structure of the ground-state energy density, the p-point Green's functions, and the effective mass of the model is derived. Through the resummation of certain contributions to all orders in ε, the relation to a coupling-constant expansion is established. In two dimensions the renormalization of the theory becomes necessary; it is performed perturbatively to second order in the nonlinearity expansion. The resulting behavior is contrasted with that in the coupling-constant expansion through a multiple-scale analysis.

In the second part of the thesis, the role of $\mathcal{PT}$ symmetry in fermionic field theories is investigated through the analysis of non-Hermitian extensions of the Nambu–Jona-Lasinio (NJL) model in $3 + 1$ dimensions. The system is modified through the addition of $\mathcal{PT}$-symmetric and anti-$\mathcal{PT}$-symmetric bilinears. Their effect on the generation of an effective fermion mass, as well as the masses of scalar and pseudoscalar mesons in the theory, is investigated. The results are supplemented by a discussion of analogous extensions of the $1 + 1$ dimensional chiral Gross-Neveu (GN) model.

Part I

$\mathcal{PT}$ Symmetry in Bosonic Systems:
Towards Renormalization of the D-Dimensional
$\phi^2(i\phi)^\varepsilon$ Quantum Field Theory

Chapter 1

Introduction to $\mathcal{PT}$ Symmetry in Bosonic Field Theories

The first model that was studied for its symmetry under combined parity reflection $\mathcal{P}$ and time reversal $\mathcal{T}$ is the quantum-mechanical system with Hamiltonian

$$H = p^2 + x^2(ix)^\varepsilon, \quad \varepsilon \in \mathbb{R}. \tag{1.1}$$

It describes a deformation of the linear harmonic-oscillator theory through the contribution $(ix)^\varepsilon$, so that the nonlinearity of the system is measured by the parameter ε. This deformation not only breaks the linearity of the underlying free theory; it also breaks the symmetry of H under Hermitian conjugation. Surprisingly, a numerical (and asymptotic) investigation of this non-Hermitian, but $\mathcal{PT}$-symmetric, system by Bender and Boettcher [21] showed that its spectrum is real, discrete, and positive for all values $\varepsilon \geq 0$, a result that was later proven analytically [22]. The intricate structure of this spectrum is shown in Figure 1.1. The real positive eigenvalues for $\varepsilon \geq 0$ grow with increasing value of ε and indicate a region of unbroken $\mathcal{PT}$ symmetry. The lower boundary of this region at $\varepsilon = 0$ is the harmonic oscillator with the well-known spectrum $E_n = 2n + 1$. The region $\varepsilon < 0$ is a phase of broken $\mathcal{PT}$ symmetry: for $-1 < \varepsilon < 0$ a finite number of the lowest energy eigenvalues remains real, but the remaining infinite number of eigenvalues become complex and form conjugate pairs. The ground-state energy E_0 remains real, but diverges as ε approaches -1 from above. For $\varepsilon \leq -1$ no real eigenvalues remain; the spectrum becomes entirely complex. Variants of the quantum-mechanical system (1.1) continue to be studied and many peculiar properties beyond its region of spectral reality are still being found [23].
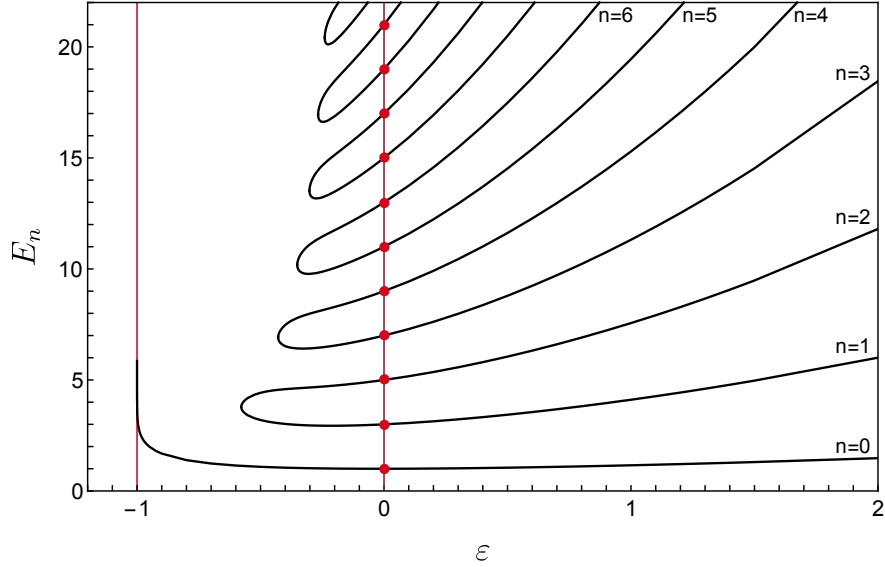
Figure 1.1: Energy spectrum of the Hamiltonian (1.1) as a function of the nonlinearity parameter ε. For $\varepsilon \geq 0$ all eigenvalues are real and positive. For $-1 < \varepsilon < 0$ a finite number of the lowest eigenvalues remain real, while all remaining eigenvalues become complex. Below $\varepsilon = -1$ no real eigenvalues exist. Adapted from [21].

The structure of (1.1) as a nonlinearity deformation of the harmonic oscillator can be traced to a series of works [24–26] of Bender et al. prior to establishing $\mathcal{PT}$ theory, in which they proposed an unconventional perturbation approach to scalar quantum field theory. This approach relied on a perturbation expansion in an *artificial* parameter, such as a measure of nonlinearity in a model, and not in a *natural* expansion parameter, such as a physical coupling constant. It has the advantage of tending to avoid or at least soften the divergent behavior that is often associated with coupling-constant expansions. Moreover, expanding in an artificial parameter preserves term-by-term the analytic dependence on physical parameters, where an expansion in a physical parameter may warp it. In [24, 25] they applied this approach to the field theory with Lagrangian density

$$\mathcal{L}(\delta) = \tfrac{1}{2}(\nabla\phi)^2 + \tfrac{1}{2}g\phi^2(\phi^2)^\delta \qquad (1.2)$$

to investigate models such as the ϕ^4 theory, which is obtained when $\delta = 1$. Notably, the system (1.2) remains Hermitian under the nonlinearity deformation

through the parameter δ, because here a quadratic term ϕ^2 is exponentiated. In addition, this quadratic structure ensures that the exponentiated quantity is positive, avoiding complex-valued contributions for noninteger values of δ; the system based on (1.2) was purposefully constructed so as to avoid spurious complex spectral solutions.

Then a decisive observation was made by Bessis and Zinn-Justin [27] when studying the quantum-mechanical Hamiltonian $H = p^2 + ix^3$ (corresponding to (1.1) at $\varepsilon = 1$) as an analogue of conformal ϕ^3 field theory arising in the study of the Yang-Lee edge singularity. Based on numerical investigations they conjectured that this system, although non-Hermitian, might have a real, positive spectrum. This led Bender and Boettcher to investigate the quantum-mechanical system (1.1), in which the nonlinearity deformation occurs through the imaginary linear factor ix, instead of a quadratic term that was present in (1.2), and finding $\mathcal{PT}$ symmetry to be the cause of the spectral reality. Other early studies of non-Hermitian systems that were found to have real spectra have since been pointed out, [28–34], but these studies remained largely disconnected until their behavior was brought into the context of $\mathcal{PT}$ theory. While this impresses the importance of what has come to be known as the Bender-Boettcher Hamiltonian (1.1) for the development of $\mathcal{PT}$ theory, it also shows the foundations that this development has had in quantum field theory.

First steps towards $\mathcal{PT}$-symmetric quantum field theory have been made in the formulation of $\mathcal{PT}$-symmetric quantum-mechanical systems as one-dimensional field theories. Early investigations addressed the scalar theories with a selfinteraction term of the form $i\phi^3$ or $-\phi^4$. The former arises in the study of the Yang-Lee edge singularity [28] and Reggeon field theory [29,30], and an application of this in the Johnson-Baker-Willey program for constructing finite massless electrodynamics has been analyzed in [35]. The latter has been studied by Symanzik [36], who pointed out the asymptotic freedom of a $-\phi^4$ theory (see also [37]). Beyond these examples, $\mathcal{PT}$ theory was found to be a powerful tool to study non-Hermitian systems that arise in the process of renormalizing initially Hermitian quantum field theories. It was demonstrated in various cases that ghost states of a renormalized theory, which appear to violate unitarity, disappear when the $\mathcal{PT}$ inner product is used and these theories are actually unitary. Examples of this are studies of the

Lee-model [38], Pauli-Villar ghosts in the Pais-Uhlenbeck model [39], as well as the vacuum-instability of the Higgs field in the standard model and of dynamical gravity breaking through gravitino condensates [40]. Further questions addressed through $\mathcal{PT}$-symmetry considerations include the behavior of the double-scaling limit in quantum field theory [41] and that of complex Hamiltonians in timelike Liouville field theory [42].

While these studies have brought attention to remarkable properties of one-dimensional field-theory analogues of quantum-mechanical systems and certain zero-dimensional models, general techniques for higher-dimensional quantum field theories were not explored until 2018: In [1] Bender, Hassanpour, Klevansky, and Sarkar began the analysis of a $\mathcal{PT}$ quantum field theory in D-dimensional Euclidean space-time that is based on the Bender-Boettcher model (1.1). They studied the system with Lagrangian density

$$\mathcal{L}(\varepsilon) = \tfrac{1}{2}(\nabla\phi)^2 + \tfrac{1}{2}\phi^2(i\phi)^\varepsilon, \tag{1.3}$$

in which $\varepsilon \in \mathbb{R}$ measures the degree of nonlinearity and ϕ is a real pseudoscalar field, which transforms under parity as

$$\mathcal{P}\,\phi(t,x)\,\mathcal{P}^{-1} = -\phi(t,-x). \tag{1.4}$$

Thus, the Lagrangian density (1.3) is not Hermitian, but preserves $\mathcal{PT}$ symmetry. Their approach is based on the unconventional nonlinearity expansion that was introduced for the Hermitian field theory (1.2), inheriting many of its advantages. In a conventional coupling-constant expansion the diagrammatic methods established for the evaluation of functional integrals are only applicable when ε (or δ) is an integer, and even then they might need to be supplemented by nonperturbative contributions [18]. In the nonlinearity expansion, on the other hand, this restriction on ε (or δ) is not present and diagrammatic methods are applicable when the expansion coefficients are brought into the form of a polynomial in the field ϕ. The difficulty lies in the logarithmic structure that the interaction terms take in the nonlinearity expansion:

$$\mathcal{L}(\delta) = \tfrac{1}{2}(\nabla\phi)^2 + \tfrac{1}{2}g\phi^2\big[1 + \sum_{n=1}^{\infty} \frac{\delta^n}{n!} \ln^n(\phi^2)\big] \tag{1.5}$$

and

$$\mathcal{L}(\varepsilon) = \tfrac{1}{2}(\nabla\phi)^2 + \tfrac{1}{2}\phi^2\big[1 + \sum_{n=1}^{\infty}\frac{\varepsilon^n}{n!}\ln^n(i\phi)\big], \tag{1.6}$$

associated with (1.2) and (1.3) respectively. While the real logarithmic terms of the Hermitian system in (1.5) were discussed by introducing a polynomial auxiliary Lagrangian density in [24, 25], new techniques were introduced in [1] to address the complex logarithmic terms in (1.6), which arise in the expansion of the $\mathcal{PT}$-symmetric system. These techniques were then used to calculate the perturbative contributions of the ground-state energy density, the Green's functions, and the effective mass to first order in ε.

The general calculations in [1] were restricted to $0 \leq D < 2$ dimensional space-time, where the model does not require renormalization. In two dimensions and beyond, however, this becomes necessary. A program for the perturbative renormalization of the theory in two dimensions, based on the nonlinearity expansion in ε, was proposed. The zero-dimensional and one-dimensional theories remain important cases for the confirmation of the calculations in [1], because the functional integrals become directly evaluable in the zero-dimensional system, and in one space-time dimension the results can be confirmed through the Rayleigh-Schrödinger perturbation theory of quantum mechanics.

In this first part of the thesis, the study begun in [1] is continued, generalizing the expansion techniques for the analysis beyond first order and working towards the proposed perturbative renormalization of the system. Instead of the model (1.3), the system with Lagrangian density

$$\mathcal{L}(\varepsilon) = \tfrac{1}{2}(\nabla\phi)^2 + \tfrac{1}{2}\mu^2\phi^2 + \tfrac{1}{2}g\mu_0^2\phi^2(i\mu_0^{1-D/2}\phi)^{\varepsilon} \tag{1.7}$$

is analyzed in D-dimensional Euclidean space-time. As before, the field ϕ is a real pseudoscalar field, $\phi(-x) = -\phi(x)$, of dimensionality $[\text{mass}]^{D/2-1}$, so that the model preserves $\mathcal{PT}$ symmetry. Contrary to (1.3) the Lagrangian density now includes the dimensional parameters of the unrenormalized mass μ, a fixed parameter μ_0 with the dimension $[\text{mass}]^1$, and a dimensionless unrenormalized coupling strength g. The parameter μ will ultimately act as a mass counterterm for the purpose of renormalization. In addition, a linear counterterm $v(\varepsilon)\phi$

is introduced into (1.7) when the renormalization is carried out. However, the Green's functions of the model that includes this term can be expressed in terms of the Green's functions for (1.7), so that, for simplicity, this linear counterterm is omitted until the perturbative renormalization is discussed.

This study is structured as follows:

In Chapter 2 the techniques that were introduced in [1] to address the complex logarithmic structure in the nonlinearity expansion of the model are generalized for the calculation of perturbation coefficients beyond first order. The derivation of a general coefficient structure in terms of only known functions is presented on the example of the normalized partition function $\mathcal{Z}(\varepsilon)$ of the theory. From this, closed-form solutions for the expansion coefficients are obtained to second order in the nonlinearity parameter ε. In addition, a second type of "leading-order" approximation, which takes into account terms to all orders in ε, is discussed, establishing a formal relation to a conventional coupling-constant expansion even at noninteger values of ε.

In Chapter 3 the coefficients of the partition function are used to approximate the ground-state energy density $\mathcal{E}(\varepsilon)$. The behavior of the expansion coefficients of $\mathcal{E}(\varepsilon)$ is illustrated in the region of $0 \leq D < 4$ space-time dimensions. Results are confirmed in the zero-dimensional and one-dimensional models using either direct integration or Rayleigh-Schrödinger perturbation theory. Through a numerical evaluation of the third-order coefficient in both of these cases the quality of the approximations is examined.

In Chapter 4 the generalized expansion techniques are applied to the calculation of the p-point Green's functions. The general coefficient structure is derived and the coefficients of both approximation schemes are evaluated algebraically to second order. As special cases, the coefficients of the one-point and two-point Green's functions are discussed and the perturbation expansion of the effective mass is obtained from the two-point Green's function.

In Chapter 5 the asymptotic behavior of the p-point Green's function coefficients in the nonlinearity expansion is examined in the limit of two-dimensional space-time. It is shown that the divergent behavior of the one-point Green's function can be removed through the introduction of a linear counterterm $v(\varepsilon)\phi$ into the Lagrangian density without breaking $\mathcal{PT}$ symmetry. The effective mass of

the model is found to diverge logarithmically in the ε expansion. This divergence is absorbed perturbatively into the mass counterterm μ included in the model. Higher-order Green's functions are found to vanish order-by-order in ε, resulting in an apparent freedom of the theory in two-dimensional space-time. This behavior is examined through the lens of the second approximation scheme, in which particular contributions to all orders in ε are resummed. The apparent freedom of the model to any finite order in the nonlinearity parameter ε is found to break down beyond all orders, demonstrating that the construction of a more sophisticated renormalization approach is necessary.

Concluding remarks are given in Chapter 6.

Central results derived in this part of the thesis have been presented in [43, 44], focusing on the renormalization program for two space-time dimensions. This program is not completed, but significant progress has been made in this study.

Chapter 2

The Logarithmic-Expansion Method

Expanding the non-Hermitian $\mathcal{PT}$-symmetric Lagrangian density (1.7),

$$\mathcal{L}(\varepsilon) = \tfrac{1}{2}(\nabla\phi)^2 + \tfrac{1}{2}\mu^2\phi^2 + \tfrac{1}{2}g\mu_0^2\phi^2(i\mu_0^{1-D/2}\phi)^\varepsilon, \tag{2.1}$$

which describes a quantum-field-theoretic analogue of the Bender-Boettcher Hamiltonian (1.1) in D-dimensional Euclidean space-time, in the nonlinearity parameter ε reveals a complex logarithmic self-interaction structure:

$$\mathcal{L}(\varepsilon) = \mathcal{L}_0 + \tfrac{1}{2}g\mu_0^2\sum_{n=1}^{\infty}\frac{\varepsilon^n}{n!}\phi^2\ln^n(i\mu_0^{1-D/2}\phi), \tag{2.2}$$

where the Lagrangian density $\mathcal{L}_0$ of the theory at $\varepsilon = 0$ (harmonic oscillator) is

$$\mathcal{L}_0 = \tfrac{1}{2}(\nabla\phi)^2 + \tfrac{1}{2}(m\mu_0)^2\phi^2 \tag{2.3}$$

with $m^2 = g + \mu^2/\mu_0^2$ denoting a dimensionless mass-like parameter. The Feynman-rules for the analysis of a field theory with such interaction terms are not obvious.

In [1] new techniques were introduced, which address the complex logarithmic interaction that arises at first order in ε. The focus of this chapter is the generalization of these techniques to resolve the interaction terms arising at higher orders in the ε expansion. These generalizations are introduced in Section 2.1 on the basis of a perturbative analysis of the normalized partition function $\mathcal{Z}(\varepsilon)$. A general expression for the partition-function coefficients in terms of known functions only is derived. In Section 2.2 this general expression is then evaluated to an

analytic closed-form solution for the first-order ε-expansion coefficient. A second type of approximation is introduced based on the summation of contributions with a similar structure to that of the first-order coefficient to all orders in ε; it is related to the conventional coupling-constant expansion. In Section 2.3 the analytic closed-form solution for the second-order ε-expansion coefficient and the approximation based on the resummation of structurally similar contributions to all orders in ε are discussed.

2.1 The Partition Function

The central difficulty in the perturbative study of the normalized partition function

$$\mathcal{Z}(\varepsilon) = \frac{1}{Z(0)} \int \mathcal{D}\phi \, e^{-\int d^D x \, \mathcal{L}(\varepsilon)}, \tag{2.4}$$

with

$$Z(0) = \int \mathcal{D}\phi \, e^{-\int d^D x \, \mathcal{L}_0} \tag{2.5}$$

being the full partition function of the model with Lagrangian density (2.3), is the logarithmic interaction structure of the Lagrangian density $\mathcal{L}(\varepsilon)$ in (2.2). Bender et al. [1] presented a way to recast the complex logarithmic self-interaction at order $O(\varepsilon)$, so that only powers of the field ϕ occur in the functional integral. It can then be evaluated using standard diagrammatic techniques, leading to an expression containing only known functions. In general, higher-order self-interaction terms can be taken into account following the same approach: In a first step, the dependence of the partition-function coefficients $\mathcal{Z}_n$ in an expansion in ε,

$$\mathcal{Z}(\varepsilon) = \sum_{n=0}^{\infty} \mathcal{Z}_n \, \varepsilon^n, \tag{2.6}$$

on the complex logarithmic self-interaction terms of $\mathcal{L}(\varepsilon)$ is determined. The complex logarithms are then replaced by real logarithms in a $\mathcal{PT}$-symmetric way, and recast into an expression containing only powers of the field ϕ. The functional integral can then be evaluated in terms of known functions.

To calculate the series expansion (2.6) of the normalized partition function, the exponential factor containing the Lagrangian density $\mathcal{L}(\varepsilon)$ in the form (2.2)

is rewritten using the defining relation of the exponential partial Bell polynomials $B_{n,k}$, see [45],

$$\exp\left(u\sum_{n=1}^{\infty}\frac{t^n}{n!}x_n\right) = 1 + \sum_{n=1}^{\infty}\frac{t^n}{n!}\sum_{k=1}^{n}u^k\, B_{n,k}(x_1,\dots,x_{n+1-k}). \tag{2.7}$$

The normalized partition function then takes the form

$$\mathcal{Z}(\varepsilon) = \frac{1}{Z(0)}\int\mathcal{D}\phi\, e^{-\int d^D x\,\mathcal{L}_0}\,\exp\left[-\tfrac{1}{2}g\mu_0^2\sum_{n=1}^{\infty}\frac{\varepsilon^n}{n!}\int d^D x\,\phi^2\,\ln^n\left(i\mu_0^{1-D/2}\phi\right)\right]$$

$$= 1 + \sum_{n=1}^{\infty}\frac{\varepsilon^n}{n!\,Z(0)}\int\mathcal{D}\phi\, e^{-\int d^D x\,\mathcal{L}_0}\sum_{k=1}^{n}\left(-\tfrac{1}{2}g\mu_0^2\right)^k B_{n,k}(I_1,\dots,I_{n+1-k}), \tag{2.8}$$

in which the arguments of the partial Bell polynomials

$$I_s = \int d^D x\,\phi^2(x)\log^s\left[i\mu_0^{1-D/2}\phi(x)\right] \tag{2.9}$$

are space-time integrals that contain the complex logarithmic interaction terms of the Lagrangian density. The polynomials $B_{n,k}$ have the explicit form [45]

$$B_{n,k}(x_1,\dots,x_{n+1-k}) = n!\sum_{c}\prod_{s=1}^{n+1-k}\frac{1}{c_s!}\left(\frac{x_s}{s!}\right)^{c_s}, \tag{2.10}$$

where the summation $\sum_c$ runs over all integers $c_1,\dots,c_{n+1-k}\geq 0$, such that:

$$\sum_{s=1}^{n+1-k}s\,c_s = c_1 + 2\,c_2 + \cdots + (n+1-k)\,c_{n+1-k} = n, \tag{2.11}$$

$$\sum_{s=1}^{n+1-k}c_s = c_1 + c_2 + \cdots + c_{n+1-k} = k. \tag{2.12}$$

The coefficients $\mathcal{Z}_n$ of the partition function (2.6) can thus be identified to be

$$\mathcal{Z}_n = \frac{1}{Z(0)}\int\mathcal{D}\phi\, e^{-\int d^D x\,\mathcal{L}_0}\sum_{k=1}^{n}\left(-\tfrac{1}{2}g\mu_0^2\right)^k\sum_{c}\prod_{s=1}^{n+1-k}\frac{1}{c_s!}\left(\frac{I_s}{s!}\right)^{c_s}. \tag{2.13}$$

To third order in ε, they are given explicitly as

$$\varepsilon^0: \quad \mathcal{Z}_0 = 1, \tag{2.14}$$

$$\varepsilon^1: \quad \mathcal{Z}_1 = \frac{1}{Z(0)} \int \mathcal{D}\phi \, e^{-\int d^D x \, \mathcal{L}_0} \left[-\tfrac{1}{2} g \mu_0^2 I_1 \right], \tag{2.15}$$

$$\varepsilon^2: \quad \mathcal{Z}_2 = \frac{1}{Z(0)} \int \mathcal{D}\phi \, e^{-\int d^D x \, \mathcal{L}_0} \left[\tfrac{1}{8} g^2 \mu_0^4 I_1^2 - \tfrac{1}{4} g \mu_0^2 I_2 \right], \tag{2.16}$$

$$\varepsilon^3: \quad \mathcal{Z}_3 = \frac{1}{Z(0)} \int \mathcal{D}\phi \, e^{-\int d^D x \, \mathcal{L}_0} \left[-\tfrac{1}{48} g^3 \mu_0^6 I_1^3 + \tfrac{1}{8} g^2 \mu_0^4 I_1 I_2 - \tfrac{1}{12} g \mu_0^2 I_3 \right]. \tag{2.17}$$

Note that in the expression (2.13) each term in the summation over the index k contains a product of k different space-time integrals, collecting the powers c_s of the integrals I_s according to (2.12). Since these integrals are independent of one another, the field $\phi(x)$ is evaluated at k distinct space-time points, say $x_1, \dots, x_k$, in these contributions to the partition-function coefficient $\mathcal{Z}_n$. To distinguish the k distinct space-time integrals more clearly, a k-dimensional multi-index notation can be used: By introducing the multi-indices

$$\alpha = (1, 2, \dots, k) \quad \text{and} \quad \beta = \Big(\underbrace{1, \dots, 1}_{c_1 \text{ copies}}, \underbrace{2, \dots, 2}_{c_2 \text{ copies}}, \dots, \underbrace{(n+1-k), \dots, (n+1-k)}_{c_{n+1-k} \text{ copies}} \Big),$$
$$\tag{2.18}$$

the product over the space-time integrals I_s becomes

$$\prod_{s=1}^{n+1-k} I_s^{c_s} = \int d^D x_\alpha \, \phi^2(x_\alpha) \log^\beta \left[i \mu_0^{1-D/2} \phi(x_\alpha) \right]. \tag{2.19}$$

The partition-function coefficient $\mathcal{Z}_n$ in (2.13) can thus be written as

$$\begin{aligned}
\mathcal{Z}_n = \sum_{k=1}^{n} \left(-\tfrac{1}{2} g \mu_0^2 \right)^k \sum_c \prod_{s=1}^{n+1-k} \frac{1}{c_s! \, (s!)^{c_s}} \int d^D x_\alpha \\
\times \frac{1}{Z(0)} \int \mathcal{D}\phi \, e^{-\int d^D x \, \mathcal{L}_0} \, \phi^2(x_\alpha) \ln^\beta \left[i \mu_0^{1-D/2} \phi(x_\alpha) \right].
\end{aligned} \tag{2.20}$$

In this form, the dependence on the complex logarithms containing the field ϕ is made explicit. The functional integral can now, in principle, be evaluated by reducing this logarithmic dependence to an expression containing only powers of the field ϕ, which then allows for the use of standard diagrammatic methods.

Following the approach of [1], the complex logarithm is separated into its real and imaginary parts:

$$\ln(i\mu_0^{1-D/2}\phi) = \tfrac{1}{2}\big[\, i\pi\, \mathrm{sgn}(\mu_0^{1-D/2}\phi) + \ln(\mu_0^{2-D}\phi^2)\,\big],\qquad (2.21)$$

in which the logarithmic contribution is now a real-valued function. While the real part of (2.21) is even in the pseudoscalar field ϕ, the imaginary part is an odd function, so that this replacement retains $\mathcal{PT}$ symmetry. Powers of the complex logarithm can be replaced in the same way, and the exponentiation can be expanded according to the binomial theorem or, in the case of the multi-index expression (2.20), the multi-binomial theorem:

$$\ln^\beta[i\mu_0^{1-D/2}\phi(x_\alpha)] = \frac{1}{2^n}\sum_{m_\alpha=0}^{\beta}\binom{\beta}{m_\alpha}\Big(i\pi\,\mathrm{sgn}[\mu_0^{1-D/2}\phi(x_\alpha)]\Big)^{m_\alpha}$$
$$\times\Big(\ln[\mu_0^{2-D}\phi^2(x_\alpha)]\Big)^{\beta-m_\alpha}, \qquad (2.22)$$

where the factors of $\tfrac{1}{2}$ from (2.21) were collected according to (2.11). The partition-function coefficient (2.20) can thus be expressed in terms of real logarithms as

$$Z_n = \frac{1}{2^n}\sum_{k=1}^{n}(-\tfrac{1}{2}g\mu_0^2)^k\sum_{c}\prod_{s=1}^{n+1-k}\frac{1}{c_s!\,(s!\,)^{c_s}}\int d^D x_\alpha\sum_{m_\alpha=0}^{\beta}\binom{\beta}{m_\alpha}(i\pi)^{m_\alpha}$$
$$\times\frac{1}{Z(0)}\int\mathcal{D}\phi\,e^{-\int d^D x\,\mathcal{L}_0}\,\phi^2(x_\alpha)\,\mathrm{sgn}^{m_\alpha}[\mu_0^{1-D/2}\phi(x_\alpha)]\,\ln^{\beta-m_\alpha}[\mu_0^{2-D}\phi^2(x_\alpha)].$$
$$(2.23)$$

A procedure for rewriting linear occurrences of the sign function and the real logarithm in terms of only powers of the field ϕ was established in [1]. To replace powers of these functions, the following generalizations of these techniques can be applied: Powers of the sign function can be rewritten using an integral identity involving the sine function, which in turn can be expanded into a series that involves only powers of the field itself

$$\mathrm{sgn}^m(\varphi) = \int_0^\infty dt\,\frac{2\sin(t\varphi^m)}{\pi\,t} = \int_0^\infty dt\sum_{\omega=0}^{\infty}\frac{2\,(-t^2)^\omega}{\pi\,(2\omega+1)!}\,\varphi^{(2\omega+1)m},\qquad (2.24)$$

where $\varphi = \mu_0^{1-D/2}\phi$ and the variable of integration t is dimensionless, ensuring the dimensional consistency of the identity. For powers of the real logarithm the

following generalization of the replica trick, see for example [46], is used

$$\ln^m(\varphi^2) = \lim_{N \to 0} \left(\frac{d}{dN}\right)^m \varphi^{2N} . \tag{2.25}$$

Note that the number N of replicas is considered generally to be an integer. The term φ^{2N} can thus be identified as a $2N$-point vertex in a diagrammatic approach to the functional integral, as remarked in [1]. However, the identity (2.25) requires N to vanish *continuously*. This remains an unresolved issue of the replica trick in general, but in cases where exact results are available, its application has been shown to yield robust results. Various confirmations of special-case results obtained with the use of (2.25) are presented throughout the following discussions, indicating the robustness of its application in this study.

With (2.24) and (2.25) the partition-function coefficient $\mathcal{Z}_n$ in (2.23) becomes:

$$\begin{aligned}
\mathcal{Z}_n = {}& \frac{1}{2^n} \sum_{k=1}^{n} \left(-\tfrac{1}{2}g\mu_0^2\right)^k \sum_c \prod_{s=1}^{n+1-k} \frac{1}{c_s!\,(s!)^{c_s}} \int d^D x_\alpha \sum_{m_\alpha=0}^{\beta} \binom{\beta}{m_\alpha} (i\pi)^{m_\alpha} \\
& \times \int_0^\infty dt_\alpha \sum_{\omega_\alpha=0}^{\infty} \frac{2\,(-t_\alpha^2)^{\omega_\alpha}}{\pi\,(2\omega_\alpha+1)!} \lim_{N_\alpha \to 0} \left(\frac{d}{dN_\alpha}\right)^{\beta-m_\alpha} \left(\mu_0^{1-D/2}\right)^{2N_\alpha+(2\omega_\alpha+1)m_\alpha} \\
& \times \frac{1}{Z(0)} \int \mathcal{D}\phi\, e^{-\int d^D x\, \mathcal{L}_0}\, [\phi(x_\alpha)]^{2(N_\alpha+1)+(2\omega_\alpha+1)m_\alpha} ,
\end{aligned} \tag{2.26}$$

where the functional integral now contains only powers of the field ϕ.

Standard diagrammatic techniques can now be used to evaluate the functional integral in terms of the free propagator $\Delta_{m\mu_0}(x)$ of the theory with Lagrangian density $\mathcal{L}_0$ given in (2.3). In general, the free propagator $\Delta_\lambda(x)$ obeys the D-dimensional Euclidean Klein-Gordon equation

$$\left(-\nabla^2 + \lambda^2\right) \Delta_\lambda(x) = \delta^{(D)}(x) \tag{2.27}$$

and thus takes the form

$$\Delta_\lambda(x) = (2\pi)^{-D/2}\, \lambda^{D/2-1}\, |x|^{1-D/2}\, \mathrm{K}_{1-D/2}(\lambda|x|) \tag{2.28}$$

containing the associated Bessel function K_ν, [47], see Appendix A. It is normalized so that

$$\int d^D x\, \Delta_\lambda(x) = \lambda^{-2} \tag{2.29}$$

and the corresponding selfloop propagator obtained at vanishing argument is

$$\Delta_\lambda(0) = \lambda^{D-2} (4\pi)^{-D/2} \Gamma\left(1 - \tfrac{D}{2}\right). \tag{2.30}$$

Note that while $\Delta_\lambda(0)$ is finite in $0 \leq D < 2$ space-time dimensions, it diverges as D approaches 2 from below due to the Γ function. Specifically, denoting $\delta = 2-D$, the selfloop propagator behaves asymptotically like

$$\Delta_\lambda(0) \sim \frac{1}{2\pi\delta}, \quad \text{as } \delta \to 0. \tag{2.31}$$

This divergent behavior is ultimately reflected in the Green's functions and necessitates the renormalization of the theory in two dimensions.

The diagrammatic methods used in the evaluation of the functional integral in (2.26) are well established and can be found in most textbooks that discuss quantum field theory, e.g. [48]. They are somewhat cumbersome in their application here, because the vertices at the k space-time points x_1 to x_k have distinct variable numbers of ends, depending on the parameters N_α, m_α, and ω_α. A detailed calculation of the general functional integral

$$\frac{1}{Z(0)} \int \mathcal{D}\phi \, e^{-\int d^D x \, \mathcal{L}_0} \, \phi^{n_1}(z_1) \dots \phi^{n_k}(z_k) \tag{2.32}$$

at k different space-time points $z_1, \dots, z_k$ with varying powers $n_1, \dots, n_k$ of the field can be found in Appendix B, in which the solution for the specific functional integral in (2.26) is demonstrated as well:

$$\frac{1}{Z(0)} \int \mathcal{D}\phi \, e^{-\int d^D x \, \mathcal{L}_0} \left[\phi(x_\alpha)\right]^{2(N_\alpha+1)+(2\omega_\alpha+1)m_\alpha}$$

$$= \left(\frac{2\Delta_{m\mu_0}(0)}{\sqrt{\pi}}\right)^k [2\Delta_{m\mu_0}(0)]^{N_\alpha+m_\alpha(\omega_\alpha+\frac{1}{2})} \sum_{l}^{\infty} \prod_{\substack{i,j=1, \\ i<j}}^{k} \frac{1}{l_{ij}!} \left[\frac{2\Delta_{m\mu_0}(x_i - x_j)}{\Delta_{m\mu_0}(0)}\right]^{l_{ij}}$$

$$\times \frac{\Gamma[N_\alpha + 2 + m_\alpha(\omega_\alpha + \frac{1}{2})]\Gamma[N_\alpha + \frac{3}{2} + m_\alpha(\omega_\alpha + \frac{1}{2})]}{\Gamma[N_\alpha + 2 + m_\alpha(\omega_\alpha + \frac{1}{2}) - \frac{1}{2}L_\alpha]} \left(\frac{1 + e^{i\pi(m_\alpha - L_\alpha)}}{2}\right). \tag{2.33}$$

Here the summation $\sum_l$ runs over all integers $l_{ij} \in [0, \infty]$ with $i, j \in [1, k] : i < j$ and the numbers L_r with $r \in [1.k]$ are defined as:

$$L_r = \sum_{i=1}^{r-1} l_{ir} + \sum_{j=r+1}^{k} l_{rj}. \tag{2.34}$$
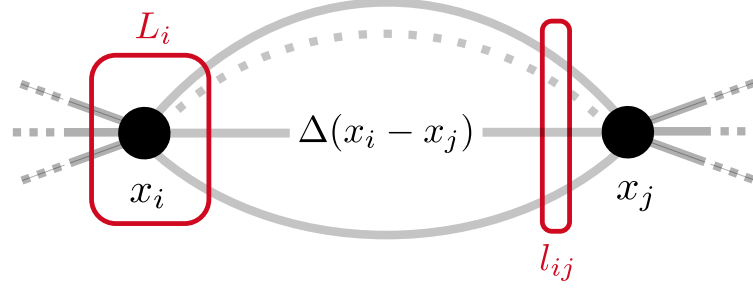
Figure 2.1: The space-time points x_i and x_j are connected by l_{ij} propagators $\Delta(x_i - x_j)$. A total of L_i propagators connect x_i to any other space-time point. The possible formation of selfloops at each vertex is suppressed in this visualization.

In a diagrammatic sense, the variables l_{ij} represent the number of propagators $\Delta_{m\mu_0}(x_i - x_j)$, connecting the space-time point x_i with x_j. The indices are restricted to $i < j$ to avoid double-counting. The numbers L_r, defined in (2.34), then denote the total number of propagators that connect a chosen space-time point x_r to *any other* space-time point x_i or x_j, excluding the number of selfloops (that is $i, j \neq r$). A schematic visualization, in which the occurrence of selfloops is suppressed, is shown in Figure 2.1. The factors involving the exponentials $e^{i\pi(m_\alpha - L_\alpha)}$ in (2.33) are a (reduced) result of the requirement that all ends of a vertex at the space-time point x_α need to either be connected to another vertex, or another end at the same vertex, forming selfloops. A detailed discussion of the combinatoric arguments involved can be found in Appendix B.

The partition-function coefficient (2.26) can thus be written as

$$
\mathcal{Z}_n = \frac{1}{2^n} \sum_{k=1}^{n} \left(-\frac{g\mu_0^2 \Delta_{m\mu_0}(0)}{\sqrt{\pi}} \right)^k \sum_{c}^{n+1-k} \prod_{s=1}^{} \frac{1}{c_s! \, (s!)^{c_s}} \int d^D x_\alpha \sum_{m_\alpha=0}^{\beta} \binom{\beta}{m_\alpha} (i\pi)^{m_\alpha}
$$

$$
\times \lim_{N_\alpha \to 0} \left(\frac{d}{dN_\alpha} \right)^{\beta - m_\alpha} \left[2\mu_0^{2-D} \Delta_{m\mu_0}(0) \right]^{N_\alpha} \sum_{l}^{\infty} \prod_{\substack{i,j=1, \\ i<j}}^{k} \frac{1}{l_{ij}!} \left[\frac{2\Delta_{m\mu_0}(x_i - x_j)}{\Delta_{m\mu_0}(0)} \right]^{l_{ij}}
$$

$$
\times \left(\frac{1 + e^{i\pi(m_\alpha - L_\alpha)}}{2} \right) \int_0^\infty dt_\alpha \sum_{\omega_\alpha=0}^{\infty} \frac{2 \, (-t_\alpha^2)^{\omega_\alpha}}{\pi \, (2\omega_\alpha + 1)!} \left[2\mu_0^{2-D} \Delta_{m\mu_0}(0) \right]^{m_\alpha(\omega_\alpha + \frac{1}{2})}
$$

$$
\times \frac{\Gamma[N_\alpha + 2 + m_\alpha(\omega_\alpha + \frac{1}{2})] \, \Gamma[N_\alpha + \frac{3}{2} + m_\alpha(\omega_\alpha + \frac{1}{2})]}{\Gamma[N_\alpha + 2 + m_\alpha(\omega_\alpha + \frac{1}{2}) - \frac{1}{2}L_\alpha]}
$$

$$
\tag{2.35}
$$

in terms of known functions only. This describes the general structure for *all*

expansion coefficients of the normalized partition function $\mathcal{Z}(\varepsilon)$ in *all* space-time dimensions D. Such a result has not been presented before. In [25] the nonlinearity expansion of the similar (but Hermitian) model (1.2) has been analyzed by introducing a polynomial auxiliary Lagrangian density, but a general form of those polynomials was not discussed [1].

Evaluating (2.35), especially the summation $\sum_l$ over the numbers of free propagators connecting different space-time points, is very intricate. The increasing complexity at high orders n is related, in particular, to the increase of the values k that have to be taken into account. Already for terms containing three or more space-time points, that is $k \geq 3$, the summation becomes intractable, but numerical evaluation remains a possible approach for these terms as long as the space-time dimension D is fixed.

The following sections of this chapter detail the derivation of closed-form solutions for the coefficients $\mathcal{Z}_1$ and $\mathcal{Z}_2$. In a diagrammatic sense, the contributions with $k = 1$ and $k = 2$ occuring therein correspond to graphs with only a single vertex or two vertices respectively. In these cases the summation over possible connections and selfloops can be accounted for. Furthermore, the contributions to (2.35) with $k = 1$ and $k = 2$ can, in fact, be evaluated independently of the order n of the coefficient, so that a summation of these terms to all orders in ε becomes possible. This presents an alternative to the ε expansion of $\mathcal{Z}(\varepsilon)$, that diagrammatically describes approximations based on an expansion in graph complexity, i.e. in the number of vertices considered. The single-vertex and two-vertex approximations to $\mathcal{Z}(\varepsilon)$ are presented in the following sections in addition to the evaluation of the ε-expansion coefficients $\mathcal{Z}_1$ and $\mathcal{Z}_2$.

Before discussing these cases, however, some general simplifications to (2.35) can be made: The summations over ω_α and integrations over t_α in (2.35) can be performed using the following identity, which is derived in Appendix C:

$$\int_0^\infty dt \sum_{\omega=0}^\infty \frac{2\,(-t^2)^\omega}{\pi\,(2\omega+1)!} \frac{\Gamma[a+m(\omega+\frac{1}{2})]\,\Gamma[b+m(\omega+\frac{1}{2})]}{\Gamma[c+m(\omega+\frac{1}{2})]} x^{m(\omega+\frac{1}{2})} = \frac{\Gamma(a)\,\Gamma(b)}{\Gamma(c)}. \tag{2.36}$$

---

[1] A study of a Hermitian model using similar techniques to those presented in this thesis has appeared recently on the arXiv [49], presenting an explicit calculation of first- and second-order coefficients. Nevertheless, a general form such as (2.35) is not derived.

The partition-function coefficient $\mathcal{Z}_n$ in (2.35) thus reduces to

$$
\mathcal{Z}_n = \frac{1}{2^n} \sum_{k=1}^{n} \left(-\frac{g\mu_0^2 \Delta_{m\mu_0}(0)}{\sqrt{\pi}} \right)^k \sum_c \prod_{s=1}^{n+1-k} \frac{1}{c_s!\,(s!)^{c_s}} \int d^D x_\alpha \sum_{m_\alpha=0}^{\beta} \binom{\beta}{m_\alpha} (i\pi)^{m_\alpha}
$$
$$
\times \lim_{N_\alpha \to 0} \left(\frac{d}{dN_\alpha} \right)^{\beta-m_\alpha} \left[2\mu_0^{2-D} \Delta_{m\mu_0}(0) \right]^{N_\alpha} \sum_{l}^{\infty} \prod_{\substack{i,j=1,\\ i<j}}^{k} \frac{1}{l_{ij}!} \left[\frac{2\Delta_{m\mu_0}(x_i - x_j)}{\Delta_{m\mu_0}(0)} \right]^{l_{ij}}
$$
$$
\times \frac{\Gamma(N_\alpha + 2)\,\Gamma(N_\alpha + \frac{3}{2})}{\Gamma(N_\alpha + 2 - \frac{1}{2}L_\alpha)} \left(\frac{1 + e^{i\pi(m_\alpha - L_\alpha)}}{2} \right).
\tag{2.37}
$$

Moreover, since the partition function $\mathcal{Z}(\varepsilon)$ is a dimensionless quantity, its coefficients $\mathcal{Z}_n$ should only depend on the dimensionless parameters g and m, not on μ_0. To confirm this, note that the general free theory propagator given in (2.28) behaves as follows when scaling the parameter λ:

$$
\Delta_{a\lambda}(x/a) = a^{D-2}\Delta_\lambda(x) \quad \text{or} \quad \Delta_\lambda(ax) = a^{2-D}\Delta_{a\lambda}(x),
\tag{2.38}
$$

and in particular

$$
\Delta_\lambda(0) = a^{2-D}\Delta_{a\lambda}(0).
\tag{2.39}
$$

Thus, by rescaling the space-time variables x_α in (2.37) according to

$$
x_j \to x'_j = \mu_0 x_j, \quad d^D x_j \to d^D x'_j = \mu_0^D d^D x_j, \quad \forall j \in [1, k]
\tag{2.40}
$$

and using (2.38) and (2.39), the partition-function coefficient can be written as:

$$
\mathcal{Z}_n = \frac{1}{2^n} \sum_{k=1}^{n} \left(-\frac{g\Delta_m(0)}{\sqrt{\pi}} \right)^k \sum_c \prod_{s=1}^{n+1-k} \frac{1}{c_s!\,(s!)^{c_s}} \int d^D x'_\alpha \sum_{m_\alpha=0}^{\beta} \binom{\beta}{m_\alpha} (i\pi)^{m_\alpha}
$$
$$
\times \lim_{N_\alpha \to 0} \left(\frac{d}{dN_\alpha} \right)^{\beta-m_\alpha} \left[2\Delta_m(0) \right]^{N_\alpha} \sum_{l}^{\infty} \prod_{\substack{i,j=1,\\ i<j}}^{k} \frac{1}{l_{ij}!} \left[\frac{2\Delta_m(x'_i - x'_j)}{\Delta_m(0)} \right]^{l_{ij}}
$$
$$
\times \frac{\Gamma(N_\alpha + 2)\,\Gamma(N_\alpha + \frac{3}{2})}{\Gamma(N_\alpha + 2 - \frac{1}{2}L_\alpha)} \left(\frac{1 + e^{i\pi(m_\alpha - L_\alpha)}}{2} \right).
\tag{2.41}
$$

Notice that the variables x'_α, determined by (2.40), are of dimension $[\text{mass}]^0$, so that the propagators $\Delta_m(x')$ are dimensionless functions. Thus (2.41) shows explicitly that the coefficients $\mathcal{Z}_n$, and hence $Z(\varepsilon)$, are dimensionless quantities.

2.2 $\mathcal{Z}_1$ and the Single-Vertex Approximation

In the following, the general structure (2.41) of the partition-function coefficient $\mathcal{Z}_n$ is evaluated for $n = 1$ and a closed-form solution is obtained. Moreover, it is shown that the simplifications, which allow the reduction of $\mathcal{Z}_1$ to an analytic form, can be applied to the single-vertex contribution ($k = 1$) in any coefficient $\mathcal{Z}_n$. These contributions are evaluated and summed to all orders n in ε as an alternative way of approximating the partition function $\mathcal{Z}(\varepsilon)$.

For $n = 1$ the summation over the index k in (2.41) contains the term with $k = 1$ only. This implies that the multi-indices defined in (2.18) become $\alpha = (1)$ and, utilizing the conditions (2.11) and (2.12), $\beta = (1)$. Thus x_α describes only a single space-time point x_1, implying that all propagators form selfloops and that all numbers l_{ij} of free propagators connecting different space-time points x_i and x_j vanish. A schematic visualization is shown in Figure 2.2. In addition, the factor in (2.41), that contains an exponential function, reduces to the requirement that m_1 has to be even. Thus, the general expression (2.41) becomes:

$$
\begin{aligned}
\mathcal{Z}_1 &= -\frac{g\Delta_m(0)}{2\sqrt{\pi}} \int d^D x_1' \sum_{\substack{m_1=0 \\ \text{even}}}^{1} (i\pi)^{m_1} \lim_{N_1 \to 0} \left(\frac{d}{dN_1}\right)^{1-m_1} \left[2\Delta_m(0)\right]^{N_1} \Gamma(N_1 + \tfrac{3}{2}) \\
&= -\frac{g\,V\Delta_m(0)}{2\sqrt{\pi}} \lim_{N_1 \to 0} \left[2\Delta_m(0)\right]^{N_1} \Gamma(N_1 + \tfrac{3}{2}) \left(\ln[2\Delta_m(0)] + \psi(N_1 + \tfrac{3}{2})\right) \\
&= -\tfrac{1}{4} g\,V\Delta_m(0) \left(\ln[2\Delta_m(0)] + \psi(\tfrac{3}{2})\right),
\end{aligned}
\tag{2.42}
$$

where $V = \int d^D x'$ denotes the volume of space-time and $\psi(x) = \Gamma'(x)/\Gamma(x)$ is the digamma function.

Similarly, the contributions with $k = 1$ in the partition-function coefficient $\mathcal{Z}_n$ in (2.41) can be evaluated for unspecified values $n \geq 1$. Since $k = 1$ implies generally that $\alpha = (1)$, these terms describe, in a diagrammatic sense, those contributions that contain only a single vertex - that at the space-time point x_1. Schematically, all such terms retain the diagrammatic structure shown in Figure 2.2. For $k = 1$ and an unspecified value n, the conditions (2.11) and (2.12) imply that $\beta = (n)$. All other arguments hold as above, especially the requirement
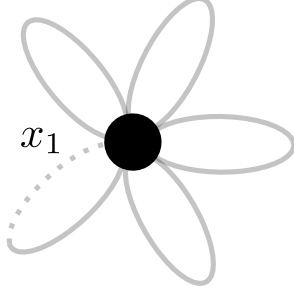
Figure 2.2: Diagrammatic visualization of the first-order ε-expansion coefficient $\mathcal{Z}_1$. All propagators form selfloops at the only space-time point x_1.

that m_1 be even. The $k = 1$ contribution to $\mathcal{Z}_n$ can thus be written as

$$
\begin{aligned}
\mathcal{Z}_n\big|_{k=1} &= -\frac{g\,V\,\Delta_m(0)}{2^n\,n!\,\sqrt{\pi}} \lim_{N_1 \to 0} \sum_{\substack{m_1=0 \\ \text{even}}}^{n} \binom{n}{m_1} (i\pi)^{m_1} \left(\frac{d}{dN_1}\right)^{n-m_1} \\
&\qquad \times \left[2\Delta_m(0)\right]^{N_1} \Gamma(N_1 + \tfrac{3}{2}) \\
&= -\frac{g\,V\,\Delta_m(0)}{2^n\,n!\,\sqrt{\pi}} \lim_{N_1 \to 0} \sum_{m_1=0}^{n} \binom{n}{m_1} \left\{\left(\frac{d}{dN_1}\right)^{m_1} \cos(\pi N_1)\right\} \\
&\qquad \times \left\{\left(\frac{d}{dN_1}\right)^{n-m_1} \left[2\Delta_m(0)\right]^{N_1} \Gamma(N_1 + \tfrac{3}{2})\right\}.
\end{aligned}
\tag{2.43}
$$

Using the general Leibniz rule [50] the summation can be evaluated, yielding:

$$
\mathcal{Z}_n\big|_{k=1} = -\frac{g\,V\,\Delta_m(0)}{2^n\,n!\,\sqrt{\pi}} \lim_{N_1 \to 0} \left(\frac{d}{dN_1}\right)^n \left[2\Delta_m(0)\right]^{N_1} \cos(\pi N_1)\,\Gamma(N_1 + \tfrac{3}{2}).
\tag{2.44}
$$

The evaluation for any specified value of n is straightforward. Furthermore, in the form (2.44) the summation of all such contributions over values $n \geq 1$, that is to all orders in ε, becomes apparent:

$$
\mathcal{Z}(\varepsilon)\big|_{k=1} = \sum_{n=1}^{\infty} \mathcal{Z}_n\big|_{k=1}\,\varepsilon^n = -\frac{g\,V\,\Delta_m(0)}{\sqrt{\pi}} \sum_{n=1}^{\infty} \frac{(\varepsilon/2)^n}{n!} \lim_{N_1 \to 0} \left(\frac{d}{dN_1}\right)^n f(N_1),
\tag{2.45}
$$

where $f(N_1) = \left[2\Delta_m(0)\right]^{N_1} \cos(\pi N_1)\,\Gamma(N_1 + \tfrac{3}{2})$. After completing this summation with a $n = 0$ term, $f(0)$, it is recognized as the Taylor series of $f(\varepsilon/2)$ around 0, and can thus be evaluated to the form

$$
\mathcal{Z}(\varepsilon)\big|_{k=1} = \tfrac{1}{2}gV\Delta_m(0) - \frac{1}{2\sqrt{\pi}}\,gV\cos(\tfrac{\pi\varepsilon}{2})\,\Gamma(\tfrac{\varepsilon+3}{2})\left[2\Delta_m(0)\right]^{1+\varepsilon/2}.
\tag{2.46}
$$

Notice that this approximation shows an explicit linear dependence on the coupling constant g. In fact, in the general coefficient structure (2.41) the coupling constant enters explicitly as g^k, i.e. exponentiated by the number of vertices considered in the respective contributions to $\mathcal{Z}_n$. The summation of the contributions with a fixed value of k over all nonlinearity expansion coefficients $\mathcal{Z}_n$ therefore, in a way, corresponds to a kth order coupling-constant approximation. But g enters also implicitly through the dimensionless mass parameter $m^2 = g + \mu^2/\mu_0^2$. Nevertheless, the coupling-constant expansion picture is suitable: By rewriting the Lagrangian density (2.1) in the form

$$\mathcal{L}(\varepsilon) = \tfrac{1}{2}(\nabla\phi)^2 + \tfrac{1}{2}(m\mu_0)^2\phi^2 + \tfrac{1}{2}g\mu_0^2\phi^2\left[(i\mu_0^{1-D/2}\phi)^\varepsilon - 1\right] \qquad (2.47)$$

one recognizes the k-vertex approximation $\mathcal{Z}(\varepsilon)|_k$ as the kth-order expansion of a model with interaction term $\tfrac{1}{2}G\mu_0^2\phi^2[(i\mu_0^{1-D/2}\phi)^\varepsilon - 1]$ in the coupling constant G at the value $G = g$. With this caveat in mind, the k-vertex approximations can be identified as coupling-constant approximations that are obtained from the nonlinearity expansion.

Relating the artificial nonlinearity expansion in ε to a natural coupling-constant expansion is of interest, because the functional integrals arising in a coupling-constant expansion for an interaction term of the form (2.47) are not evaluable for general values of ε by means of standard diagrammatic methods. The nonlinearity expansion thus not only allows one to address theories that have self-interactions with non-integer exponents of the field, but makes sense of the coupling-constant approximation in such theories as well.

On the other hand, for integer values of ε, a coupling-constant expansion of (2.47) can be evaluated directly and its first-order result can be compared to the general approximation coefficient $\mathcal{Z}(\varepsilon)|_{k=1}$. The calculation is straightforward and agrees with the result in (2.46), which serves as a confirmation of the behavior for the $k = 1$ contributions to the general partition-function coefficients $\mathcal{Z}_n$ in (2.41).

2.3 $\mathscr{Z}_2$ and the Two-Vertex Approximation

In order to determine the partition-function coefficient $\mathscr{Z}_2$ from (2.41), two contributions need to be considered: A single-vertex term when $k = 1$, which is determined by the expression (2.44) found in the last section, and a two-vertex term, when $k = 2$.

Evaluating the single-vertex contribution (2.44) for $n = 2$ yields the result:

$$\mathscr{Z}_2\big|_{k=1} = -\frac{g\,V\,\Delta_m(0)}{16}\left[\left(\ln[2\Delta_m(0)] + \psi(\tfrac{3}{2})\right)^2 + \psi^{(1)}(\tfrac{3}{2}) - \pi^2\right], \qquad (2.48)$$

where $\psi^{(1)}(x) = (d/dx)\,\psi(x)$ is the polygamma function of first order.

For the remaining $k = 2$ term in (2.41) with $n = 2$, the multi-index $\alpha = (1, 2)$ implies that this contribution contains two vertices at the space-time points x_1 and x_2. This is shown schematically in Figure 2.3. The space-time points are in general connected by l_{12} free propagators $\Delta_m(x_1 - x_2)$. Contrary to the single-vertex terms, the summation $\sum_l$ in (2.41) does contribute as a summation over this single variable l_{12} here, and $L_1 = l_{12} = L_2$ according to (2.34). The multi-index $\beta = (1, 1)$ is specified by the conditions (2.11) and (2.12). Thus, for $n = k = 2$ the general expression (2.41) becomes:

$$
\begin{aligned}
\mathscr{Z}_2\big|_{k=2} = {}& \frac{g^2\Delta_m^2(0)}{8\pi}\int d^D x_1'\, d^D x_2'\, \sum_{m_1=0}^{1}\sum_{m_2=0}^{1}(i\pi)^{m_1+m_2} \\
& \times \lim_{N_1,N_2\to 0}\left(\frac{d}{dN_1}\right)^{1-m_1}\left(\frac{d}{dN_2}\right)^{1-m_2}[2\Delta_m(0)]^{N_1+N_2} \\
& \times \sum_{l_{12}=0}^{\infty}\frac{1}{l_{12}!}\left[\frac{2\Delta_m(x_1'-x_2')}{\Delta_m(0)}\right]^{l_{12}}\left(\frac{1+\mathrm{e}^{i\pi(m_1-l_{12})}}{2}\right)\left(\frac{1+\mathrm{e}^{i\pi(m_2-l_{12})}}{2}\right) \\
& \times \frac{\Gamma(N_1+2)\,\Gamma(N_1+\tfrac{3}{2})}{\Gamma(N_1+2-\tfrac{1}{2}l_{12})}\,\frac{\Gamma(N_2+2)\,\Gamma(N_2+\tfrac{3}{2})}{\Gamma(N_2+2-\tfrac{1}{2}l_{12})}.
\end{aligned}
$$

$$(2.49)$$

The factors containing the exponential functions $\mathrm{e}^{i\pi(m_1-l_{12})}$ and $\mathrm{e}^{i\pi(m_2-l_{12})}$ imply that this expression splits into two parts: one in which l_{12} is summed over only even numbers, and for which $m_1 = m_2 = 0$, and another with odd values of l_{12}, in
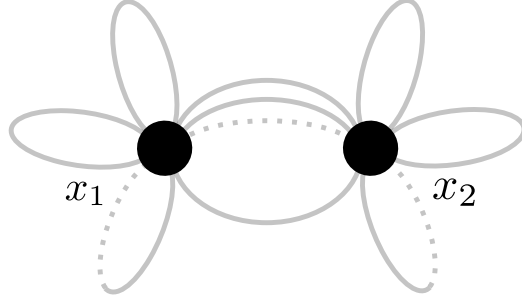
Figure 2.3: Diagrammatic visualization of the two-vertex contribution $\mathcal{Z}_2|_{k=2}$ in the second-order ε-expansion coefficient $\mathcal{Z}_2$.

which $m_1 = m_2 = 1$. Rescaling $l_{12} \to 2l$ and $l_{12} \to 2l + 1$ in these contributions respectively, (2.49) takes the form

$$
\begin{aligned}
\mathcal{Z}_2\big|_{k=2} = \frac{g^2 \Delta_m^2(0)}{8\pi} &\int d^D x_1' d^D x_2' \lim_{N_1, N_2 \to 0} \Bigg(\Bigg\{ \Bigg(\frac{d}{dN_1} \Bigg) \Bigg(\frac{d}{dN_2} \Bigg) \left[2\Delta_m(0) \right]^{N_1+N_2} \\
&\times \sum_{l=0}^{\infty} \frac{1}{(2l)!} \left[\frac{2\Delta_m(x_1' - x_2')}{\Delta_m(0)} \right]^{2l} \frac{\Gamma(N_1+2)\Gamma(N_1+\frac{3}{2})}{\Gamma(N_1+2-l)} \frac{\Gamma(N_2+2)\Gamma(N_2+\frac{3}{2})}{\Gamma(N_2+2-l)} \Bigg\} \\
&- \pi^2 \left[2\Delta_m(0) \right]^{N_1+N_2} \Gamma(N_1+2) \Gamma(N_2+2) \frac{2\Delta_m(x_1'-x_2')}{\Delta_m(0)} \\
&\times \sum_{l=0}^{\infty} \frac{1}{(2l+1)!} \left[\frac{2\Delta_m(x_1' - x_2')}{\Delta_m(0)} \right]^{2l} \frac{\Gamma(N_1+\frac{3}{2})}{\Gamma(N_1+\frac{3}{2}-l)} \frac{\Gamma(N_2+\frac{3}{2})}{\Gamma(N_2+\frac{3}{2}-l)} \Bigg).
\end{aligned}
\tag{2.50}
$$

Rewriting the fractions of Γ functions with the use of Euler's reflection formula [50] according to

$$
\frac{\Gamma(x+1)}{\Gamma(x+1-l)} = (-1)^l \frac{\Gamma(-x+l)}{\Gamma(-x)},
\tag{2.51}
$$

and rewriting

$$
(2l)! = 2^{2l} l! \, \frac{\Gamma(\frac{1}{2}+l)}{\Gamma(\frac{1}{2})} \quad \text{and} \quad (2l+1)! = 2^{2l} l! \, \frac{\Gamma(\frac{3}{2}+l)}{\Gamma(\frac{3}{2})},
\tag{2.52}
$$

the summations over l in (2.50) can be identified as Gaussian hypergeometric functions [51]

$$
{}_2F_1(a,b;c;z) = \sum_{l=0}^{\infty} \frac{z^l}{l!} \frac{\Gamma(a+l)}{\Gamma(a)} \frac{\Gamma(b+l)}{\Gamma(b)} \frac{\Gamma(c)}{\Gamma(c+l)}.
\tag{2.53}
$$

The expression (2.50) then reads:

$$
\mathcal{Z}_2\big|_{k=2} = \frac{g^2 \Delta_m^2(0)}{8\pi} \int d^D x_1' d^D x_2' \lim_{N_1,N_2 \to 0}
$$

$$
\times \left(\left\{ \left(\frac{d}{dN_1}\right)\left(\frac{d}{dN_2}\right) [2\Delta_m(0)]^{N_1+N_2} \Gamma(N_1 + \tfrac{3}{2})\Gamma(N_2 + \tfrac{3}{2}) \right. \right.
$$

$$
\times {}_2F_1\left[-(N_1+1), -(N_2+1); \tfrac{1}{2}; \left(\tfrac{\Delta_m(x_1'-x_2')}{\Delta_m(0)}\right)^2 \right] \Big\}
$$

$$
- \pi^2 [2\Delta_m(0)]^{N_1+N_2} \Gamma(N_1+2)\Gamma(N_2+2) \frac{2\Delta_m(x_1'-x_2')}{\Delta_m(0)}
$$

$$
\left. \times {}_2F_1\left[-(N_1+\tfrac{1}{2}), -(N_2+\tfrac{1}{2}); \tfrac{3}{2}; \left(\tfrac{\Delta_m(x_1'-x_2')}{\Delta_m(0)}\right)^2 \right] \right).
$$

(2.54)

Shifting the integration variable $x_1' \to x' + x_2'$ and using the explicit expressions

$$
{}_2F_1(-\tfrac{1}{2}, -\tfrac{1}{2}; \tfrac{3}{2}; z^2) = \frac{(2z^2+1)\sin^{-1}(z)}{4z} + \frac{3}{4}\sqrt{1-z^2}, \tag{2.55}
$$

$$
{}_2F_1(-1, -1; \tfrac{1}{2}; z^2) = 2z^2 + 1, \tag{2.56}
$$

and the derivatives

$$
\lim_{N \to 0}\left(\frac{d}{dN}\right) {}_2F_1[-(N+1), -1; \tfrac{1}{2}; z^2] = 2z^2, \tag{2.57}
$$

$$
\lim_{N \to 0}\left(\frac{d}{dN}\right) {}_2F_1[-1, -(N+1); \tfrac{1}{2}; z^2] = 2z^2, \tag{2.58}
$$

as well as

$$
\lim_{N_1,N_2 \to 0}\left(\frac{d}{dN_1}\right)\left(\frac{d}{dN_2}\right) {}_2F_1[-(N_1+1), -(N_2+1); \tfrac{1}{2}; z^2]
$$

$$
= 2z^2 + \tfrac{2}{3}z^4 \, {}_3F_2(1,1,1; \tfrac{15}{2}, 3; z^2)
$$

$$
= 12z\sqrt{1-z^2}\sin^{-1}(z) + (4z^2+2)[\sin^{-1}(z)]^2 - 12z^2,
$$

(2.59)

results in the expression

$$
\mathcal{Z}_2\big|_{k=2} = \frac{g^2\,V^2\,\Delta_m^2(0)}{32}\left(\ln[2\Delta_m(0)] + \psi(\tfrac{3}{2}) \right)^2
$$

$$
+ \frac{g^2\,V\,\Delta_m^2(0)}{16}\left\{ \left(\ln[2\Delta_m(0)] + \psi(\tfrac{3}{2}) \right)^2 + 2\left(\ln[2\Delta_m(0)] + \psi(\tfrac{3}{2}) \right) - 6 \right\}
$$

$$
\times \int d^D x' \left[\tfrac{\Delta_m(x')}{\Delta_m(0)} \right]^2
$$

$$
+ \frac{g^2\,V\,\Delta_m^2(0)}{16} \int d^D x' \left\{ 3\tfrac{\Delta_m(x')}{\Delta_m(0)} \sqrt{1 - [\tfrac{\Delta_m(x')}{\Delta_m(0)}]^2} \left(2\sin^{-1}[\tfrac{\Delta_m(x')}{\Delta_m(0)}] - \pi \right) \right.
$$

$$
\left. + (2[\tfrac{\Delta_m(x')}{\Delta_m(0)}]^2 + 1)\sin^{-1}[\tfrac{\Delta_m(x')}{\Delta_m(0)}]\left(\sin^{-1}[\tfrac{\Delta_m(x')}{\Delta_m(0)}] - \pi \right) \right\}.
$$

(2.60)

The integral over the square of the propagator (2.28)

$$\int d^D x' \left[\frac{\Delta_m(x')}{\Delta_m(0)}\right]^2 = \frac{(1 - \frac{D}{2})}{\Delta_m(0)} m^{-2} \tag{2.61}$$

can be evaluated using the identity $\int_0^\infty dt\, t\, \mathrm{K}_\nu^2(t) = \frac{1}{2}\Gamma(1 - \nu)\Gamma(1 + \nu)$ of the associated Bessel function K_ν, see [51]. The space-time integration in the last term of (2.60), however, is quite intricate, but can be evaluated numerically for given dimension D. Together with the $\mathcal{Z}_2|_{k=1}$ contribution (2.48) the second-order partition-function coefficient $\mathcal{Z}_2$ of the ε expansion of $\mathcal{Z}(\varepsilon)$ thus has the form:

$$
\begin{aligned}
\mathcal{Z}_2 = {} & \frac{g^2\, V^2\, \Delta_m^2(0)}{32} \left(\ln[2\Delta_m(0)] + \psi(\tfrac{3}{2})\right)^2 \\
& + \frac{g^2\, V\, m^{-2} \Delta_m(0)}{16} (1 - \tfrac{D}{2}) \left\{ \left(\ln[2\Delta_m(0)] + \psi(\tfrac{3}{2})\right)^2 \right. \\
& \left. + 2\left(\ln[2\Delta_m(0)] + \psi(\tfrac{3}{2})\right) - 6 \right\} \\
& + \frac{g^2\, V\, \Delta_m^2(0)}{16} \int d^D x' \left\{ 3\frac{\Delta_m(x')}{\Delta_m(0)} \sqrt{1 - [\frac{\Delta_m(x')}{\Delta_m(0)}]^2} \left(2\sin^{-1}[\frac{\Delta_m(x')}{\Delta_m(0)}] - \pi\right) \right. \\
& \left. + (2[\tfrac{\Delta_m(x')}{\Delta_m(0)}]^2 + 1)\sin^{-1}[\tfrac{\Delta_m(x')}{\Delta_m(0)}] \left(\sin^{-1}[\tfrac{\Delta_m(x')}{\Delta_m(0)}] - \pi\right) \right\} \\
& - \frac{g\, V\, \Delta_m(0)}{16} \left[\left(\ln[2\Delta_m(0)] + \psi(\tfrac{3}{2})\right)^2 + \psi^{(1)}(\tfrac{3}{2}) - \pi^2\right].
\end{aligned}
\tag{2.62}
$$

Similar to the vertex approximation $\mathcal{Z}(\varepsilon)|_{k=1}$ presented in Section 2.2, which took into account the single-vertex contributions arising at all orders in ε, a summation of all two-vertex contributions is possible as well. The first step towards such an approximation is the calculation of the $k = 2$ contribution in the partition-function coefficient $\mathcal{Z}_n$ in (2.41) for a general value $n \geq 2$. Schematically, all such contributions retain the diagrammatic structure shown in Figure 2.3. The evaluation proceeds as for $n = 2$ above: $\alpha = (1, 2)$ and the summation $\sum_l$ contributes as a summation over the single variable l_{12}, where $L_1 = l_{12} = L_2$ according to (2.34). Again, the factors containing the exponential functions $\mathrm{e}^{i\pi(m_1 - l_{12})}$ and $\mathrm{e}^{i\pi(m_2 - l_{12})}$ imply that the expression splits into two parts: one in which l_{12} is summed over even values, for which the summations over m_1 and m_2 are restricted to even values, and another with only odd values of l_{12}, for which m_1 and m_2 are required

to be odd as well. Thus the $k = 2$ contribution to $\mathcal{Z}_n$ in (2.41) becomes

$$
\mathcal{Z}_n\big|_{k=2} = \frac{g^2\,V\,\Delta_m^2(0)}{2^n\,\pi} \sum_c \prod_{s=1}^{n-1} \frac{1}{c_s!\,(s!)^{c_s}} \int d^D x'\, \lim_{N_1,N_2\to 0}
$$
$$
\times \left\{ \sum_{\substack{l_{12}=0 \\ \text{even}}}^\infty \frac{1}{l_{12}!} \left[\frac{2\Delta_m(x')}{\Delta_m(0)}\right]^{l_{12}} \sigma_{\text{even}} + \sum_{\substack{l_{12}=0 \\ \text{odd}}}^\infty \frac{1}{l_{12}!} \left[\frac{2\Delta_m(x')}{\Delta_m(0)}\right]^{l_{12}} \sigma_{\text{odd}} \right\},
$$

(2.63)

where, with the for now unspecified multi-index $\beta = (\beta_1, \beta_2)$,

$$
\sigma_{\text{even/odd}} = \sum_{\substack{m_1=0 \\ \text{even/odd}}}^{\beta_1} \binom{\beta_1}{m_1} (i\pi)^{m_1} \left(\frac{d}{dN_1}\right)^{\beta_1-m_1} [2\Delta_m(0)]^{N_1} \frac{\Gamma(N_1+2)\,\Gamma(N_1+\frac{3}{2})}{\Gamma(N_1+2-\frac{1}{2}l_{12})}
$$
$$
\times \sum_{\substack{m_2=0 \\ \text{even/odd}}}^{\beta_2} \binom{\beta_2}{m_2} (i\pi)^{m_2} \left(\frac{d}{dN_2}\right)^{\beta_2-m_2} [2\Delta_m(0)]^{N_2} \frac{\Gamma(N_2+2)\,\Gamma(N_2+\frac{3}{2})}{\Gamma(N_2+2-\frac{1}{2}l_{12})}.
$$

(2.64)

The summations in $\sigma_{\text{even/odd}}$ can be evaluated as versions of the general Leibniz rule [50]:

$$
\sum_{\substack{m=0 \\ \text{even}}}^{p} \binom{p}{m} (i\pi)^m \left(\frac{d}{dN}\right)^{p-m} f(N)
$$
$$
= \sum_{m=0}^{p} \binom{p}{m} \left[\left(\frac{d}{dN}\right)^m \cos(\pi N)\right] \left[\left(\frac{d}{dN}\right)^{p-m} f(N)\right]
$$
$$
= \left(\frac{d}{dN}\right)^p \cos(\pi N)\, f(N),
$$

(2.65)

and similarly

$$
\sum_{\substack{m=0 \\ \text{odd}}}^{p} \binom{p}{m} (i\pi)^m \left(\frac{d}{dN}\right)^{p-m} f(N) = \left(\frac{d}{dN}\right)^p i\sin(\pi N)\, f(N).
$$

(2.66)

Then (2.64) becomes either

$$
\sigma_{\text{even}} = \left(\frac{d}{dN_1}\right)^{\beta_1} \left(\frac{d}{dN_2}\right)^{\beta_2} [2\Delta_m(0)]^{N_1+N_2} \cos(\pi N_1)\cos(\pi N_2)
$$
$$
\times \frac{\Gamma(N_1+2)\,\Gamma(N_1+\frac{3}{2})}{\Gamma(N_1+2-\frac{1}{2}l_{12})} \frac{\Gamma(N_2+2)\,\Gamma(N_2+\frac{3}{2})}{\Gamma(N_2+2-\frac{1}{2}l_{12})}
$$

(2.67)

or

$$
\begin{aligned}
\sigma_{\text{odd}} = -& \left(\frac{d}{dN_1}\right)^{\beta_1} \left(\frac{d}{dN_2}\right)^{\beta_2} [2\Delta_m(0)]^{N_1+N_2} \sin(\pi N_1)\sin(\pi N_2) \\
&\times \frac{\Gamma(N_1+2)\,\Gamma(N_1+\frac{3}{2})}{\Gamma(N_1+2-\frac{1}{2}l_{12})} \frac{\Gamma(N_2+2)\,\Gamma(N_2+\frac{3}{2})}{\Gamma(N_2+2-\frac{1}{2}l_{12})}.
\end{aligned}
\tag{2.68}
$$

And thus the coefficient contributions $\mathcal{Z}_n|_{k=2}$ in (2.63) are found to be

$$
\begin{aligned}
\mathcal{Z}_n|_{k=2} = \frac{g^2\,V\,\Delta_m^2(0)}{2^n\,\pi} \sum_c \prod_{s=1}^{n-1}& \frac{1}{c_s!\,(s!)^{c_s}} \int d^D x'\; \lim_{N_1,N_2\to 0} \left(\frac{d}{dN_1}\right)^{\beta_1}\left(\frac{d}{dN_2}\right)^{\beta_2} \\
\times \Bigg\{ & [2\Delta_m(0)]^{N_1+N_2}\cos(\pi N_1)\cos(\pi N_2) \\
\times \sum_{\substack{l_{12}=0 \\ \text{even}}}^{\infty}& \frac{1}{l_{12}!}\left[\frac{2\Delta_m(x')}{\Delta_m(0)}\right]^{l_{12}} \frac{\Gamma(N_1+2)\,\Gamma(N_1+\frac{3}{2})}{\Gamma(N_1+2-\frac{1}{2}l_{12})}\frac{\Gamma(N_2+2)\,\Gamma(N_2+\frac{3}{2})}{\Gamma(N_2+2-\frac{1}{2}l_{12})} \\
- & [2\Delta_m(0)]^{N_1+N_2}\sin(\pi N_1)\sin(\pi N_2) \\
\times \sum_{\substack{l_{12}=0 \\ \text{odd}}}^{\infty}& \frac{1}{l_{12}!}\left[\frac{2\Delta_m(x')}{\Delta_m(0)}\right]^{l_{12}} \frac{\Gamma(N_1+2)\,\Gamma(N_1+\frac{3}{2})}{\Gamma(N_1+2-\frac{1}{2}l_{12})}\frac{\Gamma(N_2+2)\,\Gamma(N_2+\frac{3}{2})}{\Gamma(N_2+2-\frac{1}{2}l_{12})} \Bigg\}.
\end{aligned}
\tag{2.69}
$$

Before evaluating the summations over l_{12}, consider the summation $\sum_c$ and the multi-index β. The conditions (2.11) and (2.12) here have the form

$$
c_1 + 2\,c_2 + \cdots + (n-1)\,c_{n-1} = n,
\tag{2.70}
$$

$$
c_1 + c_2 + \cdots + c_{n-1} = 2.
\tag{2.71}
$$

In general, all but two numbers c_j and c_{n-j} with $j \in [1, n-1]$ will vanish, and these two have the value $c_j = c_{n-j} = 1$ to satisfy the conditions (2.70) and (2.71). A special case can occur for even values of n, in which only the coefficient $c_{n/2} = 2$ does not vanish. The conditions (2.70) and (2.71) thus result in the multi-index $\beta = (j, n-j)$, which includes the special case when $j = n/2$. This allows one to rewrite the summation

$$
\begin{aligned}
\sum_c \prod_{s=1}^{n-1}& \frac{1}{c_s!\,(s!)^{c_s}} \left[\left(\frac{d}{dN_1}\right)^{\beta_1} g(N_1)\right]\left[\left(\frac{d}{dN_2}\right)^{\beta_2} h(N_2)\right] \\
= & \frac{1}{2n!}\sum_{j=1}^{n-1}\binom{n}{j}\left[\left(\frac{d}{dN_1}\right)^{j} g(N_1)\right]\left[\left(\frac{d}{dN_2}\right)^{n-j} h(N_2)\right]
\end{aligned}
\tag{2.72}
$$

over generic functions g and h, and by completing this sum with a $j = 0$ and $j = n$ term, evaluate it as the general Leibniz rule [50]:

$$\frac{1}{2n!} \sum_{j=1}^{n-1} \binom{n}{j} \left[\left(\frac{d}{dN_1} \right)^j g(N_1) \right] \left[\left(\frac{d}{dN_2} \right)^{n-j} h(N_2) \right]$$

$$= \left[\left(\frac{d}{dN} \right)^n \frac{g(N)h(N)}{2n!} \right] - \frac{g(N_1)}{2n!} \left[\left(\frac{d}{dN_2} \right)^n h(N_2) \right] - \frac{h(N_2)}{2n!} \left[\left(\frac{d}{dN_1} \right)^n g(N_1) \right].$$
$$(2.73)$$

With this, the derivatives in the coefficient (2.69) can be rewritten, yielding the expression

$$Z_n \big|_{k=2} = \frac{g^2 \, V \, \Delta_m^2(0)}{2^{n+1} n! \, \pi} \int d^D x' \, \lim_{N \to 0} \left(\frac{d}{dN} \right)^n [2\Delta_m(0)]^{2N}$$

$$\times \left\{ \cos^2(\pi N) \sum_{\substack{l_{12}=0 \\ \text{even}}}^{\infty} \frac{1}{l_{12}!} \left[\frac{2\Delta_m(x')}{\Delta_m(0)} \right]^{l_{12}} \left[\frac{\Gamma(N+2)\,\Gamma(N+\frac{3}{2})}{\Gamma(N+2-\frac{1}{2}l_{12})} \right]^2 \right.$$

$$\left. - \sin^2(\pi N) \sum_{\substack{l_{12}=0 \\ \text{odd}}}^{\infty} \frac{1}{l_{12}!} \left[\frac{2\Delta_m(x')}{\Delta_m(0)} \right]^{l_{12}} \left[\frac{\Gamma(N+2)\,\Gamma(N+\frac{3}{2})}{\Gamma(N+2-\frac{1}{2}l_{12})} \right]^2 \right\} \qquad (2.74)$$

$$- \frac{g^2 \, V \, \Delta_m^2(0)}{2^n n! \, \pi} \int d^D x' \, \lim_{N \to 0} \left(\frac{d}{dN} \right)^n [2\Delta_m(0)]^N \cos(\pi N)$$

$$\times \sum_{\substack{l_{12}=0 \\ \text{even}}}^{\infty} \frac{1}{l_{12}!} \left[\frac{2\Delta_m(x')}{\Delta_m(0)} \right]^{l_{12}} \frac{\Gamma(N+2)\,\Gamma(N+\frac{3}{2})}{\Gamma(N+2-\frac{1}{2}l_{12})} \frac{\Gamma(2)\,\Gamma(\frac{3}{2})}{\Gamma(2-\frac{1}{2}l_{12})}.$$

The summations over even or odd values of l_{12} can now be performed in the same way as for $n = 2$ above, see the discussion of equation (2.50), leading to the result

$$Z_n \big|_{k=2} = \frac{g^2 \, V \, \Delta_m^2(0)}{2^{n+1} \, n! \, \pi} \int d^D x' \, \lim_{N \to 0} \left(\frac{d}{dN} \right)^n [2\Delta_m(0)]^{2N} \left\{ - \sin^2(\pi N)\,\Gamma(N+2)^2 \right.$$

$$\times \frac{2\Delta_m(x')}{\Delta_m(0)} \, {}_2F_1\left[-(N+\tfrac{1}{2}), -(N+\tfrac{1}{2}); \tfrac{3}{2}; \left(\tfrac{\Delta_m(x')}{\Delta_m(0)}\right)^2 \right]$$

$$\left. + \cos^2(\pi N)\,\Gamma(N+\tfrac{3}{2})^2 \, {}_2F_1\left[-(N+1), -(N+1); \tfrac{1}{2}; \left(\tfrac{\Delta_m(x')}{\Delta_m(0)}\right)^2 \right] \right\}$$

$$- \frac{g^2 \, V \, \Delta_m^2(0)}{2^n \, n! \, \pi} \int d^D x' \, \lim_{N \to 0} \left(\frac{d}{dN} \right)^n [2\Delta_m(0)]^N \cos(\pi N)\,\Gamma(\tfrac{3}{2})\,\Gamma(N+\tfrac{3}{2})$$

$$\times {}_2F_1\left[-(N+1), -1; \tfrac{1}{2}; \left(\tfrac{\Delta_m(x')}{\Delta_m(0)}\right)^2 \right].$$
$$(2.75)$$

In this form the two-vertex contributions to $\mathcal{Z}_n$ can be summed to all orders n in ε as follows:

$$\mathcal{Z}(\varepsilon)\big|_{k=2} = \sum_{n=2}^{\infty} \mathcal{Z}_n\big|_{k=2} \, \varepsilon^n = \frac{g^2 \, V \, \Delta_m^2(0)}{2\pi} \sum_{n=2}^{\infty} \frac{(\varepsilon/2)^n}{n!} \lim_{N\to 0} \left(\frac{d}{dN}\right)^n f(N), \quad (2.76)$$

where

$$\begin{aligned}
f(N) = \int d^D x' \bigg\{ &[2\Delta_m(0)]^{2N} \cos^2(\pi N) \, \Gamma(N+\tfrac{3}{2})^2 \\
&\times \, {}_2F_1\Big[-(N+1), -(N+1); \tfrac{1}{2}; \big(\tfrac{\Delta_m(x')}{\Delta_m(0)}\big)^2\Big] \\
&- [2\Delta_m(0)]^{2N} \sin^2(\pi N) \, \Gamma(N+2)^2 \, \tfrac{2\Delta_m(x')}{\Delta_m(0)} \\
&\times \, {}_2F_1\Big[-(N+\tfrac{1}{2}), -(N+\tfrac{1}{2}); \tfrac{3}{2}; \big(\tfrac{\Delta_m(x')}{\Delta_m(0)}\big)^2\Big] \\
&- \sqrt{\pi} \, [2\Delta_m(0)]^N \cos(\pi N) \, \Gamma(N+\tfrac{3}{2}) \\
&\times \, {}_2F_1\Big[-(N+1), -1; \tfrac{1}{2}; \big(\tfrac{\Delta_m(x')}{\Delta_m(0)}\big)^2\Big]\bigg\}.
\end{aligned} \qquad (2.77)$$

The summation (2.76) is recognizable as the Taylor series of $f(\varepsilon/2)$ around 0 without the $n = 0$ and $n = 1$ terms. Therefore, completing the summation results in the two-vertex approximation of the partition function:

$$\mathcal{Z}(\varepsilon)\big|_{k=2} = \frac{g^2 \, V \, \Delta_m^2(0)}{2\pi} \Big\{ f(\varepsilon/2) - f(0) - \tfrac{1}{2}\varepsilon \lim_{N\to 0} \Big(\frac{d}{dN}\Big) f(N) \Big\}. \qquad (2.78)$$

The first derivative of $f(N)$ can be performed using the derivative (2.57) of the Gaussian hypergeometric function and is found to vanish in the limit $N \to 0$. Thus the two-vertex approximation of the partition function $\mathcal{Z}(\varepsilon)$ reads:

$$\begin{aligned}
\mathcal{Z}(\varepsilon)\big|_{k=2} = &\, \frac{g^2 \, V^2 \, \Delta_m^2(0)}{8} + \frac{g^2 \, V \, m^{-2} \Delta_m(0)}{4}\big(1 - \tfrac{D}{2}\big) + \frac{g^2 \, V \, \Delta_m^2(0)}{2\pi} \int d^D x' \\
&\times \bigg\{ [2\Delta_m(0)]^\varepsilon \cos^2(\tfrac{\pi\varepsilon}{2})\Gamma(\tfrac{\varepsilon+3}{2})^2 \, {}_2F_1\Big[-\tfrac{\varepsilon+2}{2}, -\tfrac{\varepsilon+2}{2}; \tfrac{1}{2}; \big(\tfrac{\Delta_m(x')}{\Delta_m(0)}\big)^2\Big] \\
&- [2\Delta_m(0)]^\varepsilon \sin^2(\tfrac{\pi\varepsilon}{2})\Gamma(\tfrac{\varepsilon+4}{2})^2 \, \tfrac{2\Delta_m(x')}{\Delta_m(0)} \, {}_2F_1\Big[-\tfrac{\varepsilon+1}{2}, -\tfrac{\varepsilon+1}{2}; \tfrac{3}{2}; \big(\tfrac{\Delta_m(x')}{\Delta_m(0)}\big)^2\Big] \\
&- \sqrt{\pi} \, [2\Delta_m(0)]^{\varepsilon/2} \cos(\tfrac{\pi\varepsilon}{2})\Gamma(\tfrac{\varepsilon+3}{2}) \, {}_2F_1\Big[-\tfrac{\varepsilon+2}{2}, -1; \tfrac{1}{2}; \big(\tfrac{\Delta_m(x')}{\Delta_m(0)}\big)^2\Big]\bigg\}.
\end{aligned}$$
$$(2.79)$$

Notice that this approximation is explicitly quadratic in the coupling constant g and can be identified as a second-order coupling-constant approximation in the sense discussed in Section 2.2. For integer values of ε such an expansion can be evaluated using standard diagrammatic methods, confirming the result (2.79) in those cases.

Overall, the study of the normalized partition function in this chapter has demonstrated how the nonlinearity-expansion techniques of [1] can be generalized beyond the application at first order, resulting in the general structure of the partition-function coefficients $\mathcal{Z}_n$. For the first-order and second-order coefficients $\mathcal{Z}_1$ and $\mathcal{Z}_2$, this general structure was reduced to closed-form solutions and a second type of approximation, based on the summation of single-vertex and two-vertex terms to all orders in ε, was presented, relating the ε expansion of $\mathcal{Z}(\varepsilon)$ to a coupling-constant expansion picture.

Before applying the generalized expansion techniques to the study of the Green's functions, the results of the partition-function analysis are used to determine the behavior of the ground-state energy density in the following chapter, illustrating the numerical analysis that is required for the evaluation of the nonlinearity expansion beyond second order as well.

Chapter 3

The Ground-State Energy Density

The reality of the energy spectrum is one of the most surprising features of the non-Hermitian quantum-mechanical system with the Bender-Boettcher Hamiltonian (1.1). It is this curious feature in which the concept of $\mathcal{PT}$ symmetry originated [21]. In this chapter the behavior of the ε expansion for the ground-state energy density $\mathcal{E}(\varepsilon)$ of the D-dimensional model is investigated through its relation to the expansion coefficients of the normalized partition function $\mathcal{Z}(\varepsilon)$.

In Section 3.1 closed-form solutions for the first- and second-order coefficients $\mathcal{E}_1$ and $\mathcal{E}_2$ are determined based on the results for the coefficients $\mathcal{Z}_1$ and $\mathcal{Z}_2$. The coefficient $\mathcal{E}_1$ is shown to agree with the result obtained by Bender et al. in [1] and their analysis is improved upon with the calculation of $\mathcal{E}_2$. Furthermore, an approximation of $\mathcal{E}(\varepsilon)$ based on the single-vertex and two-vertex contributions $\mathcal{Z}(\varepsilon)|_{k=1}$ and $\mathcal{Z}(\varepsilon)|_{k=2}$ is obtained.

In Section 3.2 and Section 3.3 the evaluation of $\mathcal{E}_1$ and $\mathcal{E}_2$ in $D = 0$ and $D = 1$ space-time dimensions is shown to coincide with the results obtained either through direct integration of the functional integral, in the case of the zero-dimensional theory, or Rayleigh-Schrödinger perturbation theory for the quantum-mechanical case.

An additional test of the general partition-function coefficient structure $\mathcal{Z}_n$ is the occurrence of volumetric divergences, which are expected to cancel in the ground-state energy density. This behavior is argued to be generally the case in Section 3.4 based on the structure of $\mathcal{Z}_n$ obtained in the previous chapter. The cancellation of volumetrically divergent contributions also allows for numerical

evaluations of the energy density by considering only the volume-independent contributions. In Section 3.5 this is demonstrated for the coefficient $\mathcal{E}_3$ in $D = 0$ and $D = 1$ dimensions. The Padé approximants based on the third-order calculation are determined and compared to the exact results to assess the quality of the approximation.

3.1 Expansion in D Dimensions

The ground-state energy density $\mathcal{E}(\varepsilon)$ is related to the normalized partition function $\mathcal{Z}(\varepsilon)$ through

$$\mathcal{E}(\varepsilon) = -\frac{1}{V}\ln[Z(0)\,\mathcal{Z}(\varepsilon)], \tag{3.1}$$

where V denotes the D-dimensional space-time volume and $Z(0)$ the partition function (2.5) of the free theory. The coefficients $\mathcal{E}_n$ of an expansion in the nonlinearity parameter ε,

$$\mathcal{E}(\varepsilon) = \sum_{n=0}^{\infty} \mathcal{E}_n\,\varepsilon^n, \tag{3.2}$$

can thus be expressed in terms of the expansion coefficients $\mathcal{Z}_n$ of the normalized partition function, whose structure (2.41) was analyzed in the previous chapter:

$$\mathcal{E}_n = \frac{1}{n!}\left(\frac{d}{d\varepsilon}\right)^n\mathcal{E}(\varepsilon)\Big|_{\varepsilon=0} = -\frac{1}{V\,n!}\left(\frac{d}{d\varepsilon}\right)^n\ln[Z(0)\,\mathcal{Z}(\varepsilon)]\Big|_{\varepsilon=0}. \tag{3.3}$$

The logarithmic derivatives are calculated using Faa' di Bruno's formula [45] in terms of the partial Bell polynomials (2.10), finding that

$$\mathcal{E}_n = \frac{1}{V\,n!}\sum_{k=1}^{n}(k-1)!\,(-1)^k\,\mathrm{B}_{n,k}[1!\,\mathcal{Z}_1, ..., (n+1-k)!\,\mathcal{Z}_{n+1-k}] \tag{3.4}$$

for $n \geq 1$ and $\mathcal{E}_0 = -\ln[Z(0)]/V$. To third order in ε the energy-density coefficients are explicitly given in terms of the partition-function coefficients as

$$\mathcal{E}_1 = -\frac{1}{V}\mathcal{Z}_1, \quad \mathcal{E}_2 = -\frac{1}{V}(\mathcal{Z}_2 - \tfrac{1}{2}\mathcal{Z}_1^2), \quad \mathcal{E}_3 = -\frac{1}{V}(\mathcal{Z}_3 - \mathcal{Z}_1\mathcal{Z}_2 + \tfrac{1}{3}\mathcal{Z}_1^3). \tag{3.5}$$
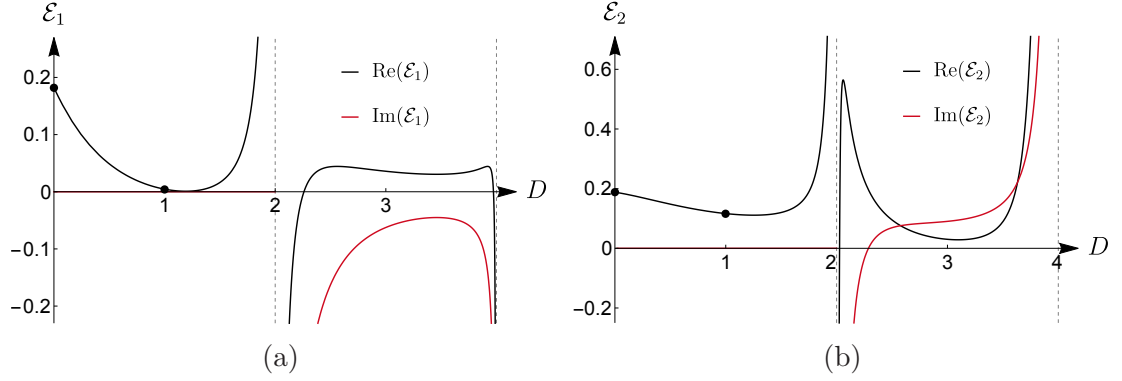
Figure 3.1: Behavior of the first-order and second-order energy-density coefficients $\mathcal{E}_1$ and $\mathcal{E}_2$ in $0 \leq D < 4$ dimensions. The black dots denote the zero-dimensional and quantum-mechanical theories, which are evaluated algebraically in Section 3.2 and Section 3.3.

Using the results (2.42) and (2.62) for the partition-function coefficients $\mathcal{Z}_1$ and $\mathcal{Z}_2$ obtained in Chapter 2, the first-order and second-order energy-density coefficients are found to be

$$\mathcal{E}_1 = \tfrac{1}{4}g\,\Delta_m(0)\left(\ln[2\Delta_m(0)] + \psi(\tfrac{3}{2})\right), \tag{3.6}$$

in agreement with the result of [1], and

$$\mathcal{E}_2 = \frac{g^2\,m^{-2}\Delta_m(0)}{16}(\tfrac{D}{2} - 1)\left\{\left(\ln[2\Delta_m(0)] + \psi(\tfrac{3}{2})\right)^2 + 2\left(\ln[2\Delta_m(0)] + \psi(\tfrac{3}{2})\right) - 6\right\}$$
$$- \frac{g^2\,\Delta_m^2(0)}{16}\int d^D x'\left\{3\tfrac{\Delta_m(x')}{\Delta_m(0)}\sqrt{1 - [\tfrac{\Delta_m(x')}{\Delta_m(0)}]^2}\left(2\sin^{-1}[\tfrac{\Delta_m(x')}{\Delta_m(0)}] - \pi\right)\right.$$
$$\left. + (2[\tfrac{\Delta_m(x')}{\Delta_m(0)}]^2 + 1)\sin^{-1}[\tfrac{\Delta_m(x')}{\Delta_m(0)}]\left(\sin^{-1}[\tfrac{\Delta_m(x')}{\Delta_m(0)}] - \pi\right)\right\}$$
$$+ \frac{g\,\Delta_m(0)}{16}\left[\left(\ln[2\Delta_m(0)] + \psi(\tfrac{3}{2})\right)^2 + \psi^{(1)}(\tfrac{3}{2}) - \pi^2\right]. \tag{3.7}$$

In Figure 3.1 the behavior of these coefficients is shown as a function of the space-time dimension in the range $0 \leq D < 4$ for $g = m = 1$, which corresponds to the model without dimensional parameters studied in [1]. The first-order energy-density coefficient shown in Figure 3.1a has a positive minimum near $D = 1.3$. Note that both energy coefficients diverge at $D = 2$, demonstrating that renormalization techniques are required in this case. Moreover, they both evaluate to finite *complex* values in the region $2 < D < 4$, and diverge again when approach-

ing $D = 4$. The transition from real values in $0 \leq D < 2$ dimensions to complex values for $2 < D < 4$ is caused by the proportionality of the selfloop propagator $\Delta_m(0)$ to $\Gamma(1 - \frac{D}{2})$, cf. (2.30), which changes sign from being a positive real function in the region $0 \leq D < 2$, to being a negative real function for $2 < D < 4$. As a result the term $\ln[2\Delta_m(0)]$ becomes a complex function in $2 < D < 4$ dimensions, and so do the ground-state energy-density coefficients $\mathcal{E}_1$ and $\mathcal{E}_2$. This behavior appears to suggest that - at least order-by-order in the nonlinearity expansion - the reality of the ground-state energy density, which is so remarkable in the quantum-mechanical Bender-Boettcher model, is not generally preserved for all dimensions in the D-dimensional quantum-field-theoretical system.

In analogy to the expansion in terms of the coefficients $\mathcal{Z}_1$ and $\mathcal{Z}_2$, the ground-state energy density $\mathcal{E}(\varepsilon)$ can also be calculated based on the single-vertex and two-vertex approximations $\mathcal{Z}(\varepsilon)|_{k=1}$ and $\mathcal{Z}(\varepsilon)|_{k=2}$ of the normalized partition function. As argued in Section 2.2, when treating m and g as independent parameters these approximations correspond to first-order and second-order coupling-constant expansion contributions. Therefore, the relation between the corresponding energy-density contributions and the partition-function contributions has the same form as for the ε-expansion coefficients, namely:

$$\mathcal{E}(\varepsilon)\big|_{k=1} = -\frac{1}{V}\mathcal{Z}(\varepsilon)\big|_{k=1}, \qquad \mathcal{E}(\varepsilon)\big|_{k=2} = -\frac{1}{V}\left[\mathcal{Z}(\varepsilon)\big|_{k=2} - \tfrac{1}{2}\mathcal{Z}(\varepsilon)\big|_{k=1}^2\right]. \quad (3.8)$$

Using the results (2.46) and (2.79) for $\mathcal{Z}(\varepsilon)|_{k=1}$ and $\mathcal{Z}(\varepsilon)|_{k=2}$ respectively, these contributions are explicitly given as

$$\mathcal{E}(\varepsilon)\big|_{k=1} = \tfrac{1}{2\sqrt{\pi}}\, g\cos(\tfrac{\pi\varepsilon}{2})\,\Gamma(\tfrac{\varepsilon+3}{2})\,[2\Delta_m(0)]^{1+\varepsilon/2} - \tfrac{1}{2}g\,\Delta_m(0), \qquad (3.9)$$

$$\begin{aligned}
\mathcal{E}(\varepsilon)\big|_{k=2} = {} & \frac{g^2\,m^{-2}\Delta_m(0)}{4}(\tfrac{D}{2}-1) - \frac{g^2\,\Delta_m^2(0)}{2\pi}\int d^D x' \\
& \times \Bigg\{[2\Delta_m(0)]^{\varepsilon}\cos^2(\tfrac{\pi\varepsilon}{2})\Gamma(\tfrac{\varepsilon+3}{2})^2\left({}_2F_1\left[-\tfrac{\varepsilon+2}{2},-\tfrac{\varepsilon+2}{2};\tfrac{1}{2};\left(\tfrac{\Delta_m(x')}{\Delta_m(0)}\right)^2\right]-1\right) \\
& - [2\Delta_m(0)]^{\varepsilon}\sin^2(\tfrac{\pi\varepsilon}{2})\Gamma(\tfrac{\varepsilon+4}{2})^2\,\tfrac{2\Delta_m(x')}{\Delta_m(0)}\,{}_2F_1\left[-\tfrac{\varepsilon+1}{2},-\tfrac{\varepsilon+1}{2};\tfrac{3}{2};\left(\tfrac{\Delta_m(x')}{\Delta_m(0)}\right)^2\right] \\
& - \sqrt{\pi}\,[2\Delta_m(0)]^{\varepsilon/2}\cos(\tfrac{\pi\varepsilon}{2})\Gamma(\tfrac{\varepsilon+3}{2})\left({}_2F_1\left[-\tfrac{\varepsilon+2}{2},-1;\tfrac{1}{2};\left(\tfrac{\Delta_m(x')}{\Delta_m(0)}\right)^2\right]-1\right)\Bigg\}.
\end{aligned}$$
$$(3.10)$$
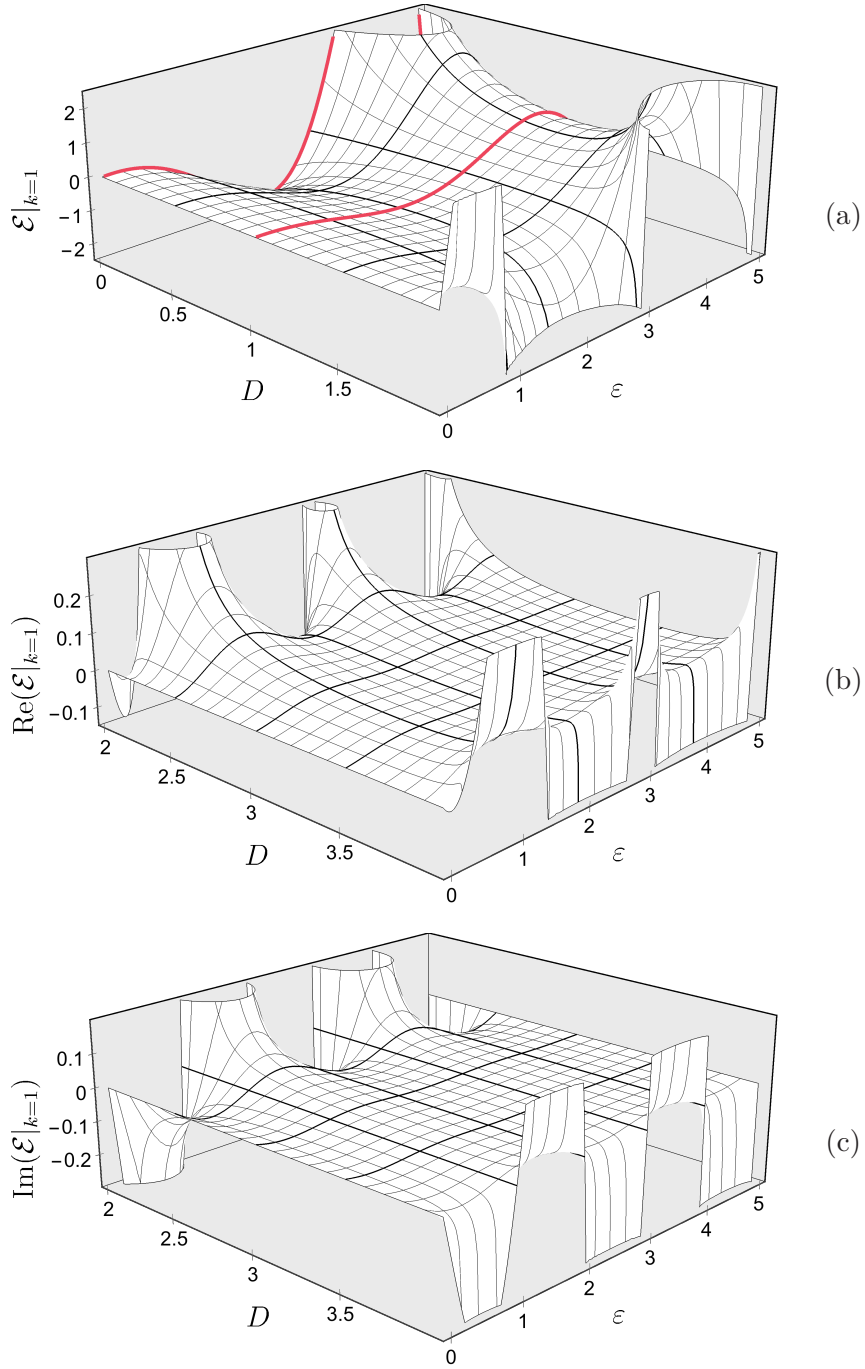
Figure 3.2: Behavior of the single-vertex approximation of the ground-state energy density as a function of the dimension D and the nonlinearity parameter ε. For $0 \leq D < 2$ the coefficient $\mathcal{E}(\varepsilon)|_{k=1}$ is real, shown in Figure 3.2a; the red lines denote the zero-dimensional and quantum-mechanical theories. For $2 < D < 4$ the coefficient becomes complex; the real and imaginary parts are displayed in Figure 3.2b and Figure 3.2c respectively.

Notice that, since the Gaussian hypergeometric function (2.53) has an expansion of the form $_2F_1(a, b; c; z) = 1 + O(z)$, all terms in the curly brackets are functions of at least order $O(\Delta_m(x'))$ in the propagator, so that the space-time integration in $\mathcal{E}(\varepsilon)|_{k=2}$ does not lead to a volumetric divergence.

The behavior of $\mathcal{E}(\varepsilon)|_{k=1}$ and $\mathcal{E}(\varepsilon)|_{k=2}$ is visualized in Figure 3.2 and Figure 3.3 respectively as a function of the space-time dimension D and the nonlinearity parameter ε. Similar to the ε-expansion coefficients, both contributions are real functions for $0 \leq D < 2$, which diverge in the limit of two dimensions, see Figure 3.2a and Figure 3.3a. The red lines in these figures denote the behavior in $D = 0$ and $D = 1$ dimensions, which is determined algebraically in the following Section 3.2 and Section 3.3. For $2 \leq D < 4$ dimensions $\mathcal{E}(\varepsilon)|_{k=1}$ and $\mathcal{E}(\varepsilon)|_{k=2}$ are generally complex functions, the real and imaginary parts of which are visualized in Figure 3.2b and Figure 3.2c, and Figure 3.3b and Figure 3.3c respectively. This behavior originates in raising the selfloop propagator $\Delta_m(0)$ to powers involving the generally noninteger parameter ε in (3.9) and (3.10).

Observe, however, that the single-vertex and two-vertex contributions $\mathcal{E}(\varepsilon)|_{k=1}$ and $\mathcal{E}(\varepsilon)|_{k=2}$ remain *real* functions for integer values of the nonlinearity parameter ε. This can not be observed in the ε expansion because of its perturbative nature in the nonlinearity parameter. The spectral reality at integer values of ε can be understood from the structure of the Lagrangian density (2.1) in the partition function (2.4): For integer values of ε the term $(i\phi)^\varepsilon$ is either purely real or purely imaginary. In the functional integral in $\mathcal{Z}(\varepsilon)$ only terms that are even in the field ϕ contribute, so that for integer ε the partition function is real. While this results in real-valued energy-density coefficients, cf. the relations (3.8), it has to be remarked, that the full ground-state energy density $\mathcal{E}(\varepsilon)$ may still be complex, due to its logarithmic relation (3.1) to the full partition function, which could be a negative.

In addition to the divergences in $D = 2$ and $D = 4$ dimensions, Figure 3.3b and Figure 3.3c illustrate that the two-vertex contribution $\mathcal{E}(\varepsilon)|_{k=2}$ has a complicated divergence structure in the region $2 < D < 4$. This demonstrates that renormalization techniques are not only required for $D = 2$ and $D = 4$ but in-between as well. It also affects the apparent complexity of $\mathcal{E}(\varepsilon)$ in these dimensions which has to be reexamined in the renormalized system for conclusive statements.
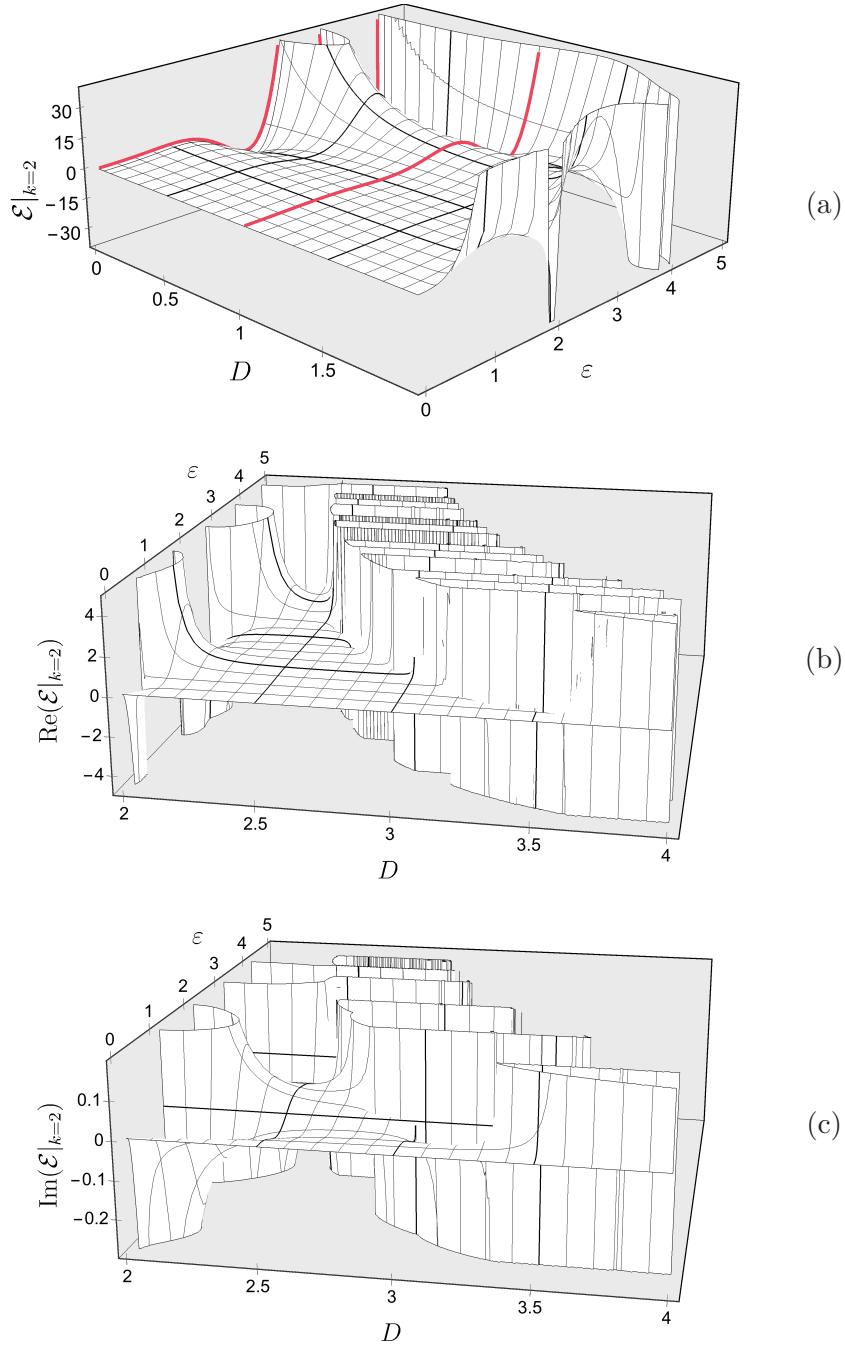
Figure 3.3: Behavior of the two-vertex approximation of the ground-state energy density as a function of the dimension D and the nonlinearity parameter ε. For $0 \leq D < 2$ the coefficient $\mathcal{E}(\varepsilon)|_{k=2}$ is real, shown in Figure 3.3a; the red lines denote the zero-dimensional and quantum-mechanical theories. For $2 < D < 4$ the coefficient becomes complex; the real and imaginary parts are displayed in Figure 3.3b and Figure 3.3c respectively.

3.2 $D = 0$ Dimensions

In the special case of zero-dimensional space-time, the theory describes a valuable toy-model that is exactly solvable. In particular, since space-time is a single point the functional integral simplifies to an ordinary integration over the (real) field and the free propagator has the form $\Delta_m(x) \equiv \Delta_m(0) = m^{-2}$. Moreover, the volume of zero-dimensional space-time is $V = 1$. For simplicity the theory is analyzed for $g = m = 1$ in the following; in this case the model corresponds to that without dimensional parameters, which was studied in [1].

For $D = 0$ the expressions (3.6) and (3.7) for the ε-expansion coefficients of the ground-state energy density become

$$\mathcal{E}_0\big|_{D=0} = -\ln(\sqrt{2\pi}) \approx -0.918938, \tag{3.11}$$

$$\mathcal{E}_1\big|_{D=0} = \tfrac{1}{4}(2 - \gamma - \ln 2) \approx 0.182409, \tag{3.12}$$

$$\mathcal{E}_2\big|_{D=0} = \tfrac{1}{64}(8\gamma - 8 + \pi^2 + 8\ln 2) \approx 0.188007. \tag{3.13}$$

The first-order result reproduces that obtained in [1]. In Appendix D the normalized partition function is calculated directly by evaluating the functional integral as an ordinary integration over the field. In particular, the values of the coefficients $\mathcal{Z}_1$ and $\mathcal{Z}_2$ are evaluated in this calculation, confirming the results (2.42) and (2.62) in $D = 0$ dimensions and thus also the ground-state energy coefficients (3.12) and (3.13). In addition, the *exact* partition function $\mathcal{Z}(\varepsilon)$ and the related ground-state energy density $\mathcal{E}(\varepsilon)$ are found to be

$$\mathcal{Z}(\varepsilon)\big|_{D=0} = \frac{2^{1/(\varepsilon+2)}}{\sqrt{2\pi}\,(1 + \varepsilon/2)}\,\Gamma(\tfrac{1}{\varepsilon+2})\,\cos(-\tfrac{\pi}{2}\,\tfrac{\varepsilon}{\varepsilon+2}) \tag{3.14}$$

and

$$\mathcal{E}(\varepsilon)\big|_{D=0} = -\ln\left[\frac{2^{1/(\varepsilon+2)}}{1 + \varepsilon/2}\,\Gamma(\tfrac{1}{\varepsilon+2})\,\cos(-\tfrac{\pi}{2}\,\tfrac{\varepsilon}{\varepsilon+2})\right]. \tag{3.15}$$

The single- and two-vertex approximations $\mathcal{E}(\varepsilon)|_{k=1}$ and $\mathcal{E}(\varepsilon)|_{k=2}$ in (3.9) and (3.10) simplify to

$$\mathcal{E}(\varepsilon)\big|_{\substack{k=1 \\ D=0}} = 2^{\varepsilon/2}\cos(\tfrac{\pi\varepsilon}{2})\,\Gamma(\tfrac{\varepsilon+3}{2})\,\tfrac{1}{\sqrt{\pi}} - \tfrac{1}{2}, \tag{3.16}$$

and

$$\mathcal{E}(\varepsilon)\big|_{\substack{k=2 \\ D=0}} = -\frac{1}{2\pi}\Big\{2^\varepsilon \cos^2(\tfrac{\pi\varepsilon}{2})\big[\sqrt{\pi}\Gamma(\varepsilon + \tfrac{5}{2}) - \Gamma(\tfrac{\varepsilon+3}{2})^2\big] - 2^\varepsilon \sin^2(\tfrac{\pi\varepsilon}{2})\sqrt{\pi}\,\Gamma(\varepsilon + \tfrac{5}{2})$$
$$- 2^{\varepsilon/2}\cos(\tfrac{\pi\varepsilon}{2})\sqrt{\pi}\,(\varepsilon + 2)\Gamma(\tfrac{\varepsilon+3}{2})\Big\} - \frac{1}{4},$$

$$\tag{3.17}$$

using in the latter that [51]

$$_2F_1(a, b; c; 1) = \frac{\Gamma(c)\,\Gamma(c - a - b)}{\Gamma(c - a)\,\Gamma(c - b)}. \tag{3.18}$$

3.3 $D = 1$ Dimension

The theory in one-dimensional space-time describes the field-theoretic equivalent of the quantum-mechanical system (1.1). While an exact evaluation of the ground-state energy density is only possible numerically, the ε-expansion coefficients $\mathcal{E}_1$ and $\mathcal{E}_2$ can be calculated following Rayleigh-Schrödinger perturbation theory. This was used in [1] to confirm the first-order behavior.

In one-dimensional space-time the free propagator (2.28) has the form $\Delta_m(x) = \frac{1}{2m}\,e^{-m|x|}$ and the selfloop amplitude becomes $\Delta_m(0) = \frac{1}{2m}$. Again, the theory is analyzed for $g = m = 1$ in the following for simplicity; here the model corresponds to that without dimensional parameters, which was studied in [1]. With these expressions the D-dimensional solutions for $\mathcal{E}_1$ and $\mathcal{E}_2$ in (3.6) and (3.7) can be evaluated, yielding

$$\mathcal{E}_1\big|_{D=1} = \tfrac{1}{8}(2 - \gamma - 2\ln 2) \approx 0.004561, \tag{3.19}$$

$$\mathcal{E}_2\big|_{D=1} = \tfrac{1}{32}\big[\psi(\tfrac{3}{2}) - 1 - \tfrac{\pi^2}{4}\ln 2 - \tfrac{1}{2}\psi(\tfrac{3}{2})^2 - \tfrac{7}{8}\zeta(3)\big] \approx 0.116445. \tag{3.20}$$

The result for $\mathcal{E}_1$ confirms that obtained in [1]. In Appendix E these ground-state energy-density coefficients are evaluated using Rayleigh-Schrödinger perturbation theory, confirming the results in (3.19) and (3.20). This indirectly verifies the correct behavior of the partition-function coefficients as well.

The single-vertex and two-vertex approximations $\mathcal{E}(\varepsilon)|_{k=1}$ and $\mathcal{E}(\varepsilon)|_{k=2}$ in (3.9) and (3.10) simplify to

$$\mathcal{E}(\varepsilon)\Big|_{\substack{k=1\\D=1}} = \cos(\tfrac{\pi\varepsilon}{2})\,\Gamma(\tfrac{\varepsilon+3}{2})\,\tfrac{1}{2\sqrt{\pi}} - \tfrac{1}{4} \tag{3.21}$$

and

$$\begin{aligned}
\mathcal{E}(\varepsilon)\Big|_{\substack{k=2\\D=1}} = &-\tfrac{1}{16} - \tfrac{1}{8\pi}\Big\{ 2\cos^2(\tfrac{\pi\varepsilon}{2})\,\Gamma(\tfrac{\varepsilon+3}{2})^2\,(\tfrac{\varepsilon+2}{2})^2\,{}_4F_3[1,1,-\tfrac{\varepsilon}{2},-\tfrac{\varepsilon}{2};\tfrac{3}{2},2,2;1] \\
&- 4\sin^2(\tfrac{\pi\varepsilon}{2})\,\Gamma(\tfrac{\varepsilon+4}{2})^2\,{}_3F_2[\tfrac{1}{2},-\tfrac{\varepsilon+1}{2},-\tfrac{\varepsilon+1}{2};\tfrac{3}{2},\tfrac{3}{2};1] \\
&- \sqrt{\pi}\cos(\tfrac{\pi\varepsilon}{2})\,\Gamma(\tfrac{\varepsilon+3}{2})(\varepsilon+2)\Big\}.
\end{aligned} \tag{3.22}$$

3.4 Volumetric Divergences

The ground-state energy density $\mathcal{E}(\varepsilon)$ does in general not depend on the volume of space-time V, even though the appearance of volumetric divergences is a general property of the partition-function coefficients $\mathcal{Z}_n$. The discussion of the energy-density coefficients $\mathcal{E}_2$ and $\mathcal{E}(\varepsilon)|_{k=2}$ in one-dimensional space-time, presented in the previous section, serves as a good example: These coefficients are related to the partition-function coefficients up to second order in the respective approximation scheme by (3.5) and (3.8). In particular, the square of the first-order coefficient $\mathcal{Z}_1$, see (2.42), or $\mathcal{Z}(\varepsilon)|_{k=1}$, see (2.46), which dependent linearly on the space-time volume, enters. But this exactly cancels the contributions of the second-order partition-function coefficients that depend quadratically on V. Thus, overall, the coefficients become volume-independent, as seen in the results of $\mathcal{E}_2$ in (3.20) and $\mathcal{E}(\varepsilon)|_{k=2}$ in (3.22).

This cancellation of volumetric divergences confirms that the partition-function coefficients $\mathcal{Z}_n$ behave correctly and understanding it is necessary for numerical evaluations when no closed-form solutions are available. In the following, the dependence of the general partition-function coefficients (2.41) on the space-time volume V is analyzed and it is shown that these divergences cancel exactly in the coefficients $\mathcal{E}_n$.

The ground-state energy density $\mathcal{E}(\varepsilon)$ is related to the partition function $\mathcal{Z}(\varepsilon)$ through the relation (3.1). This relation is a version of the exponential formula [52]

(or the polymer expansion [53]): In the diagrammatic sense, the energy density contains only the fully connected contributions of the partition function. In particular, this is the case order-by-order in ε, so that $\mathcal{E}_n$ contains only the fully connected contributions of $\mathcal{Z}_n$:

$$\mathcal{E}_n = -\frac{1}{V}\, \mathcal{Z}_n\big|_{\text{connected}}. \tag{3.23}$$

Arguing that the connected contributions depend linearly on the volume V then implies that $\mathcal{E}(\varepsilon)$ (and its coefficients $\mathcal{E}_n$) are independent of the volume.

In the general structure (2.41) of the coefficients $\mathcal{Z}_n$ the only space-time dependence can arise from powers of the free propagators $\Delta_m(x_i - x_j)$ connecting different space-time points. Any dependence on $\Delta_m(0)$ describes selfloops and does therefore not depend on the space-time variables; they do not affect the volumetric divergences. The space-time dependence of the coefficients $\mathcal{Z}_n$ can therefore be argued on the basis of the space-time integrals

$$\int d^D x_\alpha \prod_{\substack{i,j=1 \\ i<j}}^{k} \Delta_m(x_i - x_j)^{l_{ij}} = \int d^D x_1 \, ... \int d^D x_k \prod_{\substack{i,j=1 \\ i<j}}^{k} \Delta_m(x_i - x_j)^{l_{ij}}, \tag{3.24}$$

where $k \in [1, n]$ and in general all $l_{ij} \in [0, \infty]$. Redefining all integration variables by $x_r \to \sum_{i=r}^{k} x_i$ renders the free propagators independent of the space-time variable x_k, resulting in the expression

$$\int d^D x_1 \, ... \int d^D x_{k-1} \prod_{\substack{i,j=1 \\ i<j}}^{k} \Delta_m\Big(\sum_{r=i}^{j-1} x_r \Big)^{l_{ij}} \underbrace{\int d^D x_k}_{V}, \tag{3.25}$$

in which a factor of the space-time volume V is apparent. Therefore, all contributions to the coefficient $\mathcal{Z}_n$ have *at least* a linear volumetric divergence.

So far, no assumption on the structure of the graph representing the product of free propagators in (3.24), that is on the values of the numbers l_{ij}, was made. If the graph representing (3.24) consists of two disconnected parts, then the space-time points x_1 to x_k can be relabeled and grouped into two sets, containing the points with indices in $S_1 = [1, k_1]$ and $S_2 = [k_1 + 1, k]$, so that all l_{ij} with $i \in S_1$ and $j \in S_2$ vanish. The product over the propagators in (3.24) then factorizes

into the form

$$
\left[\int d^D x_1 \ldots d^D x_{k_1} \prod_{\substack{i,j=1 \\ i<j}}^{k_1} \Delta_m(x_i - x_j)^{l_{ij}} \right] \left[\int d^D x_{k_1+1} \ldots d^D x_k \prod_{\substack{i,j=k_1+1 \\ i<j}}^{k} \Delta_m(x_i - x_j)^{l_{ij}} \right]
$$
(3.26)

and the previous redefinition of integration variables can be applied for both parts individually. Therefore, an overall at least quadratic dependence on the volume V arises.

This argument applies generally, so that (3.24) is proportional to the volume V raised to the power of *at least* the number of disconnected parts in the graph it represents. If (3.24) represents a fully disconnected graph, that is a graph with k disconnected parts, it consequently is proportional to at least V^k. But in this case all $l_{ij} = 0$, so that (3.24) is, in fact, exactly proportional to V^k. This, in turn, implies that (3.24) is proportional to the volume V raised to the power of *exactly* the number of disconnected parts in the graph it represents. In particular, a fully connected graph gives rise to a linear dependence on the space-time volume. Thus, the connected contributions of all $\mathcal{Z}_n$, and $\mathcal{Z}(\varepsilon)$ accordingly, are linearly dependent on V, such that the ground-state energy density $\mathcal{E}(\varepsilon)$, and all $\mathcal{E}_n$, are independent of the space-time volume.

3.5 The Third-Order Coefficient $\mathcal{E}_3$

For energy-density coefficients beyond second order in the nonlinearity expansion the evaluation of the general partition-function coefficient in (2.41) and consequently the energy-density coefficient in (3.4) becomes unwieldy. However, these coefficients can be calculated numerically. As argued in Section 3.4, the occurrence of volumetric divergences can be circumvented by considering only those contributions to (2.41) that correspond to connected graphs. To illustrate this, the third-order ground-state energy-density coefficient $\mathcal{E}_3$ is in this section determined numerically from (2.41) for $D = 0$ and $D = 1$ dimensional space-time and $g = m = 1$. In these cases, the exact third-order solution can be accessed through direct evaluation (zero-dimensional theory) or Rayleigh-Schrödinger perturbation theory (one-dimensional theory) for comparison.

The difficulty of evaluating the connected part of the partition-function co-efficient (2.41) lies in the summation $\sum_l$ over the numbers l_{ij} of propagators $\Delta_m(x_i - x_j)$ connecting the space-time points x_i and x_j. By limiting the maximum number of intermediate propagators l_{ij}, and studying the behavior of the result as a function of this maximum, a good approximation can be found. For the results that are presented in the following, the upper limits of the summation $\sum_l$ were increased successively up to 20. The resulting approximation of the energy coefficient based on these partial sums displays an oscillatory behavior with a growing amplitude in both $D = 0$ and $D = 1$ dimension. An approximate solution for the energy coefficient $\mathcal{E}_3$ can be found using Shanks and Euler transforms [50, 54] to extrapolate these results:

$$\mathcal{E}_3\big|_{D=0} \approx -0.234883 \quad \text{and} \quad \mathcal{E}_3\big|_{D=1} \approx -0.077953. \tag{3.27}$$

For the zero-dimensional theory, the energy-density coefficients $\mathcal{E}_n$ can be determined exactly to any order through the partition-function coefficients, whose evaluation is described in Appendix D. The exact result for the third-order coefficient is

$$\mathcal{E}_3\big|_{D=0} \approx -0.235768, \tag{3.28}$$

which confirms the quality of the approximate solution in (3.27).

For the one-dimensional case, the coefficients of the ground-state energy density can be determined using Rayleigh-Schrödinger perturbation theory, see Appendix E. The third-order coefficient $\mathcal{E}_3$ found in this way is

$$\mathcal{E}_3\big|_{D=1} \approx -0.077952, \tag{3.29}$$

confirming the quality of the approximate solution in (3.27) as well.

Having found the coefficients up to third order in the ε expansion of the ground-state energy density $\mathcal{E}(\varepsilon)$ in $D = 0$ and $D = 1$ dimensions, one can calculate the corresponding Padé approximants [54] for different values of ε to improve upon the approximation of $\mathcal{E}(\varepsilon)$. The closed-form solution for $\mathcal{E}(\varepsilon)$ in $D = 0$ dimensional space-time, see (3.15), offers a reference point to judge the quality of these Padé approximants in comparison to the exact result. For the

	M=0	M=1	M=2	M=3
L=0	-0.918938	-0.766740	-0.637049	-0.720208
L=1	-0.736529	-6.864121	-0.683985	
L=2	-0.548523	-0.652946		
L=3	-0.783406			

(a) $D = 0$, $\varepsilon = 1$

	M=0	M=1	M=2	M=3
L=0	-0.918938	-0.657794	-0.387252	-0.883171
L=1	-0.554119	-1.262664	-0.507806	
L=2	0.197903	-0.339175		
L=3	-1.681161			

(b) $D = 0$, $\varepsilon = 2$

Table 3.1: $[L/M]$ Padé approximants for $L, M \leq 3$ resulting from the energy-density coefficients $\mathcal{E}_n$ up to third order and for $\varepsilon = 1$ and $\varepsilon = 2$ in $D = 0$.

one-dimensional theory such a reference can be determined through the numerical solution to the eigenvalue equation based on the Hamiltonian (1.1).

In Table 3.1 and Table 3.2 the Padé results of the zero-dimensional and one-dimensional theory at $\varepsilon = 1$ and $\varepsilon = 2$, corresponding to interactions of the form $i\phi^3$ and $-\phi^4$, are shown. The exact result (3.15) for $D = 0$ evaluates to

$$\mathcal{E}(\varepsilon = 1)\big|_{D=0} \approx -0.667163, \tag{3.30}$$

$$\mathcal{E}(\varepsilon = 2)\big|_{D=0} \approx -0.421588. \tag{3.31}$$

In $D = 1$ space-time dimension the exact ground-state energy densitiy at $\varepsilon = 1$ and $\varepsilon = 2$ is found numerically to be

$$\mathcal{E}(\varepsilon = 1)\big|_{D=1} \approx 0.578134, \tag{3.32}$$

$$\mathcal{E}(\varepsilon = 2)\big|_{D=1} \approx 0.738575. \tag{3.33}$$

	M=0	M=1	M=2	M=3
L=0	0.5	0.504603	0.659568	0.544528
L=1	0.504561	0.499814	0.586198	
L=2	0.621006	0.574311		
L=3	0.543052			

(a) $D = 1$, $\varepsilon = 1$

	M=0	M=1	M=2	M=3
L=0	0.5	0.509292	9.895253	0.375440
L=1	0.509122	0.499817	0.847741	
L=2	0.974901	0.708268		
L=3	0.351275			

(b) $D = 1$, $\varepsilon = 2$

Table 3.2: $[L/M]$ Padé approximants for $L, M \leq 3$ resulting from the energy-density coefficients $\mathcal{E}_n$ up to third order for $\varepsilon = 1$ and $\varepsilon = 2$ in $D = 1$, corresponding to quantum-mechanical theories with interactions of the form $i\phi^3$ and $-\phi^4$.

The $[2/1]$ and $[1/2]$ Padé approximants in the first sub-diagonal and super-diagonal of all tables give reasonable upper and lower bounds bracketing the exact results. Moreover, considering the approximants with $L + M \leq 2$, resulting from at most the second-order ε-expansion coefficients, shows that a good approximation for the ground-state energy density $\mathcal{E}(\varepsilon)$ is only reached after including the third-order coefficients.

Overall, it was demonstrated in this chapter how to approximate the ground-state energy density in the nonlinearity expansion and in the vertex-approximation scheme based on the general coefficient structure (2.41) of the normalized partition function. Closed-form solutions of the first-order and second-order coefficients in both approximation schemes were derived and their behavior was discussed for $0 \leq D < 4$ space-time dimensions: While these coefficients are real-valued functions in the region $0 \leq D < 2$ they become generally complex in $2 < D < 4$ dimensions, suggesting a possible departure from the remarkable spectral reality found in the

quantum-mechanical Bender-Boettcher model (1.1) - at least to finite order in the expansions. However, the vertex-approximation coefficients, in which terms to all orders in ε are resummed, display the noteworthy feature of remaining real for integer values of the nonlinearity parameter even in $2 < D < 4$ dimensions. This may reflect an underlying property of the ground-state energy density $\mathcal{E}(\varepsilon)$ that emerges beyond all orders in ε. Moreover, using the numerically evaluated third-order ε-expansion coefficient $\mathcal{E}_3$, the quality of an approximation based on the Padé approximants of the nonlinearity expansion to third order was demonstrated by comparison to the exact results in the zero-dimensional and one-dimensional model.

In addition, the appearance of non-volumetric divergences in the ground-state energy-density coefficients, found in two dimensions and beyond, indicate that renormalization techniques are required. It is in particular necessary to reexamine the reality of the ground-state energy density in these dimensions after renormalization. The perturbative renormalization of the two-dimensional model is investigated in Chapter 5 after the discussion of the Green's functions in the following.

Chapter 4

The Green's Functions

Similar to the quantum-mechanical Bender-Boettcher model, the quantum-field-theoretic analogue (1.7) describes a family of systems that are characterized by the nonlinearity parameter ε and by their $\mathcal{PT}$ symmetry, which is reflected in the complex nature of the interaction term $(i\phi)^\varepsilon$. By generalizing the techniques proposed in [1], it was demonstrated in Chapter 2 for the partition function how the unusual complex logarithmic self-interaction structure that arises when expanding this theory in the nonlinearity parameter can be addressed. These techniques apply equally to the analysis of the Green's functions.

In Section 4.1 the general ε-expansion structure of the connected p-point Green's function is determined in terms of known functions only, particularly the propagator (2.28) of the free theory ($\varepsilon = 0$) with Lagrangian density (2.3).

The evaluation of this coefficient structure is demonstrated on the examples of the first-order and second-order coefficients in Section 4.2 and Section 4.3: Closed-form solutions for these ε-expansion coefficients are obtained and, like for the partition function, a second approximation, based on the summation of structurally similar contributions to all orders in ε, is analyzed. The results for the one-point and two-point Green's functions are presented.

In Section 4.4 the effective mass of the D-dimensional theory is determined from the expansion of the two-point Green's function to second order.

4.1 The General Coefficient Structure

The p-point Green's function is defined as

$$G_p(\varepsilon; y_1, \ldots, y_p) = \frac{1}{Z(0)\mathcal{Z}(\varepsilon)} \int \mathcal{D}\phi \, e^{-\int d^D x \, \mathcal{L}(\varepsilon)} \, \phi(y_1) \ldots \phi(y_p), \qquad (4.1)$$

where $\mathcal{Z}(\varepsilon)$ is the normalized partition function given in (2.4), and $Z(0)$ is the full partition function of the free theory, that is at $\varepsilon = 0$, see (2.5). Expanding (4.1) into a series of the form

$$G_p(\varepsilon; y_1, \ldots, y_p) = \sum_{n=0}^{\infty} G_{p,n}(y_1, \ldots, y_p) \, \varepsilon^n \qquad (4.2)$$

in the nonlinearity parameter ε requires not only the expansion of the functional integral, but also that one takes into account the ε expansion of $\mathcal{Z}(\varepsilon)$ in the denominator. This expansion of $\mathcal{Z}(\varepsilon)$, as described in Chapter 2, contains exclusively contributions that are represented diagrammatically by graphs on only *internal* points x_α, that is space-time points, which are integrated over. Such graphs are commonly referred to as vacuum bubbles. The functional integral in (4.1), however, contains in addition the *external* points y_1 to y_p, which are not integrated over. It is a well-established feature of the p-point Green's function (4.1) that the vacuum bubbles in the denominator exactly cancel the vacuum-bubble contributions of the remaining functional integral, see for example [48]. That is to say, only contributions that are represented by graphs in which every part is connected to at least one external point remain. This does not exclude graphs with disconnected parts, as long as each part contains an external point. One may write

$$G_p(\varepsilon; y_1, \ldots, y_p) = \frac{1}{Z(0)} \int \mathcal{D}\phi \, e^{-\int d^D x \, \mathcal{L}(\varepsilon)} \, \phi(y_1) \ldots \phi(y_p) \Big|_{\text{non-vacuum}} \qquad (4.3)$$

to emphasize the structural similarity to the normalized partition function (2.4).

Note that, because diagrammatically every disconnected part contributing to the expression (4.3) contains an external point, over which space-time is not integrated, $G_p(\varepsilon; y_1, \ldots, y_p)$ does not contain any volumetric divergences. The rescaling argument presented in Section 3.4, which showed that every discon-

nected part of a vacuum-bubble graph contributes an overall factor V, does not apply here, because (at least) one of the space-time points to be considered is an external point. Nevertheless, the general generating-function relation does apply: (4.3) contains various contributions represented by graphs with disconnected (non-vacuum) parts, which can be generated from only the fully connected contributions. It thus suffices to study the *connected p-point Green's function*:

$$G_p^c(\varepsilon; y_1, \dots, y_p) = \frac{1}{Z(0)} \int \mathcal{D}\phi \, e^{-\int d^D x \, \mathcal{L}(\varepsilon)} \, \phi(y_1) \dots \phi(y_p) \Big|_{\text{connected}}. \qquad (4.4)$$

Expanding the connected Green's functions in the nonlinearity parameter ε now proceeds in the same way as the expansion of the normalized partition function $\mathcal{Z}(\varepsilon)$ in Chapter 2. The complex logarithmic interaction terms of the expanded Lagrangian density $\mathcal{L}(\varepsilon)$ are expressed in only powers of the field ϕ, yielding in analogy to (2.26) the expansion coefficient:

$$
\begin{aligned}
G_{p,n}^c(y_1, \dots, y_p) = \\
\frac{1}{2^n} \sum_{k=1}^n \left(-\frac{g\mu_0^2}{2} \right)^k \sum_c \prod_{s=1}^{n+1-k} \frac{1}{c_s! \, (s!)^{c_s}} \int d^D x_\alpha \sum_{m_\alpha=0}^\beta \binom{\beta}{m_\alpha} (i\pi)^{m_\alpha} \\
\times \int_0^\infty dt_\alpha \sum_{\omega_\alpha=0}^\infty \frac{2 \, (-t_\alpha^2)^{\omega_\alpha}}{\pi \, (2\omega_\alpha + 1)!} \lim_{N_\alpha \to 0} \left(\frac{d}{dN_\alpha} \right)^{\beta - m_\alpha} (\mu_0^{1-D/2})^{2N_\alpha + (2\omega_\alpha+1)m_\alpha} \\
\times \frac{1}{Z(0)} \int \mathcal{D}\phi \, e^{-\int d^D x \, \mathcal{L}_0} \, \phi(y_1) \dots \phi(y_p) \, [\phi(x_\alpha)]^{2(N_\alpha+1)+(2\omega_\alpha+1)m_\alpha} \Big|_{\text{connected}},
\end{aligned}
\qquad (4.5)
$$

where the summation $\sum_c$ takes place over all integers $c_1, \dots, c_{n+1-k} \geq 0$ such that the conditions (2.11) and (2.12) are satisfied.

Before evaluating the general functional integral in (4.5), consider the special case of the coefficients at $n = 0$, which correspond to (4.4) at $\varepsilon = 0$:

$$G_{p,0}^c(y_1, \dots, y_p) = \frac{1}{Z(0)} \int \mathcal{D}\phi \, e^{-\int d^D x \, \mathcal{L}_0} \, \phi(y_1) \dots \phi(y_p) \Big|_{\text{connected}}. \qquad (4.6)$$

For odd values of p the integral is an odd function of the field ϕ and therefore vanishes. Moreover, since the field ϕ occurs only linearly at the space-time points y_1 to y_p, these points are diagrammatically connected pairwise by the propagator $\Delta_{m\mu_0}$ of the free theory. That is, even when p is even, (4.6) is represented by a

fully connected graph only for $p = 2$, where it corresponds to a single propagator connecting y_1 and y_2. Therefore,

$$G_{p,0}^c(y_1, \dots, y_p) = \begin{cases} \Delta_{m\mu_0}(y_1 - y_2), & \text{for} \quad p = 2, \\ 0, & \text{for} \quad p \neq 2. \end{cases} \tag{4.7}$$

In general, the functional integral in (4.5) is evaluated in terms of only known functions in the same way as in the partition function, see (2.33). A detailed calculation of the general integral

$$\frac{1}{Z(0)} \int \mathcal{D}\phi \, e^{-\int d^D x \, \mathcal{L}_0} \, \phi^{n_1}(z_1) \dots \phi^{n_k}(z_k) \tag{4.8}$$

can be found in Appendix B. There, the special case of the functional integral arising in (4.5) is evaluated as well:

$$\frac{1}{Z(0)} \int \mathcal{D}\phi \, e^{-\int d^D x \, \mathcal{L}_0} \, \phi(y_1) \dots \phi(y_p) \left[\phi(x_\alpha)\right]^{2(N_\alpha+1)+(2\omega_\alpha+1)m_\alpha} =$$

$$\left[\tfrac{1}{2}\Delta_{m\mu_0}(0)\right]^{p/2} \left(\frac{2\Delta_{m\mu_0}(0)}{\sqrt{\pi}}\right)^k \left[2\Delta_{m\mu_0}(0)\right]^{N_\alpha+m_\alpha(\omega_\alpha+\frac{1}{2})} \sum_l^\infty \prod_{\substack{i,j=1, \\ i<j}}^{k+p} \frac{1}{l_{ij}!}$$

$$\times \left[\frac{2\Delta_{m\mu_0}(z_i - z_j)}{\Delta_{m\mu_0}(0)}\right]^{l_{ij}} \frac{\Gamma[N_\alpha + 2 + m_\alpha(\omega_\alpha + \frac{1}{2})]\,\Gamma[N_\alpha + \frac{3}{2} + m_\alpha(\omega_\alpha + \frac{1}{2})]}{\Gamma[N_\alpha + 2 + m_\alpha(\omega_\alpha + \frac{1}{2}) - \frac{1}{2}L_\alpha]}$$

$$\times \left(\frac{1 + e^{i\pi(m_\alpha - L_\alpha)}}{2}\right) \left\{\prod_{r=1}^p \frac{1}{\Gamma(\frac{3}{2} - \frac{1}{2}L_{k+r})} \left(\frac{1 + e^{i\pi(1 - L_{k+r})}}{2}\right)\right\}, \tag{4.9}$$

where the summation $\sum_l$ runs over all integers $l_{ij} \in [0, \infty]$ with $i, j \in [1, k+p]$: $i < j$ and the numbers L_r with $r \in [1, k+p]$ are defined as in (2.34). The space-time points z_1 to z_{k+p} combine the internal points x_α and the external points y_1 to y_p; $z_i = x_i \, \forall i \in [1, k]$ and the additional space-time points y_1 to y_p are denoted as z_{k+1} to z_{k+p}.

Notice that since the field ϕ occurs linearly at the external space-time points, in a diagrammatic representation only exactly one propagator can connect these points to other space-time points. In (4.9) one finds this behavior in the term

within curly brackets: The factor containing the exponential function requires that an odd number of propagators are connected to each external point, and the Γ function in the denominator implies that this contribution vanishes for all odd numbers except the value one.

With the functional integral (4.9) the ε-expansion coefficients (4.5) of the connected p-point Green's function can be written as

$$G_{p,n}^c(y_1,\dots,y_p) =$$

$$\frac{1}{2^n}\left[\frac{\Delta_{m\mu_0}(0)}{2}\right]^{p/2}\sum_{k=1}^n\left(-\frac{g\mu_0^2\Delta_{m\mu_0}(0)}{\sqrt{\pi}}\right)^k\sum_c{}^{n+1-k}\prod_{s=1}^{}\frac{1}{c_s!\,(s!)^{c_s}}\int d^Dx_\alpha\sum_{m_\alpha=0}^{\beta}\binom{\beta}{m_\alpha}$$

$$\times (i\pi)^{m_\alpha}\lim_{N_\alpha\to 0}\left(\frac{d}{dN_\alpha}\right)^{\beta-m_\alpha}[2\mu_0^{2-D}\Delta_{m\mu_0}(0)]^{N_\alpha}\sum_l^{\infty}\prod_{\substack{i,j=1,\\i<j}}^{k+p}\frac{1}{l_{ij}!}\left[\frac{2\Delta_{m\mu_0}(z_i-z_j)}{\Delta_{m\mu_0}(0)}\right]^{l_{ij}}$$

$$\times\int_0^\infty dt_\alpha\sum_{\omega_\alpha=0}^{\infty}\frac{2\,(-t_\alpha^2)^{\omega_\alpha}}{\pi\,(2\omega_\alpha+1)!}\frac{\Gamma[N_\alpha+2+m_\alpha(\omega_\alpha+\frac{1}{2})]\,\Gamma[N_\alpha+\frac{3}{2}+m_\alpha(\omega_\alpha+\frac{1}{2})]}{\Gamma[N_\alpha+2+m_\alpha(\omega_\alpha+\frac{1}{2})-\frac{1}{2}L_\alpha]}$$

$$\times[2\mu_0^{2-D}\Delta_{m\mu_0}(0)]^{m_\alpha(\omega_\alpha+\frac{1}{2})}\left(\frac{1+e^{i\pi(m_\alpha-L_\alpha)}}{2}\right)\left\{\prod_{r=1}^{p}\left(\frac{1+e^{i\pi(1-L_{k+r})}}{2\Gamma(\frac{3}{2}-\frac{1}{2}L_{k+r})}\right)\right\}\Bigg|_{\text{connected}}$$

$$(4.10)$$

in terms of known functions only. As for the partition-function coefficients (2.35) in Chapter 2, some simplifications can be made: The summations over ω_α and integrations over t_α can be performed according to the identity (2.36), see Appendix C, yielding

$$G_{p,n}^c(y_1,\dots,y_p) =$$

$$\frac{1}{2^n}\left[\frac{\Delta_{m\mu_0}(0)}{2}\right]^{p/2}\sum_{k=1}^n\left(-\frac{g\mu_0^2\Delta_{m\mu_0}(0)}{\sqrt{\pi}}\right)^k\sum_c{}^{n+1-k}\prod_{s=1}^{}\frac{1}{c_s!\,(s!)^{c_s}}\int d^Dx_\alpha\sum_{m_\alpha=0}^{\beta}\binom{\beta}{m_\alpha}$$

$$\times (i\pi)^{m_\alpha}\lim_{N_\alpha\to 0}\left(\frac{d}{dN_\alpha}\right)^{\beta-m_\alpha}[2\mu_0^{2-D}\Delta_{m\mu_0}(0)]^{N_\alpha}\sum_l^{\infty}\prod_{\substack{i,j=1,\\i<j}}^{k+p}\frac{1}{l_{ij}!}\left[\frac{2\Delta_{m\mu_0}(z_i-z_j)}{\Delta_{m\mu_0}(0)}\right]^{l_{ij}}$$

$$\times\frac{\Gamma(N_\alpha+2)\,\Gamma(N_\alpha+\frac{3}{2})}{\Gamma(N_\alpha+2-\frac{1}{2}L_\alpha)}\left(\frac{1+e^{i\pi(m_\alpha-L_\alpha)}}{2}\right)\left\{\prod_{r=1}^{p}\left(\frac{1+e^{i\pi(1-L_{k+r})}}{2\Gamma(\frac{3}{2}-\frac{1}{2}L_{k+r})}\right)\right\}\Bigg|_{\text{connected}}.$$

$$(4.11)$$

Furthermore, the dependence on the dimensional parameter μ_0 can be simplified by denoting

$$z_j = z'_j/\mu_0, \quad \forall j \in [1, k+p]. \tag{4.12}$$

For $z'_1 = \mu_0 x_1$ to $z'_k = \mu_0 x_k$, this is the same rescaling of internal space-time points as in the calculation of the partition function, see (2.40). The additional variables $z'_{k+1} = \mu_0 y_1$ to $z'_{k+p} = \mu_0 y_p$ denote dimensionless versions of the external space-time points. By utilizing the scaling behavior (2.38) and (2.39) of the general propagator Δ_λ, the propagators in (4.11) can then be rewritten as

$$\Delta_{m\mu_0}(z) = \Delta_{m\mu_0}(z'/\mu_0) = \mu_0^{D-2}\,\Delta_m(z'), \tag{4.13}$$

where now $\Delta_m(z')$ is again a function of dimension $[\text{mass}]^0$ and the dependence on the dimensional parameter μ_0 is factored out explicitly. Taking care to rescale the space-time integrals as well, the expression (4.11) becomes

$$G^c_{p,n}(y_1, \dots, y_p) =$$

$$\frac{1}{2^n}\left[\frac{\mu_0^{D-2}\Delta_m(0)}{2}\right]^{p/2} \sum_{k=1}^{n}\left(-\frac{g\Delta_m(0)}{\sqrt{\pi}}\right)^k \sum_c \prod_{s=1}^{n+1-k}\frac{1}{c_s!\,(s!\,)^{c_s}}\int d^D x'_\alpha \sum_{m_\alpha=0}^{\beta}\binom{\beta}{m_\alpha}$$

$$\times (i\pi)^{m_\alpha}\lim_{N_\alpha\to 0}\left(\frac{d}{dN_\alpha}\right)^{\beta-m_\alpha}[2\Delta_m(0)]^{N_\alpha}\sum_l^{\infty}\prod_{\substack{i,j=1,\\i<j}}^{k+p}\frac{1}{l_{ij}!}\left[\frac{2\Delta_m(z'_i - z'_j)}{\Delta_m(0)}\right]^{l_{ij}}$$

$$\times \frac{\Gamma(N_\alpha + 2)\,\Gamma(N_\alpha + \frac{3}{2})}{\Gamma(N_\alpha + 2 - \frac{1}{2}L_\alpha)}\left(\frac{1 + e^{i\pi(m_\alpha - L_\alpha)}}{2}\right)\left\{\prod_{r=1}^{p}\left(\frac{1 + e^{i\pi(1 - L_{k+r})}}{2\Gamma(\frac{3}{2} - \frac{1}{2}L_{k+r})}\right)\right\}\Bigg|_{\text{connected}}.$$

$$\tag{4.14}$$

This describes the coefficients of the connected Green's function in terms of known functions only, paralleling the result (2.41) for the partition-function coefficients. Similar to the coefficients $\mathcal{Z}_n$, the main difficulty lies in the evaluation of the summation $\sum_l$ over the numbers l_{ij} of propagators connecting space-time points z_i to z_j. Unlike in the case of the partition function, this difficulty increases not only with the number k of internal space-time points which need to be considered, but also with p, the number of external space-time points in the coefficients $G^c_{p,n}(y_1, \dots, y_p)$. The chances of calculating closed-form solutions for these
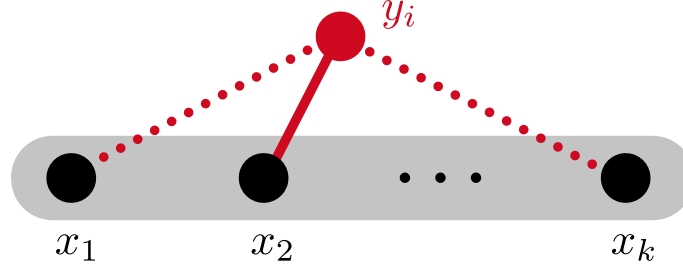
Figure 4.1: Schematic visualization of the connections between external (red) and internal (black) space-time points in the functional integral of the Green's functions.

coefficients in the same way as for the partition function seem bleak, as it would require a maximum of $k + p \leq 2$ space-time points, internal and external. But each external point can only be connected to one different space-time point, as described by the factor in curly brackets, which requires that $L_{k+r} = 1 \, \forall r \in [1, p]$. Moreover, to describe a fully connected graph, pairwise connections among the external points are excluded, such that the only remaining possibilities are to connect every external space-time point to exactly one of the internal space-time points. This still allows for multiple possible ways to form these connections when the number of internal points k is larger than one.

A schematic visualization is given in Figure 4.1: Each external point y_i, with $i \in [1, p]$, has to be connected through a single propagator to one of the internal points x_1 to x_k to form a fully connected graph. The internal space-time points x_1 to x_k are fully connected among each other, indicated through the grey obround shape. Shown is the example of a connection from y_i to x_2 as a solid red line, while the options of connecting y_i to another point are illustrated as dotted red lines. The combinations of these possible options from all p external points result in fully connected graphs and all of these possible graphs have to be taken into account. While specifying the possible connections explicitly can be tedious, it retains the possibility to calculate closed-form solutions for the first-order and second-order coefficients $G^c_{p,1}(y_1, \dots, y_p)$ and $G^c_{p,2}(y_1, \dots, y_p)$ using the same techniques that were utilized in the calculation of the partition-function coefficients; they are evaluated in the following Section 4.2 and Section 4.3.

For coefficients beyond second order, and in particular the contributions to (4.14) with $k \geq 3$ internal points, the summation over the numbers l_{ij} becomes

very intricate. Their calculation relies on the numerical evaluation, similar to the third-order energy-density coefficient $\mathcal{E}_3$ discussed in Section 3.5. The connectedness of the graphs considered in such numerical calculations can be taken into account using, for example, the algebraic connectivity (Fiedler value) [55]. However, these calculations require that the dimension D of space-time is specified.

Observe as well, that the coefficients $G^c_{p,n}(y_1, \ldots, y_p)$ in (4.14) depend on a dimensional parameter only in the form of the overall factor of $\mu_0^{(D/2-1)p}$, which is independent of the order n of the coefficient in the ε expansion. The p-point Green's function $G^c_p(\varepsilon; y_1, \ldots, y_p)$ thus has the dimension $[\text{mass}]^{(D/2-1)p}$. This is in agreement with the expectation that one can obtain by considering $G^c_p(\varepsilon; y_1, \ldots, y_p)$ as the (normalized) expectation value

$$G^c_p(\varepsilon; y_1, \ldots, y_p) = \left. \frac{\langle \Omega | \, T\phi(y_1) \ldots \phi(y_p) \, | \Omega \rangle}{\langle \Omega | \Omega \rangle} \right|_{\text{connected}} \tag{4.15}$$

of p fields, which are each of dimension $[\text{mass}]^{D/2-1}$; here $|\Omega\rangle$ denotes the ground-state of the interacting theory and T denotes the time-ordering symbol [48].

4.2 The First-Order Coefficient and the Single-Vertex Approximation

In the following, the first-order ε-expansion coefficient $G^c_{p,1}(y_1, \ldots, y_p)$ of the connected p-point Green's function is determined from the general coefficient structure in (4.14). This general result is then evaluated specifically for the one-point and two-point Green's functions $G^c_1(\varepsilon; y_1)$ and $G^c_2(\varepsilon; y_1, y_2)$. Both the general and the specific solutions are confirmed to agree with those previously obtained in [1]. In addition, the single-vertex approximation $G^c_p(\varepsilon; y_1, \ldots, y_p)|_{k=1}$ of the p-point Green's function is calculated; that is the $k = 1$ contribution is evaluated for every coefficient $G^c_{p,n}(y_1, \ldots, y_p)$ in (4.14) and these contributions are then summed to all orders n in ε. Again, the general result is evaluated specifically for the one-point and two-point Green's functions.

At first order in ε, that is for $n = 1$, the general coefficient structure in (4.14) consists of only a single contribution with $k = 1$. Similar to the calculation of
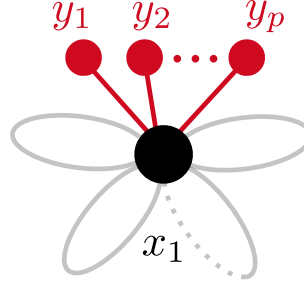
Figure 4.2:   Diagrammatic visualization of the first-order ε-expansion coefficient $G^c_{p,1}(y_1, \dots, y_p)$ of the p-point Green's function. All external points y_1 to y_p are connected to the single internal point x_1 by a single propagator each, indicated as red lines. Adapted from [43].

the partition-function coefficient $\mathcal{Z}_1$ in Section 2.2, the multi-indices defined by (2.18) become $\alpha = (1)$ and $\beta = (1)$, utilizing the conditions (2.11) and (2.12). Thus x_α describes only a single internal space-time point x_1. Contrary to the partition-function calculation, the external space-time points y_1 to y_p have to be taken into account as well. As pointed out in the discussion of the general coefficients (4.14), the external points are connected by only a single propagator to other space-time points. Any connection between two external points separates that pair from the remaining space-time points, especially from x_1, so that the only possible fully connected contribution consists of all external points being connected to x_1; a schematic visualization of this is shown in Figure 4.2. In particular, this specifies the values of all numbers l_{ij} of propagators connecting the various space-time points, namely $l_{1j} = 1\,\forall j \in [2, p+1]$ and all others vanish, that is $l_{ij} = 0\,\forall i \in [2, p]$. Accordingly, $L_1 = p$, signifying that a total of p propagators connect x_1 to the external space-time points. With this, the general coefficient structure (4.14) simplifies to

$$
\begin{aligned}
G^c_{p,1}(y_1, \dots, y_p) = &- \frac{g\Delta_m(0)}{2\sqrt{\pi}} \left[\frac{\mu_0^{D-2}\Delta_m(0)}{2}\right]^{p/2} \int d^D x'_1 \sum_{m_1=0}^{1} (i\pi)^{m_1} \\
&\times \lim_{N_1 \to 0} \left(\frac{d}{dN_1}\right)^{1-m_1} [2\Delta_m(0)]^{N_1} \prod_{r=1}^{p} \left[\frac{2\Delta_m(x'_1 - y'_r)}{\Delta_m(0)}\right] \quad (4.16)\\
&\times \frac{\Gamma(N_1 + 2)\,\Gamma(N_1 + \frac{3}{2})}{\Gamma(N_1 + 2 - \frac{p}{2})} \left(\frac{1 + e^{i\pi(m_1 - p)}}{2}\right).
\end{aligned}
$$

For odd values of p the factor involving the exponential $e^{i\pi(m_1-p)}$ implies that m_1 has to be odd as well, that is $m_1 = 1$. In this case, (4.16) becomes

$$G^c_{p,1}(y_1, \dots, y_p) = -\frac{ig\pi\Delta_m(0)}{4\Gamma(2-\frac{p}{2})} \left[\frac{2\mu_0^{D-2}}{\Delta_m(0)}\right]^{p/2} \int d^D x'_1 \prod_{r=1}^p \Delta_m(x'_1 - y'_r). \quad (4.17)$$

Conversely, for even values of p the factor involving the exponential $e^{i\pi(m_1-p)}$ implies that m_1 has to be even, that is $m_1 = 0$. In this case, (4.16) reduces to

$$\begin{aligned}
G^c_{p,1}(y_1, \dots, y_p) = & -\frac{g\Delta_m(0)}{4\Gamma(2-\frac{p}{2})} \left[\frac{2\mu_0^{D-2}}{\Delta_m(0)}\right]^{p/2} \int d^D x'_1 \prod_{r=1}^p \Delta_m(x'_1 - y'_r) \\
& \times \left(\ln[2\Delta_m(0)] + \psi(\tfrac{3}{2}) + \psi(2) - \psi(2-\tfrac{p}{2})\right).
\end{aligned} \quad (4.18)$$

As special cases of the expressions (4.17) and (4.18) for the first-order ε-expansion coefficients of the p-point Green's function consider $p = 0$, $p = 1$ and $p = 2$: In the case that $p = 0$, no external points are included and the expression (4.18) for the coefficient $G^c_{0,1}$ takes the form:

$$G^c_{0,1} = \mathcal{Z}^c_1 = \mathcal{Z}_1 = -\tfrac{1}{4}gV\Delta_m(0)\left(\ln[2\Delta_m(0)] + \psi(\tfrac{3}{2})\right). \quad (4.19)$$

This denotes the connected part of the partition-function coefficient $\mathcal{Z}^c_1$, but since $\mathcal{Z}_1$ is represented by an inherently connected graph, it is, in fact, equivalent to $\mathcal{Z}_1$ as given in (2.42).

For $p = 1$ one finds the first-order ε-expansion coefficient of the one-point Green's function from (4.17) to be

$$G^c_{1,1}(y_1) = -igm^{-2}\mu_0^{D/2-1}\sqrt{\tfrac{1}{2}\pi\Delta_m(0)}, \quad (4.20)$$

using the normalization (2.29) of the propagator; $\int d^D x' \, \Delta_m(x') = m^{-2}$. This agrees with the result in [1] for the theory without dimensional parameters when choosing $g = m = 1$ and $\mu_0 = 1$. In Figure 4.3 the behavior of (4.20) is shown as a function of the space-time dimension D for $g = m = 1$ and $\mu_0 = 1$ in the range $0 \leq D < 4$. Notice in particular the divergence of the coefficient at $D = 2$, confirming that renormalization techniques are required. For $D = 0$ and $D = 1$ the result for $G^c_{1,1}$ can also be determined through direct integration and Rayleigh-Schrödinger
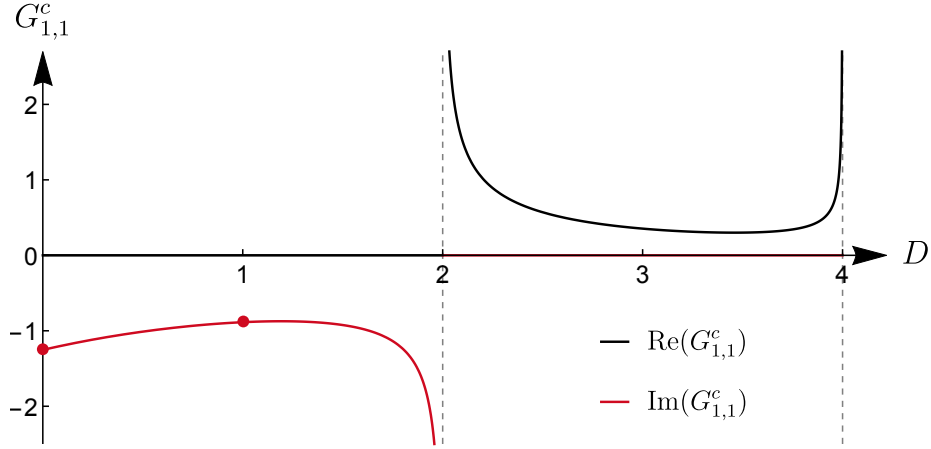
Figure 4.3: Behavior of the first-order ε-expansion coefficient $G^c_{1,1}$ of the one-point Green's function in $0 \leq D < 4$ dimensions. The red dots denote the zero-dimensional and quantum-mechanical theories.

perturbation theory, yielding the values $G^c_{1,1}|_{D=0} = -\sqrt{\pi/2}\, i \approx -1.253314\, i$ and $G^c_{1,1}|_{D=1} = -\frac{1}{2}\sqrt{\pi}\, i \approx -0.886227\, i$, which are visualized in Figure 4.3 as red dots and confirm the result (4.20) in these cases. Moreover, the coefficient changes from imaginary values in the region $0 \leq D < 2$ to real values when $2 < D < 4$ due to the behavior of the selfloop propagator, and diverges again when approaching $D = 4$.

At $p = 2$ the first-order coefficient of the two-point Green's function is

$$G^c_{2,1}(y_1, y_2) = g\, \mu_0^{D-2}\, K_1 \int d^D x_1'\, \Delta_m(x_1' - y_1')\Delta_m(x_1' - y_2') \qquad (4.21)$$

based on (4.18), with the constant dimensionless term

$$K_1 = -\tfrac{1}{2}\Big(\ln[2\Delta_m(0)] + \psi(\tfrac{3}{2}) + 1\Big). \qquad (4.22)$$

Here recall that $y_1' = \mu_0 y_1$ and $y_2' = \mu_0 y_2$ are dimensionless versions of the external space-time variables. Again, the result agrees with that in [1] for the theory without dimensional parameters.

In order to bring the general expressions (4.17) and (4.18) for the first-order Green's function coefficient $G^c_{p,1}(y_1, \ldots, y_p)$ into the form of the general result presented in [1], the function $\Gamma(2 - p/2)$ in the denominator of (4.17) and (4.18) has to be rewritten. For odd values of p, that is for the expression (4.17), this

can be done using Euler's reflection formula [50], so that:

$$\frac{i\pi}{\Gamma(2-\frac{p}{2})} = i\,\Gamma(\tfrac{p}{2}-1)\sin[\pi(\tfrac{p}{2}-1)] = (-i)^p\,\Gamma(\tfrac{p}{2}-1). \tag{4.23}$$

With this (4.17) becomes

$$G^c_{p,1}(y_1,\ldots,y_p) = -\tfrac{1}{2}(-i)^p g\,\mu_0^{(D/2-1)p}\,\Gamma(\tfrac{p}{2}-1)\big[\tfrac{1}{2}\Delta_m(0)\big]^{1-p/2}$$
$$\times \int d^D x_1' \prod_{r=1}^{p} \Delta_m(x_1'-y_r'). \tag{4.24}$$

This is the result of [1], here including dimensional parameters. In [1] it was also found that this result for odd values of p remains valid for even values of $p \geq 4$ as well. This can be seen from the expression (4.18) as follows: For even values of $p \geq 4$ the function $\Gamma(2-p/2)$ in the denominator becomes singular and the only term in which this singularity is canceled is $\psi(2) - \psi(2-\frac{p}{2})$. One can rewrite

$$\begin{aligned}
\frac{\psi(2)-\psi(2-\frac{p}{2})}{\Gamma(2-\frac{p}{2})} &= \lim_{N\to 0}\Big(\frac{d}{dN}\Big)\frac{\Gamma(N+2)}{\Gamma(N+2-\frac{p}{2})} \\
&= \lim_{N\to 0}\Big(\frac{d}{dN}\Big)\big[(N+1)\,N\,(N-1)\ldots(N+2-\tfrac{p}{2})\big] \\
&= \lim_{N\to 0}\Big(\frac{d}{dN}\Big)\big[(1)\,N\,(-1)\ldots(2-\tfrac{p}{2})\big] \\
&= (-1)^{p/2-2}\,(\tfrac{p}{2}-2)! = (-i)^p\,\Gamma(\tfrac{p}{2}-1),
\end{aligned} \tag{4.25}$$

when $p \geq 4$. With this (4.18) takes the form of (4.24) as well, reflecting the behavior described in [1]. Notice, however, that (4.24) is neither valid for $p = 2$, nor for $p = 0$, while (4.17) and (4.18) do describe the behavior of the first-order ε-expansion coefficients of the general p-point Green's function in these cases.

Beyond the evaluation of the general Green's function coefficients (4.14) at first order ($n = 1$), the calculation of the $k = 1$ contribution to these coefficients can be performed at any order n in a very similar way. This approach was previously introduced in Section 2.2 for the partition-function coefficients $\mathcal{Z}_n$. Here the only conceptual difference is that the connections of the external space-time points have to be specified before continuing with the evaluation, as established for $n = 1$ above. After that, the remaining calculation parallels the discussion of the single-vertex approximation of the partition-function coefficient in Section 2.2.

For $k = 1$ and an unspecified value n, the conditions (2.11) and (2.12) specify that in the summation $\sum_c$ only $c_n = 1$, while $c_1 = \cdots = c_{n-1} = 0$. This implies that $\alpha = (1)$ and $\beta = (n)$. These terms generally describe, in a diagrammatic sense, those contributions that contain only a single internal point x_1. In the same way as for $n = 1$, the only possible fully connected contribution therefore consists of all external points being connected to x_1, which is schematically shown in Figure 4.2. Again, this determines the values of all numbers l_{ij} of propagators connecting the various space-time points, namely $l_{1j} = 1 \,\forall j \in [2, p+1]$ and $l_{ij} = 0 \,\forall i \in [2, p]$, so that in particular $L_1 = p$, signifying that p propagators connect x_1 to the external space-time points. The general coefficient structure (4.14) then becomes

$$
G_{p,n}^c(y_1, \ldots, y_p)\big|_{k=1} = -\frac{g\Delta_m(0)}{2^n \, n! \, \sqrt{\pi}} \left[\frac{\mu_0^{D-2}\Delta_m(0)}{2} \right]^{p/2} \int d^D x_1' \sum_{m_1=0}^{n} \binom{n}{m_1} (i\pi)^{m_1}
$$

$$
\times \lim_{N_1 \to 0} \left(\frac{d}{dN_1} \right)^{n-m_1} [2\Delta_m(0)]^{N_1} \prod_{r=1}^{p} \left[\frac{2\Delta_m(x_1' - y_r')}{\Delta_m(0)} \right]
$$

$$
\times \frac{\Gamma(N_1 + 2)\,\Gamma(N_1 + \tfrac{3}{2})}{\Gamma(N_1 + 2 - \tfrac{p}{2})} \left(\frac{1 + e^{i\pi(m_1 - p)}}{2} \right).
$$

$$(4.26)$$

The factor involving the exponential $e^{i\pi(m_1 - p)}$ implies that for odd values of p the summation over m_1 contains only the odd values of m_1, while for even values of p it contains only the even values of m_1. But these summations can be evaluated as special cases of the Leibniz rule [50] in the same way as discussed in the calculation of the partition-function coefficients, see (2.65) and (2.66), resulting in the expression

$$
G_{p,n}^c(y_1, \ldots, y_p)\big|_{k=1} = -\frac{g\Delta_m(0)}{2^n \, n! \, \sqrt{\pi}} \left[\frac{2\mu_0^{D-2}}{\Delta_m(0)} \right]^{p/2} \int d^D x_1' \prod_{r=1}^{p} \Delta_m(x_1' - y_r')
$$

$$
\times \lim_{N_1 \to 0} \left(\frac{d}{dN_1} \right)^{n} [2\Delta_m(0)]^{N_1} \frac{\Gamma(N_1 + 2)\,\Gamma(N_1 + \tfrac{3}{2})}{\Gamma(N_1 + 2 - \tfrac{p}{2})} \quad (4.27)
$$

$$
\times \begin{cases} \cos(\pi N_1), & \text{for } p \text{ even,} \\ i \, \sin(\pi N_1), & \text{for } p \text{ odd.} \end{cases}
$$

Similar to the partition-function coefficients $\mathcal{Z}_n|_{k=1}$ in (2.44), the evaluation for any specified value of n is straightforward.

Moreover, the expression (4.27) can be summed over all values $n \geq 1$, that is to all orders in ε, as

$$
\begin{aligned}
G_p^c(\varepsilon; y_1, \dots, y_p)\big|_{k=1} &= \sum_{n=1}^{\infty} \varepsilon^n\, G_{p,n}^c(y_1, \dots, y_p)\big|_{k=1} \\
&= -\frac{g\,\Delta_m(0)}{\sqrt{\pi}} \left[\frac{2\mu_0^{D-2}}{\Delta_m(0)}\right]^{p/2} \sum_{n=1}^{\infty} \frac{(\varepsilon/2)^n}{n!} \lim_{N_1 \to 0} \left(\frac{d}{dN_1}\right)^n f(N_1) \\
&\quad \times \int d^D x_1' \prod_{r=1}^{p} \Delta_m(x_1' - y_r'),
\end{aligned}
$$

(4.28)

where

$$
f(N_1) = [2\Delta_m(0)]^{N_1} \frac{\Gamma(N_1 + 2)\,\Gamma(N_1 + \tfrac{3}{2})}{\Gamma(N_1 + 2 - \tfrac{p}{2})} \begin{cases} \cos(\pi N_1), & \text{for } p \text{ even,} \\ i\,\sin(\pi N_1), & \text{for } p \text{ odd.} \end{cases}
$$

(4.29)

Completing the summation in (4.28) with a $n = 0$ term, $f(0)$, it is recognized as the Taylor series of $f(\varepsilon/2)$ around 0, and can thus be evaluated to the form

$$
\begin{aligned}
G_p^c(\varepsilon; y_1, \dots, y_p)\big|_{k=1} &= -\frac{i\,g}{2\sqrt{\pi}} \left[\frac{2\mu_0^{D-2}}{\Delta_m(0)}\right]^{p/2} [2\Delta_m(0)]^{1+\varepsilon/2}\, \sin(\tfrac{\pi\varepsilon}{2}) \\
&\quad \times \frac{\Gamma(\tfrac{\varepsilon}{2} + 2)\,\Gamma(\tfrac{\varepsilon}{2} + \tfrac{3}{2})}{\Gamma(\tfrac{\varepsilon}{2} + 2 - \tfrac{p}{2})} \int d^D x_1' \prod_{r=1}^{p} \Delta_m(x_1' - y_r')
\end{aligned}
$$

(4.30)

for odd values of p, and

$$
\begin{aligned}
G_p^c(\varepsilon; y_1, \dots, y_p)\big|_{k=1} &= -\frac{g}{2\sqrt{\pi}} \left[\frac{2\mu_0^{D-2}}{\Delta_m(0)}\right]^{p/2} \int d^D x_1' \prod_{r=1}^{p} \Delta_m(x_1' - y_r') \\
&\quad \times \left([2\Delta_m(0)]^{1+\varepsilon/2} \cos(\tfrac{\pi\varepsilon}{2}) \frac{\Gamma(\tfrac{\varepsilon}{2} + 2)\,\Gamma(\tfrac{\varepsilon}{2} + \tfrac{3}{2})}{\Gamma(\tfrac{\varepsilon}{2} + 2 - \tfrac{p}{2})} - \frac{\sqrt{\pi}\Delta_m(0)}{\Gamma(2 - \tfrac{p}{2})}\right)
\end{aligned}
$$

(4.31)

for even values of p. These describe the single-vertex approximation of the connected p-point Green's function.
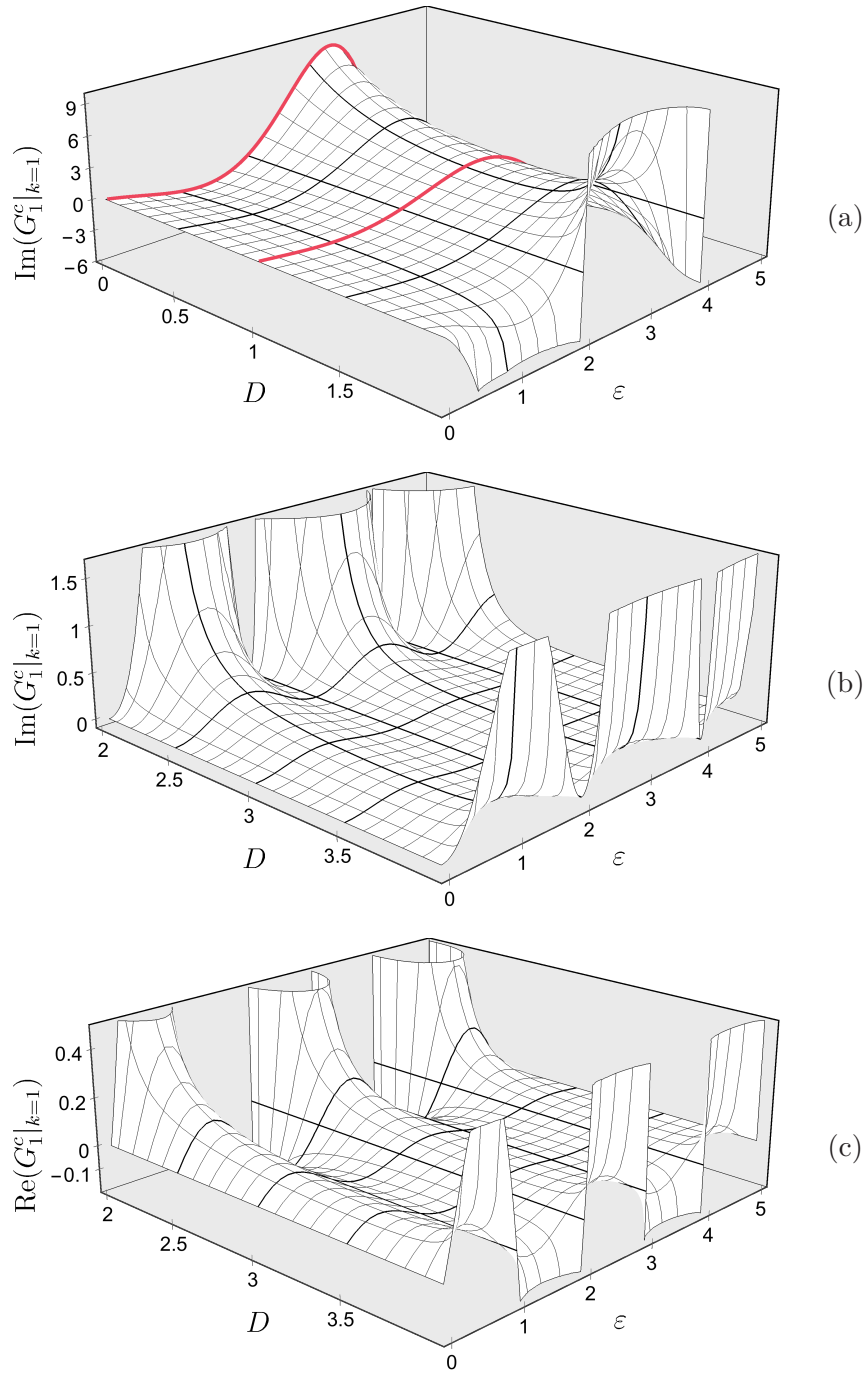
Figure 4.4: Behavior of the single-vertex approximation of the one-point Green's function as a function of the dimension D and the nonlinearity parameter ε. For $0 \leq D < 2$ the coefficient $G_1^c(\varepsilon; y_1)|_{k=1}$ is imaginary, shown in Figure 4.4a; the red lines denote the zero-dimensional and quantum-mechanical theories. For $2 < D < 4$ the coefficient becomes complex; the imaginary and real parts are displayed in Figure 4.4b and Figure 4.4c respectively.

For $p = 0$ the expression (4.31) reduces to the single-vertex approximation $\mathcal{Z}(\varepsilon)|_{k=1}$ of the normalized partition function obtained previously in (2.46). The approximation of the one-point Green's function is obtained from (4.30) to be:

$$G_1^c(\varepsilon; y_1)\big|_{k=1} = -igm^{-2}\mu_0^{D/2-1} \sqrt{\frac{2\Delta_m(0)}{\pi}} \left[2\Delta_m(0)\right]^{\varepsilon/2} \sin(\tfrac{\pi\varepsilon}{2}) \Gamma[\tfrac{\varepsilon}{2} + 2], \quad (4.32)$$

using the normalization (2.29) of the propagator. The behavior of $G_1^c(\varepsilon; y_1)|_{k=1}$ is visualized in Figure 4.4 as a function of the space-time dimension D and the non-linearity parameter ε. Similar to the first-order ε-expansion coefficient $G_{1,1}^c(y_1)$ in (4.20), the single-vertex approximation is an imaginary function for $0 \leq D < 2$, that diverges in the limit of two dimensions, see Figure 4.4a. The red lines indicate the behavior at $D = 0$ and $D = 1$. For $2 < D < 4$ dimensions, $G_1^c(\varepsilon; y_1)|_{k=1}$ is generally a complex function due to the negative selfloop propagator (2.30). Its imaginary and real parts are visualized in Figure 4.4b and Figure 4.4c respectively. In the limit of four-dimensional space-time, $G_1^c(\varepsilon; y_1)|_{k=1}$ diverges again.

Observe that, while $G_1^c(\varepsilon; y_1)|_{k=1}$ is generally a complex function in $2 < D < 4$ dimensions, its real part vanishes for odd values of ε, resulting in an imaginary solution resembling the behavior in $0 \leq D < 2$ dimensions. These cases correspond to an odd imaginary self-interaction term in the Lagrangian density $\mathcal{L}(\varepsilon)$, see (2.1), so that this imaginary nature of the one-point Green's function coefficients is expected. Due to the perturbative expansion in ε, this feature is not apparent in the nonlinearity expansion, but it reemerges here in the vertex approximation where terms to all orders in ε are taken into account.

Furthermore, because of the sine function in (4.32), the single-vertex approximation vanishes for even values of ε in all dimensions. For an even nonlinearity parameter the self-interaction term in the Lagrangian density is even as well, so that the expectation value of the field ϕ - and thus the one-point Green's function - is expected to vanish. Again, this feature is not apparent in the nonlinearity expansion but reemerges in the single-vertex approximation.

For the two-point Green's function, (4.31) reduces to

$$G_2^c(\varepsilon; y_1, y_2)\big|_{k=1} = g\,\mu_0^{D-2}\,\kappa_1(\varepsilon) \int d^D x'\, \Delta_m(x' - y_1')\Delta_m(x' - y_2'), \quad (4.33)$$

with

$$\kappa_1(\varepsilon) = 1 - \frac{\varepsilon + 2}{\sqrt{\pi}} \left[2\Delta_m(0)\right]^{\varepsilon/2} \cos(\tfrac{\pi\varepsilon}{2}) \, \Gamma[\tfrac{\varepsilon+3}{2}]. \tag{4.34}$$

Note that $\kappa_1(0)$, and thus $G_2^c(0; y_1, y_2)|_{k=1}$, vanishes as expected from the coupling-constant expansion interpretation of the vertex approximation established in (2.47). In addition, (4.34) is a real-valued function in all space-time dimensions for integer values of ε: For even values the (possibly negative) selfloop propagator is raised to an integer power while for odd values the possibly imaginary contribution vanishes due to the cosine function.

4.3 The Second-Order Coefficient and the Two-Vertex Approximation

To evaluate the general ε-expansion coefficient (4.14) of the p-point Green's function at second order in the nonlinearity parameter, that is for $n = 2$, two contributions need to be considered: A single-vertex term when $k = 1$, and a two-vertex term, when $k = 2$. The single-vertex term is determined by the expression (4.27) obtained in Section 4.2, and takes the form

$$\begin{aligned}
G_{p,2}^c(y_1, \dots, y_p)\big|_{k=1} = -\frac{g\,\Delta_m(0)}{16\,\Gamma(2 - \frac{p}{2})} \left[\frac{2\mu_0^{D-2}}{\Delta_m(0)}\right]^{p/2} \int d^D x_1' \prod_{r=1}^{p} \Delta_m(x_1' - y_r') \\
\times \left\{ \left(\ln[2\Delta_m(0)] + \psi(\tfrac{3}{2}) + \psi(2) - \psi(2 - \tfrac{p}{2}) \right)^2 \right. \\
\left. + \psi^{(1)}(\tfrac{3}{2}) + \psi^{(1)}(2) - \psi^{(1)}(2 - \tfrac{p}{2}) - \pi^2 \right\}
\end{aligned} \tag{4.35}$$

for even values of p, and

$$\begin{aligned}
G_{p,2}^c(y_1, \dots, y_p)\Big|_{k=1} = -\frac{i\,g\,\pi\,\Delta_m(0)}{8\,\Gamma(2 - \frac{p}{2})} \left[\frac{2\mu_0^{D-2}}{\Delta_m(0)}\right]^{p/2} \int d^D x_1' \prod_{r=1}^{p} \Delta_m(x_1' - y_r') \\
\times \left(\ln[2\Delta_m(0)] + \psi(\tfrac{3}{2}) + \psi(2) - \psi(2 - \tfrac{p}{2}) \right)
\end{aligned} \tag{4.36}$$

for odd values of p.

The calculation of the two-vertex term, on the other hand, is somewhat more involved: Similar to the single-vertex contribution, the external points are con-
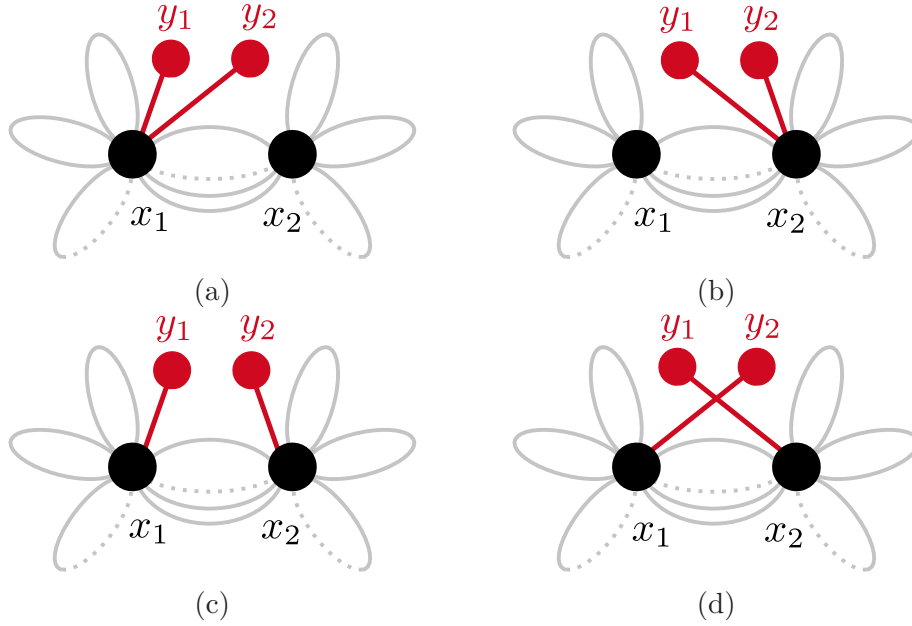
Figure 4.5: Diagrammatic visualization of connected graphs in the two-vertex contribution $G^c_{p,2}(y_1, \dots, y_p)|_{k=2}$ for the case $p = 2$. Adapted from [43].

nected by only a single propagator to other space-time points and any connection between two external points separates that connected pair from the remaining space-time points. The only possible fully connected contributions therefore consist of all external points being connected to either x_1 or x_2 and those internal points being connected to one another. Contrary to the single-vertex case, there is more than one way of connecting the external points $y_1, \dots, y_p$ to the internal points x_1 and x_2. A schematic visualization for two external points is shown in Figure 4.5. Furthermore, the summation over the number l_{12} of propagators connecting the two internal points x_1 and x_2 has to be evaluated. An example of this summation was calculated in Chapter 2 for the two-vertex contribution of the partition-function coefficients $\mathcal{Z}_n$ and the techniques employed therein can be generalized for the summation here.

Due to the length and complexity of the calculation, the result for the general two-vertex contribution $G^c_{p,n}(y_1, \dots, y_p)|_{k=2}$ of the nth-order Green's function coefficient is directly given in the following. A detailed calculation can be found in Appendix F. The general result is then evaluated for $n = 2$ and combined with the single-vertex contribution (4.35) or (4.36) to determine the second-order

ε-expansion coefficient $G^c_{p,2}(y_1, \dots, y_p)$ of the p-point Green's function. Then, the result for the general two-vertex contribution is summed to all order in ε, that is over n, to find the two-vertex approximation $G^c_p(\varepsilon; y_1, \dots, y_p)|_{k=2}$ of the full Green's function.

The general two-vertex contribution $G^c_{p,n}(y_1, \dots, y_p)|_{k=2}$ of the nth-order Green's function coefficient has the form

$$
G^c_{p,n}(y_1, \dots, y_p)\big|_{k=2} =
$$
$$
\frac{g^2 \Delta_m^2(0)}{2^{n+1} n! \, \pi} \left[\frac{2\mu_0^{D-2}}{\Delta_m(0)} \right]^{p/2} \int d^D x_1' d^D x_2' \, \lim_{N \to 0} \left(\frac{d}{dN} \right)^n
$$
$$
\times \left\{ \sum_{\substack{q=0 \\ \text{even}}}^{p} \{\Sigma\Pi\Delta(p,q)\} \left[\cos^2(\pi N)\, L_{\text{even}}(N,N) - \sin^2(\pi N)\, L_{\text{odd}}(N,N) \right.\right.
$$
$$
\left. - \cos(\pi N)\, L_{\text{even}}(N,0) - \cos(\pi N)\, L_{\text{even}}(0,N) \right]
$$
$$
+ \sum_{\substack{q=0 \\ \text{odd}}}^{p} \{\Sigma\Pi\Delta(p,q)\} \left[\cos^2(\pi N)\, L_{\text{odd}}(N,N) - \sin^2(\pi N)\, L_{\text{even}}(N,N) \right.
$$
$$
\left.\left. - \cos(\pi N)\, L_{\text{odd}}(N,0) - \cos(\pi N)\, L_{\text{odd}}(0,N) \right] \right\}
$$

$$(4.37)$$

for even values of p, and

$$
G^c_{p,n}(y_1, \dots, y_p)\big|_{k=2} =
$$
$$
\frac{g^2 \Delta_m^2(0)}{2^{n+1} n! \, \pi} \left[\frac{2\mu_0^{D-2}}{\Delta_m(0)} \right]^{p/2} \int d^D x_1' d^D x_2' \, \lim_{N \to 0} \left(\frac{d}{dN} \right)^n \sum_{\substack{q=0 \\ \text{odd}}}^{p} \{\Sigma\Pi\Delta(p,q)\}
$$
$$
\times \left[2i \, \sin(\pi N) \, \cos(\pi N)\, L_{\text{even}}(N,N) + 2i \, \sin(\pi N) \, \cos(\pi N)\, L_{\text{odd}}(N,N) \right.
$$
$$
\left. - 2i \, \sin(\pi N)\, L_{\text{even}}(N,0) - 2i \, \sin(\pi N)\, L_{\text{odd}}(0,N) \right]
$$

$$(4.38)$$

for odd values of p. Here the factor $\{\Sigma\Pi\Delta(p,q)\}$ denotes the possible ways in which q of the external points y_1 to y_p can be connected to the internal point x_1, while $p - q$ points are connected to x_2,

$$
\{\Sigma\Pi\Delta(p,q)\} = \frac{1}{q! \, (p-q)!} \sum_{\sigma} \left[\prod_{i=1}^{q} \Delta_m(x_1' - y_{\sigma(i)}') \right] \left[\prod_{j=q+1}^{p} \Delta_m(x_2' - y_{\sigma(j)}') \right],
$$

$$(4.39)$$

given in terms of the summation $\sum_\sigma$ over all permutations of the external points y_1 to y_p. The dependence of (4.39) on the space-time variables is suppressed in the arguments of $\{\Sigma\Pi\Delta(p,q)\}$ for brevity. The functions $L_{\text{even}}(N_1, N_2)$ and $L_{\text{odd}}(N_1, N_2)$ are given as:

$$
L_{\text{even}}(N_1, N_2) =
$$

$$
[2\Delta_m(0)]^{N_1+N_2} \frac{\Gamma(N_1+2)\,\Gamma(N_1+\frac{3}{2})}{\Gamma(N_1+2-\frac{q}{2})} \frac{\Gamma(N_2+2)\,\Gamma(N_2+\frac{3}{2})}{\Gamma(N_2+2-\frac{p-q}{2})}
$$

$$
\times \left\{ -1 + {}_2F_1\left[-(N_1+1-\tfrac{q}{2}), -(N_2+1-\tfrac{p-q}{2}); \tfrac{1}{2}; \left(\tfrac{\Delta_m(x_1'-x_2')}{\Delta_m(0)} \right)^2 \right] \right\}
\tag{4.40}
$$

and

$$
L_{\text{odd}}(N_1, N_2) =
$$

$$
\frac{2\Delta_m(x_1'-x_2')}{\Delta_m(0)} \, [2\Delta_m(0)]^{N_1+N_2} \frac{\Gamma(N_1+2)\,\Gamma(N_1+\frac{3}{2})}{\Gamma(N_1+\frac{3}{2}-\frac{q}{2})} \frac{\Gamma(N_2+2)\,\Gamma(N_2+\frac{3}{2})}{\Gamma(N_2+\frac{3}{2}-\frac{p-q}{2})}
$$

$$
\times {}_2F_1\left[-(N_1+\tfrac{1}{2}-\tfrac{q}{2}), -(N_2+\tfrac{1}{2}-\tfrac{p-q}{2}); \tfrac{3}{2}; \left(\tfrac{\Delta_m(x_1'-x_2')}{\Delta_m(0)} \right)^2 \right];
$$

$$
\tag{4.41}
$$

the dependence on the space-time variables, as well as the values p and q, is suppressed in the arguments of $L_{\text{even}}(N_1, N_2)$ and $L_{\text{odd}}(N_1, N_2)$ for brevity.

In the case of the second-order ε-expansion coefficient, that is for $n = 2$, the expressions (4.37) and (4.38) reduce to the form

$$
G_{p,2}^c(y_1, \ldots, y_p)\big|_{k=2} =
$$

$$
\frac{g^2\Delta_m^2(0)}{8\pi} \left[\frac{2\mu_0^{D-2}}{\Delta_m(0)} \right]^{p/2} \int d^D x_1' d^D x_2'
$$

$$
\times \left\{ \sum_{\substack{q=0 \\ \text{even}}}^{p} \{\Sigma\Pi\Delta(p,q)\} \left[\lim_{N_1,N_2\to 0} \frac{d}{dN_1} \frac{d}{dN_2} L_{\text{even}}(N_1, N_2) - \pi^2 L_{\text{odd}}(0,0) \right] \right.
\tag{4.42}
$$

$$
\left. + \sum_{\substack{q=0 \\ \text{odd}}}^{p} \{\Sigma\Pi\Delta(p,q)\} \left[\lim_{N_1,N_2\to 0} \frac{d}{dN_1} \frac{d}{dN_2} L_{\text{odd}}(N_1, N_2) - \pi^2 L_{\text{even}}(0,0) \right] \right\}
$$

for even values of p, and

$$G_{p,2}^c(y_1, \ldots, y_p)\big|_{k=2} = \tfrac{1}{4}i\, g^2 \Delta_m^2(0) \left[\frac{2\mu_0^{D-2}}{\Delta_m(0)}\right]^{p/2} \int d^D x_1' d^D x_2' \sum_{\substack{q=0 \\ \text{odd}}}^{p} \{\Sigma\Pi\Delta(p, q)\}$$

$$\times \lim_{N\to 0}\left[\frac{d}{dN} L_{\text{even}}(0, N) + \frac{d}{dN} L_{\text{odd}}(N, 0)\right]$$

(4.43)

for odd values of p. Together with the results (4.35) and (4.36) for the single-vertex contribution, this determines the general second-order ε-expansion coefficient $G_{p,2}^c(y_1, \ldots, y_p)$ of the p-point Green's function as

$$G_{p,2}^c(y_1, \ldots, y_p) = G_{p,2}^c(y_1, \ldots, y_p)\big|_{k=1} + G_{p,2}^c(y_1, \ldots, y_p)\big|_{k=2}.$$

(4.44)

Special cases include the following: For $p = 0$ the expression (4.44) reduces to the connected part of the second-order coefficient of the normalized partition function previously obtained in (2.62). Contrary to the first-order coefficient $\mathcal{Z}_1^c = \mathcal{Z}_1$, the connected part $\mathcal{Z}_2^c$ is not identical to the full coefficient $\mathcal{Z}_2$. However, as established in Chapter 3, it is identical to $-V\mathcal{E}_2$ and the result (3.7) presented there indeed agrees with that obtained from (4.44) at $p = 0$.

For $p = 1$, one finds the second-order ε-expansion coefficient of the one-point Green's function to be

$$G_{1,2}^c(y_1) = -\tfrac{1}{2}igm^{-2}\mu_0^{D/2-1}\sqrt{\tfrac{1}{2}\Delta_m(0)\pi}\left(\ln[2\Delta_m(0)] + \psi(2)\right)$$

$$+ \tfrac{1}{4}ig^2 m^{-4}\mu_0^{D/2-1}\sqrt{\tfrac{1}{2}\Delta_m(0)\pi}\left\{\left(\ln[2\Delta_m(0)] + \psi(\tfrac{3}{2})\right)(3 - \tfrac{D}{2})\right.$$

$$\left. + (D - 2) + 2\Delta_m(0)\, m^2\int d^D x'\left(1 + \tfrac{\Delta_m(x')}{\Delta_m(0)}\right)^2\ln[1 + \tfrac{\Delta_m(x')}{\Delta_m(0)}]\right\},$$

(4.45)

using the normalization (2.29) of the propagator, the integral (2.61) over its square, and the derivatives of the hypergeometric functions

$$\lim_{N\to 0}\left(\frac{d}{dN}\right){}_2F_1[-\tfrac{1}{2}, -(N+1); \tfrac{1}{2}; z^2] =$$

$$(1 + z)^2\ln(1 + z) + (1 - z)^2\ln(1 - z) - 2z^2$$

(4.46)
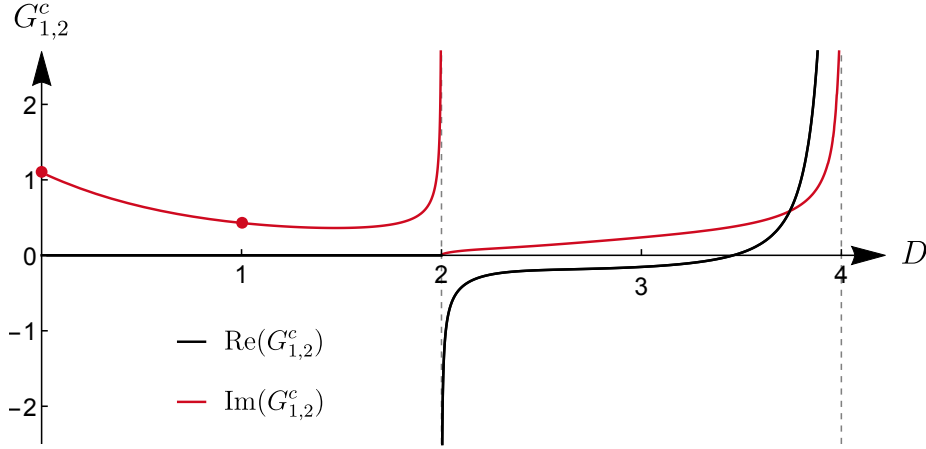
Figure 4.6: Behavior of the second-order ε-expansion coefficient $G^c_{1,2}$ of the one-point Green's function in $0 \le D < 4$ dimensions. The red dots denote the zero-dimensional and quantum-mechanical theories (4.48) and (4.49).

and

$$\lim_{N \to 0} \left(\frac{d}{dN} \right) {}_2F_1[-N, -\tfrac{1}{2}; \tfrac{3}{2}; z^2] =$$
$$(2z)^{-1} \left[(1+z)^2 \ln(1+z) - (1-z)^2 \ln(1-z) - 2z \right].$$
(4.47)

In Figure 4.6 the behavior of $G^c_{1,2}(y_1)$ is visualized as a function of the space-time dimension in the region $0 \le D < 4$ for $g = m = 1$ and $\mu_0 = 1$. Notice in particular the divergence of the coefficient at $D = 2$ and $D = 4$. For $D = 0$ and $D = 1$ the result for $G^c_{1,2}(y_1)$ can also be determined through direct integration or Rayleigh-Schrödinger perturbation theory, yielding the values

$$G^c_{1,2}|_{D=0} = i\sqrt{\pi/8} \left[-2 + \gamma + \tfrac{9}{2} \ln 2 + \tfrac{3}{2}\psi(\tfrac{3}{2}) \right] \approx 1.097347\,i,$$
(4.48)

$$G^c_{1,2}|_{D=1} = i\sqrt{\pi} \left[\tfrac{1}{48}\pi^2 - \tfrac{13}{16} + \tfrac{1}{4}\gamma + \ln 2 + \tfrac{5}{16}\psi(\tfrac{3}{2}) \right] \approx 0.428882\,i,$$
(4.49)

which are visualized in Figure 4.6 as red dots and confirm the result (4.45) in these cases. Moreover, the coefficient changes from imaginary values in the region $0 \le D < 2$ to complex values when $2 < D < 4$, similar to the first-order coefficient $G^c_{1,1}(y_1)$ in (4.20).

For $p = 2$, one finds the second-order coefficient of the two-point Green's function to be

$$G_{2,2}^c(y_1, y_2) = \mu_0^{D-2}\left(gK_2 + g^2K_3\right)\int d^D x'\, \Delta_m(x' - y_1')\Delta_m(x' - y_2')$$
$$+ g^2\mu_0^{D-2}\int d^D x_1'\, d^D x_2'\,\Delta(x_1' - y_1')\Delta(x_2' - y_2')\,f(x_1' - x_2'), \tag{4.50}$$

in terms of the dimensionless constants

$$K_2 = -\tfrac{1}{8}\left\{\left(\ln[2\Delta_m(0)] + \psi(\tfrac{3}{2}) + 1\right)^2 + \psi^{(1)}(\tfrac{3}{2}) - \pi^2 - 1\right\} \tag{4.51}$$

and

$$K_3 = \tfrac{1}{4}\Delta_m(0)\int d^D x'\left\{\frac{\Delta_m(x')}{\Delta_m(0)}\sqrt{1 - \left[\frac{\Delta_m(x')}{\Delta_m(0)}\right]^2}\left(2\sin^{-1}\left[\frac{\Delta(x')}{\Delta(0)}\right] - \pi\right)\right.$$
$$+ \sin^{-1}\left[\frac{\Delta_m(x')}{\Delta_m(0)}\right]\left(\sin^{-1}\left[\frac{\Delta_m(x')}{\Delta_m(0)}\right] - \pi\right) \tag{4.52}$$
$$\left. + \left[\frac{\Delta_m(x')}{\Delta_m(0)}\right]^2\left(\log[2\Delta_m(0)] + \psi(\tfrac{3}{2}) - 2\right)\right\},$$

and the function

$$f(x) =$$
$$\tfrac{1}{2}\Delta_m(x)\left\{\sin^{-1}\left[\frac{\Delta_m(x)}{\Delta_m(0)}\right]\left(\sin^{-1}\left[\frac{\Delta_m(x)}{\Delta_m(0)}\right] - \pi\right) + \tfrac{1}{2}\left(\ln[2\Delta_m(0)] + \psi(\tfrac{3}{2}) + 1\right)^2 - 2\right\}$$
$$+ \Delta_m(0)\left\{\sin^{-1}\left[\frac{\Delta_m(x)}{\Delta_m(0)}\right]\sqrt{1 - \left[\frac{\Delta_m(x)}{\Delta_m(0)}\right]^2} + +\tfrac{1}{2}\pi\left(1 - \sqrt{1 - \left[\frac{\Delta_m(x)}{\Delta_m(0)}\right]^2}\right)\right\}. \tag{4.53}$$

In addition to the evaluation of the second-order ε-expansion coefficient, the general two-vertex contributions in (4.37) and (4.38) can be summed to all orders $n \geq 2$ in ε. Much like for the summation of the two-vertex contribution of the partition-function coefficients in Section 2.3, the sum

$$G_p^c(\varepsilon; y_1, \dots, y_p)\big|_{k=2} = \sum_{n=2}^{\infty} G_{p,n}^c(y_1, \dots, y_p)\big|_{k=2}\,\varepsilon^n$$
$$= \frac{g^2\,\Delta_m^2(0)}{2\pi}\left[\frac{2\mu_0^{D-2}}{\Delta_m(0)}\right]^{p/2}\sum_{n=2}^{\infty}\frac{(\varepsilon/2)^n}{n!}\lim_{N\to 0}\left(\frac{d}{dN}\right)^n w(N), \tag{4.54}$$

with

$$
\begin{aligned}
w(N) = \int d^D x_1' d^D x_2' \Big\{ &\sum_{\substack{q=0 \\ \text{even}}}^{p} \{\Sigma\Pi\Delta(p,q)\} \Big[\cos^2(\pi N)\, L_{\text{even}}(N,N) \\
&- \sin^2(\pi N)\, L_{\text{odd}}(N,N) - \cos(\pi N)\, L_{\text{even}}(N,0) - \cos(\pi N)\, L_{\text{even}}(0,N) \Big] \\
&+ \sum_{\substack{q=0 \\ \text{odd}}}^{p} \{\Sigma\Pi\Delta(p,q)\} \Big[\cos^2(\pi N)\, L_{\text{odd}}(N,N) - \sin^2(\pi N)\, L_{\text{even}}(N,N) \\
&- \cos(\pi N)\, L_{\text{odd}}(N,0) - \cos(\pi N)\, L_{\text{odd}}(0,N) \Big] \Big\}
\end{aligned}
$$

(4.55)

for even values of p, and

$$
\begin{aligned}
w(N) = \int d^D x_1' d^D x_2' \sum_{\substack{q=0 \\ \text{odd}}}^{p} \{\Sigma\Pi\Delta(p,q)\} \Big[&2i\,\sin(\pi N)\,\cos(\pi N)\, L_{\text{even}}(N,N) \\
&+ 2i\,\sin(\pi N)\,\cos(\pi N)\, L_{\text{odd}}(N,N) - 2i\,\sin(\pi N)\, L_{\text{even}}(N,0) \\
&- 2i\,\sin(\pi N)\, L_{\text{odd}}(0,N) \Big]
\end{aligned}
$$

(4.56)

for odd values of p, can be recognized as the Taylor series of $w(\varepsilon/2)$ around 0 without the $n=0$ and $n=1$ terms. The functions $\{\Sigma\Pi\Delta(p,q)\}$, $L_{\text{even}}(N_1, N_2)$, and $L_{\text{odd}}(N_1, N_2)$ in $w(N)$ are given in (4.39), (4.40), and (4.41) respectively; their dependence on the space-time variables is suppressed for brevity. Completing the summation then results in the two-vertex approximation of the p-point Green's function:

$$
\begin{aligned}
&G_p^c(\varepsilon; y_1, \dots, y_p)\big|_{k=2} = \\
&\frac{g^2\, \Delta_m^2(0)}{2\pi} \left[\frac{2\mu_0^{D-2}}{\Delta_m(0)} \right]^{p/2} \Big\{ w(\varepsilon/2) - w(0) - \tfrac{1}{2}\varepsilon \lim_{N\to 0} \Big(\frac{d}{dN} \Big) w(N) \Big\}.
\end{aligned}
$$

(4.57)

The first derivative of $w(N)$ is found overall to vanish in the limit $N \to 0$.

In the special case that $p = 0$, the expression (4.57) reduces to the connected part of $\mathcal{Z}(\varepsilon)\big|_{k=2}$ in (2.79), which corresponds to the two-vertex approximation of the energy density $-V\mathcal{E}(\varepsilon)\big|_{k=2}$ in (3.10).
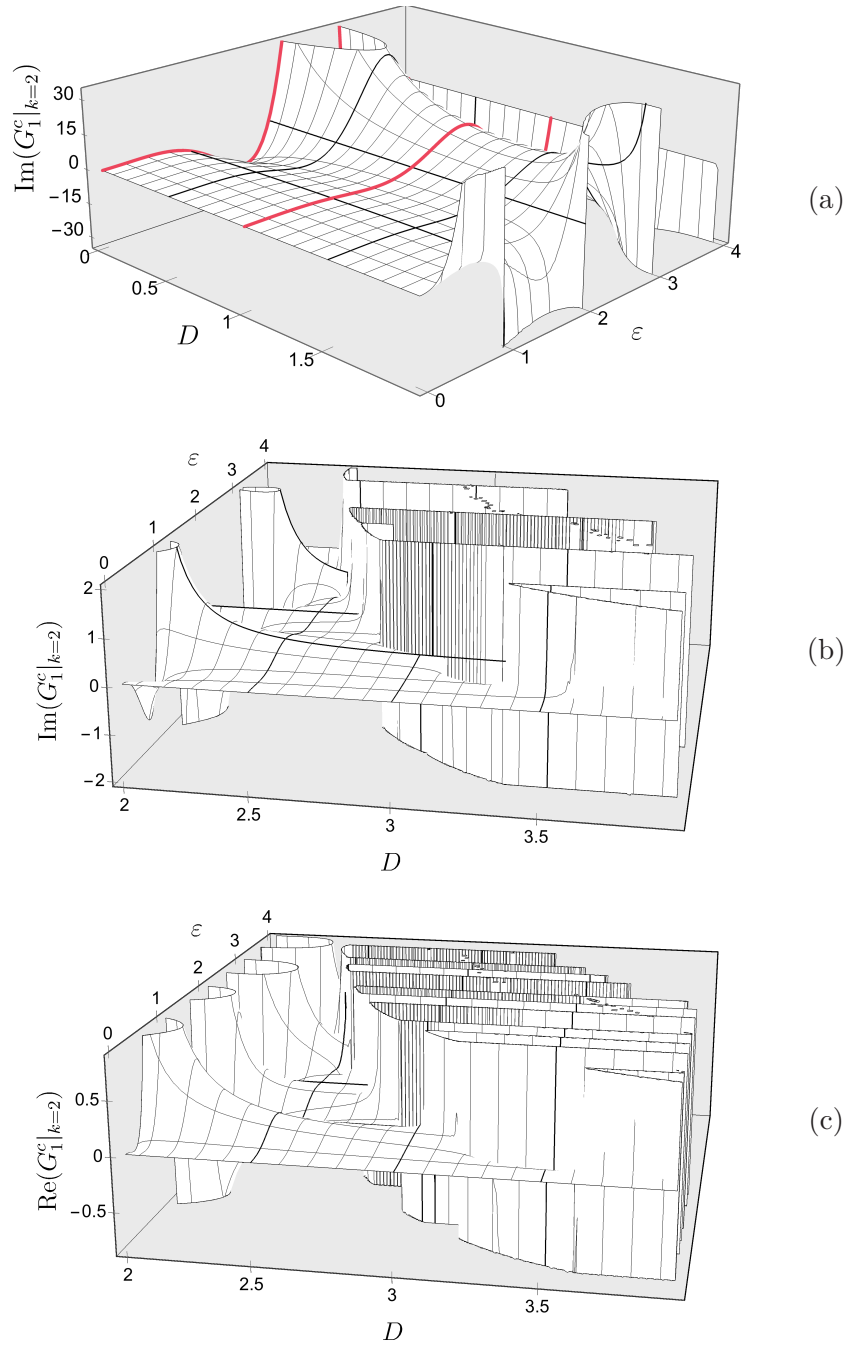
Figure 4.7: Behavior of the two-vertex approximation of the one-point Green's function as a function of the dimension D and the nonlinearity parameter ε. For $0 \leq D < 2$ the coefficient $G_1^c(\varepsilon; y_1)|_{k=2}$ is imaginary, shown in Figure 4.7a; the red lines denote the zero-dimensional and quantum-mechanical theories. For $2 < D < 4$ the coefficient becomes complex; the imaginary and real parts are displayed in Figure 4.7b and Figure 4.7c respectively.

For $p = 1$ the two-vertex approximation to the one-point Green's function is found to be

$$
\begin{aligned}
G_1^c(\varepsilon; y_1)\big|_{k=2} = \\
2i\, \frac{g^2 m^{-2}}{\pi} \sqrt{\tfrac{1}{2}\Delta_m(0)}\, \mu_0^{D/2-1}\, \sin(\tfrac{\pi\varepsilon}{2})\, \Gamma(\tfrac{\varepsilon+4}{2}) \Big([2\Delta_m(0)]^\varepsilon \cos(\tfrac{\pi\varepsilon}{2})\, \Gamma(\tfrac{\varepsilon+3}{2}) \\
\times \Big\{ \int d^D x'\, \Delta_m(0) \Big({}_2F_1\Big[-\tfrac{\varepsilon+1}{2}, -\tfrac{\varepsilon+2}{2}; \tfrac{1}{2}; \big(\tfrac{\Delta_m(x')}{\Delta_m(0)}\big)^2 \Big] - 1 \Big) \\
+ (\varepsilon+2) \int d^D x'\, \Delta_m(x')\, {}_2F_1\Big[-\tfrac{\varepsilon}{2}, -\tfrac{\varepsilon+1}{2}; \tfrac{3}{2}; \big(\tfrac{\Delta_m(x')}{\Delta_m(0)}\big)^2 \Big] \Big\} \\
- \sqrt{\pi}m^{-2} [2\Delta_m(0)]^{\varepsilon/2} \big[1 + \tfrac{1}{2}(\varepsilon+1)(1 - D/2)] \Big),
\end{aligned}
\tag{4.58}
$$

using the normalization (2.29) of the propagator and the integral (2.61) over its square. The behavior of $G_1^c(\varepsilon; y_1)|_{k=2}$ is shown in Figure 4.7 as a function of the space-time dimension D and the nonlinearity parameter ε. Similar to the single-vertex result in (4.32), it is an imaginary function for $0 \le D < 2$, that diverges in the limit of two dimensions, see Figure 4.7a. The red lines indicate the behavior for $D = 0$ and $D = 1$. In $2 < D < 4$ dimensions (4.58) is generally a complex function due to the dependence on the selfloop propagator, which is negative in this region and is raised to generally noninteger powers involving the parameter ε. The imaginary and real parts of $G_1^c(\varepsilon; y_1)|_{k=2}$ are shown in Figure 4.7b and Figure 4.7c respectively. Similar to the two-vertex approximation of the energy density $\mathcal{E}(\varepsilon)|_{k=2}$ in (3.10), cf. Figure 3.3, a complicated divergence structure is found the region $2 < D < 4$. This again demonstrates that renormalization techniques are not only required for $D = 2$ and $D = 4$ but in-between as well.

In addition, the two-vertex contribution (4.58) is found to vanish in all dimensions for even values of ε due to the sine function, and in $2 < D < 4$ its real part vanishes for odd values of ε, so that $G_1^c(\varepsilon; y_1)|_{k=2}$ becomes a purely imaginary function in this region, like for $0 \le D < 2$. These features were also observed for the single-vertex approximation in (4.32) and it was argued there that they are to be expected based on the structure of the Lagrangian density. They are not apparent in the nonlinearity expansion due to its perturbative nature but reemerge in the single-vertex and two-vertex approximations where terms to all orders in ε are taken into account.

In the case of the two-vertex approximation of the two-point Green's function, that is when $p = 2$, (4.57) becomes

$$
G_2^c(\varepsilon; y_1, y_2)\big|_{k=2} = g^2 \mu_0^{D-2} \Big\{ \kappa_2(\varepsilon) \int d^D x_1' \, \Delta_m(x_1' - y_1') \Delta_m(x_1' - y_2')
$$
$$
+ \int d^D x_1' d^D x_2' \, \Delta(x_1' - y_1') \Delta(x_2' - y_2') \, h(x_1' - x_2') \Big\}
\tag{4.59}
$$

in terms of

$$
\kappa_2(\varepsilon) =
$$
$$
\frac{2}{\pi} \Delta_m(0) \int d^D x' \Big(-\frac{\sqrt{\pi}}{2} \varepsilon \, \cos(\tfrac{\pi\varepsilon}{2}) \, [2\Delta_m(0)]^{\varepsilon/2} \, \Gamma(\tfrac{\varepsilon}{2} + \tfrac{3}{2}) \, (\tfrac{\varepsilon+2}{2}) \, \big(\tfrac{\Delta_m(x')}{\Delta_m(0)}\big)^2
$$
$$
+ \cos(\tfrac{\pi\varepsilon}{2})^2 \, [2\Delta_m(0)]^{\varepsilon} \, \Gamma(\tfrac{\varepsilon}{2} + \tfrac{3}{2})^2 \, (\tfrac{\varepsilon+2}{2}) \Big\{ {}_2F_1\Big[-\tfrac{\varepsilon+2}{2}, -\tfrac{\varepsilon}{2}; \tfrac{1}{2}; \big(\tfrac{\Delta_m(x')}{\Delta_m(0)}\big)^2 \Big] - 1 \Big\}
$$
$$
- \sin(\tfrac{\pi\varepsilon}{2})^2 \, [2\Delta_m(0)]^{\varepsilon} \, \Gamma(\tfrac{\varepsilon}{2} + 2)^2 \, (\varepsilon + 1) \tfrac{\Delta_m(x')}{\Delta_m(0)} \, {}_2F_1\Big[-\tfrac{\varepsilon+1}{2}, -\tfrac{\varepsilon-1}{2}; \tfrac{3}{2}; \big(\tfrac{\Delta_m(x')}{\Delta_m(0)}\big)^2 \Big] \Big),
$$
$$
\tag{4.60}
$$

and

$$
h(x) = \frac{2}{\pi} \, \cos(\tfrac{\pi\varepsilon}{2})^2 \, [2\Delta_m(0)]^{\varepsilon} \, \Gamma(\tfrac{\varepsilon}{2} + \tfrac{3}{2})^2 \, (\tfrac{\varepsilon+2}{2})^2 \, \tfrac{2\Delta_m(x)}{\Delta_m(0)} \, {}_2F_1\Big[-\tfrac{\varepsilon}{2}, -\tfrac{\varepsilon}{2}; \tfrac{3}{2}; \big(\tfrac{\Delta_m(x)}{\Delta_m(0)}\big)^2 \Big]
$$
$$
- \frac{2}{\pi} \, \sin(\tfrac{\pi\varepsilon}{2})^2 \, [2\Delta_m(0)]^{\varepsilon} \, \Gamma(\tfrac{\varepsilon}{2} + 2)^2 \, \Big\{ {}_2F_1\Big[-\tfrac{\varepsilon+1}{2}, -\tfrac{\varepsilon+1}{2}; \tfrac{1}{2}; \big(\tfrac{\Delta_m(x)}{\Delta_m(0)}\big)^2 \Big] - 1 \Big\}
$$
$$
- \frac{2}{\pi} \, \sqrt{\pi} \tfrac{\Delta_m(x)}{\Delta_m(0)} \, \cos(\tfrac{\pi\varepsilon}{2}) \, [2\Delta_m(0)]^{\varepsilon/2} \, \Gamma(\tfrac{\varepsilon}{2} + \tfrac{3}{2}) \, (\varepsilon + 2) + \tfrac{\Delta_m(x)}{\Delta_m(0)}.
$$
$$
\tag{4.61}
$$

Note that $\kappa_2(\varepsilon)$ and $h(x)$, and thus $G_2^c(\varepsilon; y_1, y_2)\big|_{k=2}$, vanish when $\varepsilon \to 0$, as expected from the coupling-constant expansion interpretation of the vertex approximation established in (2.47). In addition, both (4.60) and (4.61) are real-valued functions in all space-time dimensions for integer values of ε due to the combinations of trigonometric functions and powers of the (possibly negative) selfloop propagator $\Delta_m(0)$, similar to the behavior of $\kappa_1(\varepsilon)$ in (4.34).

4.4 The Effective Mass

Having derived the general closed-form behavior of the p-point Green's functions to second order in the ε expansion of the model, as well as their single-vertex and two-vertex approximations, this section closes the general discussion of the Green's functions by remarking upon the behavior of the effective mass $M(\varepsilon)$ of the theory.

The effective mass is defined through the Fourier transform of the two-point Green's function as

$$M^2(\varepsilon) = \lim_{p \to 0} \widehat{G_2^c}(\varepsilon; p)^{-1}. \tag{4.62}$$

In the previous sections, $G_2^c(\varepsilon; y_1, y_2)$ was determined in position space, finding its nonlinearity expansion to second order to be of the form

$$
\begin{aligned}
G_2^c(\varepsilon; y_1, y_2) = \mu_0^{D-2} \Big\{ &\Delta_m(y_1' - y_2') + g\,\varepsilon K_1 \int d^D x'\, \Delta_m(x' - y_1')\Delta_m(x' - y_2') \\
&+ \varepsilon^2(gK_2 + g^2 K_3) \int d^D x'\, \Delta_m(x' - y_1')\Delta_m(x' - y_2') \\
&+ \varepsilon^2 g^2 \int d^D x_1' d^D x_2'\, \Delta(x_1' - y_1')\Delta(x_2' - y_2')\, f(x_1' - x_2') \Big\},
\end{aligned}
\tag{4.63}
$$

where $y_1' = \mu_0 y_1$ and $y_2' = \mu_0 y_2$ are dimensionless space-time variables, and K_1, K_2, K_3, and $f(x')$ are given in (4.22), (4.51), (4.52), and (4.53) respectively. The space-time integrals in this expansion form convolutions, so that obtaining $\widehat{G_2^c}(\varepsilon; p)$ is straightforward:

$$
\begin{aligned}
\widehat{G_2^c}(\varepsilon; p) = \mu_0^{-2} \Big\{ &\widehat{\Delta}_m(p') + g\,\varepsilon K_1 \widehat{\Delta}_m(p')^2 + \varepsilon^2(gK_2 + g^2 K_3)\widehat{\Delta}_m(p')^2 \\
&+ \varepsilon^2 g^2\, \widehat{f}(p')\,\widehat{\Delta}_m(p')^2 \Big\},
\end{aligned}
\tag{4.64}
$$

where $p' = p\mu_0^{-1}$ is the dimensionless momentum variable, so that all functions are dimensionless expressions and the only dimensional dependence is explicit in the overall factor μ_0^{-2}; that is $\widehat{G_2^c}(\varepsilon; p)$ has the expected dimension $[\text{mass}]^{-2}$.

(a) First-order coefficient M_1^2.   (b) Second-order coefficient M_2^2.
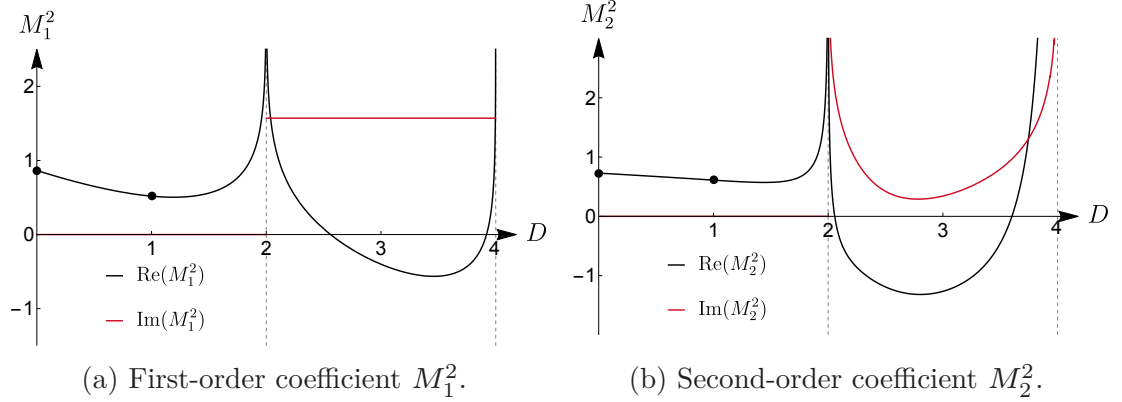
Figure 4.8: Behavior of the first-order and second-order effective mass coefficients M_1^2 and M_2^2 in $0 \leq D < 4$ dimensions. The black dots denote the zero-dimensional and quantum-mechanical theories in (4.71), (4.72), (4.74), and (4.75).

By expanding the inverse of the two-point Green's function in terms of the momentum-space ε-expansion coefficients

$$\widehat{G}_2^c(\varepsilon; p) = \sum_{n=0}^{\infty} \widehat{G}_{2,n}^c(p)\, \varepsilon^n, \tag{4.65}$$

one obtains the expansion coefficients of the effective mass, given by

$$M^2(\varepsilon) = \sum_{n=0}^{\infty} M_n^2\, \varepsilon^n, \tag{4.66}$$

to be

$$\varepsilon^0 :\; M_0^2 = [\widehat{G}_{2,0}^c(0)]^{-1} = \mu_0^2 \widehat{\Delta}_m(0)^{-1} = (m\mu_0)^2, \tag{4.67}$$

$$\varepsilon^1 :\; M_1^2 = -\,\widehat{G}_{2,1}^c(0)\, [\widehat{G}_{2,0}^c(0)]^{-2} = -g\, m^{-2} K_1\, (m\mu_0)^2, \tag{4.68}$$

$$\varepsilon^2 :\; M_2^2 = [\widehat{G}_{2,1}^c(0)]^2\, [\widehat{G}_{2,0}^c(0)]^{-3} - \widehat{G}_{2,2}^c(0)\, [\widehat{G}_{2,0}^c(0)]^{-2}$$
$$= -\, gm^{-2}\, (m\mu_0)^2 \left\{ K_2 + g[K_3 + \hat{f}(0) - m^{-2}K_1^2\,] \right\}, \tag{4.69}$$

using that $\widehat{\Delta}_m(p') = 1/(p'^2 + m^2)$. The term $\hat{f}(0) = \int d^D x'\, f(x')$ is a dimensionless constant.

In Figure 4.8 the behavior of the first-order and second-order mass coefficients M_1^2 and M_2^2 is shown as a function of the space-time dimension D for $g = m = 1$ and $\mu_0 = 1$ in the range $0 \leq D < 4$. Note in particular that both coefficients diverge at $D = 2$, demonstrating that renormalization techniques are required

in this case. Moreover, they evaluate to finite *complex* values in dimensions $2 < D < 4$, and diverge again when approaching $D = 4$. The special cases of the zero-dimensional and quantum-mechanical models are denoted as black dots. In $D = 0$, $\Delta(x) = \Delta(0) = 1$, so (4.67) to (4.69) simplify to

$$\varepsilon^0 : M_0^2|_{D=0} = 1, \tag{4.70}$$

$$\varepsilon^1 : M_1^2|_{D=0} = \tfrac{1}{2}\big[\ln 2 + \psi(\tfrac{3}{2}) + 1\big] \approx 0.865, \tag{4.71}$$

$$\varepsilon^2 : M_2^2|_{D=0} = \tfrac{1}{8}\big[\psi'(\tfrac{3}{2}) + \tfrac{1}{2}\pi^2 - 4\pi + 12\big] \approx 0.729. \tag{4.72}$$

In $D = 1$, $\Delta(x) = \tfrac{1}{2}e^{-|x|}$ and $\Delta(0) = \tfrac{1}{2}$, so the constants are easily evaluated, resulting in:

$$\varepsilon^0 : M_0^2\big|_{D=1} = 1, \tag{4.73}$$

$$\varepsilon^1 : M_1^2\big|_{D=1} = \tfrac{1}{2}\big[\psi(\tfrac{3}{2}) + 1\big] \approx 0.518, \tag{4.74}$$

$$\varepsilon^2 : M_2^2\big|_{D=1} \approx 0.611. \tag{4.75}$$

When approximating the two-point Green's function in terms of the single-vertex and two-vertex contributions

$$G_2^c(\varepsilon; y_1, y_2) =$$
$$\mu_0^{D-2} \bigg\{ \Delta_m(y_1' - y_2') + g\,\mu_0^{D-2}\,\kappa_1(\varepsilon) \int d^D x'\, \Delta_m(x' - y_1')\Delta_m(x' - y_2')$$
$$+ g^2 \mu_0^{D-2}\kappa_2(\varepsilon) \int d^D x'\, \Delta_m(x' - y_1')\Delta_m(x' - y_2')$$
$$+ g^2 \mu_0^{D-2} \int d^D x_1' d^D x_2'\, \Delta(x_1' - y_1')\Delta(x_2' - y_2')\, h(x_1' - x_2') \bigg\}, \tag{4.76}$$

with $\kappa_1(\varepsilon)$ given in (4.34), $\kappa_2(\varepsilon)$ in (4.60), and $h(x')$ in (4.61), the Fourier transform becomes

$$\widehat{G}_2^c(\varepsilon; p) = \mu_0^{-2} \Big\{ \widehat{\Delta}_m(p') + g\,\kappa_1(\varepsilon)\,\widehat{\Delta}_m(p')^2 + g^2\,[\kappa_2(\varepsilon) + \hat{h}(p')]\,\widehat{\Delta}_m(p')^2 \Big\}. \tag{4.77}$$

As argued in Section 2.2, when treating m and g as independent parameters the vertex approximations correspond to first-order and second-order coupling-constant expansion coefficients and the relation between the effective mass coeffi-

Figure 4.9: Behavior of the single-vertex approximation of the effective mass as a function of the dimension D and the nonlinearity parameter ε. For $0 \leq D < 2$ the coefficient $M^2|_{k=1}$ is real, shown in Figure 4.9a; the red lines denote the zero-dimensional and quantum-mechanical theories. For $2 < D < 4$ the coefficient becomes complex; the real and imaginary parts are displayed in Figure 4.9b and Figure 4.9c respectively.

cients and the coefficients in (4.77) has the same form as for the ε expansion:

$$M^2\big|_{k=0} = [\widehat{G}_2^c(0)\big|_{k=0}]^{-1} = [\widehat{G}_{2,0}^c(0)]^{-1} = (m\mu_0)^2, \tag{4.78}$$

$$M^2\big|_{k=1} = -\,\widehat{G}_2^c(0)\big|_{k=1}\,[\widehat{G}_{2,0}^c(0)]^{-2} = -g\,m^{-2}\kappa_1(\varepsilon)\,(m\mu_0)^2, \tag{4.79}$$

$$M^2\big|_{k=2} = \widehat{G}_2^c(0)\big|_{k=1}^2\,[\widehat{G}_{2,0}^c(0)]^{-3} - \widehat{G}_2^c(0)\big|_{k=2}\,[\widehat{G}_{2,0}^c(0)]^{-2}$$
$$= -\,g^2 m^{-4}\,(m\mu_0)^2\,\{m^2[\kappa_2(\varepsilon) + \widehat{h}(0)] - \kappa_1(\varepsilon)^2\}. \tag{4.80}$$

The behavior of the single-vertex and two-vertex approximations $M^2\big|_{k=1}$ and $M^2\big|_{k=2}$ is shown in Figure 4.9 and Figure 4.10 respectively as a function of the space-time dimension D and the nonlinearity parameter ε. Both contributions are real functions in the region $0 \leq D < 2$, which diverge in the limit of two dimensions, see Figure 4.9a and Figure 4.10a, where the behavior in $D = 0$ and $D = 1$ dimension is indicated as red lines. Similar to previous vertex approximations they become generally complex functions in $2 < D < 4$ dimensions; their real and imaginary parts are visualized in Figure 4.9b and Figure 4.9c, and Figure 4.10b and Figure 4.10c respectively. However, observe that the vertex approximations of the effective mass remain purely real functions for integer values of ε, as previously indicated for the functions $\kappa_1(\varepsilon)$ given in (4.34), $\kappa_2(\varepsilon)$ in (4.60), and $h(x)$ in (4.61).

Overall, the analysis in this chapter has demonstrated how the nonlinearity-expansion techniques of [1], that were generalized in Chapter 2, can be used to determine the behavior of the p-point Green's functions. The general coefficient structure was presented and evaluated to closed-form solutions at first and second order in ε. This analysis was supplemented with the discussion of the vertex approximation based on the resummation of contributions with only a single or two internal space-time points to all orders in ε.

Furthermore, the general results for the p-point Green's function were specified, in particular for the special cases of the one-point Green's function and, based on the two-point Green's function result, the effective mass of the theory. These cases demonstrate that the renormalization of the theory becomes necessary in, and above, two space-time dimensions. A first step towards this is presented in the following chapter with the perturbative renormalization in two dimensions.
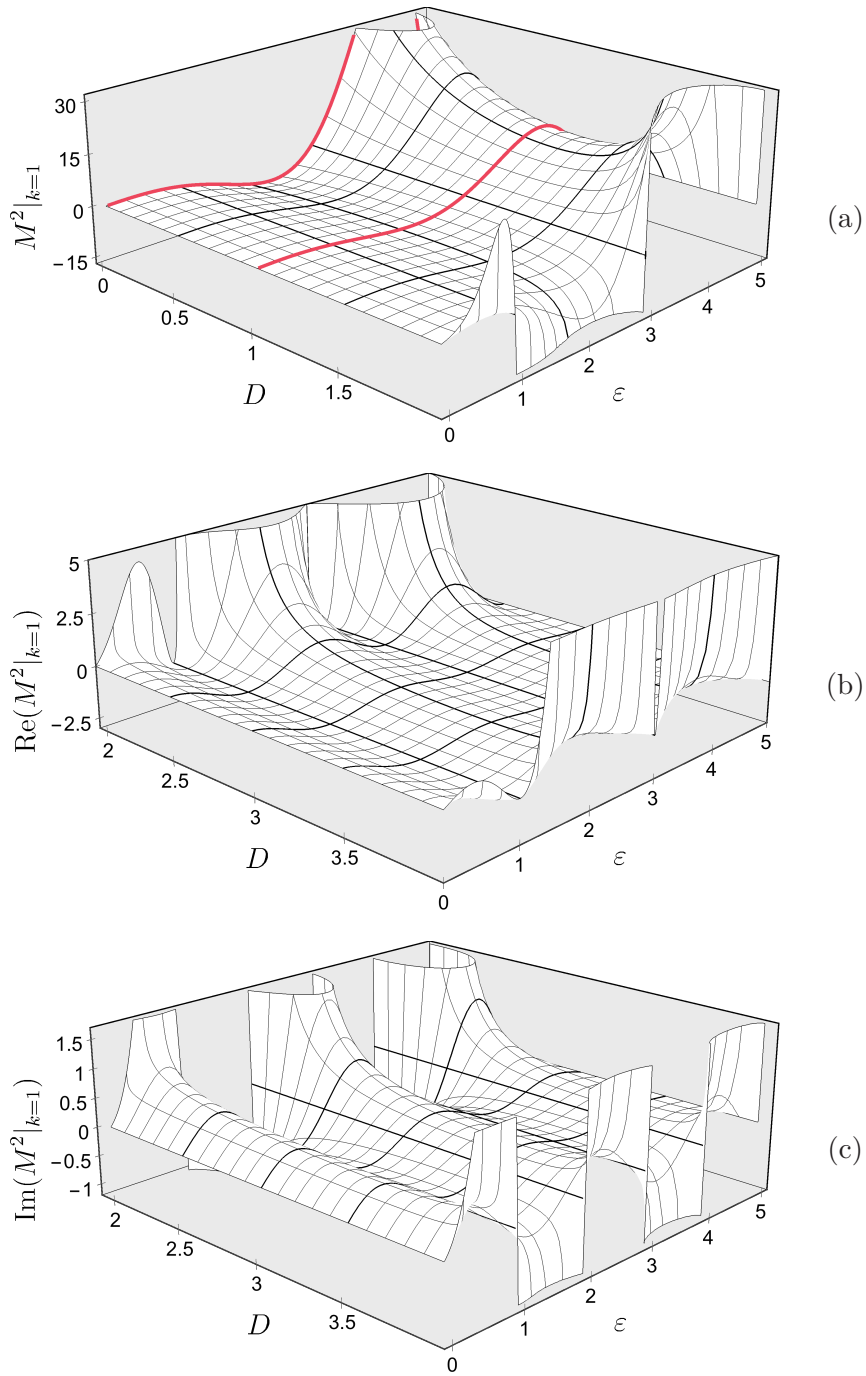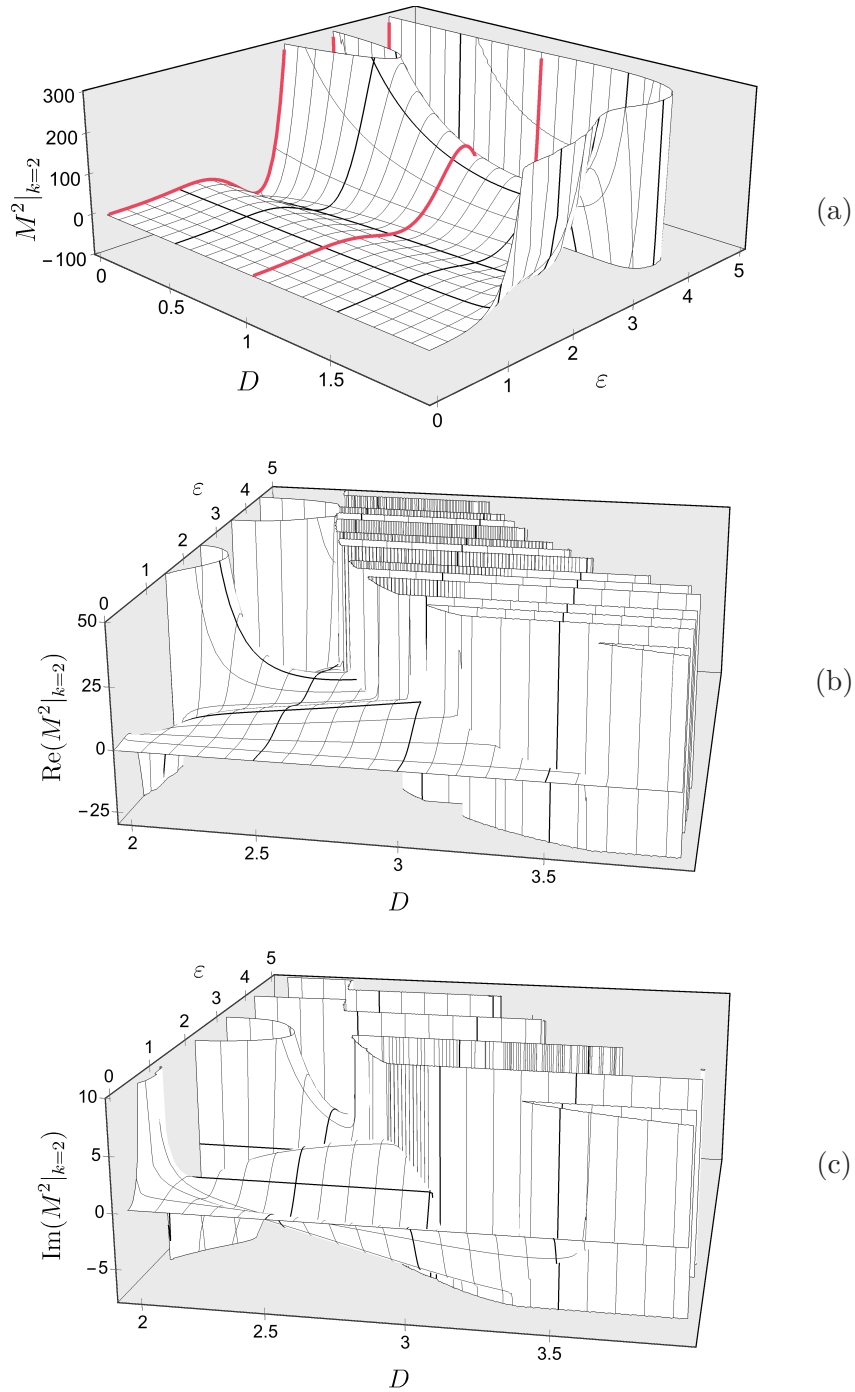
Figure 4.10: Behavior of the two-vertex approximation of the effective mass as a function of the dimension D and the nonlinearity parameter ε. For $0 \le D < 2$ the coefficient $M^2|_{k=2}$ is real, shown in Figure 4.10a; the red lines denote the zero-dimensional and quantum-mechanical theories. For $2 < D < 4$ the coefficient becomes complex; the real and imaginary parts are displayed in Figure 4.10b and Figure 4.10c respectively.

Chapter 5

Towards Perturbative Renormalization in Two Dimensions

So far, the discussion of the nonlinearity expansion of the $\mathcal{PT}$-symmetric quantum-field-theory analogue of the Bender-Boettcher model (1.1) has focused on developing the general techniques introduced in [1] beyond the initial first-order results, aiming to study the behavior of the theory in greater detail and establishing the nonlinearity expansion as a promising approach to non-Hermitian $\mathcal{PT}$-symmetric field theories in D space-time dimensions. In Chapter 2 to Chapter 4 the technical aspects of this expansion at higher orders have been examined in detail and were applied to determine the behavior of the ground-state energy density $\mathcal{E}(\varepsilon)$, the connected Green's functions $G_p^c(\varepsilon; y_1, \dots, y_p)$ and the effective mass $M^2(\varepsilon)$ to second order in the nonlinearity parameter ε. Moreover, by resumming certain contributions of these coefficients to all order in ε, the connection to a common coupling-constant expansion of the theory was examined, which allows one to analyze the perturbative study of the model from a different angle.

A noteworthy feature, which was remarked upon by Bender, Hassanpour, Klevansky and Sarkar in [1], is that the propagator of the underlying free theory with Lagrangian density (2.3) diverges when approaching the two-dimensional case, that is $D \to 2^-$. This divergence is reflected in the expansion coefficients of the ground-state energy density, see Chapter 3, of the one-point and two-point Green's functions, and of the effective mass, see Chapter 4. The theory requires renormalization. In fact, as the behavior of the two-vertex approximation of these quantities has illustrated, the renormalization of the model is necessary for $D \geq 2$.

In this study, the renormalization program for $D = 2$ dimensions, proposed in [1], is considered; it is presented in this chapter. Using the dimensional regularization $\delta = 2 - D$, Section 5.1 gives the analysis of the behavior of the Green's functions and the effective mass in the limit $\delta \to 0$. In Section 5.2 it is then demonstrated that the divergent behavior found for $G_1^c(\varepsilon; y_1)$ can be addressed through the introduction of a linear counterterm $v(\varepsilon)\phi$ into the Lagrangian density. Then the divergence found for $G_2^c(\varepsilon; y_1, y_2)$, and in turn for the effective mass $M^2(\varepsilon)$, is countered through perturbative mass renormalization, which is performed to second order in ε in Section 5.3. Finally a multiple-scale analysis in ε and δ is investigated in Section 5.4, centering on the single-vertex and two-vertex approximations of the Green's functions, and the behavior observed is contrasted with that found in the ε perturbation expansion.

Central results of this analysis can be found in [43] and [44].

5.1 Divergence Structure in Two Dimensions

The general nth-order Green's function coefficient $G_{p,n}^c(y_1, \ldots, y_p)$ in (4.14) depends on the dimension D of space-time due to the free-theory propagators $\Delta_m(x)$ and $\Delta_m(0)$ in (2.28) and (2.30):

$$\Delta_m(x) = (2\pi)^{-D/2}\, m^{D/2-1}\, |x|^{1-D/2}\, \mathrm{K}_{1-D/2}(m|x|) \tag{5.1}$$

and

$$\Delta_m(0) = m^{D-2}\, (4\pi)^{-D/2}\, \Gamma\!\left(1 - \tfrac{D}{2}\right). \tag{5.2}$$

As remarked upon in (2.31), when denoting $\delta = 2 - D$, the selfloop propagator diverges asymptotically like

$$\Delta_m(0) \sim \frac{1}{2\pi\delta} + O(1), \quad \text{as } \delta \to 0. \tag{5.3}$$

The propagator $\Delta_m(x)$ on the other hand does not diverge, but behaves as

$$\Delta_m(x) \sim \frac{1}{2\pi}\, \mathrm{K}_0(m|x|) + O(\delta), \quad \text{as } \delta \to 0. \tag{5.4}$$

Using (5.3) and (5.4), the structure of the leading-order behavior for the general Green's function coefficients in (4.14),

$$
G_{p,n}^c(y_1,\ldots,y_p) =
$$

$$
\frac{1}{2^n}\left[\frac{\mu_0^{D-2}\Delta_m(0)}{2}\right]^{p/2}\sum_{k=1}^n\left(-\frac{g\Delta_m(0)}{\sqrt{\pi}}\right)^k\sum_{c}{}^{n+1-k}\prod_{s=1}\frac{1}{c_s!\,(s!\,)^{c_s}}\int d^Dx_\alpha'\sum_{m_\alpha=0}^\beta\binom{\beta}{m_\alpha}
$$

$$
\times\,(i\pi)^{m_\alpha}\lim_{N_\alpha\to 0}\left(\frac{d}{dN_\alpha}\right)^{\beta-m_\alpha}[2\Delta_m(0)]^{N_\alpha}\sum_{l}^\infty\prod_{\substack{i,j=1,\\i<j}}^{k+p}\frac{1}{l_{ij}!}\left[\frac{2\Delta_m(z_i'-z_j')}{\Delta_m(0)}\right]^{l_{ij}}
$$

$$
\times\,\frac{\Gamma(N_\alpha+2)\,\Gamma(N_\alpha+\frac{3}{2})}{\Gamma(N_\alpha+2-\frac{1}{2}L_\alpha)}\left(\frac{1+e^{i\pi(m_\alpha-L_\alpha)}}{2}\right)\left\{\prod_{r=1}^p\left(\frac{1+e^{i\pi(1-L_{k+r})}}{2\Gamma(\frac{3}{2}-\frac{1}{2}L_{k+r})}\right)\right\}\Big|_{\text{connected}},
$$
$$(5.5)$$

is found as follows:

The overall factor $\Delta_m(0)^{p/2}$ is of the order $O(\delta^{-p/2})$. Similarly, for any fixed values of k, the factor $\Delta_m(0)^k$ is of the order $O(\delta^{-k})$. In addition, the summation in m_α over derivatives $(\frac{d}{dN_\alpha})^{\beta-m_\alpha}[2\Delta_m(0)]^{N_\alpha}$ contributes terms of the order $[O(1)+\cdots+O(\ln^n\delta)]$, using the definition (2.18) of the multi-index β and the restriction (2.11) to find the highest possible power of logarithms that can occur. This only modifies the degree of divergence by sub-leading contributions. Finally, the summation $\sum_l$ is a function of the term $\Delta_m(z)/\Delta_m(0)$, which, according to (5.3) and (5.4), is of the order $O(\delta)$. It thus suppresses the degree of divergence. To obtain the leading-order behavior in the limit $\delta\to 0$, only the minimally connected contributions, which contain the least factors of $\Delta_m(z)/\Delta_m(0)$, have to be considered. For the $k+p$ space-time points in (5.5), at least $k+p-1$ connections, i.e. factors $\Delta_m(z)/\Delta_m(0)$, are required. Thus the summation $\sum_l$ suppresses the asymptotic behavior by at least $O(\delta^{k+p-1})$. Overall, the nth-order Green's function coefficient generally behaves as

$$
G_{p,n}^c(y_1,\ldots,y_p)\sim O(\delta^{p/2-1})\left[O(1)+O(\ln\delta)+\ldots+O(\ln^n\delta)\right],\quad\text{as }\delta\to 0.
$$
$$(5.6)$$

Notably, the algebraic asymptotic behavior does not depend on the order n of the expansion in ε. Leading-order terms of the asymptotic δ expansion arise at every order in the nonlinearity parameter ε.

The structural analysis of the asymptotics in (5.6) leads to some noteworthy observations: The ε-expansion coefficients of the one-point Green's function $G_1^c(\varepsilon; y_1)$ diverge as $\delta^{-1/2}$ in the limit of the two-dimensional theory. For the two-point Green's function $G_2^c(\varepsilon; y_1, y_2)$ the algebraic δ dependence becomes a constant, but the additional logarithmic terms still result in the divergence of the ε-expansion coefficients. Accordingly, this also implies that the expansion coefficients of the effective mass diverge logarithmically. For all higher-order Green's functions, that is for $p \geq 3$, the positive exponent of the algebraic δ dependence overrides the logarithmic divergences and the ε-expansion coefficients vanish in the two-dimensional theory. Therefore, to any finite order in the nonlinearity parameter ε, the theory is free in two dimensions!

The following two sections address the perturbative renormalization of the one-point Green's function and of the effective mass, while the apparent freedom of the model is reexamined through the lens of the single-vertex and two-vertex approximations thereafter.

5.2 Divergence of the One-Point Green's Function

In the limit of two-dimensional space-time, $\delta \to 0$, the one-point Green's function diverges as $\delta^{-1/2}$. Since $G_1^c(\varepsilon; y_1)$ is not directly measurable, this divergence can be removed through the introduction of a linear counterterm of the form $-v(\varepsilon)\phi$ into the Lagrangian density, so that

$$\mathcal{L}_v(\varepsilon) = \tfrac{1}{2}(\nabla\phi)^2 + \tfrac{1}{2}\mu^2\phi^2 + \tfrac{1}{2}g\mu_0^2\phi^2(i\mu_0^{1-D/2}\phi)^\varepsilon - v(\varepsilon)\phi. \tag{5.7}$$

The factor $v(\varepsilon) = \sum_{j=1}^{\infty} v_j\,\varepsilon^j$ has the dimension $[\text{mass}]^{1+D/2}$. When $v(\varepsilon)$ is imaginary such a counterterm is consistent with $\mathcal{PT}$ symmetry, because the field changes sign under parity reflection (1.4) and $v(\varepsilon)$ changes sign under time reversal, which acts as complex conjugation.

The dependence of the connected Green's functions $G_p^c(v, \varepsilon)$ of the theory (5.7) on the coefficients v_j of the linear counterterm can be examined in terms of the Green's functions of the theory without the counterterm studied previously:

Consider the general form (4.4) of the connected Green's functions,

$$
\begin{aligned}
G_p^c(v, \varepsilon; y_1, \dots, y_p) &= \frac{1}{Z(0)} \int \mathcal{D}\phi \, e^{-\int d^D x \, \mathcal{L}_v(\varepsilon)} \, \phi(y_1) \dots \phi(y_p) \Big|_{\text{connected}} \\
&= \frac{1}{Z(0)} \int \mathcal{D}\phi \, e^{-\int d^D x \, \mathcal{L}(\varepsilon)} \, \phi(y_1) \dots \phi(y_p) \\
&\quad \times \exp\Big[\int d^D x \, \phi(x) \sum_{j=1}^{\infty} v_j \, \varepsilon^j \Big] \Big|_{\text{connected}}.
\end{aligned}
\tag{5.8}
$$

Using the generating function relation (2.7) of the exponential partial Bell polynomials, this takes the form

$$
\begin{aligned}
&G_p^c(v, \varepsilon; y_1, \dots, y_p) = \\
&G_p^c(\varepsilon; y_1, \dots, y_p) + \sum_{r=1}^{\infty} \frac{\varepsilon^r}{r!} \sum_{j=1}^{r} \mathrm{B}_{r,j}\big[1! \, v_1, \dots, (r+1-j)! \, v_{r+1-j}\big] \\
&\times \int d^D x_1 \dots d^D x_j \, \frac{1}{Z(0)} \int \mathcal{D}\phi \, e^{-\int d^D x \, \mathcal{L}(\varepsilon)} \, \phi(y_1) \dots \phi(y_p) \phi(x_1) \dots \phi(x_j) \Big|_{\text{connected}} \\
&= G_p^c(\varepsilon; y_1, \dots, y_p) + \sum_{r=1}^{\infty} \frac{\varepsilon^r}{r!} \sum_{j=1}^{r} \mathrm{B}_{r,j}\big[1! \, v_1, \dots, (r+1-j)! \, v_{r+1-j}\big] \\
&\times \int d^D x_1 \dots d^D x_j \, G_{p+j}^c(\varepsilon; y_1, \dots, y_p, x_1, \dots, x_j)
\end{aligned}
\tag{5.9}
$$

in terms of the Green's functions of the theory without linear counterterm.

When writing $G_p^c(\varepsilon; y_1, \dots, y_p)$ in the ε expansion (4.2), and expanding

$$
G_p^c(v, \varepsilon; y_1, \dots, y_p) = \sum_{n=0}^{\infty} G_{p,n}^c(v; y_1, \dots, y_p) \, \varepsilon^n
\tag{5.10}
$$

similarly, the coefficients $G_{p,n}^c(v; y_1, \dots, y_p)$ are determined from (5.9) to be of the form $G_{p,0}^c(v; y_1, \dots, y_p) = G_{p,0}^c(y_1, \dots, y_p)$ when $n = 0$, and

$$
\begin{aligned}
&G_{p,n}^c(v; y_1, \dots, y_p) = \\
&G_{p,n}^c(y_1, \dots, y_p) + \sum_{r=1}^{n} \frac{1}{r!} \sum_{j=1}^{r} \mathrm{B}_{r,j}\big[1! \, v_1, \dots, (r+1-j)! \, v_{r+1-j}\big] \\
&\times \int d^D x_1 \dots d^D x_j \, G_{p+j,n-r}^c(y_1, \dots, y_p, x_1, \dots, x_j)
\end{aligned}
\tag{5.11}
$$

for $n \geq 1$ in terms of the Green's function coefficients of the theory without the linear counterterm. The first-order and second-order coefficients have the explicit form:

$$G^c_{p,1}(v; y_1, \dots, y_p) = G^c_{p,1}(y_1, \dots, y_p) + v_1 \int d^D x_1 \, G^c_{p+1,0}(y_1, \dots, y_p, x_1), \quad (5.12)$$

$$\begin{aligned} G^c_{p,2}(v; y_1, \dots, y_p) = {}& G^c_{p,2}(y_1, \dots, y_p) + v_1 \int d^D x_1 \, G^c_{p+1,1}(y_1, \dots, y_p, x_1) \\ & + \tfrac{1}{2} v_1^2 \int d^D x_1 d^D x_2 \, G^c_{p+2,0}(y_1, \dots, y_p, x_1, x_2) \qquad (5.13) \\ & + v_2 \int d^D x_1 \, G^c_{p+1,0}(y_1, \dots, y_p, x_1). \end{aligned}$$

Observe that in the relation (5.11), the last contribution in the summation over r, i.e. when $r = n$, is proportional to the coefficients $G^c_{p+j,0}$. As initially remarked in (4.7), these coefficients vanish for all values $p + j \neq 2$, including in particular all values $p \geq 2$ (since $j \geq 1$). The terms with $r \in [1, n-1]$, however, only contain the counterterm coefficients v_1 to v_{n-1}. Thus, when $p \geq 2$, the coefficient v_n arises earliest at order $O(\varepsilon^{n+1})$. For $p = 1$, on the other hand, one contribution with $r = n$ does not vanish: that with $j = 1$. (Using that $\mathrm{B}_{n,1}(1! \, v_1, \dots, n! \, v_n) = n! \, v_n$, this contribution is readily found to be $v_n \int d^D x \, G^c_{2,0}(y_1, x) = v_n (m\mu_0)^{-2}$.) In the one-point Green's function the coefficient v_n thus arises already at order $O(\varepsilon^n)$. Accordingly, the counterterm coefficients are, in fact, determined by the behavior of the one-point Green's function.

The coefficients of $v(\varepsilon)$ are chosen to cancel the divergence of the coefficient $G^c_{1,n}(v; y_1)$ in the limit $\delta \to 0$ order-by-order in the nonlinearity expansion. To second order they take the explicit form

$$v_1 = \tfrac{1}{2} i g \mu_0^2 \, \delta^{-1/2} \qquad \text{and} \qquad v_2 = \tfrac{1}{4} i g \mu_0^2 \, \delta^{-1/2} \left[\psi(2) - \ln \pi - \ln \delta \right] \qquad (5.14)$$

based on the asymptotic behavior of (5.12) and (5.13). Note that these coefficients are imaginary so that the linear counterterm is in fact consistent with $\mathcal{PT}$ symmetry. The resulting one-point Green's function vanishes to second order.

According to (5.6) all coefficients v_n of the counterterm diverge as $\delta^{-1/2}$ at leading order. Notably, this implies that the Bell polynomials in (5.11) diverge like $\delta^{-j/2}$, as can be seen from the condition (2.12). This exactly cancels the suppression of the divergence in the Green's function coefficients $G^c_{p+j,n-r} \sim O(\delta^{(p+j)/2-1})$ which accompany the Bell polynomials, so that the overall divergence structure of the p-point Green's function coefficients of the theory with the linear counterterm remains generally unchanged for $p \geq 2$; the counterterm absorbs only the divergence of the one-point Green's function.

Because the general divergence structure of the higher-order Green's functions remains unchanged by the linear counterterm contributions, the following discussion of the mass renormalization does not include them. Nevertheless, all considerations remain equally valid when including these terms; they are dropped for the sake of brevity.

5.3 The Mass Counterterm

The study of the model with the Lagrangian density $\mathcal{L}(\varepsilon)$ in (2.1), discussed throughout previous chapters, includes the dimensional mass parameter μ that is often implicitly contained in the dimensionless parameter $m^2 = g + \mu^2/\mu_0^2$. The parameter μ will here act as a mass counterterm, canceling the logarithmic divergences that the effective mass $M^2(\varepsilon)$ inherits from the two-point Green's function in the ε expansion.

In Section 4.4 the nonlinearity expansion of the effective mass was examined, presenting the expansion coefficients to second order explicitly, see (4.67) to (4.69):

$$\varepsilon^0 : \ M_0^2 = (m\mu_0)^2, \tag{5.15}$$

$$\varepsilon^1 : \ M_1^2 = -\,g\,m^{-2}K_1\,(m\mu_0)^2, \tag{5.16}$$

$$\varepsilon^2 : \ M_2^2 = -\,gm^{-2}\,(m\mu_0)^2\,\{K_2 + g[K_3 + \hat{f}(0) - m^{-2}K_1^2]\}, \tag{5.17}$$

with K_1, K_2, K_3, and $\hat{f}(0)$ determined by (4.22), (4.51), (4.52), and (4.53). With the asymptotic behavior of $\Delta_m(0)$ and $\Delta_m(x)$ in (5.3) and (5.4) the leading-order asymptotic behavior of these coefficients is evaluated exactly, finding the following results.

At order $O(\varepsilon^0)$ in the nonlinearity expansion, the coefficient of the effective mass behaves as

$$M_0^2 = (m\mu_0)^2 = \mu^2 + g\mu_0^2, \quad \text{as } \delta \to 0; \tag{5.18}$$

the coefficient is constant.

At first order in ε, the effective-mass coefficient has the form

$$M_1^2 \sim \tfrac{1}{2}g\mu_0^2\left[\psi(\tfrac{3}{2}) + 1 - \ln\pi\right] - \tfrac{1}{2}g\mu_0^2 \ln\delta + O(\delta), \quad \text{as } \delta \to 0. \tag{5.19}$$

The coefficient diverges like $\ln\delta$ in the limit of two space-time dimensions. It is independent of m and therefore also of μ. This implies that the mass counterterm μ in (5.18) has to absorb divergences, which arise at higher orders in the ε expansion.

The second-order coefficient of the effective mass behaves like

$$M_2^2 \sim \tfrac{1}{8}g\mu_0^2\Big\{\left(\psi^{(1)}(\tfrac{3}{2}) - \pi^2 - 1 + [\psi(\tfrac{3}{2}) + 1 - \ln\pi]^2 + 4\pi g m^{-2}\right)$$
$$- 2\ln\delta\,[\psi(\tfrac{3}{2}) + 1 - \ln\pi] + \ln^2\delta\Big\} + O(\delta) \tag{5.20}$$

in the limit $\delta \to 0$. Notably, the constant term depends on m^{-2} and therefore on μ. Such a dependence on μ is suspected to arise beyond second order as well, and may initially appear troubling. However, since absorbing the $O(\varepsilon^1)$ divergence into μ results in a divergent counterterm, $\mu \to \infty$ as $\delta \to 0$, the factor $m^{-2} = 1/(g + \mu^2/\mu_0^2)$ vanishes. The divergent behavior at order $O(\varepsilon^2)$ can thus effectively be absorbed into the counterterm, disregarding the μ dependence of M_2^2.

Thus, to second order in the nonlinearity parameter ε, the mass counterterm is of the form:

$$\mu^2 = \tfrac{1}{2}\varepsilon g\mu_0^2 \ln\delta + \tfrac{1}{8}\varepsilon^2 g\mu_0^2\left(2\ln\delta\,[\psi(\tfrac{3}{2}) + 1 - \ln\pi] - \ln^2\delta\right) \tag{5.21}$$

up to a constant of dimension $[\text{mass}]^2$, which is determined by the experimental value of the renormalized mass.

5.4 Multiple-Scale Analysis

Besides the perturbative expansion in the nonlinearity parameter ε, the Green's functions have been examined in another approximation scheme in Chapter 4. These vertex approximations relied on the resummation of contributions in the ε-expansion coefficients with only a single or two internal space-time points to all orders in ε. The single-vertex approximation in (4.30) and (4.31), and the two-vertex approximation in (4.57) can also be examined in the limit of two space-time dimensions ($\delta \to 0$) to understand the asymptotic behavior of the p-point Green's functions in this limit better.

Using the asymptotic behavior (5.3) and (5.4) of the propagators to analyze the single-vertex approximation in (4.30) and (4.31), one finds that the leading-order asymptotic behavior takes the form

$$
\begin{aligned}
G_p^c(\varepsilon; y_1, \dots, y_p)\Big|_{k=1} \sim &-\frac{g}{2\sqrt{\pi}} \left(\pi\delta\right)^{p/2-1-\varepsilon/2} \frac{\Gamma(\frac{\varepsilon}{2}+2)\,\Gamma(\frac{\varepsilon}{2}+\frac{3}{2})}{\Gamma(\frac{\varepsilon}{2}+2-\frac{p}{2})} \cos(\tfrac{\pi\varepsilon}{2}) \\
&\times \int d^{2-\delta}x_1' \prod_{r=1}^{p} K_0(m|x_1'-y_r'|), \quad \text{as } \delta \to 0,
\end{aligned}
\tag{5.22}
$$

for even values of p, and

$$
\begin{aligned}
G_p^c(\varepsilon; y_1, \dots, y_p)\Big|_{k=1} \sim &-\frac{ig}{2\sqrt{\pi}} \left(\pi\delta\right)^{p/2-1-\varepsilon/2} \frac{\Gamma(\frac{\varepsilon}{2}+2)\,\Gamma(\frac{\varepsilon}{2}+\frac{3}{2})}{\Gamma(\frac{\varepsilon}{2}+2-\frac{p}{2})} \sin(\tfrac{\pi\varepsilon}{2}) \\
&\times \int d^{2-\delta}x_1' \prod_{r=1}^{p} K_0(m|x_1'-y_r'|), \quad \text{as } \delta \to 0,
\end{aligned}
\tag{5.23}
$$

for odd values of p. (Note that for $p = 2$ (4.31) contains an additional term, which is, however, of order $O(\delta^{p/2-1})$ and does thus not contribute at leading order.)

Remarkably, this single-vertex approximation is of the order $O(\delta^{p/2-1-\varepsilon/2})$, contrasting the $O(\delta^{p/2-1})$ behavior of the ε-expansion coefficients. Through the summation to all orders in ε, which constitutes the vertex-approximation scheme, the logarithmic contributions in the ε-expansion coefficients, cf. (5.6), are re-summed to an algebraic form, which promotes a divergent behavior of this approximation. This resembles the summation of logarithms employed by Cheng and Wu in high energy quantum electrodynamics [56]. Notably, the algebraic

dependence of the asymptotic behavior on ε affects the apparent freedom of the theory, which was obtained to all finite orders in ε in Section 5.1: For values $\varepsilon > 1$, the single-vertex approximation of the *three-point* Green's function becomes divergent, even though the ε-expansion coefficients vanish at each order in ε. Similarly, even-higher-order Green's functions diverge in the limit $\delta \to 0$ for sufficiently large values of ε.

Analyzing the asymptotic behavior of the two-vertex approximation (4.57) of the p-point Green's function is somewhat more cumbersome. The leading contribution depends in particular on the behavior of the function $L_{odd}(\frac{\varepsilon}{2}, \frac{\varepsilon}{2})$ in $w(\varepsilon/2)$ given by (4.41), which scales as $O(\delta^{1-\varepsilon})$ when $\delta \to 0$. Together with the prefactors in (4.57) the general leading-order asymptotic behavior of the two-vertex approximation is thus found to be of the order

$$G_p^c(\varepsilon; y_1, \dots, y_p)\big|_{k=2} \sim O(\delta^{p/2-1-\varepsilon}), \quad \text{as } \delta \to 0. \tag{5.24}$$

Notably, this is not of the same order as the single-vertex approximation in (5.22) and (5.23); the summation to all orders in ε here promotes a divergent behavior even further. For example, the two-vertex approximation of the three-point Green's function already diverges for $\varepsilon > 1/2$. The asymptotic behavior of the single-vertex and two-vertex approximations suggests that in higher-order vertex approximations the divergent behavior is promoted even further, so that at any given value of ε sufficiently high-order vertex approximations of all Green's functions diverge.

The apparent freedom of the theory in two space-time dimensions, observed in the nonlinearity expansion in Section 5.1, arises as a feature of the finite-order ε expansion, but breaks down when considering the vertex-approximation scheme that takes into account terms to all orders in ε. For further investigations of the $\mathcal{PT}$-symmetric $\phi^2(i\phi)^\varepsilon$ quantum field theory it is therefore imperative that a robust renormalization scheme is developed, which takes the divergence of high-order Green's functions that emerges beyond any finite order in the nonlinearity parameter into account.

Chapter 6

Concluding Remarks

The nonlinearity expansion was introduced as a powerful perturbation technique to address open questions of quantum field theory in [24–26] and it was adapted for the analysis of non-Hermitian $\mathcal{PT}$-symmetric quantum-field-theory models in [1]. This first part of the thesis has expanded upon the discussion in [1] in multiple ways:

The nonlinearity-expansion techniques introduced in [1] for a $\phi^2(i\phi)^\varepsilon$ theory without dimensional quantities were generalized beyond their application in first-order calculations for the corresponding model that includes dimensional parameters. They were then used to determine the general coefficient structure of the normalized partition function $\mathcal{Z}(\varepsilon)$ and the connected p-point Green's functions $G_p^c(\varepsilon; y_1, \ldots, y_p)$. Algebraic closed-form solutions were presented for these functions to second order and the coefficients of the related ground-state energy density $\mathcal{E}(\varepsilon)$ and of the effective mass $M^2(\varepsilon)$ were derived. The system was furthermore examined through first- and second-order vertex approximations which relate the nonlinearity expansion to the common coupling-constant expansion picture. These technical advances emphasize the conclusion of [1] that the nonlinearity expansion is a powerful technique that enables the investigation of non-Hermitian $\mathcal{PT}$-symmetric quantum field theories in D-dimensional Euclidean space-time. They also illustrate that the results of this artificial expansion can be related to an expansion in a natural parameter, such as the coupling constant, which allows one to examine the behavior of these theories from multiple perspectives.

The analysis of the ground-state energy-density coefficients of the $\phi^2(i\phi)^\varepsilon$ theory in both approximation schemes suggests that the characteristic spectral reality found in the quantum-mechanical case is retained in all space-time dimensions $D < 2$. In $2 < D < 4$ dimensions, however, these coefficients become complex functions. But the appearance of divergences in the vertex-approximation coefficients of the ground-state energy density, of the Green's functions, and of the effective mass indicate that the theory requires renormalization in this region. The apparent breakdown of the spectral reality in two dimensions and beyond therefore has to be reexamined after the renormalization of the system.

A first step towards renormalizing the theory in two dimensions was made in a perturbative scheme: Using a linear counterterm $v(\varepsilon)\phi$ and a mass counterterm the divergent behavior of the one-point Green's function and the effective mass were renormalized to second order in ε. In addition, the asymptotic analysis of the general Green's function coefficient structure indicated that all p-point Green's functions with $p > 2$ vanish in two dimensions, resulting in an apparently free theory. An analysis in the vertex-approximation scheme, however, signals that this freedom is an artifact of the perturbative nature of the nonlinearity expansion, which holds to any finite order in ε but not beyond all orders. As such, a perturbative renormalization scheme would appear unsuitable and a new robust scheme is required.

Overall, the technical generalizations presented in this first part allowed for significant progress towards understanding the behavior of the non-Hermitian $\mathcal{PT}$-symmetric $\phi^2(i\phi)^\varepsilon$ theory in D-dimensional space-time and first steps towards the renormalization of the system were made.

Part II

$\mathcal{PT}$ Symmetry in Fermionic Systems: Non-Hermitian Extensions of the Nambu–Jona-Lasinio model

---

Chapter 7

Introduction to $\mathcal{PT}$ Symmetry in Fermionic Field Theories

In 2010, Jones-Smith and Mathur [57] brought attention to a subtle but essential difference of fermionic $\mathcal{PT}$ theory compared to the bosonic case: While time reversal in a bosonic theory is always *even*, that is the time-reveral operator $\mathcal{T}$ satisfies $\mathcal{T}^2 = +1$, a fermionic system can have *odd* time reversal $\mathcal{T}^2 = -1$. This is a well established property of fermionic systems, see for example [58], but it becomes essential when considering a theory that is centered around the behavior under combined parity-reflection and time-reversal operations, namely $\mathcal{PT}$ theory.

On a fundamental level, the difference between systems with even and odd time reversal can be seen in the composition of the unbroken $\mathcal{PT}$-symmetry regime. Considering $\mathcal{PT}$-symmetric quantum mechanics for simplicity, one finds generally that the symmetry $[H, \mathcal{PT}] = 0$ of the Hamiltonian implies that, when ψ is an eigenstate with eigenvalue E, then the state $\mathcal{PT}\psi$ has the complex conjugate eigenvalue E^*, since $\mathcal{T}$ is an antilinear operation. When $\mathcal{T}^2 = +1$, an unbroken symmetry, that is when the eigenstate ψ itself is $\mathcal{PT}$-symmetric $\mathcal{PT}\psi = \psi$, thus entails that the energy is real, and vice-versa. However, for a system in which $\mathcal{T}^2 = -1$, there exists no state which satisfies $\mathcal{PT}\psi = \psi$ (as can be seen by operating with $\mathcal{PT}$ on both sides of the equation, implying that $-\psi = \psi$). Therefore, the characteristic reality of the eigenvalues in the unbroken $\mathcal{PT}$-symmetry phase does not originate in the symmetry of the eigenstate, but rather in the degeneracy of the states ψ and $\mathcal{PT}\psi$. This occurrence of doubly degenerate real eigenvalues in the unbroken phase for $\mathcal{T}^2 = -1$ is analogous to Kramer's theorem in conventional quantum mechanics [59] and differs fundamentally from the case when $\mathcal{T}^2 = +1$.

A more immediate consequence of having odd instead of even time reversal is the structure of the operator $\mathcal{T}$. Evidently, the time-reversal operator satisfying $\mathcal{T}^2 = -1$ differs from the one satisfying $\mathcal{T}^2 = +1$. But this affects the question of whether or not an interaction term is $\mathcal{PT}$-symmetric or not. Consider, for example, the system with Hamiltonian density

$$\mathcal{H} = \bar{\psi}(-i\gamma^k \partial_k + m_0 + g\gamma_5)\psi, \tag{7.1}$$

which was introduced in [60] and extends the Hamiltonian density of the free Dirac fermion by a non-Hermitian pseudoscalar mass term. Here the mass parameter $g \in \mathbb{R}$, and γ_5 denotes the fifth Dirac matrix [58]. Following the recent discussion in [61] one observes:

In $1 + 1$ dimensional space-time the Dirac matrices are

$$\gamma^0 = \begin{pmatrix} 0 & 1 \\ 1 & 0 \end{pmatrix}, \quad \gamma^1 = \begin{pmatrix} 0 & 1 \\ -1 & 0 \end{pmatrix}, \quad \gamma_5 = \gamma^0 \gamma^1, \tag{7.2}$$

and the parity-reflection and time-reversal operators are given by

$$
\begin{aligned}
\mathcal{P} &: \psi(t, \mathbf{x}) \to \mathcal{P}\psi(t, \mathbf{x})\mathcal{P}^{-1} = \gamma^0 \psi(t, -\mathbf{x}), \\
\mathcal{T} &: \psi(t, \mathbf{x}) \to \mathcal{T}\psi(t, \mathbf{x})\mathcal{T}^{-1} = \gamma^0 \psi^*(-t, \mathbf{x}).
\end{aligned}
\tag{7.3}
$$

In particular, $\mathcal{T}^2 = +1$, that is time-reversal is even. And notably, the pseudoscalar mass term $g\gamma_5$ in (7.1) is $\mathcal{PT}$-symmetric, that is it commutes with the $\mathcal{PT}$ operator: $[\mathcal{PT}, g\gamma_5] = 0$. The modified Dirac fermion therefore describes a $\mathcal{PT}$-symmetric system in $1 + 1$ dimensions.

In $3 + 1$ dimensional space-time, on the other hand, the Dirac matrices are

$$\gamma^0 = \begin{pmatrix} \mathbb{1} & 0 \\ 0 & -\mathbb{1} \end{pmatrix}, \quad \gamma^k = \begin{pmatrix} 0 & \sigma^k \\ -\sigma^k & 0 \end{pmatrix}, \quad \gamma_5 = i\gamma^0 \gamma^1 \gamma^2 \gamma^3, \tag{7.4}$$

where σ^k with $k \in [1, 3]$ are the Pauli matrices. The parity-reflection and time-reversal operators are now given by

$$
\begin{aligned}
\mathcal{P} &: \psi(t, \mathbf{x}) \to \mathcal{P}\psi(t, \mathbf{x})\mathcal{P}^{-1} = \gamma^0 \psi(t, -\mathbf{x}), \\
\mathcal{T} &: \psi(t, \mathbf{x}) \to \mathcal{T}\psi(t, \mathbf{x})\mathcal{T}^{-1} = i\gamma^1 \gamma^3 \psi^*(-t, \mathbf{x}).
\end{aligned}
\tag{7.5}
$$

Contrary to the $1+1$ dimensional version, here $\mathcal{T}^2 = -1$, that is time reversal is odd. Furthermore, the pseudoscalar mass term $g\gamma_5$ in (7.1) now anticommutes with the $\mathcal{PT}$ operator: $\{\mathcal{PT}, g\gamma_5\} = 0$. It is an anti-$\mathcal{PT}$-symmetric term, and thus the model (7.1), having $\mathcal{PT}$-symmetric and anti-$\mathcal{PT}$-symmetric contributions, has no overall $\mathcal{PT}$ symmetry in $3+1$ dimensions.

This illustrates how the question of evenness or oddness of the time reversal $\mathcal{T}$ can influence the symmetry of the model under consideration. But remarkably, whether $\mathcal{PT}$-symmetric or not, the dispersion relation of the non-Hermitian model (7.1) studied in [60] remains the same: From the equation of motion associated with $\mathcal{H}$ in (7.1),

$$(i\not{\partial} - m_0 - g\gamma_5)\psi(t, \mathbf{x}) = 0, \tag{7.6}$$

multiplication with $(i\not{\partial} + m_0 - g\gamma_5)$ gives rise to the Klein-Gordon equation

$$(\partial^2 + m^2)\psi(t, \mathbf{x}) = 0, \quad \text{with} \quad m^2 = m_0^2 - g^2. \tag{7.7}$$

The effective mass m of the theory is therefore only real in the presence of a sufficiently large bare mass term m_0. If the bare mass vanishes, however, the effective mass m is inherently complex, independent of the parameter g. When the model is $\mathcal{PT}$ symmetric, as in $1+1$ dimensions, (7.7) describes a system with phases of broken and unbroken $\mathcal{PT}$ symmetry, transitioning at $m_0^2 = g^2$. However, even without $\mathcal{PT}$ symmetry being present, as in $3+1$ dimensions, these spectral phases are maintained.

This simple example shows that odd time-reversal symmetry has a significant effect on $\mathcal{PT}$ theories and it raises immediate questions: For one, while the $3+1$ dimensional version of the non-Hermitian model with Hamiltonian density (7.1) is not $\mathcal{PT}$ symmetric, a bilinear interaction term other than the pseudoscalar mass term $g\gamma_5$ can preserve $\mathcal{PT}$ symmetry. In [61] two such models of $\mathcal{PT}$ fermions in $3+1$ dimensions were identified and their dispersion relations were studied. Furthermore, the existence of real mass solutions (7.7) in the presence of a finite bare mass m_0 challenges the idea that it is $\mathcal{PT}$ symmetry causing the occurrence of real solutions. Including other non-Hermitian non-$\mathcal{PT}$-symmetric interaction terms instead of the pseudoscalar mass $g\gamma_5$ could clarify this relation. Beyond these variations of the model (7.1), the breakdown of a phase with real mass

solutions in the absence of a bare mass term, even in the $\mathcal{PT}$-symmetric model in $1+1$ dimensions, is a curious feature that raises the question as to which role higher-order interactions play. A discussion of the (bosonic, that is $\mathcal{T}^2 = +1$) quantum-mechanical system with Hamiltonian of the form

$$H = p^2 + (m_0^2 - g^2)x^2 - Gx^4 \tag{7.8}$$

in [62] (see also [63]) illustrates the idea, that higher-order interactions might mimic the effect of m_0 and restore a regime with real solutions: For $G = m_0 = 0$ the system has complex eigenvalues. But for $G \neq 0$ it was demonstrated that the system is spectrally equivalent to a Hermitian Hamiltonian with a real spectrum for all values of g and m_0, in particular for $m_0 = 0$.

In the context of relativistic fermionic quantum theory, a suitable model to study the influence of higher-order interactions on modified Dirac fermions, such as (7.1), is the Nambu–Jona-Lasinio (NJL) model [64,65]. It is briefly introduced, modified, and analyzed throughout this part of the thesis. Central results of this study were previously presented in two papers [66, 67]. The following discussion combines these studies and presents all essential features of the topic.

While $\mathcal{PT}$ theory has become a highly active field of research, there are still relatively few studies of fermionic theories. Following the formalism of Jones-Smith and Mathur [57] for odd time-reversal symmetry, Bender and Klevansky have studied $\mathcal{PT}$-symmetric representations of fermionic algebras [68]. This work was expanded upon in [69] and [70,71], relating it to an early study of Mostafazadeh [72] on fermionic algebras in pseudo-Hermitian quantum mechanics as well. In addition, Jones-Smith and Mathur demonstrated in [73] that when incorporating odd time-reversal symmetry, $\mathcal{PT}$ fermions might give rise to new types of flavor oscillations in the context of the standard model, establishing the potential relevance of such models to neutrino physics. Non-Hermitian neutrino oscillations were investigated further in [74], and in [75] Alexandre, Bender, and Millington proposed a non-Hermitian Yukawa model, which presents a possible explanation for small masses of light neutrinos. The generation of light neutrino masses through the presence of axion-like particles has recently been discussed in other non-Hermitian Yukawa-type models [76, 77] as well. The discussion of

non-Hermitian fermions beyond that in (7.1) within this thesis is of direct interest to these ongoing developments in fermionic $\mathcal{PT}$ theory. In particular, the qualitative behavior of the modified NJL model might be of interest to non-Hermitian Yukawa-type models, since such models can, at least in principle, be obtained from the two-body interactions of the NJL model through partial bosonization [78]. In fact, the investigations in [76, 77] have taken some of these aspects into account and demonstrated qualitative agreements.

This study is structured as follows:

In Chapter 8 the NJL model is introduced and modified through non-Hermitian bilinear terms. All possible terms of this nature are identified and their behavior under $\mathcal{PT}$ symmetry and chiral symmetry is discussed. The question of the Lorentz symmetry of the model is addressed as well.

In Chapter 9 the gap equation of the modified NJL model is derived for all non-Hermitian extensions and the effective mass solutions for all models are evaluated in the chiral limit of vanishing bare mass. Their behavior is discussed in the light of dynamical mass generation.

In Chapter 10 the meson mass equation is derived and solved for all models that allow for dynamically generated fermion masses.

In Chapter 11 the discussion of the modified NJL model is supplemented by the analysis of similar non-Hermitian extensions to the chiral Gross-Neveu (GN) model which can be considered as a $1+1$ dimensional analogue of the NJL system.

Concluding remarks are presented in Chapter 12.

Chapter 8

The Modified Nambu–Jona-Lasinio Model

The NJL model [64, 65] is a fermionic theory in which masses for Dirac fermions are generated through an attractive chirally symmetric two-body interaction of bare fermions. This mass generation of the individual fermion, as well as that of mesonic (fermion-antifermion) bound states, is a consequence of spontaneous chiral symmetry breaking within the model. In this it parallels the Bardeen-Cooper-Schrieffer theory of superconductivity [79], where the generated bound states are instead pairs of like particles, namely electrons with opposite spin (Cooper-pairs). First proposed before the development of quantum chromodynamics (QCD), the NJL model was initially constructed as a nucleon theory. It has since been reinterpreted as an effective theory with quark degrees of freedom, which approximates the behavior of QCD in the low-energy limit. A detailed overview of the development within this context can be found, for example, in [80]. The introduction of the NJL model and its modification through non-Hermitian terms in this chapter closely follows the presentation in the previously published analyses of this subject in [66, 67].

For two flavors of quarks ($N_f = 2$), the Hamiltonian density of the standard NJL model has the form

$$\mathcal{H}_{\mathrm{NJL}} = \bar{\psi}(-i\gamma^k \partial_k + m_0)\psi - G[(\bar{\psi}\psi)^2 + (\bar{\psi}i\gamma_5\vec{\tau}\psi)^2] \tag{8.1}$$

in terms of the Dirac matrices γ with $k \in [1, 3]$, the isospin SU(2) matrices $\vec{\tau}$, and the two-body coupling strength G. In addition, (8.1) includes a bare fermion mass $m_0 = m_u = m_d$. While the two-body interaction term is chirally symmetric, the

mass term m_0 breaks this symmetry explicitly. In the limit of vanishing bare mass, (8.1) describes a chirally symmetric theory that allows the study of spontaneous symmetry breaking; this limit is therefore commonly referred to as the chiral limit of the theory. In this case, a sufficiently strong two-body interaction generates an effective fermion mass, which is identified with the valence quark mass in the context of QCD, and furthermore gives rise to a massless Nambu-Goldstone boson in form of the pseudoscalar bound state. Including a small bare mass term m_0 (relative to the effective mass generated in the chiral limit) affects the fermion and meson masses only slightly. Therefore, even though m_0 breaks the chiral symmetry of the system, the model is called *approximately* symmetric. The resulting light pseudoscalar bound state, referred to as a pseudo-Goldstone boson, is identified with the pion in QCD. The generation of the effective fermion mass, as well as the masses of both the scalar (σ meson) and the pseudoscalar (π meson) bound states is discussed in detail in the following chapters.

While chiral symmetry breaking can be studied within the NJL model to great effect, it has to be stressed that it is inherently an effective model which is not renormalizable in $3 + 1$ dimensional space-time and requires the specification of a regularization scheme, such as the four-momentum Euclidean cutoff scheme used in this thesis. The model does not describe a consistent physical system by itself and has to be understood as an approximation in the context of a more general theory, such as QCD. Nevertheless it is not necessary to identify the fermions of the NJL model with quarks; it can be discussed as a general fermionic model with chiral symmetry. However, the numerical analyses in this thesis are based on quantities established within the QCD interpretation: A four-momentum Euclidean cutoff scale of $\Lambda = 1015$ MeV is used for the purpose of regularization and the two-body coupling strength is chosen as $G\Lambda^2 = 3.93$, see [80].

8.1 Non-Hermitian Extension

In the following study, the $3+1$ dimensional NJL model (8.1) is modified through the introduction of various possible non-Hermitian bilinear terms. These bilinears of the fermionic field ψ and its conjugate $\bar{\psi}$ have the general form $\bar{\psi}\Gamma\psi$, containing

a complex 4×4 matrix Γ. The Hamiltonian density of such a model has the form

$$\mathcal{H} = \bar{\psi}(-i\gamma^k \partial_k + m_0 + g\Gamma)\psi - G[(\bar{\psi}\psi)^2 + (\bar{\psi}i\gamma_5\vec{\tau}\psi)^2], \tag{8.2}$$

where $g \in \mathbb{R}$ is the associated coupling constant.

To identify all possible non-Hermitian modifications Γ, consider the complete set of 4×4 matrices, as generated by the Dirac matrices γ: Any matrix can be written as a real superpositions of the following 32 matrices:

$$\begin{matrix} \mathbb{1}, & \gamma_5, & \gamma^\mu, & \gamma_5\gamma^\mu, & \gamma^\mu\gamma^\nu, \\ i\mathbb{1}, & i\gamma_5, & i\gamma^\mu, & i\gamma_5\gamma^\mu, & i\gamma^\mu\gamma^\nu, \end{matrix} \tag{8.3}$$

where $\mu \leq \nu$ denote the spin indices. They behave, from left to right, as scalars, pseudoscalars, vectors, pseudovectors, and antisymmetric second-rank tensors under observer Lorentz transformations. Based on these matrices, the following structurally distinct modifications are identified

$$\begin{matrix} \mathbb{1}, & \gamma_5, & A_\mu\gamma^\mu, & \gamma_5 B_\mu\gamma^\mu, & F_{\mu\nu}\gamma^\mu\gamma^\nu, \\ i\mathbb{1}, & i\gamma_5, & iA_\mu\gamma^\mu, & i\gamma_5 B_\mu\gamma^\mu, & iF_{\mu\nu}\gamma^\mu\gamma^\nu, \end{matrix} \tag{8.4}$$

in which A_μ and B_μ are real vector elements, and $F_{\mu\nu}$ are real elements of an antisymmetric matrix. Considering that including an imaginary unit into any bilinear changes it from being symmetric under Hermitian conjugation to being antisymmetric, and vice versa, demonstrates that only half of the terms in (8.4) result in non-Hermitian modifications in the model (8.2). Namely those, for which Γ takes one of the forms

$$i\mathbb{1}, \quad \gamma_5, \quad iA_\mu\gamma^\mu, \quad i\gamma_5 B_\mu\gamma^\mu, \quad F_{\mu\nu}\gamma^\mu\gamma^\nu. \tag{8.5}$$

These terms establish the non-Hermitian extensions of the NJL model that are considered in the following analysis.

Notice that the bilinears $\bar{\psi}\Gamma\psi$, with Γ being one of the terms in (8.5), are either Lorentz scalars or Lorentz pseudoscalars, depending in particular on the behavior of the background fields A_μ, B_μ, and $F_{\mu\nu}$ under Lorentz transformations. In the pseudoscalar case the modified NJL model (8.2) is not Lorentz invariant.

Nonetheless, these systems are analyzed for the following reason: Like the NJL model itself, the modified versions have to be understood as effective models which result as approximations of a more fundamental theory. It has been proposed that such an approximation process can result in the occurrence of Lorentz-symmetry-breaking terms [81–83]. The nature of this process, especially in the context of $\mathcal{PT}$-symmetric and non-Hermitian models, is the topic of ongoing investigation. Therefore, the inclusion of Lorentz pseudoscalar bilinears in the modified NJL model has not been ruled out in this discussion. Moreover, one finds that the calculation of fermion and meson masses in the following analyses is not affected by the behavior of the background fields under Lorentz transformations.

Under the combined parity reflection $\mathcal{P}$ and time reversal $\mathcal{T}$ in 3+1 dimensional space-time, as given in (7.5), only two of the non-Hermitian bilinears $\bar{\psi}\Gamma\psi$, with Γ as in (8.5), are symmetric, that is $[\mathcal{PT}, \Gamma] = 0$:

$$\Gamma_{PT_1} = i\gamma_5 B_\mu \gamma^\mu \qquad \text{and} \qquad \Gamma_{PT_2} = F_{\mu\nu}\gamma^\mu\gamma^\nu. \tag{8.6}$$

For these terms, the modified NJL model (8.2) is a $\mathcal{PT}$-symmetric theory. The bilinears based on the remaining three choices of Γ in (8.5) are anti-$\mathcal{PT}$-symmetric, that is $\{\mathcal{PT}, \Gamma\} = 0$, and will in the following be referred to as

$$\Gamma_{aPT_1} = iA_\mu \gamma^\mu, \qquad \Gamma_{aPT_2} = \gamma_5, \qquad \Gamma_{aPT_3} = i\mathbb{1}. \tag{8.7}$$

While the bilinears themselves are anti-$\mathcal{PT}$-symmetric, the modified NJL models that include these terms have no such overall symmetry. They are non-Hermitian and non-$\mathcal{PT}$-symmetric systems.

Moreover, out of the five non-Hermitian bilinears based on (8.5), only two preserve chiral symmetry: Only

$$\Gamma_{aPT_1} = iA_\mu \gamma^\mu \qquad \text{and} \qquad \Gamma_{PT_1} = i\gamma_5 B_\mu \gamma^\mu \tag{8.8}$$

anticommute with γ_5, so that the bilinears $\bar{\psi}\Gamma_{PT_1}\psi$ and $\bar{\psi}\Gamma_{aPT_1}\psi$ are invariant under the axial flavor transformation $\psi \to e^{i\alpha\vec{\tau}\gamma_5}\psi$, where $\alpha \in \mathbb{R}$. Combined with the symmetry under the vector flavor transformation $\psi \to e^{i\alpha\vec{\tau}}\psi$, which is satisfied by all bilinears $\bar{\psi}\Gamma\psi$ based on (8.5), one therefore finds that only the modified

NJL models with the non-Hermitian extensions in (8.8) are chirally symmetric theories. In the models based on

$$\Gamma_{PT_2} = F_{\mu\nu}\gamma^\mu\gamma^\nu, \qquad \Gamma_{aPT_2} = \gamma_5, \qquad \Gamma_{aPT_3} = i\mathbb{1} \qquad (8.9)$$

chiral symmetry is broken explicitly, similar to the effect of the bare mass term m_0. The limit of vanishing bare mass is thus not a chiral limit.

Taking previous analyses of non-Hermitian Dirac fermions into account, the study of the modified NJL model can be seen from two perspectives: On one hand, the non-Hermitian Dirac fermions display a curious breakdown of real mass solutions in the limit of vanishing bare fermion mass [60, 61]. Studying the mass generation in the modified NJL model thus allows one to address the question of whether two-body interactions can mimic the effect of a bare mass term and restore a region of real mass solutions even in the limit of vanishing bare fermion mass. The investigation of all possible non-Hermitian extensions of the NJL model, not only $\mathcal{PT}$ symmetric ones, furthermore addresses the question which role $\mathcal{PT}$ symmetry plays in the generation of real solutions. This aspect is explored further by contrasting the results of the $3 + 1$ dimensional modified NJL model with those of the $1 + 1$ dimensional analogue, the modified chiral Gross-Neveu model. On the other hand, the modified NJL model can be seen as precisely that: a non-Hermitian extension of the standard NJL model. This rather raises the question of how the behavior of the NJL model, in form of the generated fermion and meson masses, is affected by the inclusion of non-Hermitian bilinear additions, be they $\mathcal{PT}$ symmetric or not.

These viewpoints come with an intuitive approach to which coupling constant is varied and which is kept fixed: The first perspective suggests a variation of the two-body coupling G, while the latter that of the non-Hermitian coupling g. Overall, it is of course primarily the relative size of both contributions that is important. In the following analyses the two-body coupling constant G is kept fixed initially, so that the modified NJL model remains connected to the context of QCD that is established in the standard NJL model. Nevertheless, the results are discussed from both points of view.

Chapter 9

The Effective Fermion Mass

The effective fermion mass m of the standard NJL model can be determined approximately in a self-consistent approach through the gap equation, which is obtained in Feynman-Dyson perturbation theory. Its study in this chapter follows [80, 84] and the presentation closely follows that of the published discussions [66, 67]. The full fermion propagator S is expressed in terms of the propagator $S^{(0)}$ of the free theory, which is unperturbed by the two-body interactions, and the proper self-energy Σ through the (algebraic) Dyson equation:

$$
iS_{\alpha\beta}(k) = iS_{\alpha\beta}^{(0)}(k) + \left[iS_{\alpha\lambda}^{(0)}(k)\right]\left[-i\Sigma_{\lambda\mu}(k)\right]\left[iS_{\mu\beta}(k)\right], \tag{9.1}
$$

where α, β, λ, and μ denote combined color, flavor, and spin indices, and k is a four-momentum dependence. At first order the proper self-energy comprises two contributions, the Hartree term and the Fock term, which are shown in the schematic visualization of (9.1) in Figure 9.1. Even though the two-body interaction of the NJL model is a point interaction, a finite range has been introduced in form of the wavy line in the diagrammatic representation for simplicity of visualization. Considering that the two-body interaction of the NJL model (8.1) consists of a scalar $(\bar{\psi}\psi)^2$ and a pseudoscalar $(\bar{\psi}i\gamma_5\vec{\tau}\psi)^2$ contribution, the proper self-energy is calculated using the appropriate Feynman rules as follows.
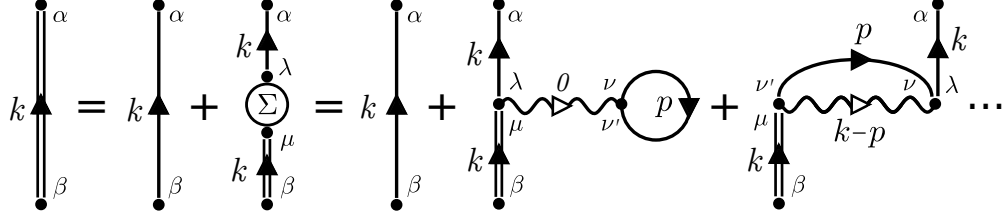
Figure 9.1: Schematic visualization of the algebraic Dyson equation to first order. Shown are in particular the Hartree and Fock terms of the proper self-energy Σ.

The Hartree term for the scalar interaction evaluates to

$$
\begin{aligned}
-i\Sigma^s_{\text{Hartree},\lambda\mu}(k) &= (-1)\int \frac{d^4p}{(2\pi)^4}\left[-i(-2G\,\delta_{\lambda\mu}\delta_{\nu\nu'})\right]\left[iS^{(0)}_{\nu\nu'}(p)\right] \\
&= 2GN_cN_f\,\delta_{\lambda\mu}\int\frac{d^4p}{(2\pi)^4}\,\text{tr}[S^{(0)}(p)],
\end{aligned}
\tag{9.2}
$$

where the factor of two originates in the symmetry of the interaction under the exchange $(\lambda,\mu)\leftrightarrow(\nu,\nu')$ and a factor of (-1) arises due to the closed fermion loop. The trace over the color and flavor indices was evaluated and tr denotes the spinor trace only. The Hartree term for the pseudoscalar interaction,

$$
-i\Sigma^{ps}_{\text{Hartree},\lambda\mu}(k) = (-1)\int\frac{d^4p}{(2\pi)^4}\left[-i(-2G(i\gamma_5\vec{\tau})_{\lambda\mu}(i\gamma_5\vec{\tau})_{\nu\nu'})\right]\left[iS^{(0)}_{\nu\nu'}(p)\right] = 0,
\tag{9.3}
$$

vanishes because of the flavor trace over $\vec{\tau}$. The Fock term of the scalar interaction becomes

$$
-i\Sigma^s_{\text{Fock},\lambda\mu}(k) = \int\frac{d^4p}{(2\pi)^4}\left[-i(-2G\,\delta_{\lambda\nu}\delta_{\nu'\mu})\right]\left[iS^{(0)}_{\nu\nu'}(p)\right] = -2G\int\frac{d^4p}{(2\pi)^4}\,S^{(0)}_{\lambda\mu}(p),
\tag{9.4}
$$

and the Fock term of the pseudoscalar interaction is

$$
\begin{aligned}
-i\Sigma^{ps}_{\text{Fock},\lambda\mu}(k) &= (-1)\int\frac{d^4p}{(2\pi)^4}\left[-i(-2G(i\gamma_5\vec{\tau})_{\lambda\nu}(i\gamma_5\vec{\tau})_{\nu'\mu})\right]\left[iS^{(0)}_{\nu\nu'}(p)\right] \\
&= 6G\,\delta_{f_\lambda f_\mu}\,\delta_{c_\lambda c_\mu}\int\frac{d^4p}{(2\pi)^4}\left[\gamma_5 S^{(0)}(p)\gamma_5\right]_{s_\lambda s_\mu},
\end{aligned}
\tag{9.5}
$$

using that the trace of $\vec{\tau}^2$ over the flavor indices is $3\delta_{f_\lambda f_\mu}$ and the trace over the color indices yields $\delta_{c_\lambda c_\mu}$.

In the context of QCD, the NJL model describes an effective model of quark interactions in the limit of large N_c while $GN_c \sim O(1)$, see [85, 86]. As such, the Hartree-Fock approximation is to be understood as a first-order contribution in a $1/N_c$ expansion, compare [87]. In this picture, only the Hartree contribution describes a leading-order term due to the dependence on the factor GN_c in (9.2). The Fock contributions are of order $O(N_c^{-1})$. Since any other next-to-leading order terms arising beyond the Hartree-Fock approximation have been disregarded, the Fock terms are omitted likewise in the following. The approximate proper self-energy thus becomes

$$-i\Sigma_{\lambda\mu}(k) = 2GN_cN_f\,\delta_{\lambda\mu}\int\frac{d^4p}{(2\pi)^4}\,\mathrm{tr}[S^{(0)}(p)]. \tag{9.6}$$

By replacing the dependence of Σ in (9.6) on the free-theory propagator $S^{(0)}$ with the full fermion propagator S, this first-order approximation can be improved upon in a self-consistent way: Together with the Dyson equation (9.1) such a replacement describes an infinite-order approximate series. Noticing furthermore that the expression in (9.6) is independent of the four-momentum k, and therefore a constant, one can identify

$$\Sigma_{\lambda\mu}^{sc}(k) = 2iGN_cN_f\,\delta_{\lambda\mu}\int\frac{d^4p}{(2\pi)^4}\,\mathrm{tr}[S(p)] = (m - m_0)\,\delta_{\lambda\mu}, \tag{9.7}$$

where m plays the role of an effective mass. This identification of the effective mass becomes clear when considering that the free-theory propagator satisfies the equation of motion

$$(\not{k} - m_0)\,S_{\alpha\beta}^{(0)}(k) = \mathbb{1}\,\delta_{\alpha\beta}. \tag{9.8}$$

Acting with $(\not{k} - m_0)$ on the Dyson equation (9.1) and identifying the proper self-energy according to (9.7) then results upon rearrangement in the equation of motion of the full fermion propagator

$$(\not{k} - m)\,S_{\alpha\beta}(k) = \mathbb{1}\,\delta_{\alpha\beta}, \tag{9.9}$$

in which the nature of m as effective mass becomes apparent. The result (9.7) for the self-energy thus determines the gap equation of the standard NJL model:

$$m = m_0 + 2iGN_cN_f\int\frac{d^4p}{(2\pi)^4}\,\mathrm{tr}[S(p)]. \tag{9.10}$$

For the Dirac fermion propagator

$$S(p) = (\not{p} - m)^{-1} = \frac{\not{p} + m}{p^2 - m^2}, \quad \text{with} \quad \text{tr}[S(p)] = \frac{4m}{p^2 - m^2}, \tag{9.11}$$

the gap equation (9.10) is evaluated in the chiral limit $(m_0 \to 0)$ and the four-momentum Euclidean cutoff regularization by letting $p_0 = ip_4$ and introducing the radial cutoff scale Λ: With $p_E^2 = p_1^2 + ... + p_4^2 = -p^2$ equation (9.10) becomes

$$1 = 8GN_cN_f \int^{\Lambda} \frac{d^4p_E}{(2\pi)^4} \frac{1}{p_E^2 + m^2} = \frac{GN_cN_f}{2\pi^2} \int_0^{\Lambda} dr \frac{2r^3}{r^2 + m^2}. \tag{9.12}$$

Integration results in the established gap equation within this regularization scheme

$$\frac{2\pi^2}{\tilde{G}N_cN_f} = 1 - \tilde{m}^2 \ln\left(1 + \frac{1}{\tilde{m}^2}\right) \tag{9.13}$$

in terms of the rescaled quantities $\tilde{m} = m\Lambda^{-1}$ and $\tilde{G} = G\Lambda^2$.

This equation can be solved in terms of the Lambert W function [88] with the result that

$$\tilde{m} = \left[\tfrac{1}{c}W_{-1}(c\,e^c) - 1\right]^{-1/2}, \quad \text{where} \quad c = \frac{2\pi^2}{\tilde{G}N_cN_f} - 1. \tag{9.14}$$

For $N_c = 3$, $N_f = 2$, and with $\Lambda = 1015$ MeV and $G\Lambda^2 = 3.93$, which are traditionally determined within the given regularization scheme from the pion decay constant $f_\pi = 93$ MeV and the quark condensate density per flavor $\langle \bar{u}u \rangle = \langle \bar{d}d \rangle = (-250\,\text{MeV})^3$, see [80], the gap equation (9.13) results in an effective mass of $m_{NJL} = 238$ MeV. In Figure 9.2 the behavior of the mass solution under variation of the two-body coupling $\tilde{G}$ is shown, demonstrating that the generation of an effective fermion mass requires sufficiently strong two-body interactions in the standard NJL model. In fact, the critical coupling $\tilde{G}_{\text{crit}}$, above which the spontaneously broken chiral symmetry gives rise to finite mass solutions, is determined by the constant c in (9.14): When c is positive no real mass is generated, but when c becomes negative a finite mass solution can be found. The phase transition arises at $c = 0$, that is $\tilde{G}_{\text{crit}} = \pi^2/3$. The behavior when including a small chiral-symmetry-breaking bare mass m_0 is shown for comparison.
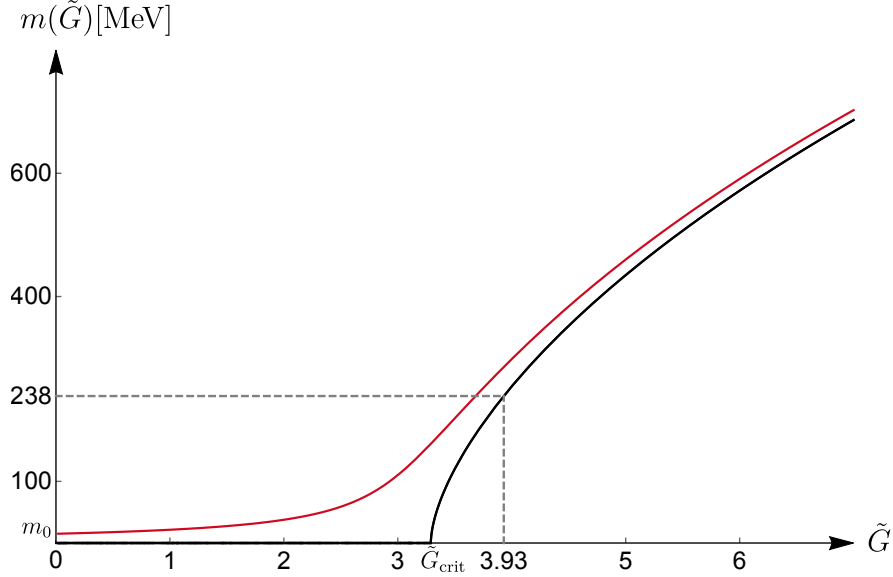
Figure 9.2: Behavior of the effective mass m of the NJL model as a function of the two-body coupling strength $\tilde{G}$. A phase transition occurs at $\tilde{G}_{\text{crit}} = \pi^2/3$, after which finite mass solutions are generated in the model. The behavior when including a small bare mass m_0 is shown as red line for comparison.

For the non-Hermitian extensions of the standard NJL model that were identified in the previous chapter, the structure of the two-body interactions remains unchanged, so that the general form of the gap equation (9.10) persists. However, the bilinear modifications in the non-Hermitian models do change the structure of the free-theory propagator (9.8), as the free theory now describes various non-Hermitian extensions of the Dirac fermion. In the general modified model with Hamiltonian density (8.2) the spinor trace $\text{tr}[S(p)]$ in the gap equation is now based on the fermion propagator satisfying the equation of motion

$$(\not{p} - m - g\Gamma)\, S(p) = \mathbb{1}, \tag{9.15}$$

with Γ being one of the non-Hermitian terms in (8.5). Evaluating these traces and the resulting gap equations is the subject of this chapter. In Section 9.1 and Section 9.2 the non-Hermitian $\mathcal{PT}$-symmetric modified models are analyzed, Section 9.3 to Section 9.5 discuss the non-Hermitian non-$\mathcal{PT}$-symmetric extensions. The results are summarized in Section 9.6.

9.1 The Fermion Mass for $\Gamma_{PT_1} = i\gamma_5 B_\mu \gamma^\mu$

The fermion propagator (9.15) for the non-Hermitian NJL model based on the $\mathcal{PT}$-symmetric and chirally symmetric extension term $\Gamma_{PT_1} = i\gamma_5 B_\mu \gamma^\mu$ is formally given as

$$S(p) = (\not{p} - m - ig\gamma_5 B_\mu \gamma^\mu)^{-1}. \tag{9.16}$$

To evaluate the spinor trace $\mathrm{tr}[S(p)]$ this expression is recast into a form with a scalar denominator: An expansion of (9.16) with the factor $(\not{p} + m + ig\gamma_5 B_\nu \gamma^\nu)$ yields the denominator

$$\begin{aligned}
& (\not{p} - m - ig\gamma_5 B_\mu \gamma^\mu)(\not{p} + m + ig\gamma_5 B_\nu \gamma^\nu) \\
& = p^2 - m^2 - g^2 B^2 - 2igm\gamma_5 B_\mu \gamma^\mu - 2igB_\mu p^\mu \gamma_5,
\end{aligned} \tag{9.17}$$

using that $\gamma_5 \gamma^\mu \not{p} - \not{p}\gamma_5 \gamma^\mu = 2p^\mu \gamma_5$. The last two terms are still not scalar, but under expansion with a factor of the same form as (9.17), but with opposite sign in those two terms, the denominator becomes

$$\begin{aligned}
& [p^2 - m^2 - g^2 B^2 - 2igm\gamma_5 B_\mu \gamma^\mu - 2igB_\mu p^\mu \gamma_5] \\
& \times [p^2 - m^2 - g^2 B^2 + 2igm\gamma_5 B_\nu \gamma^\nu + 2igB_\nu p^\nu \gamma_5] \\
& = (p^2 - m^2 - g^2 B^2)^2 - 4g^2 m^2 B^2 + 4g^2 (B_\mu p^\mu)^2.
\end{aligned} \tag{9.18}$$

Thus the fermion propagator (9.16) takes the form

$$S(p) = \frac{(\not{p} + m + ig\gamma_5 B_\mu \gamma^\mu)[p^2 - m^2 - g^2 B^2 + 2igm\gamma_5 B_\nu \gamma^\nu + 2igB_\nu p^\nu \gamma_5]}{(p^2 - m^2 - g^2 B^2)^2 - 4g^2 m^2 B^2 + 4g^2 (B_\mu p^\mu)^2}. \tag{9.19}$$

The spinor trace of the terms in the numerator vanishes for all but the combinations $\mathrm{tr}[\gamma^\mu \gamma^\nu] = 4\eta^{\mu\nu}$ and $\mathrm{tr}[\mathbb{1}] = 4$, resulting in the trace of the fermion propagator

$$\mathrm{tr}[S(p)] = \frac{4m(p^2 - m^2 + g^2 B^2)}{(p^2 - m^2 - g^2 B^2)^2 - 4g^2 m^2 B^2 + 4g^2 (B_\mu p^\mu)^2}. \tag{9.20}$$

In the chiral limit of vanishing bare mass, the gap equation (9.10) thus becomes

$$m = \frac{2iGN_cN_f}{(2\pi)^4} I_{PT_1},$$

(9.21)

with

$$I_{PT_1} = 4m \int d^4p \, \frac{p^2 - m^2 + g^2B^2}{(p^2 - m^2 - g^2B^2)^2 - 4g^2m^2B^2 + 4g^2(B_\mu p^\mu)^2}.$$

(9.22)

The four-momentum integral (9.22) can be evaluated in the Euclidean four-momentum cutoff regularization by first transforming to Euclidean coordinates, that is letting $p_0 = ip_4$ and choosing $B_0 = iB_4$ so that $p_E^2 = p_1^2 + ... + p_4^2 = -p^2$, $B_E^2 = -B^2$, and $B_\mu p^\mu = -B_E \cdot p_E$ in the Euclidean dot product:

$$I_{PT_1} = -4im \int d^4p_E \, \frac{p_E^2 + m^2 + g^2B_E^2}{(p_E^2 + m^2 - g^2B_E^2)^2 + 4g^2m^2B_E^2 + 4g^2(B_E \cdot p_E)^2}.$$

(9.23)

In a spherical coordinate system with zenith direction B_E, the product $B_E \cdot p_E = |B_E||p_E|\cos\theta$ depends only on the radial component $|p_E|$ and the zenithal angle θ. The four-momentum cutoff scale Λ is then introduced as a radial integration limit, yielding:

$$I_{PT_1} = -16i\pi m \int_0^\Lambda dr \, \frac{r(r^2 + m^2 + g^2B_E^2)}{4g^2B_E^2} \int_0^\pi d\theta \frac{\sin^2\theta}{f(r) - \sin^2\theta},$$

(9.24)

with $f(r) = (r^2 + m^2 + g^2B_E^2)^2/4g^2B_E^2r^2$. Evaluating the angular integration

$$\int_0^\pi d\theta \frac{\sin^2\theta}{f(r) - \sin^2\theta} = \pi\left(\sqrt{\frac{f(r)}{f(r) - 1}} - 1\right)$$

(9.25)

then results in the radial integral

$$I_{PT_1} = 16i\pi^2m \int_0^\Lambda dr \, \frac{r(r^2 + m^2 + g^2B_E^2)}{4g^2B_E^2}$$
$$\times \left(1 - \frac{r^2 + m^2 + g^2B_E^2}{\sqrt{(r^2 + m^2 + g^2B_E^2)^2 - 4g^2B_E^2r^2}}\right),$$

(9.26)

which can be performed using established integral identities, see for example [51].

The resulting gap equation (9.21) has the form

$$
\begin{aligned}
\frac{2\pi^2}{\tilde{G}N_cN_f} = \frac{1}{4\tilde{g}^2}\Bigg\{ &\sqrt{(1+\tilde{m}^2-\tilde{g}^2)^2+4\tilde{g}^2\tilde{m}^2}(1+\tilde{m}^2+7\tilde{g}^2) \\
&- (\tilde{m}^2+\tilde{g}^2)(2+\tilde{m}^2+7\tilde{g}^2)-1+4\tilde{g}^2(2\tilde{g}^2-\tilde{m}^2) \\
&\times \ln\left[\frac{1}{2\tilde{m}^2}\left(\sqrt{(1+\tilde{m}^2-\tilde{g}^2)^2+4\tilde{g}^2\tilde{m}^2}+1+\tilde{m}^2-\tilde{g}^2\right)\right]\Bigg\}
\end{aligned}
$$

$$(9.27)$$

in terms of the rescaled quantities $\tilde{m} = m\Lambda^{-1}$, $\tilde{G} = G\Lambda^2$, and $\tilde{g} = g|B_E|\Lambda^{-1}$, which is proportional to the amplitude of the background field. In the limit of vanishing coupling g, (9.27) simplifies to the gap equation (9.13) of the standard NJL model within this regularization scheme.

The effective mass solution m of the gap equation can now be determined through the intersection of the function on the right-hand side of (9.27) with the real positive constant left-hand side, which is determined through $N_c = 3$, $N_f = 2$, the choice of the cutoff scale $\Lambda = 1015$ MeV, and the two-body interaction strength $\tilde{G} = 3.93$ for comparison with the standard NJL model as $g \to 0$. In Figure 9.3 the behavior of the right-hand side of (9.27) is shown as a function of the (scaled) effective mass $\tilde{m}$ at various values of the coupling $\tilde{g}$, while the constant left-hand side is visualized as a dashed horizontal line.

In the limit of vanishing $\tilde{g}$ the right-hand side reaches a finite maximum at $\tilde{m} = 0$, see Figure 9.3a, and the intersection with the dashed horizontal line lies at $m_{NJL} \approx 0.2349\Lambda \approx 238$ MeV, giving rise to the standard NJL model solution.

For any non-vanishing coupling $0 < \tilde{g} \leq 1$ the right-hand side has a singularity at $\tilde{m} = 0$, see Figure 9.3a and Figure 9.3b, which guarantees an intersection with the finite constant left-hand side, and thus the existence of a real mass solution of this $\mathcal{PT}$-symmetric non-Hermitian model at small couplings $\tilde{g}$.

But for coupling values $\tilde{g} > 1$ the singularity vanishes and the right-hand side reaches a finite maximum at $\tilde{m} = 0$ again, see Figure 9.3c. The height of this maximum decreases with increasing $\tilde{g}$. One finds that for coupling values $\tilde{g} > \tilde{g}_{\mathrm{crit}} \approx 1.261$ the maximum falls below the dashed line, so that an intersection with the left-hand side can no longer be found. Therefore, the gap equation no longer has a real mass solution in this region.

(a) $0 \leq \tilde{g} \leq 0.1$

(b) $0.1 \leq \tilde{g} \leq 0.8$
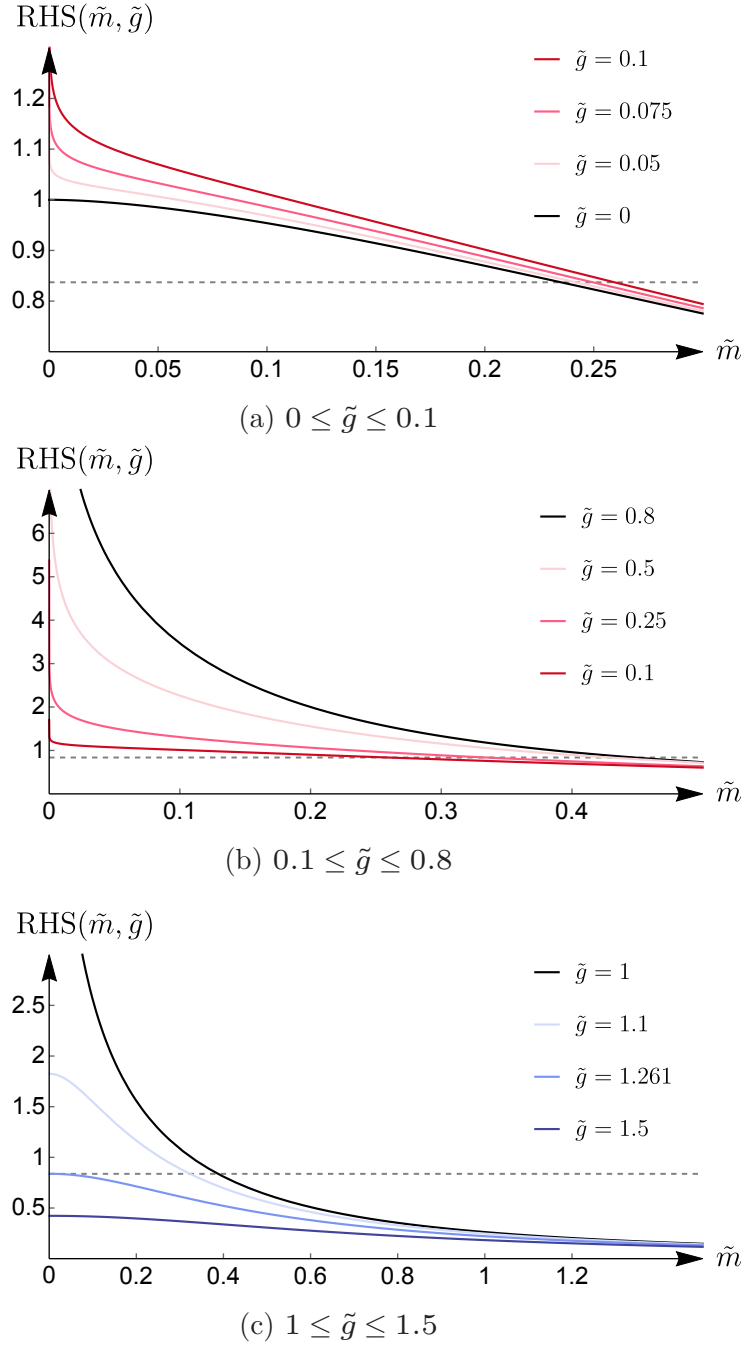

(c) $1 \leq \tilde{g} \leq 1.5$

Figure 9.3: Behavior of the right-hand side of (9.27) as a function of the scaled mass $\tilde{m}$ for given ranges of the scaled coupling constant $\tilde{g}$ (curves). The constant left-hand side is plotted as a dashed horizontal line for fixed values of G and Λ. Adapted from [66].
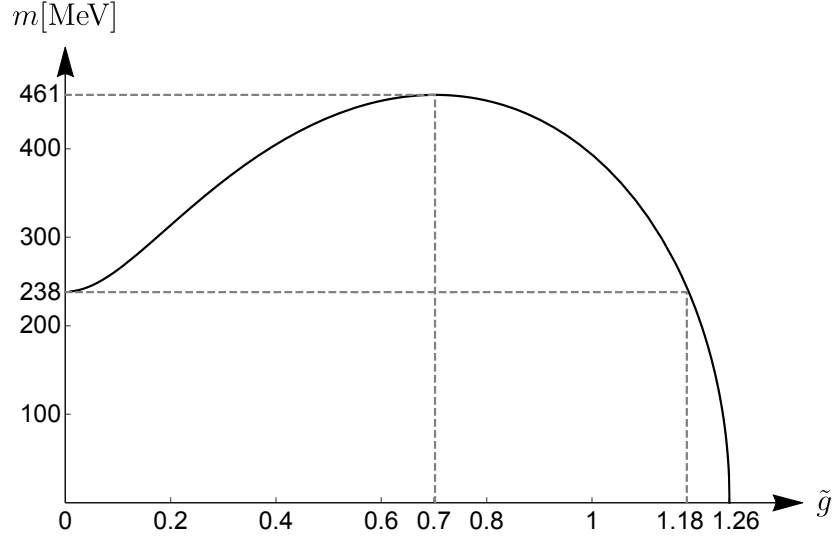
Figure 9.4: The behavior of the effective fermion mass solution to the gap equation (9.27) is shown as a function of the scaled coupling constant $\tilde{g}$. Adapted from [66].

The behavior of the real mass solution m of the gap equation is shown in Figure 9.4 as a function of $\tilde{g}$. Starting at the mass of the standard NJL model when $\tilde{g} = 0$, the solution increases to a maximum of $m \approx 460.870$ MeV at a coupling value of $\tilde{g} \approx 0.702$. Thereafter it decreases with increasing coupling until breaking down at the critical value of $\tilde{g}_{\text{crit}} \approx 1.261$. Notably, for all coupling values below $\tilde{g}_{\text{dyn}} \approx 1.183$, an increase in mass compared to m_{NJL} is generated dynamically through the $\mathcal{PT}$-symmetric non-Hermitian extension term.

The equivalent of a bare mass m_0 in the range of the up quark mass, $m_u = (1.7 - 3.3)$ MeV, is obtained at coupling values $\tilde{g} \approx (0.025 - 0.034)$ or $\tilde{g} \approx (1.181 - 1.182)$. For the equivalent of a bare down quark, $m_d = (4.1 - 5.8)$ MeV, coupling values $\tilde{g} \approx (0.038 - 0.046)$ or $\tilde{g} \approx (1.179 - 1.181)$ are required. The coupling is expected to be small, and therefore lie in the first range given.

When considering the model as an extension of a non-Hermitian Dirac fermion, that is treating the two-body coupling $\tilde{G}$ as a variable, one obtains the behavior visualized in Figure 9.5: The singularity of the right-hand side of (9.27) for values $0 < \tilde{g} \leq 1$ implies that mass solutions exist for all values of $\tilde{G}$, softening the phase transition of the standard NJL model ($\tilde{g} = 0$) similar to the inclusion of a finite bare mass m_0, cf. Figure 9.2, but without breaking chiral symmetry explicitly.
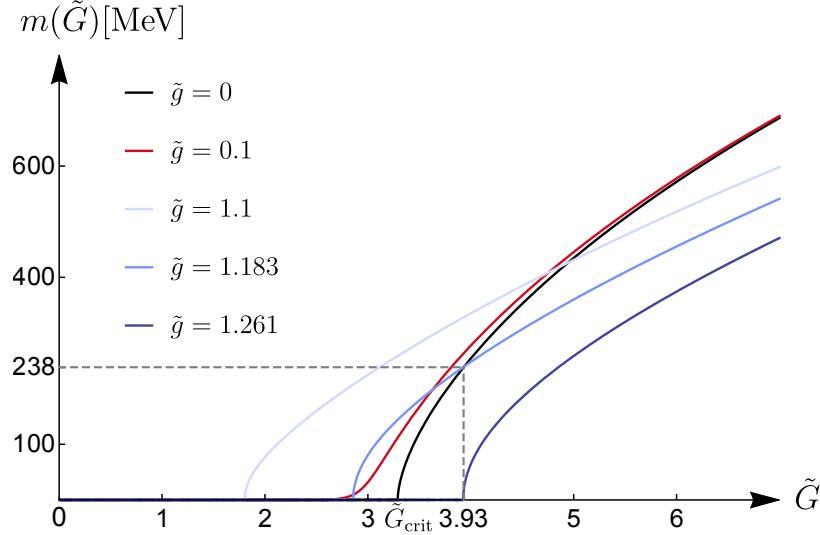
Figure 9.5: Behavior of the effective mass solution as a function of the two-body coupling strength $\tilde{G}$ for different values of the (scaled) bilinear-coupling constant $\tilde{g}$.

However, for values $\tilde{g} > 1$ the finite maximum of the right-hand side of (9.27) implies that an abrupt phase transition similar to that of the standard NJL model is restored. Nevertheless, as seen in Figure 9.5, the large-G behavior of the mass solution for such values of $\tilde{g}$ differs from that of the standard NJL model. The non-Hermitian bilinear term here modifies the two-body interaction rather than mimicking the effect of including a bare mass term.

Altogether, the modified NJL model based on the $\mathcal{PT}$ and chirally symmetric bilinear extension $\Gamma_{PT_1} = i\gamma_5 B_\mu \gamma^\mu$ admits real, effective mass solutions in the chiral limit of vanishing bare mass m_0 within a finite region of coupling values up to a critical coupling $\tilde{g}_{\text{crit}}$. This represents a phase of unbroken $\mathcal{PT}$ symmetry in the system, that is generally missing without the inclusion of the two-body interactions. When compared to the standard NJL model, mass is generated dynamically due to the extension term for $\tilde{g} < \tilde{g}_{\text{dyn}}$; larger coupling values $\tilde{g}_{\text{dyn}} < \tilde{g} < \tilde{g}_{\text{crit}}$ result in an effective mass loss. As a function of the two-body coupling G the mass solution shows two distinct behaviors: For $\tilde{g} \leq 1$ the phase transition of the standard NJL model is softened, resembling the inclusion of a bare mass m_0, though here the mass solution vanishes in the limit of $G = 0$. For coupling values $\tilde{g} > 1$ an abrupt phase transition like that of the standard NJL model is restored.

9.2 The Fermion Mass for $\Gamma_{PT_2} = F_{\mu\nu}\gamma^\mu\gamma^\nu$

In the non-Hermitian NJL model based on the $\mathcal{PT}$-symmetric, but chiral-symmetry-breaking, extension term $\Gamma_{PT_2} = F_{\mu\nu}\gamma^\mu\gamma^\nu$, with $F_{\mu\nu} = -F_{\nu\mu}$ being real, the fermion propagator (9.15) is formally given as

$$S(p) = (\not{p} - m - gF_{\mu\nu}\gamma^\mu\gamma^\nu)^{-1}. \tag{9.28}$$

To evaluate the spinor trace $\mathrm{tr}[S(p)]$ in the gap equation, one first recasts this expression into a form with a scalar denominator: By expanding (9.28) with the factor $(\not{p} - m + gF_{\alpha\beta}\gamma^\alpha\gamma^\beta)$, the denominator becomes

$$
\begin{aligned}
& (\not{p} - m - gF_{\mu\nu}\gamma^\mu\gamma^\nu)\,(\not{p} - m + gF_{\alpha\beta}\gamma^\alpha\gamma^\beta) \\
&= (p^2 + m^2 - 2g^2 f_1) - 2m\not{p} - 4gF_{\mu\nu}p^\nu\gamma^\mu + 8ig^2 f_2\gamma_5,
\end{aligned}
\tag{9.29}
$$

utilizing that $F_{\mu\nu}(\gamma^\mu\gamma^\nu\not{p} - \not{p}\gamma^\mu\gamma^\nu) = 4F_{\mu\nu}p^\nu\gamma^\mu$ and $F_{\mu\nu}F_{\alpha\beta}\gamma^\mu\gamma^\nu\gamma^\alpha\gamma^\beta = 2f_1\mathbb{1} - 8if_2\gamma_5$, with

$$f_1 = 2(F_{01}^2 + F_{02}^2 + F_{03}^2 - F_{12}^2 - F_{13}^2 - F_{23}^2) = \mathrm{tr}[F^2], \tag{9.30}$$

$$f_2 = (F_{01}F_{23} - F_{02}F_{13} + F_{03}F_{12}) = \mathrm{Pf}(F). \tag{9.31}$$

The expression (9.29) is not yet scalar, but when expanded with a factor having the opposite sign in all non-scalar contributions, the denominator takes the desired form:

$$
\begin{aligned}
& \big[(p^2 + m^2 - 2g^2 f_1) - 2m\not{p} - 4gF_{\mu\nu}p^\nu\gamma^\mu + 8ig^2 f_2\gamma_5\big] \\
& \times \big[(p^2 + m^2 - 2g^2 f_1) + 2m\not{p} + 4gF_{\alpha\beta}p^\beta\gamma^\alpha - 8ig^2 f_2\gamma_5\big] \\
&= (p^2 + m^2 - 2g^2 f_1)^2 - 4m^2 p^2 + 64g^4 f_2^2 + 16g^2 p^\mu F_{\mu\nu}F^\nu{}_\alpha p^\alpha,
\end{aligned}
\tag{9.32}
$$

where $\{\gamma^\mu, \gamma^\nu\} = 2\eta^{\mu\nu}$, $\{\gamma^\mu, \gamma_5\} = 0$, and $F_{\mu\nu} = -F_{\nu\mu}$ was used. The fermion propagator (9.28) can thus be written as

$$S(p) = \frac{(\not{p} - m + gF_{\mu\nu}\gamma^\mu\gamma^\nu)\big[(p^2 + m^2 - 2g^2 f_1) + 2m\not{p} + 4gF_{\alpha\beta}p^\beta\gamma^\alpha - 8ig^2 f_2\gamma_5\big]}{(p^2 + m^2 - 2g^2 f_1)^2 - 4m^2 p^2 + 64g^4 f_2^2 + 16g^2 p^\mu F_{\mu\nu}F^\nu{}_\alpha p^\alpha}. \tag{9.33}$$

When evaluating the spinor trace of this propagator, almost all terms in the numerator vanish. With $\mathrm{tr}[\mathbb{1}] = 4$, $\mathrm{tr}[\gamma^\mu \gamma^\nu] = 4\eta^{\mu\nu}$, and $F_\mu{}^\mu = 0$ one finds that

$$\mathrm{tr}[S(p)] = \frac{4m(p^2 - m^2 + 2g^2 f_1)}{(p^2 + m^2 - 2g^2 f_1)^2 - 4m^2 p^2 + 64g^4 f_2^2 + 16g^2 p^\mu F_{\mu\nu} F^\nu{}_\alpha p^\alpha}, \quad (9.34)$$

so that, in the limit of vanishing bare mass, the gap equation (9.10) becomes

$$m = \frac{2iG N_c N_f}{(2\pi)^4} I_{PT_2}, \quad (9.35)$$

with

$$I_{PT_2} = \int d^4 p \, \frac{4m(p^2 - m^2 + 2g^2 f_1)}{(p^2 + m^2 - 2g^2 f_1)^2 - 4m^2 p^2 + 64g^4 f_2^2 + 16g^2 p^\mu F_{\mu\nu} F^\nu{}_\alpha p^\alpha}. \quad (9.36)$$

To evaluate this gap equation in the Euclidean four-momentum cutoff regularization, one first changes to a Euclidean system by denoting $p_0 = ip_4$ and choosing $F_{0k} = iF_{4k}$, $\forall k \in [1,3]$, so that $p^2 = -p_E^2$ and $p^\mu F_{\mu\nu} F^\nu{}_\alpha p^\alpha = -p_E \cdot F_E \cdot F_E \cdot p_E$ in terms of the Euclidean dot product, where the (now complex) matrix F_E is

$$F_E = \begin{bmatrix} 0 & F_{41} & F_{42} & F_{43} \\ -F_{41} & 0 & F_{12} & F_{13} \\ -F_{42} & -F_{12} & 0 & F_{23} \\ -F_{43} & -F_{13} & -F_{23} & 0 \end{bmatrix}. \quad (9.37)$$

The momentum integral (9.36) then becomes

$$I_{PT_2} = \int d^4 p_E \, \frac{-4im(p_E^2 + m^2 - 2g^2 f_1)}{(p_E^2 - m^2 + 2g^2 f_1)^2 + 4m^2 p_E^2 + 64g^4 f_2^2 - 16g^2 p_E \cdot F_E \cdot F_E \cdot p_E}. \quad (9.38)$$

In principle, the momentum cutoff Λ can now be introduced as a radial bound of the integral, but in the form (9.38) the dependence of the momentum integral on F_E is somewhat unwieldy. However, when the matrix F_E is diagonalizable, it is orthogonally diagonalizable [89], so that one can find a transformation Q with $Q^T Q = \mathbb{1}$ and $Q^T F_E Q = \mathrm{diag}(\lambda_1, -\lambda_1, \lambda_2, -\lambda_2)$ in terms of

$$\lambda_{1,2} = \frac{1}{2}\sqrt{f_1 \mp \sqrt{f_1^2 + 16 f_2^2}}. \quad (9.39)$$

Applying such an orthogonal transformation to the Euclidean four-momentum $p_E \to Q\, p_E$ leaves the integral measure invariant, but yields a much more convenient dependence of the integral I_{PT_2} on the momentum components:

$$
\begin{aligned}
I_{PT_2} = -\, 4im \int^{\Lambda} d^4 p_E \, (p_E^2 + m^2 - 2g^2 f_1) \Big[(p_E^2 - m^2 + 2g^2 f_1)^2 + 4m^2 p_E^2 \\
+\, 64 g^4 f_2^2 - 16 g^2 \lambda_1^2 (p_4^2 + p_1^2) - 16 g^2 \lambda_2^2 (p_2^2 + p_3^2) \Big]^{-1}.
\end{aligned}
\tag{9.40}
$$

From the structure of the eigenvalues in (9.39) one observes that F_E is diagonalizable if f_2 does not vanish. Given the form of f_2 in (9.31), this is equivalent to the requirement that $f_2^2 = \mathrm{Det}(F)$ does not vanish, which is only a minor restriction that is assumed to be the case in the following analysis.

In order to evaluate (9.40), one can now rewrite the four-momentum integration in two sets of polar coordinates with $p_4 = R_1 \cos\phi_1$, $p_1 = R_1 \sin\phi_1$ and $p_2 = R_2 \cos\phi_2$, $p_3 = R_2 \sin\phi_2$ with $\phi_1, \phi_2 \in [0, 2\pi]$:

$$
\begin{aligned}
I_{PT_2} = -\, 16 i \pi^2 m \int^{\Lambda} dR_1 dR_2 \, R_1 R_2 (R_1^2 + R_2^2 + m^2 - 2g^2 f_1) \\
\times \Big[(R_1^2 + R_2^2 - m^2 + 2g^2 f_1)^2 + 4m^2 (R_1^2 + R_2^2) + 64 g^4 f_2^2 \\
-\, 16 g^2 (\lambda_1^2 R_1^2 + \lambda_2^2 R_2^2) \Big]^{-1},
\end{aligned}
\tag{9.41}
$$

where Λ is the upper bound for $\sqrt{R_1^2 + R_2^2}$. And in a polar coordinate system for R_1 and R_2, that is $R_1 = r \cos\theta$ and $R_2 = r \sin\theta$, with $\theta \in [0, \pi/2]$ and $r \in [0, \Lambda]$ the integral I_{PT_2} thus becomes

$$
I_{PT_2} = -16 i \pi^2 m \int_0^{\Lambda} dr \, r^3 (r^2 + m^2 - 2g^2 f_1) \int_0^{\pi/2} d\theta \, \frac{\cos\theta \sin\theta}{A(r) - B(r) \cos^2\theta},
\tag{9.42}
$$

where

$$
A(r) = (r^2 + m^2 - 2g^2 f_1^2) + 64 g^4 f_2^2 + 4 g^2 r^2 \Big(f_1 - \sqrt{f_1^2 + 16 f_2^2} \Big),
\tag{9.43}
$$

$$
B(r) = -\, 8 g^2 r^2 \sqrt{f_1^2 + 16 f_2^2}.
\tag{9.44}
$$

The angular integral is a standard integral, see for example [51], so that

$$I_{PT_2} = -i\pi^2 m \int_0^\Lambda dr \, \frac{r(r^2 + m^2 - 2g^2 f_1)}{g^2 \sqrt{f_1^2 + 16 f_2^2}} \ln\left[1 - \frac{B(r)}{A(r)}\right], \tag{9.45}$$

which can be rewritten as

$$\begin{aligned} I_{PT_2} =\, & \frac{i\pi^2 m}{2g^2 \sqrt{f_1^2 + 16 f_2^2}} \int_0^{\Lambda^2} dz \, (z + m^2 - 2g^2 f_1) \\ & \times \left[\ln(z + a_1) + \ln(z + a_2) - \ln(z + a_3) - \ln(z + a_4)\right], \end{aligned} \tag{9.46}$$

with

$$a_{1,2} = m^2 - 2g^2 \sqrt{f_1^2 + 16 f_2^2} \pm \sqrt{4m^2 g^2 (f_1 - \sqrt{f_1^2 + 16 f_2^2})}, \tag{9.47}$$

$$a_{3,4} = m^2 + 2g^2 \sqrt{f_1^2 + 16 f_2^2} \pm \sqrt{4m^2 g^2 (f_1 + \sqrt{f_1^2 + 16 f_2^2})}. \tag{9.48}$$

Integration and some simplification yields:

$$\begin{aligned} I_{PT_2} = \frac{-i\Lambda^3 \pi^2 \tilde{m}}{2\tilde{g}^2 \sqrt{1 + f^2}} \Big[& 4\tilde{g}^2 \sqrt{1 + f^2} - (\tilde{a}_1 + 1)\ln(\tfrac{1+\tilde{a}_1}{\tilde{a}_1})(\tilde{m}^2 - 2\tilde{g}^2 + \tfrac{1-\tilde{a}_1}{2}) \\ & - (\tilde{a}_2 + 1)\ln(\tfrac{1+\tilde{a}_2}{\tilde{a}_2})(\tilde{m}^2 - 2\tilde{g}^2 + \tfrac{1-\tilde{a}_2}{2}) \\ & + (\tilde{a}_3 + 1)\ln(\tfrac{1+\tilde{a}_3}{\tilde{a}_3})(\tilde{m}^2 - 2\tilde{g}^2 + \tfrac{1-\tilde{a}_3}{2}) \\ & + (\tilde{a}_4 + 1)\ln(\tfrac{1+\tilde{a}_4}{\tilde{a}_4})(\tilde{m}^2 - 2\tilde{g}^2 + \tfrac{1-\tilde{a}_4}{2}) \Big] \end{aligned} \tag{9.49}$$

in terms of the rescaled quantities $\tilde{m} = m\Lambda^{-1}$, $\tilde{a} = a\Lambda^{-2}$, $\tilde{g}^2 = g^2 f_1 \Lambda^{-2}$, and $f = 4f_2/f_1 \in \mathbb{R}$. The resulting gap equation (9.35) has the form

$$\begin{aligned} \frac{2\pi^2}{\tilde{G} N_c N_f} = \frac{1}{8\tilde{g}^2 \sqrt{1 + f^2}} \Big[& 4\tilde{g}^2 \sqrt{1 + f^2} - (\tilde{a}_1 + 1)\ln(\tfrac{1+\tilde{a}_1}{\tilde{a}_1})(\tilde{m}^2 - 2\tilde{g}^2 + \tfrac{1-\tilde{a}_1}{2}) \\ & - (\tilde{a}_2 + 1)\ln(\tfrac{1+\tilde{a}_2}{\tilde{a}_2})(\tilde{m}^2 - 2\tilde{g}^2 + \tfrac{1-\tilde{a}_2}{2}) \\ & + (\tilde{a}_3 + 1)\ln(\tfrac{1+\tilde{a}_3}{\tilde{a}_3})(\tilde{m}^2 - 2\tilde{g}^2 + \tfrac{1-\tilde{a}_3}{2}) \\ & + (\tilde{a}_4 + 1)\ln(\tfrac{1+\tilde{a}_4}{\tilde{a}_4})(\tilde{m}^2 - 2\tilde{g}^2 + \tfrac{1-\tilde{a}_4}{2}) \Big], \end{aligned} \tag{9.50}$$

where $\tilde{G} = G\Lambda^2$. In the limit of vanishing coupling g, (9.50) simplifies to the gap equation (9.13) of the standard NJL model within this regularization scheme.
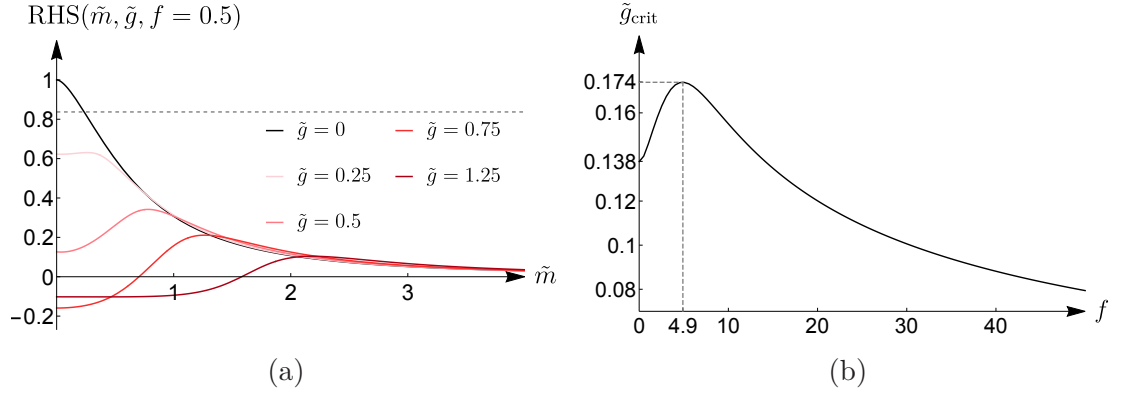
Figure 9.6: (a) Behavior of the right-hand side of the gap equation (9.50) as a function of the scaled mass $\tilde{m}$ for different values of the coupling $\tilde{g}$. The value for $f = 0.5$ is fixed, but this case is representative of the general behavior. The dashed horizontal line represents the left-hand side of the gap equation. (b) Behavior of the critical coupling value $\tilde{g}_{\text{crit}}$ up to which the gap equation (9.50) has real mass solutions as a function of f. Both figures are adapted from [67].

In Figure 9.6a the behavior of the right-hand side of (9.50) is shown as a function of the (scaled) effective mass $\tilde{m}$ at various values of the coupling $\tilde{g}$, while the real positive constant left-hand side, determined by $N_c = 3$, $N_f = 2$, and $\tilde{G} = 3.93$ for comparison with the standard NJL model, is visualized as a dashed horizontal line. The parameter f is fixed at $f = 0.5$, but the behavior is representative of other values. For small coupling values the behavior of the right-hand side deviates only slightly from that of the standard NJL model ($\tilde{g} = 0$). In particular, the right-hand side reaches a finite maximum which exceeds the dashed horizontal line for sufficiently small coupling values $\tilde{g}$, so that a real fermion mass solution $\tilde{m}$ can be found. Beyond a critical value $\tilde{g}_{\text{crit}}$, however, the right-hand side falls below the dashed line and real mass solutions no longer exist. The behavior of this critical coupling value is shown in Figure 9.6b as a function of the parameter f. Notably, it vanishes asymptotically for large values of f.

In Figure 9.7 the behavior of the real mass solution m of the gap equation is shown as a function of the coupling $\tilde{g}$ for different values of f. One observes that independent of f, the effective mass *decreases* as the coupling constant $\tilde{g}$ increases: the $\mathcal{PT}$-symmetric extension Γ_{PT_2} always results in an effective mass loss. The dynamical generation of a bare quark mass is not possible in this model.
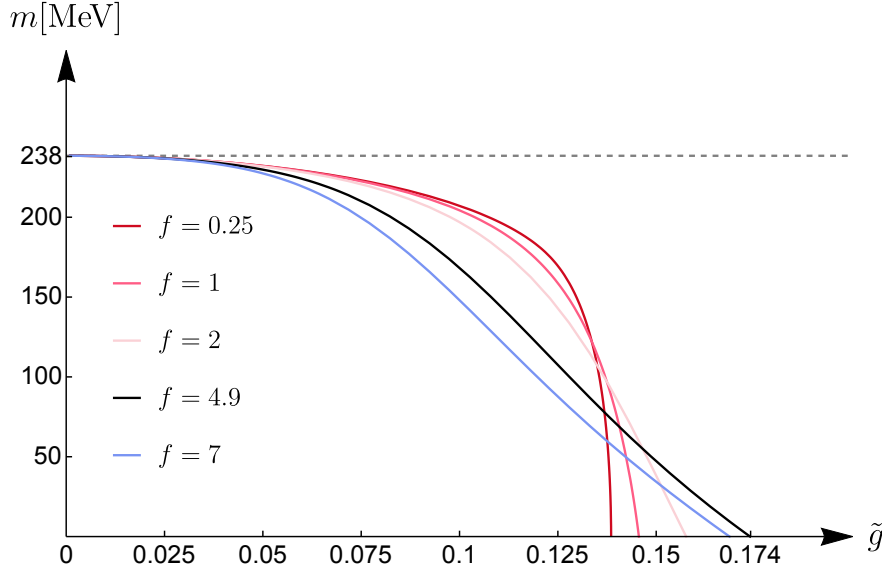
Figure 9.7: The behavior of the effective fermion mass solution of the gap equation (9.50) is shown as a function of the coupling constant $\tilde{g}$ up to the corresponding critical coupling value for different values of f. Adapted from [67].

In Figure 9.8 the model is considered as an extension of a non-Hermitian Dirac fermion and the mass solution is shown as a function of the two-body coupling $\tilde{G}$. For small coupling values $\tilde{g}$, where the behavior of the right-hand side of (9.50) resembles that of the standard NJL model, see Figure 9.6a, the mass solution behaves similar to the standard NJL solution as well - the phase transition occurs at larger values of G with increasing $\tilde{g}$ and is softened to some extent with increasing values of the parameter f. However, for sufficiently large values $\tilde{g}$ this behavior changes and the gap equation can admit multiple mass solutions in a finite range of the two-body coupling G. An increase of the parameter f reduces the size of this region. It is remarked that the occurrence of a region in which the gap equation has multiple mass solutions, as well as the qualitative change of its right-hand side with increasing bilinear coupling $\tilde{g}$, resembles to some extent the behavior of the standard NJL model at finite densities, cf. [80]. The investigation of non-Hermitian extensions to the NJL model at finite temperature and density and of this resemblance is the subject of ongoing investigation.

Altogether, the modified NJL model based on the $\mathcal{PT}$-symmetric, but chiral-symmetry-breaking, bilinear extension $\Gamma_{PT_2} = F_{\mu\nu}\gamma^\mu\gamma^\nu$ admits real effective mass
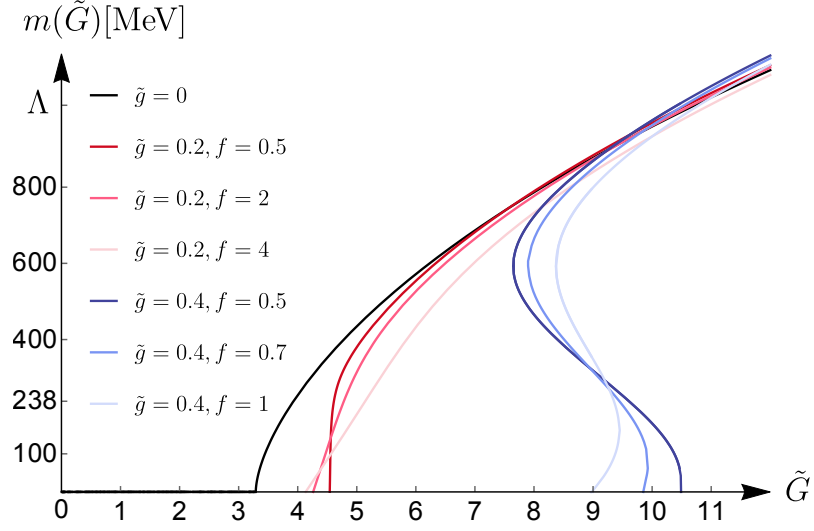
Figure 9.8: Behavior of the effective mass solution as a function of the two-body coupling strength $\tilde{G}$ for different values of the (scaled) bilinear-coupling constant $\tilde{g}$ and the parameter f.

solutions in the limit of vanishing bare mass m_0 within a finite region of coupling values $\tilde{g}$ up to a critical coupling $\tilde{g}_{\text{crit}}$. This represents a phase of unbroken $\mathcal{PT}$ symmetry in the system. But contrary to the non-Hermitian extension Γ_{PT_1}, the dynamical generation of mass is not possible within this model and the effect of a bare mass term m_0 can not be mimicked through the non-Hermitian extension. The bilinear term lessens the effect of the two-body interaction and results in an effective mass loss. As a function of the two-body coupling G the mass solution initially resembles the standard NJL solution, with the critical value of the two-body coupling increasing with increasing values of $\tilde{g}$. But for sufficiently large bilinear coupling values $\tilde{g}$ a region in which the gap equation admits multiple mass solutions forms.

9.3 The Fermion Mass for $\Gamma_{aPT_1} = iA_\mu\gamma^\mu$

The modified NJL model based on the non-Hermitian non-$\mathcal{PT}$-symmetric but chirally symmetric term $\Gamma_{aPT_1} = iA_\mu\gamma^\mu$ is structurally similar to the model based on Γ_{PT_1}, that is discussed in Section 9.1. The fermion propagator is formally given

as

$$S(p) = (\not{p} - m - igA_\mu\gamma^\mu)^{-1}. \tag{9.51}$$

By expansion with $(\not{p} + m - igA_\nu\gamma^\nu)$ the propagator takes the form

$$S(p) = \frac{\not{p} + m - iA_\mu\gamma^\mu}{p^2 - m^2 - g^2A^2 - 2igA_\mu p^\mu}, \tag{9.52}$$

which has a scalar denominator. The spinor trace is then readily obtained:

$$\text{tr}[S(p)] = \frac{4m}{p^2 - m^2 - g^2A^2 - 2igA_\mu p^\mu}. \tag{9.53}$$

In the chiral limit of vanishing bare mass, the gap equation (9.10) thus becomes

$$m = \frac{2iGN_cN_f}{(2\pi)^4} I_{aPT_1} = \frac{2iGN_cN_f}{(2\pi)^4} \int d^4p \frac{4m}{p^2 - m^2 - g^2A^2 - 2igA_\mu p^\mu}. \tag{9.54}$$

The regularization of the integral within the Euclidean four-momentum cutoff scheme can be performed as described in Section 9.1: The cutoff Λ is introduced as a bound of the radial integration after transforming to Euclidean coordinates with $p_0 = ip_4$ and $A_0 = iA_4$, so that $p^2 = -p_E^2$, $A^2 = -A_E^2$, and $A_\mu p^\mu = -A_E \cdot p_E$. In a spherical system with zenith direction A_E, the integral I_{aPT_1} then becomes

$$I_{aPT_1} = \frac{8\pi m}{g\,|A_E|} \int_0^\Lambda dr\, r^2 \int_0^\pi d\theta\, \frac{\sin^2\theta}{f(r) + \cos\theta}, \tag{9.55}$$

where $f(r) = (r^2 + m^2 - g^2A_E^2)/(-2igr|A_E|)$. Both the angular integral and the resulting radial integral are standard integrals, that can be found for example in [51], yielding

$$\begin{aligned}
I_{aPT_1} = \frac{i\Lambda^3\pi^2\tilde{m}}{\tilde{g}^2}\Big\{ & 4\tilde{m}^2\tilde{g}^2 \ln\Big[\frac{1}{2\tilde{m}^2}\Big(\sqrt{(1+\tilde{m}^2+\tilde{g}^2)^2 - 4\tilde{g}^2\tilde{m}^2} + 1 + \tilde{m}^2 + \tilde{g}^2\Big)\Big] \\
& - (1+\tilde{m}^2+\tilde{g}^2)\sqrt{(1+\tilde{m}^2+\tilde{g}^2)^2 - 4\tilde{g}^2\tilde{m}^2} + 1 \\
& + (\tilde{m}^2 - \tilde{g}^2)(2+\tilde{m}^2+\tilde{g}^2)\Big\},
\end{aligned} \tag{9.56}$$

in terms of the rescaled quantities $\tilde{m} = m\Lambda^{-1}$ and $\tilde{g} = g|A_E|\Lambda^{-1}$, which is proportional to the amplitude of the background field.
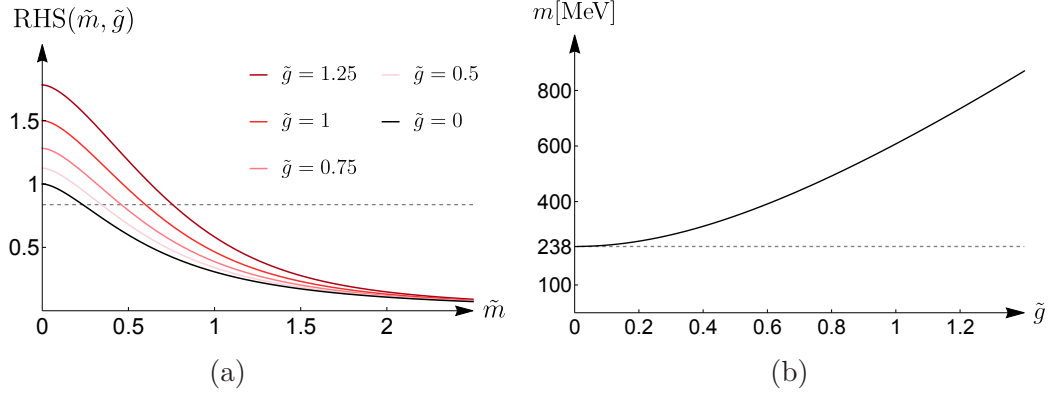
Figure 9.9: (a) Behavior of the right-hand side of the gap equation (9.57) as a function of the scaled mass $\tilde{m}$ for different values of the coupling $\tilde{g}$. The dashed horizontal line represents the left-hand side of the gap equation. (b) Behavior of the effective fermion mass solution m as a function of the scaled coupling constant $\tilde{g}$. Both figures are adapted from [67].

The resulting gap equation (9.54) has the form

$$
\frac{2\pi^2}{\tilde{G}N_c N_f} = \frac{1}{4\tilde{g}^2}\Big\{ (1 + \tilde{m}^2 + \tilde{g}^2)\sqrt{(1 + \tilde{m}^2 + \tilde{g}^2)^2 - 4\tilde{g}^2\tilde{m}^2} - 1
$$
$$
- 4\tilde{m}^2\tilde{g}^2 \ln\Big[\frac{1}{2\tilde{m}^2}\Big(\sqrt{(1 + \tilde{m}^2 + \tilde{g}^2)^2 - 4\tilde{g}^2\tilde{m}^2} + 1 + \tilde{m}^2 + \tilde{g}^2 \Big)\Big]
$$
$$
- (\tilde{m}^2 - \tilde{g}^2)(2 + \tilde{m}^2 + \tilde{g}^2)\Big\},
$$

$$(9.57)$$

where $\tilde{G} = G\Lambda^2$. In the limit of vanishing coupling g, the gap equation (9.13) of the standard NJL model within this regularization scheme is recovered.

Notably, the right-hand side of the gap equation (9.57) is a real-valued function of the (scaled) mass $\tilde{m}$ and the coupling constant $\tilde{g}$, the behavior of which is shown in Figure 9.9a as a function of $\tilde{m}$ for various values of $\tilde{g}$. The real positive constant left-hand side at $N_c = 3$, $N_f = 2$, and $\tilde{G} = 3.93$ for comparison with the standard NJL model is visualized as a dashed horizontal line. A finite maximum of the right-hand side is reached at $\tilde{m} = 0$, whose height increases with increasing $\tilde{g}$. Therefore, an intersection with the dashed horizontal line, and thus a real fermion mass solution, can always be found.
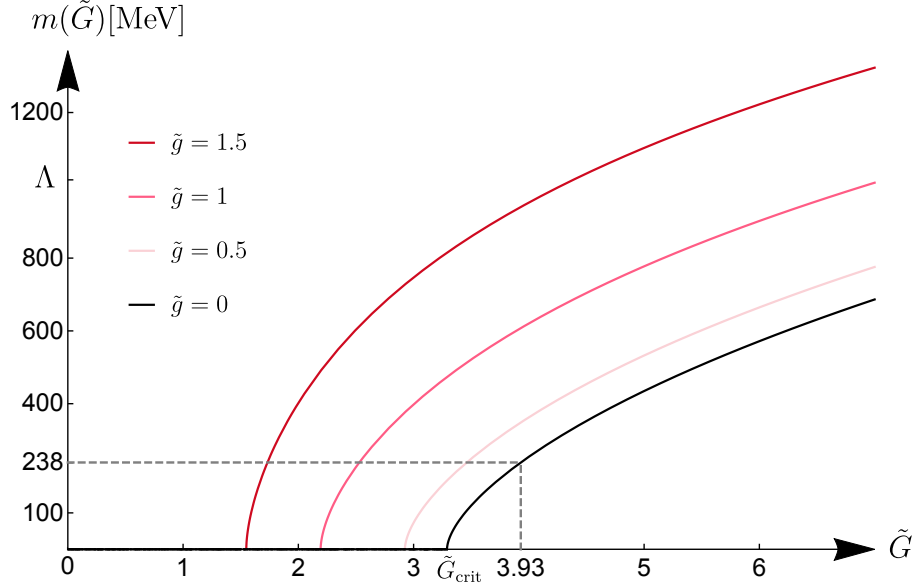
Figure 9.10: Behavior of the effective mass solution as a function of the two-body coupling strength $\tilde{G}$ for different values of the (scaled) bilinear-coupling constant $\tilde{g}$.

In Figure 9.9b the behavior of the real mass solution m of the gap equation is shown as a function of the coupling $\tilde{g}$. The mass increases monotonically with $\tilde{g}$ and, in contrast to the $\mathcal{PT}$-symmetric models discussed previously, is not restricted to a finite coupling region. An increased mass compared to m_{NJL} is generated dynamically through the non-Hermitian non-$\mathcal{PT}$-symmetric extension term Γ_{aPT_1}. The equivalent of a bare up quark mass, $m_u = (1.7 - 3.3)$ MeV, is obtained at the coupling value $\tilde{g} \approx (0.059 - 0.083)$ and for the the equivalent of a bare down quark, $m_d = (4.1 - 5.8)$ MeV, a coupling value of $\tilde{g} \approx (0.092 - 0.110)$ is required.

In Figure 9.10 the model is considered as an extension of a non-Hermitian Dirac fermion, that is the two-body coupling G is treated as a variable, and the effective fermion mass is shown as a function of $\tilde{G}$. The qualitative behavior of the mass solution of the standard NJL model without bare mass is generally preserved while the critical value of the coupling $\tilde{G}$, beyond which the chiral symmetry of the model is spontaneously broken, decreases as the bilinear coupling constant $\tilde{g}$ increases. Even though the non-Hermitian bilinear results in an increase of the effective mass, it does not mimic the effect of a bare mass term in the sense that it softens the phase transition as a function of the two-body coupling; it rather modifies the effect of the two-body interaction.

Altogether, the modified NJL model based on the non-$\mathcal{PT}$-symmetric, but chirally symmetric, extension $\Gamma_{aPT_1} = iA_\mu\gamma^\mu$ admits real, effective fermion mass solutions in the chiral limit of vanishing bare mass m_0, even though $\mathcal{PT}$ symmetry is explicitly broken. These solutions are not restricted to a finite coupling region and dynamically generate mass compared to the standard NJL model. In addition, when treating the two-body coupling as a variable the general behavior of the effective fermion mass as a function of G remains qualitatively unchanged: the generation of an effective fermion mass requires a sufficiently strong two-body interaction. The critical value of the two-body coupling decreases with an increasing strength $\tilde{g}$ of the non-Hermitian non-$\mathcal{PT}$-symmetric bilinear term.

9.4 The Fermion Mass for $\Gamma_{aPT_2} = \gamma_5$

In the modified NJL model based on the non-Hermitian, non-$\mathcal{PT}$-symmetric, and chiral-symmetry-breaking extension term $\Gamma_{aPT_2} = \gamma_5$, the fermion propagator (9.15) is formally given as

$$S(p) = (\not{p} - m - g\gamma_5)^{-1}. \tag{9.58}$$

An expansion with $(\not{p} + m - g\gamma_5)$ results straightforwardly in the form

$$S(p) = \frac{\not{p} + m - g\gamma_5}{p^2 - m^2 + g^2}, \quad \text{with} \quad \text{tr}[S(p)] = \frac{4m}{p^2 - m^2 + g^2}. \tag{9.59}$$

In the limit of vanishing bare mass the gap equation (9.10) thus becomes

$$m = \frac{2iGN_cN_f}{(2\pi)^4} I_{aPT_2} = \frac{2iGN_cN_f}{(2\pi)^4} \int d^4p \frac{4m}{p^2 - m^2 + g^2}. \tag{9.60}$$

The argument of the momentum integral only depends on the square of the four-momentum, so that the introduction of a radial cutoff Λ in Euclidean coordinates for the purpose of regularization follows immediately by letting $p_0 = ip_4$,

so that $p^2 = -p_E^2 = -r^2$:

$$I_{aPT_2} = -8im\pi^2 \int_0^\Lambda dr \frac{r^3}{r^2 + m^2 - g^2}. \tag{9.61}$$

Subsequently, performing the integration yields

$$I_{aPT_2} = 4i\Lambda^3\pi^2\tilde{m}\left[(\tilde{m}^2 - \tilde{g}^2)\ln\left(1 + \frac{1}{\tilde{m}^2 - \tilde{g}^2}\right) - 1\right], \tag{9.62}$$

in terms of the rescaled parameters $\tilde{m} = m\Lambda^{-1}$ and $\tilde{g} = g\Lambda^{-1}$. The resulting gap equation (9.60) has the form

$$\frac{2\pi^2}{\tilde{G}N_cN_f} = 1 - (\tilde{m}^2 - \tilde{g}^2)\ln\left(1 + \frac{1}{\tilde{m}^2 - \tilde{g}^2}\right), \tag{9.63}$$

where $\tilde{G} = G\Lambda^2$.

In the limit of vanishing coupling g, (9.63) clearly simplifies to the gap equation (9.13) of the standard NJL model within this regularization scheme. In fact, the gap equation (9.63) is structurally identical to that of the standard NJL model, with $\tilde{m}^2 - \tilde{g}^2 = \tilde{m}_{NJL}^2$. Accordingly, the real fermion mass solution $\tilde{m}$ has the form

$$\tilde{m} = \sqrt{\tilde{g}^2 + \tilde{m}_{NJL}^2} = \sqrt{\tilde{g}^2 + [\tfrac{1}{c}W_{-1}(ce^c) - 1]^{-1}}, \tag{9.64}$$

using the solution (9.14) of the standard NJL model with $c = 2\pi^2/\tilde{G}N_cN_f - 1$.

In Figure 9.11 the behavior of this real mass solution m of the gap equation is shown as a function of the coupling $\tilde{g}$. The mass increases monotonically with $\tilde{g}$ like in the case discussed in Section 9.3 and, in contrast to the $\mathcal{PT}$-symmetric models discussed previously, it is not restricted to a finite coupling region. An increased mass compared to m_{NJL} is generated dynamically. The equivalent of a bare up quark mass, $m_u = (1.7-3.3)$ MeV, is obtained at the coupling value $\tilde{g} \approx (0.028-0.039)$ and for the equivalent of a bare down quark, $m_d = (4.1-5.8)$ MeV, a coupling value of $\tilde{g} \approx (0.044-0.052)$ is required.
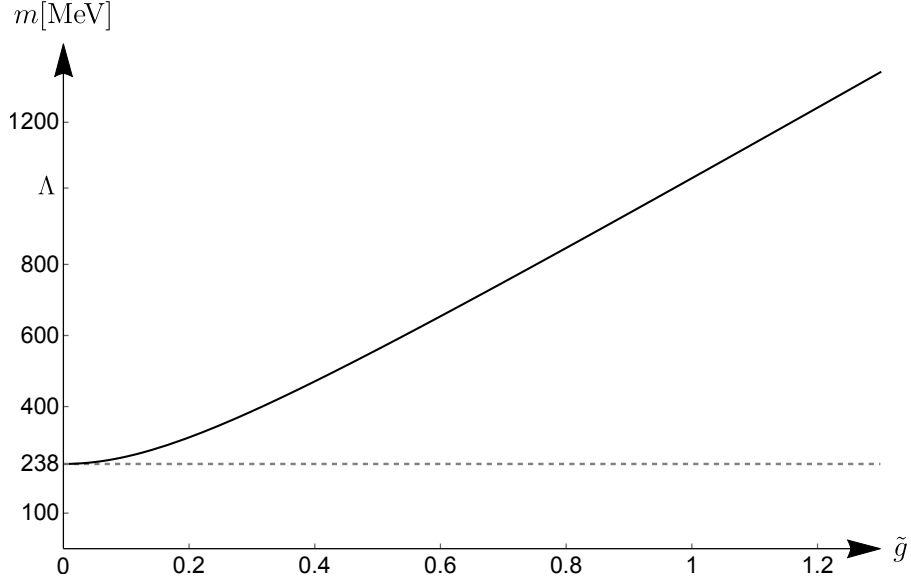
Figure 9.11: The behavior of the effective fermion mass solution (9.64) is shown as a function of the scaled coupling constant $\tilde{g}$. Adapted from [67].

When considering the model as an extension of a non-Hermitian Dirac fermion, that is treating the two-body coupling G as a variable, the effective fermion mass behaves as shown in Figure 9.12. Independent of the bilinear coupling $\tilde{g}$ a nontrivial, real effective fermion mass is obtained only when $\tilde{G} > \tilde{G}_{\text{crit}} = \pi^2/3$; that is the transition occurs at the same two-body coupling value as in the standard NJL model. (For smaller values of $\tilde{G}$ the Lambert W function in (9.64) becomes complex.) The value of the effective fermion mass at $\tilde{G}_{\text{crit}}$ is $\tilde{m}(\tilde{G}_{\text{crit}}, \tilde{g}) = \tilde{g}$; the inclusion of the chiral-symmetry-breaking bilinear term results in a discontinuous transition. For every coupling $\tilde{G} > \tilde{G}_{\text{crit}}$ the effective mass increases with increasing values of the bilinear coupling $\tilde{g}$, similar to the case shown in Figure 9.11.

Altogether, the modified NJL model based on the non-$\mathcal{PT}$-symmetric, non-chirally-symmetric extension $\Gamma_{aPT_2} = \gamma_5$ admits real effective fermion mass solutions in the limit of vanishing bare mass m_0, even though $\mathcal{PT}$ symmetry is explicitly broken. It resembles the solution found in Section 9.3: The real mass is not restricted to a finite coupling region and dynamically generates a mass increase compared to the standard NJL model. Contrary to the solution in Section 9.3 the critical value of the two-body coupling $\tilde{G}$ remains unaffected by the non-Hermitian extension and the transition becomes discontinuous.
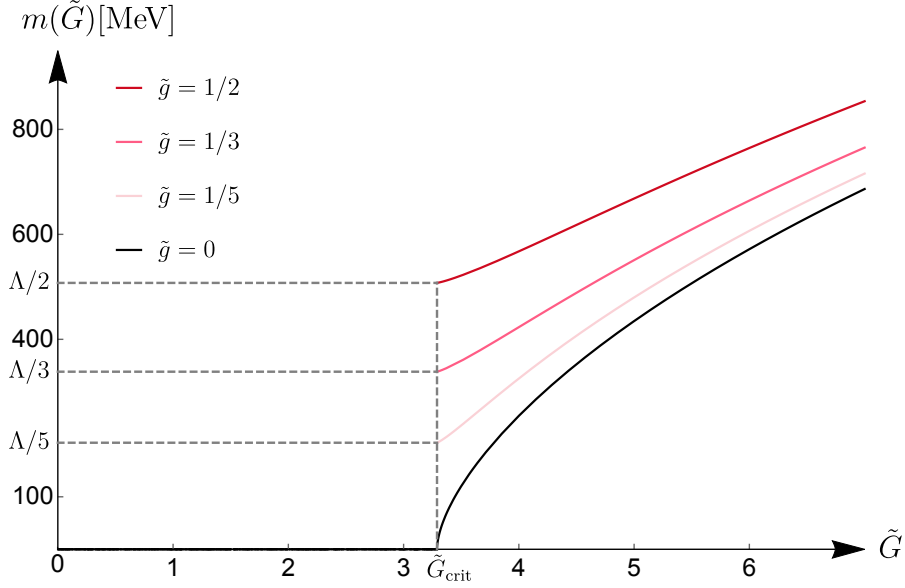
Figure 9.12: Behavior of the effective mass solution as a function of the two-body coupling strength $\tilde{G}$ for different values of the (scaled) bilinear-coupling constant $\tilde{g}$.

9.5 The Fermion Mass for $\Gamma_{aPT_3} = i\mathbb{1}$

The non-Hermitian, non-$\mathcal{PT}$-symmetric, and chiral-symmetry-breaking model based on the extension term $\Gamma_{aPT_3} = i\mathbb{1}$ has the fermion propagator

$$S(p) = (\not{p} - m - ig)^{-1}, \tag{9.65}$$

which, in essence, corresponds to that of the standard NJL model with the mass shifted to $m + ig$. Accordingly, the trace of the propagator takes the form

$$\mathrm{tr}[S(p)] = \frac{4(m + ig)}{p^2 - (m + ig)^2}, \tag{9.66}$$

and in the limit of vanishing bare mass the gap equation (9.10) becomes

$$\frac{2\pi^2}{\tilde{G}N_cN_f} = \frac{\tilde{m} + i\tilde{g}}{\tilde{m}}\left\{1 - (\tilde{m} + i\tilde{g})^2 \ln\left[\frac{1 + (\tilde{m} + i\tilde{g})^2}{(\tilde{m} + i\tilde{g})^2}\right]\right\} \tag{9.67}$$

in the Euclidean four-momentum cutoff regularization scheme, where $\tilde{m} = m\Lambda^{-1}$ and $\tilde{g} = g\Lambda^{-1}$. In the limit of vanishing coupling g, (9.67) simplifies to the gap

equation (9.13) of the standard NJL model within this regularization scheme. For non-vanishing coupling values $\tilde{g}$, the right-hand side of (9.67) takes on inherently complex values for real masses $\tilde{m}$, so that an intersection with the real constant left-hand side can not be found. Thus the gap equation has no real effective fermion mass solutions.

Overall, the modified NJL model based on Γ_{aPT_3} is the only non-Hermitian bilinear extension of the NJL model that does not admit real fermionic masses. This is independent of the (real) two-body coupling G, because the left-hand side of (9.67) remains a real constant.

9.6 Summary of the Fermion Masses

The effect of the five possible non-Hermitian bilinear extensions of the NJL model on the generated effective fermion mass was investigated through the analysis of the self-consistent gap equation in the limit of vanishing bare mass. For all but the case of the bilinear based on $\Gamma_{aPT_3} = i\mathbb{1}$ the modified gap equation admits real mass solutions. In the $\mathcal{PT}$-symmetric models based on $\Gamma_{PT_1} = i\gamma_5 B_\mu \gamma^\mu$ and $\Gamma_{PT_2} = F_{\mu\nu}\gamma^\mu\gamma^\nu$ these solutions arise in a finite region up to a critical coupling strength $\tilde{g}_{\text{crit}}$, signifying a phase of unbroken $\mathcal{PT}$ symmetry in the system. For $\Gamma_{aPT_1} = iA_\mu \gamma^\mu$ and $\Gamma_{aPT_2} = \gamma_5$ on the other hand, any coupling value $\tilde{g}$ results in real masses, which is remarkable given that these models are neither Hermitian nor $\mathcal{PT}$ symmetric.

A dynamical mass generation through the inclusion of a non-Hermitian bilinear can be observed for the terms based on Γ_{PT_1}, Γ_{aPT_1}, and Γ_{aPT_2}. The $\mathcal{PT}$-symmetric modification based on Γ_{PT_2}, however, resulted in an effective mass loss at all coupling-constant values. Nevertheless, in this it shows an intriguing resemblance to the effect of a finite density in the standard NJL model. The discussion of non-Hermitian extensions to the NJL model at finite temperature and density is the subject of ongoing investigations and will be presented in future work.

Furthermore, by considering the behavior of the effective mass under variation of the two-body coupling strength G the following distinction between the three bilinear terms that generate mass dynamically could be made. For the two

non-$\mathcal{PT}$-symmetric terms Γ_{aPT_1} and Γ_{aPT_2} the general behavior of the standard NJL model is qualitatively preserved to a large extent. Notably a transition from the existence of only the vanishing mass solution at small two-body coupling values to finite mass solutions beyond a critical value G_{crit} remains intact. In the $\mathcal{PT}$-symmetric model based on Γ_{PT_1} this behavior can also be found when considering a large bilinear coupling value $\tilde{g} = g|B_E|\Lambda^{-1} > 1$. Therefore, the modifications based on Γ_{aPT_1} and Γ_{aPT_2}, as well as on the strong bilinear-coupling regime of Γ_{PT_1}, generate mass dynamically by modifying the effect of the two-body interaction rather than by mimicking the inclusion of a bare mass m_0. However, at small coupling values of the bilinear term based on Γ_{PT_1} the standard-NJL-model transition was softened instead, resembling the effect of a finite bare mass term without breaking chiral symmetry explicitly.

Chapter 10

The Meson Masses

A central feature of the standard NJL model is that it allows one to study the mechanism of spontaneous chiral symmetry breaking. Without a chiral-symmetry-breaking bare mass term, this is in particular manifested in the existence of a massless Nambu-Goldstone boson in the form of the pseudoscalar mesonic bound state. In the approximately chirally symmetric case when a small bare mass term is included, this bound state gains a small mass as well. As the discussion of fermion mass generation in the previous chapter has established, modifying the NJL model through the inclusion of non-Hermitian bilinear terms can result in the dynamical generation of increased fermion masses which are comparable to a bare mass term. Such a mass generation was observed in the systems based on the $\mathcal{PT}$-symmetric extension $\Gamma_{PT_1} = i\gamma_5 B_\mu \gamma^\mu$ as well as for the non-$\mathcal{PT}$-symmetric terms $\Gamma_{aPT_1} = iA_\mu \gamma^\mu$ and $\Gamma_{aPT_2} = \gamma_5$. While the last extension term breaks chiral symmetry, similar to a bare mass term m_0, the former two do not - they generate the equivalent of a bare mass term without breaking chiral symmetry explicitly. In this chapter, the effect of these three non-Hermitian extensions of the NJL model on the mass of the scalar and pseudoscalar mesonic bound states, which in the context of QCD are identified as the σ and π mesons, is investigated in detail. This analysis closely follows that of the published discussion in [67].

Recall that the study of the fermion mass served to establish the relation between higher-order interaction terms, in the form of the NJL two-body interaction, and non-Hermitian extensions, in particular those that are $\mathcal{PT}$ symmetric. In this aspect, the modified NJL model can be viewed as either an extension of

the non-Hermitian modified Dirac fermions or an extension of the standard NJL model. The following study of the mesonic bound states focuses on the role of chiral symmetry in the modified NJL model, and as such it is inherently tied to the perspective of extending the standard NJL model through non-Hermitian bilinears.

Similar to the analysis of the gap equation for the fermion mass, the meson mass equations for the scalar and pseudoscalar bound state can be derived following the approach of [80] and [84] to the standard NJL model: the effective meson interaction $V_{\alpha\alpha',\beta\beta'}$, in which all relevant degrees of freedom are denoted in the indices α, α', β, and β', is expressed in terms of the bare two-body interaction $V^{(0)}_{\alpha\alpha',\beta\beta'}$ of the model and the (proper) polarization insertion $\Pi_{\lambda\lambda',\mu\mu'}$ as

$$-iV_{\alpha\alpha',\beta\beta'}(k) = -iV^{(0)}_{\alpha\alpha',\beta\beta'}(k) + \left[-iV^{(0)}_{\alpha\alpha',\lambda\lambda'}(k)\right]\left[-i\Pi_{\lambda\lambda',\mu\mu'}(k)\right]\left[-iV_{\mu\mu',\beta\beta'}(k)\right]. \tag{10.1}$$

Considering that the two-body interaction of the NJL model (8.1) consists of a scalar $(\bar\psi\psi)^2$ and a pseudoscalar $(\bar\psi i\gamma_5\vec\tau\psi)^2$ contribution, one can analyze (10.1) for these contributions separately, writing

$$V^{(0)}_{\alpha\alpha',\beta\beta'}(k) = V^{(0)}(k)\,\delta_{\alpha\alpha'}\delta_{\beta\beta'} \tag{10.2}$$

or

$$V^{(0)}_{\alpha\alpha',\beta\beta'}(k) = V^{(0)}(k)\,(i\gamma_5\vec\tau)_{\alpha\alpha'}(i\gamma_5\vec\tau)_{\beta\beta'} \tag{10.3}$$

respectively. Identifying the contributions of the effective interaction accordingly then leads (10.1) to become

$$-iV(k) = -iV^{(0)}(k) + \left[-iV^{(0)}(k)\right]\left[-i\Pi^{s/ps}(k)\right]\left[-iV(k)\right], \tag{10.4}$$

where $\Pi^s(k) = \delta_{\lambda\lambda'}\Pi^s_{\lambda\lambda',\mu\mu'}(k)\delta_{\mu\mu'}$ and $\Pi^{ps}(k) = (i\gamma_5\vec\tau)_{\lambda\lambda'}\Pi^{ps}_{\lambda\lambda',\mu\mu'}(k)(i\gamma_5\vec\tau)_{\mu\mu'}$ for the scalar and pseudoscalar case respectively. This is a geometric progression and can thus be summed to the form

$$-iV(k) = \frac{-iV^{(0)}(k)}{1 + V^{(0)}(k)\,\Pi^{s/ps}(k)}. \tag{10.5}$$
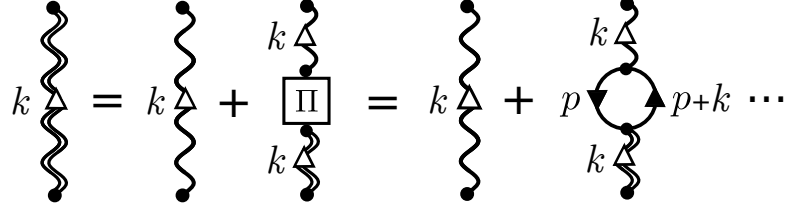
Figure 10.1: Schematic visualization of equation (10.4) for the effective meson interaction to first order, where the polarization insertion corresponds to a closed fermion loop.

The pole of (10.5) corresponds to the pole of the general scalar or pseudoscalar bound-state propagator, which lies at $k^2 = m^2_{s/ps}$, denoting the mass of the scalar or pseudoscalar meson as $m_{s/ps}$. These masses are therefore determined by the equation

$$1 + V^{(0)}(k)\,\Pi^{s/ps}(k) = 0 \quad \text{at} \quad k^2 = m^2_{s/ps}. \tag{10.6}$$

At the lowest perturbative order, the polarization insertion corresponds to a closed fermion loop, shown diagrammatically in Figure 10.1. Furthermore identifying that $V^{(0)}(k) = -2G$ [1] for the NJL model (8.1) thus results in

$$V^{(0)}(k)\left[-i\Pi^s(k)\right] = -\frac{2GN_cN_f}{(2\pi)^4}\int d^4p\,\mathrm{tr}[S^{(0)}(p+k)S^{(0)}(p)] \tag{10.7}$$

for the scalar vertex function and

$$V^{(0)}(k)\left[-i\Pi^{ps}(k)\right] = \frac{2GN_cN_f}{(2\pi)^4}\int d^4p\,\mathrm{tr}[\gamma_5 S^{(0)}(p+k)\gamma_5 S^{(0)}(p)] \tag{10.8}$$

for each pseudoscalar channel. Similar to the gap equation, this first-order approximation can be improved self-consistently by replacing the free fermion propagator $S^{(0)}$ with the full propagator S.

Using the gap equation (9.10) at vanishing bare mass,

$$m = \frac{2iGN_cN_f}{(2\pi)^4}\,I = \frac{2iGN_cN_f}{(2\pi)^4}\int d^4p\,\mathrm{tr}[S(p)], \tag{10.9}$$

---

[1] Note that this follows the commonly used convention of identifying the two-body interaction in the Hamiltonian density as $\frac{1}{2}V$ and denoting with V the interaction between a pair of particles *counted once*. The factor of two in $V^{(0)}(k) = -2G$ explicitly accounts for the symmetry of the interaction under particle exchange.

the meson mass equation (10.6) can thus be written as

$$R^{s/ps}(k) - I/m = 0 \quad \text{at } k^2 = m_{s/ps}^2, \tag{10.10}$$

with

$$R^s(k) = \int d^4p \, \text{tr}[S(p+k)S(p)], \tag{10.11}$$

$$R^{ps}(k) = -\int d^4p \, \text{tr}[\gamma_5 S(p+k)\gamma_5 S(p)], \tag{10.12}$$

and where I, as defined in (10.9), is evaluated through

$$I = \tfrac{1}{2} \int d^4p \left(\text{tr}[S(p+k)] + \text{tr}[S(p)] \right). \tag{10.13}$$

For the Dirac fermion propagator

$$S(p) = (\not{p} - m)^{-1} = \frac{\not{p} + m}{p^2 - m^2}, \tag{10.14}$$

with $m = m_{NJL}$ being the effective fermion mass (9.14) determined by the gap equation (9.10) in the chiral limit, this is readily calculated, leading to the expressions

$$R_{NJL}^s(k) = \int d^4p \, \frac{4(p^2 + p_\mu k^\mu + m^2)}{[(p+k)^2 - m^2](p^2 - m^2)}, \tag{10.15}$$

$$R_{NJL}^{ps}(k) = \int d^4p \, \frac{4(p^2 + p_\mu k^\mu - m^2)}{[(p+k)^2 - m^2](p^2 - m^2)}, \tag{10.16}$$

as well as

$$I_{NJL} = \int d^4p \, \frac{4m \left(p^2 + p_\mu k^\mu - m^2 \right) + 2k^2}{[(p+k)^2 - m^2](p^2 - m^2)}. \tag{10.17}$$

The meson mass equation (10.10) then takes the form of the established conditions

$$0 = (k^2 - 4m^2) \int d^4p \frac{1}{[(p+k)^2 - m^2](p^2 - m^2)} \quad \text{at} \quad k^2 = m_s^2 \tag{10.18}$$

for the mass m_s of the scalar σ meson bound state, and

$$0 = k^2 \int d^4p \frac{1}{[(p+k)^2 - m^2](p^2 - m^2)} \quad \text{at} \quad k^2 = m_{ps}^2 \tag{10.19}$$

for the pseudoscalar π meson mass m_{ps}, cf. [80]. They yield the apparent solutions that

$$m_s^2 = 4m^2 = 4m_{NJL}^2 \quad \text{and} \quad m_{ps}^2 = 0, \tag{10.20}$$

the latter of which is the Nambu-Goldstone mode in this model, in which chiral symmetry is spontaneously broken. An additional simultaneous solution of m_s and m_{ps} can be found when the momentum integral in (10.18) and (10.19) vanishes. In the Euclidean four-momentum cutoff regularization scheme this happens at $|k| = m_{s/ps} \approx 0.712\Lambda$. Besides the Nambu-Goldstone mode and its chiral partner, the meson mass spectrum of the NJL model therefore contains an additional finite mass solution that describes a scalar/pseudoscalar mode degeneracy. However, since this state is heavier than the sum of its constituent fermions, i.e. $m_{s/ps} > 2m_{NJL} \approx 0.469\Lambda$, this mode degeneracy likely describes a resonance rather than a bound-state solution.

Paralleling the discussion of the gap equation, the evaluation of the self-consistent approximation of the meson masses given above persists structurally when extending the NJL model through non-Hermitian bilinear terms, since the two-body interaction remains unchanged. The influence of the bilinear modifications is accounted for in the fermion propagator of the extended model, satisfying the equation of motion (9.15):

$$(\not{p} - m - g\Gamma)\,S(p) = \mathbb{1}. \tag{10.21}$$

In the following, the meson masses are obtained for the non-Hermitian extensions that allow for the dynamical generation of fermion mass. First, the extension based on $\Gamma_{aPT_2} = \gamma_5$, which, like m_0, breaks chiral symmetry explicitly, is analyzed. Then the effect of the chirally symmetric modifications $\Gamma_{aPT_1} = iA_\mu\gamma^\mu$ and $\Gamma_{PT_1} = i\gamma_5 B_\mu\gamma^\mu$ are studied, raising the question as to which role $\mathcal{PT}$ symmetry plays. In the $\mathcal{PT}$-symmetric model, dynamical fermion mass generation is, in addition, restricted to a finite coupling region. The analysis of the $\mathcal{PT}$ extension of the model on the meson masses is restricted to this region accordingly.

10.1 The Meson Masses for $\Gamma_{aPT_2} = \gamma_5$

In the modified NJL model based on the non-Hermitian, non-$\mathcal{PT}$-symmetric, and chiral-symmetry-breaking extension term $\Gamma_{aPT_2} = \gamma_5$, the spinor traces (10.11) to (10.13) are evaluated using the fermion propagator in the form (9.59) discussed in Section 9.4. They take the explicit form

$$R^s_{aPT_2}(k) = \int d^4p \, \frac{4(p^2 + p_\mu k^\mu + m^2 + g^2)}{[(p+k)^2 - m^2 + g^2]\,(p^2 - m^2 + g^2)}, \tag{10.22}$$

$$R^{ps}_{aPT_2}(k) = \int d^4p \, \frac{4(p^2 + p_\mu k^\mu - m^2 - g^2)}{[(p+k)^2 - m^2 + g^2]\,(p^2 - m^2 + g^2)}, \tag{10.23}$$

$$\frac{I_{aPT_2}}{m} = \int d^4p \, \frac{4(p^2 + p_\mu k^\mu - m^2 + g^2) + 2k^2}{[(p+k)^2 - m^2 + g^2]\,(p^2 - m^2 + g^2)}, \tag{10.24}$$

in which the effective fermion mass m is given by (9.64). The meson mass equation (10.10) thus becomes

$$0 = (k^2 - 4m^2) \int d^4p \frac{1}{[(p+k)^2 - m^2 + g^2](p^2 - m^2 + g^2)} \tag{10.25}$$

at $k^2 = m_s^2$ for the scalar mode, and

$$0 = (k^2 + 4g^2) \int d^4p \frac{1}{[(p+k)^2 - m^2 + g^2](p^2 - m^2 + g^2)}, \tag{10.26}$$

at $k^2 = m_{ps}^2$ for the pseudoscalar mode.

These resemble the equations (10.18) and (10.19) of the standard NJL model, but show one significant difference: The apparent solution of the pseudoscalar meson is no longer massless, signifying the breakdown of the Nambu-Goldstone mode. This is to be expected, considering that the non-Hermitian term $\Gamma_{aPT_2} = \gamma_5$ breaks the chiral symmetry of the model explicitly. Instead, one finds that

$$m_{ps}^2 = -4g^2, \tag{10.27}$$

that is the pseudoscalar π meson of this model is a *tachyonic* state with mass

$m_{ps} = \pm 2ig$. At the same time, the apparent scalar meson mass solution of (10.25) remains structurally unchanged compared to the standard NJL case (10.18). However, the effective fermion mass m of this model, as determined in (9.64), depends on the coupling strength g, such that

$$m_s^2 = 4m^2 = 4(m_{NJL}^2 + g^2). \tag{10.28}$$

That is to say, the dynamical mass generation of the effective fermion mass is reflected in the mass generation of the σ meson.

Moreover, similar to the standard NJL model, the scalar and pseudoscalar meson mass equations (10.25) and (10.26) admit an additional simultaneous solution, when the momentum integral vanishes. In fact, the coupling dependence of the effective fermion mass, $m^2 = m_{NJL}^2 + g^2$, exactly counteracts the coupling dependence of this momentum integral. That is, it is found to be the same integral that occurs in the meson mass equations of the standard NJL model. Accordingly, the resulting scalar/pseudoscalar mode degeneracy remains unaffected by the chiral symmetry breaking due to the non-Hermitian extension and has the same mass as the degenerate solution of the standard NJL model; namely $m_{s/ps} \approx \pm 0.712\Lambda$ in the Euclidean four-momentum cutoff regularization. Contrary to the standard NJL model, this scalar/pseudoscalar meson mode degeneracy can in principle be lighter than the sum of the constituent fermions when the coupling constant g exceeds values $g \approx 0.268\Lambda$. However, in this coupling region the effective fermion mass exceeds values of $m \approx 0.356\Lambda = 361$ MeV, which corresponds to a significant current quark mass of about 123 MeV.

Altogether, extending the NJL model based on the non-$\mathcal{PT}$-symmetric, non-chirally-symmetric term $\Gamma_{aPT_2} = \gamma_5$ results in a dynamical mass gain of the scalar σ meson, reflecting the effective mass generation of the fermion. However, it appears to act as a tachyonic instability of the pseudoscalar π meson. Despite the fact that the Nambu-Goldstone mode becomes tachyonic, the combination of the non-degenerate scalar and pseudoscalar meson masses $m_s^2 + m_{ps}^2 = 4m_{NJL}^2$ remains unchanged from the NJL model. The mass of the scalar/pseudoscalar meson mode degeneracy in the standard NJL model remains unaffected by this non-Hermitian extension of the model.

10.2 The Meson Masses for $\Gamma_{aPT_1} = iA_\mu \gamma^\mu$

In the modified NJL model based on the non-Hermitian, non-$\mathcal{PT}$-symmetric, but chirally symmetric term $\Gamma_{aPT_1} = iA_\mu \gamma^\mu$, the spinor traces in the meson mass equation (10.10) are evaluated for the fermion propagator (9.52). With this propagator, the terms (10.11) to (10.13) become

$$
\begin{aligned}
R^s_{aPT_1}(k) = \int d^4 p \, 4(p^2 + p_\mu k^\mu + m^2 - g^2 A^2 - 2ig A_\mu p^\mu - ig A_\mu k^\mu) \\
\times \left\{ [(p+k)^2 - m^2 - g^2 A^2 - 2ig A_\mu (p+k)^\mu] \right. \\
\left. \times (p^2 - m^2 - g^2 A^2 - 2ig A_\mu p^\mu) \right\}^{-1},
\end{aligned} \tag{10.29}
$$

$$
\begin{aligned}
R^{ps}_{aPT_1}(k) = \int d^4 p \, 4(p^2 + p_\mu k^\mu - m^2 - g^2 A^2 - 2ig A_\mu p^\mu - ig A_\mu k^\mu) \\
\times \left\{ [(p+k)^2 - m^2 - g^2 A^2 - 2ig A_\mu (p+k)^\mu] \right. \\
\left. \times (p^2 - m^2 - g^2 A^2 - 2ig A_\mu p^\mu) \right\}^{-1},
\end{aligned} \tag{10.30}
$$

as well as

$$
\begin{aligned}
\frac{I_{aPT_1}}{m} = \int d^4 p \, 4(p^2 + p_\mu k^\mu - m^2 - g^2 A^2 - 2ig A_\mu p^\mu - ig A_\mu k^\mu) + 2k^2) \\
\times \left\{ [(p+k)^2 - m^2 - g^2 A^2 - 2ig A_\mu (p+k)^\mu] \right. \\
\left. \times (p^2 - m^2 - g^2 A^2 - 2ig A_\mu p^\mu) \right\}^{-1},
\end{aligned} \tag{10.31}
$$

in which the fermion mass m is the solution to the gap equation (9.57) discussed in Section 9.3. The meson mass equation (10.10) thus takes the form

$$
\begin{aligned}
0 = (k^2 - 4m^2) \int d^4 p \left\{ [(p+k)^2 - m^2 - g^2 A^2 - 2ig A_\mu (p+k)^\mu] \right. \\
\left. \times (p^2 - m^2 - g^2 A^2 - 2ig A_\mu p^\mu) \right\}^{-1}
\end{aligned} \tag{10.32}
$$

at $k^2 = m_s^2$ for the scalar mode, and

$$
\begin{aligned}
0 = k^2 \int d^4 p \left\{ [(p+k)^2 - m^2 - g^2 A^2 - 2ig A_\mu (p+k)^\mu] \right. \\
\left. \times (p^2 - m^2 - g^2 A^2 - 2ig A_\mu p^\mu) \right\}^{-1}
\end{aligned} \tag{10.33}
$$

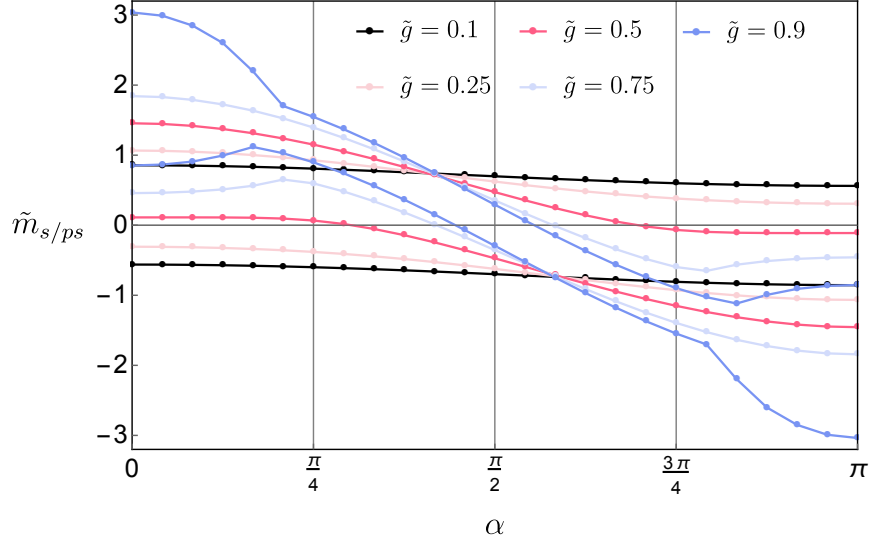at $k^2 = m_{ps}^2$ for the pseudoscalar mode.

Figure 10.2: Behavior of the meson mass $\tilde{m}_{s/ps}$ of the scalar/pseudoscalar mode degeneracy as a function of the angle α between the Euclidean background field and the Euclidean meson momentum for different values of the coupling constant $\tilde{g}$. Adapted from [67].

Again, a close resemblance to the meson mass equations (10.18) and (10.19) of the standard NJL model can be noticed: Both apparent solutions,

$$m_s^2 = 4m^2 \qquad \text{and} \qquad m_{ps}^2 = 0, \qquad (10.34)$$

are structurally identical to the solutions (10.20). In particular, the presence of the massless pseudoscalar mode as the Nambu-Goldstone boson of the theory remains intact, since the chiral symmetry is preserved by the non-Hermitian extension Γ_{aPT_1}. Likewise, the structure of the scalar σ meson remains unchanged, although it now reflects the mass generation of the fermion mass m.

In addition, the appearance of identical four-momentum integrals in both meson mass equations (10.32) and (10.33) indicates the existence of a simultaneous meson mass solution, as was the case in the standard NJL model. But due to the dependence of this momentum integral on the term $A_\mu k^\mu$, this solution is not constant, as in the standard NJL model or in Section 10.1. It varies with the angle between the background field A_μ and the meson momentum k_μ. In the Euclidean four-momentum cutoff regularization the mass solution can be determined numerically as a function of the angle α between the the Euclidean background
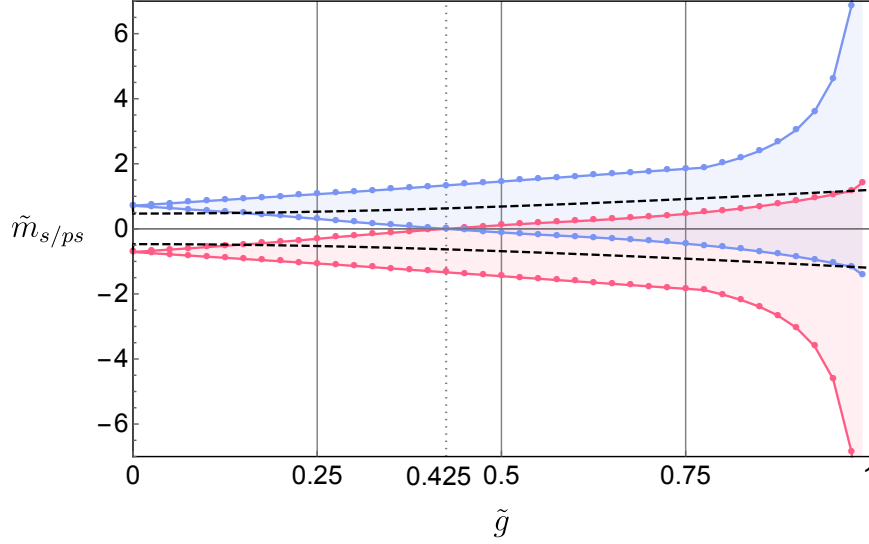
Figure 10.3: Behavior of the region of mass in the scalar/pseudoscalar mode degeneracy that is accessible through variation of the angle α as a function of the bilinear-coupling constant $\tilde{g}$. The dashed black line denotes the behavior of $2m$, with m being the fermion mass solution of the model, see Figure 9.9b. Adapted from [67].

field A_E and the Euclidean meson momentum k_E from the roots of the integral. The behavior of this solution as a function of α is visualized in Figure 10.2 for various small coupling values $\tilde{g} = g|A_E|\Lambda^{-1} < 1$, which are in particular proportional to the amplitude of the background field. Figure 10.3 shows the behavior of the extremal values that the meson mass takes when varying α as a function of the coupling $\tilde{g}$. The shaded regions indicate that all mass values between these extrema are realized at some angle α, because the mass varies continuously in the angle. Notably, arbitrarily small or vanishing degenerate meson masses $m_{s/ps}$ can be found for coupling values larger than $\tilde{g} \approx 0.425$, but such coupling values also generate a significant fermion mass in the model. The dashed black line denotes the behavior of $2m$, where m is the effective fermion mass of this model. At small coupling values $\tilde{g}$ the mode degeneracy is heavier than the sum of its constituent fermions for all angles α, i.e. $\tilde{m}_{s/ps} > 2m$, so that this state is likely a resonance rather than a bound-state solution.

Altogether, extending the NJL model based on the non-$\mathcal{PT}$-symmetric, but chirally symmetric term $\Gamma_{aPT_1} = iA_\mu\gamma^\mu$ results in a dynamical mass gain of the scalar σ meson, reflecting the effective mass generation of the fermion, and

a massless pseudoscalar π meson as the Nambu-Goldstone boson of this model in which chiral symmetry is spontaneously broken. An additional scalar/pseudoscalar mode degeneracy of the meson masses, which depends intricately on the amplitude of the background field and its angle relative to the meson momentum, can be found.

10.3 The Meson Masses for $\Gamma_{PT_1} = i\gamma_5 B_\mu \gamma^\mu$

In the modified NJL model based on the non-Hermitian, but $\mathcal{PT}$-symmetric and chirally symmetric extension term $\Gamma_{PT_1} = i\gamma_5 B_\mu \gamma^\mu$, real fermion masses are generated dynamically within a finite region of coupling values smaller than $\tilde{g}_{\text{dyn}} = g_{\text{dyn}}|B_E|\Lambda^{-1} \approx 1.183$. In particular, at small bilinear-coupling values $\tilde{g} \leq 1$ the non-Hermitian extension mimics the inclusion of a bare mass term m_0. To study the effect of the extension on the meson masses the spinor traces (10.11) to (10.13) are evaluated using the fermion propagator in the form (9.19),

$$
S(p) = \frac{(\not{p} + m + ig\gamma_5 B_\mu \gamma^\mu)\left[p^2 - m^2 - g^2 B^2 + 2igm\gamma_5 B_\nu \gamma^\nu + 2igB_\nu p^\nu \gamma_5\right]}{(p^2 - m^2 - g^2 B^2)^2 - 4g^2 m^2 B^2 + 4g^2 (B_\mu p^\mu)^2},
$$
(10.35)

discussed in Section 9.1. This propagator simplifies less than in the case of the models discussed previously, and results in somewhat cumbersome expressions for (10.11) to (10.13). But when combined in the meson mass equation (10.10) additional simplifications are possible, resulting in the equations

$$
0 = \int d^4 p \left[(k^2 - 4m^2)a(p,k) + 8g^2 b(p,k)\right]
$$
$$
\times \left\{\left[\left((p+k)^2 - m^2 - g^2 B^2\right)^2 - 4g^2 m^2 B^2 + 4g^2\left(B_\mu(p+k)^\mu\right)^2\right] \right.
$$
(10.36)
$$
\left. \times \left[(p^2 - m^2 - g^2 B^2)^2 - 4g^2 m^2 B^2 + 4g^2 (B_\mu p^\mu)^2\right]\right\}^{-1}
$$

at $k^2 = m_s^2$ for the scalar mode, and

$$
0 = \int d^4 p \left[k^2 a(p,k) + 8g^2 b(p,k)\right]
$$
$$
\times \left\{\left[\left((p+k)^2 - m^2 - g^2 B^2\right)^2 - 4g^2 m^2 B^2 + 4g^2\left(B_\mu(p+k)^\mu\right)^2\right] \right.
$$
(10.37)
$$
\left. \times \left[(p^2 - m^2 - g^2 B^2)^2 - 4g^2 m^2 B^2 + 4g^2 (B_\mu p^\mu)^2\right]\right\}^{-1}
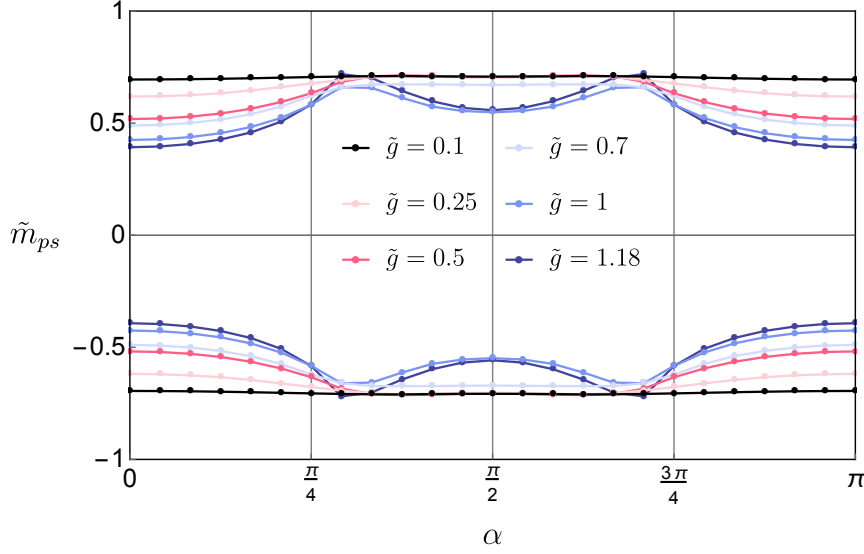$$

Figure 10.4: Behavior of the meson mass $\tilde{m}_{ps}$ of the pseudoscalar mode as a function of the angle α between the Euclidean background field and the Euclidean meson momentum for different values of the coupling constant $\tilde{g}$. Adapted from [67].

at $k^2 = m_{ps}^2$ for the pseudoscalar mode, where

$$a(p,k) = [(p+k)^2 - m^2 + g^2B^2](p^2 - m^2 + g^2B^2) \\ + 4g^2[B^2 p_\mu (p+k)^\mu - (B_\mu p^\mu)(B_\nu (p+k)^\nu)], \tag{10.38}$$

$$b(p,k) = 2(p_\mu k^\mu)(B_\nu k^\nu)(B_\alpha p^\alpha) - B^2(p_\mu k^\mu)^2 + p^2 k^2 B^2 \\ - k^2(B_\mu p^\mu)^2 - p^2(B_\mu k^\mu)^2. \tag{10.39}$$

Notably, the vector products in $b(p,k)$ show an overall proportionality to $|k|^2$, so that the equation (10.37) admits a vanishing mass solution of the pseudoscalar π meson. Thus, as in Section 10.2, the non-Hermitian extension Γ_{PT_1} does not disrupt the presence of the Nambu-Goldstone boson, because the chiral symmetry of the model is preserved. In addition, the pseudoscalar meson mass equation (10.37) permits a second possible solution that can be found through numerical evaluation of the momentum integral in the Euclidean four-momentum cutoff regularization scheme. This solution depends, in particular, on the angle α between the Euclidean background field B_E and the Euclidean pion momentum k_E.

The behavior of this second pseudoscalar mode solution is visualized in Figure 10.4 as a function of α for various coupling values $\tilde{g} = g|B_E|\Lambda^{-1}$ in the
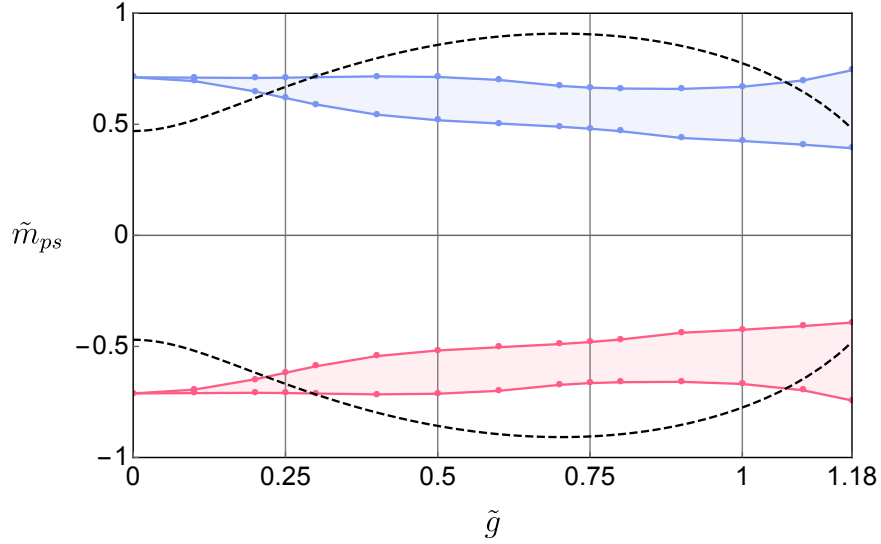
Figure 10.5: Behavior of the region of masses in the pseudoscalar mode that is accessible through variation of α as a function of the bilinear-coupling constant $\tilde{g}$. The dashed black line denotes the behavior of $2m$, with m being the fermion mass solution of the model, see Figure 9.4. Adapted from [67].

region where a fermion mass is dynamically generated, that is $\tilde{g} < \tilde{g}_{\mathrm{dyn}} \approx 1.183$. Figure 10.5 shows the behavior of the extremal values that the pseudoscalar meson mass takes when varying α as a function of the coupling $\tilde{g}$ in the same region. The shaded areas indicate that all mass values between the extrema are realized at some angle α, since the mass varies continuously with the angle. Notably, for all coupling values $\tilde{g}$ and angles α this solution of the meson mass has finite real values. The dashed black line denotes the behavior of $2m$, where m is the effective fermion mass of this model. At small coupling values $\tilde{g}$, where the system mimics the generation of a small current quark mass through the inclusion of a finite bare mass m_0, the pseudoscalar mode is heavier than the sum of its constituent fermions, $\tilde{m}_{ps} > 2m$, so that this state is likely a resonance rather than a bound-state solution.

Contrary to the standard NJL model and the modified NJL models discussed previously, the second solution of the pseudoscalar mode is not a simultaneous solution of the scalar mode. Furthermore, the meson mass equation (10.36) does in general not have an apparent solution, which factors out of the momentum integral, as was the case in the other models discussed so far. Specifically, the σ
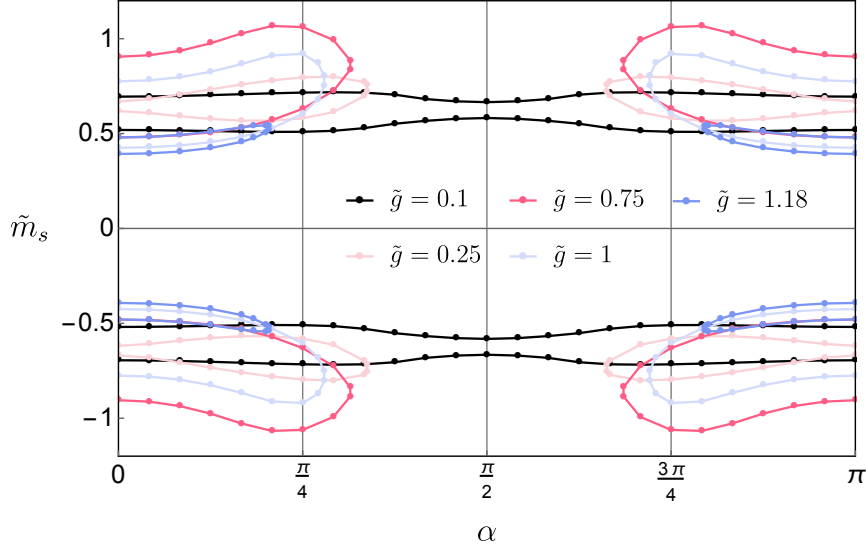
Figure 10.6: Behavior of the meson mass $\tilde{m}_s$ of the scalar mode as a function of the angle α between the Euclidean background field and the Euclidean meson momentum for different values of the coupling constant $\tilde{g}$. Adapted from [67].

meson does not have a mass solution which is proportional only to the effective fermion mass m of the model.

Evaluating the equation (10.36) numerically in the Euclidean four-momentum cutoff regularization, one finds two possible solutions, which both depend on the coupling constant $\tilde{g}$ as well as the angle α between the Euclidean background field B_E and the Euclidean scalar-meson momentum k_E. Their behavior is shown in Figure 10.6 for various fixed values of the coupling constant $\tilde{g}$ as a function of the angle α. Note that for small coupling values below $\tilde{g} \approx 0.107$ the real mass solutions exist for all angles α, but at larger couplings the solutions begin to break down around $\alpha = \pi/2$. Nevertheless, the σ meson mass solutions never break down entirely (for all α), and a real solution can always be found at some angle. Where scalar meson mass solutions exist, they are continuous functions of the coupling, so that all masses between the extremal values are realized. The behavior of the extremal values is shown in Figure 10.7 as a function of the coupling constant $\tilde{g}$ in the region where an effective fermion mass is generated dynamically ($\tilde{g} < \tilde{g}_{\text{dyn}} \approx 1.183$). The accessible mass values between these extrema are indicated as shaded regions. When the real mass solutions begin to break down
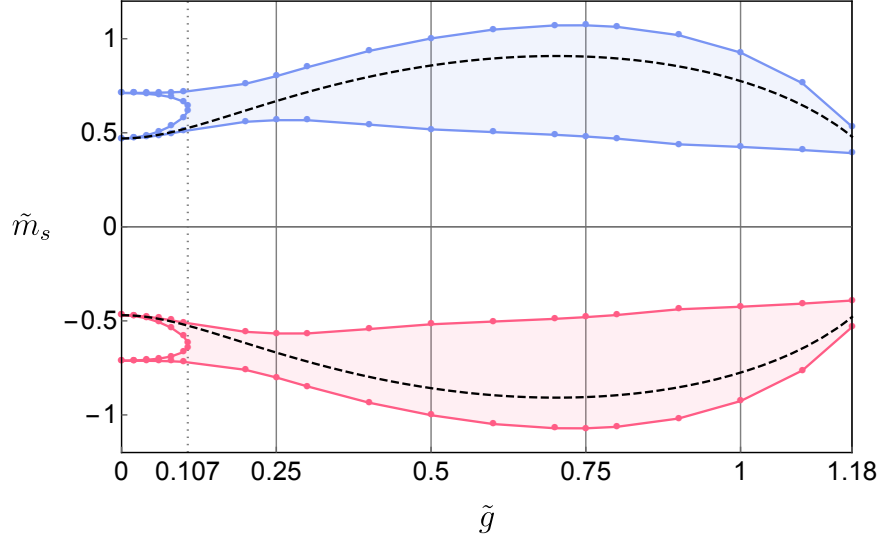
Figure 10.7: Behavior of the region of masses in the scalar mode that is accessible through variation of α as a function of the bilinear-coupling constant $\tilde{g}$. The dashed black line denotes the behavior of $2m$, with m being the fermion mass solution of the model, see Figure 9.4. Adapted from [67].

around $\alpha = \pi/2$ at sufficiently large coupling values, the two separated solutions of the scalar mode merge at the boundary, as can be seen in Figure 10.6. The initially separate regions of accessible σ meson mass solutions at small coupling constants $\tilde{g} < 0.107$ therefore combine into a single region in Figure 10.7. The dashed black line again denotes the behavior of $2m$, where m is the effective fermion mass of this model. At small coupling values $\tilde{g}$ both scalar-mode solutions are heavier than the sum of the constituent fermions, $\tilde{m}_s \geq 2m$, so that these states are likely resonances rather than a bound-state solutions.

One special case of the scalar meson mass shall be emphasized: When the Euclidean background field B_E is parallel to the meson momentum k_E, that is $\alpha = 0$, the function $b(p, k)$ in (10.39) vanishes, resulting in the apparent scalar-meson mass of the standard NJL model $m_s^2 = 4m^2$ and the presence of a scalar/pseudoscalar mode degeneracy. Here the effective fermion mass m is given as solution to the gap equation (9.27) and depends on the coupling strength g of the bilinear term. The case of $\alpha = 0$ is, in addition, a special case of the modified Dirac fermion with Hamiltonian density

$$\mathcal{H} = \bar{\psi}(-i\gamma^k \partial_k + ig\gamma_5 B_\mu \gamma^\mu)\psi, \tag{10.40}$$

obtained at $G = 0$, as well: From its dispersion relation

$$0 = (p^2 - g^2 B^2)^2 + 4g^2 (B_\mu p^\mu)^2 \qquad \text{at} \quad p^2 = m^2 \qquad (10.41)$$

the effective mass is found to be $m^2 = g^2 B^2 \exp[\mp 2i\alpha]$, describing generally complex solutions, see [61], but for $\alpha = 0$ it simplifies to the real result $m^2 = g^2 B^2$.

Altogether, extending the NJL model based on the $\mathcal{PT}$-symmetric and chirally symmetric term $\Gamma_{PT_1} = i\gamma_5 B_\mu \gamma^\mu$ results in a massless pseudoscalar π meson as the Nambu-Goldstone boson of this model. In addition, a finite pseudoscalar-meson mass solution, which depends intricately on the amplitude of the background field and its angle relative to the meson momentum, is found. Moreover, two scalar-meson mass solutions, which are both independent from the pseudoscalar mode and do generally not form a mode degeneracy, can be obtained. Similar to the finite mass solution of the pseudoscalar meson, these solutions show an intricate dependence on the amplitude of the background field and its angle relative to the meson momentum. They can break down for specific angles α and bilinear coupling strengths $\tilde{g} = g|B_E|\Lambda^{-1}$.

10.4 Summary of the Meson Masses

The effect of non-Hermitian bilinear extensions of the NJL model on the mass of the scalar- and pseudoscalar-meson bound states was studied for those models in which the extension results in the dynamical mass generation of the fermion. Namely, the bilinears based on the chirally symmetric terms $\Gamma_{PT_1} = i\gamma_5 B_\mu \gamma^\mu$ and $\Gamma_{aPT_1} = iA_\mu \gamma^\mu$, as well as the chiral-symmetry-breaking term $\Gamma_{aPT_2} = \gamma_5$, were considered.

In both chirally symmetric models one finds that the pseudoscalar π meson is a massless state, identifying it as the Nambu-Goldstone boson. The existence of this solution thus remains expectedly unaffected by the inclusion of chirally symmetric bilinears into the standard NJL model. This is in particular independent of the fact that Γ_{PT_1} is $\mathcal{PT}$ symmetric, while Γ_{aPT_1} results in a non-Hermitian, non-$\mathcal{PT}$-symmetric system. Including the chiral-symmetry-breaking term Γ_{aPT_2} acts as a tachyonic instability of the pseudoscalar-meson mode.

A structural difference between the $\mathcal{PT}$-symmetric and the non-$\mathcal{PT}$-symmetric models is found for the scalar σ meson: In the non-$\mathcal{PT}$-symmetric models based on Γ_{aPT_1} and Γ_{aPT_2} the mass of the scalar meson, $m_s^2 = 4m^2$, remains structurally unchanged compared to the standard NJL model and depends on the bilinear coupling strength g only indirectly through the effective fermion mass m. In the $\mathcal{PT}$-symmetric model, on the other hand, the mass of the scalar-meson mode depends intricately on $\tilde{g} = g|B_E|\Lambda^{-1}$, as well as the angle of the background field B_E to the meson momentum. This distinction is furthermore reflected in the existence of a meson-mode degeneracy. When modifying the standard NJL model through a bilinear based on Γ_{aPT_1} or Γ_{aPT_2} a scalar/pseudoscalar mode degeneracy continues to exist. In fact, for Γ_{aPT_2} the mass of this state remains unaffected by the extension term. For the extension based on Γ_{aPT_1} the state depends intricately on the coupling strength $\tilde{g} = g|A_E|\Lambda^{-1}$ and the angle of the background field to the meson momentum, but it remains present in the system. In the $\mathcal{PT}$-symmetric model based on Γ_{PT_1} a meson-mode degeneracy does generally not exist. These additional meson mass solutions, degenerate or not, are, at small coupling values where small current quark masses are generated, heavier than their constituent fermions and thus likely resonance states rather than bound-state solutions.

Chapter 11

The Modified Gross-Neveu Model

The analysis of the self-consistent gap equation in Chapter 9 and of the self-consistent meson-mass equations in Chapter 10 has demonstrated that non-Hermitian bilinear extensions of the $3 + 1$ dimensional NJL model provide a fertile ground for the study of $\mathcal{PT}$ symmetry in fermionic field theories. However, like the standard NJL model, these systems come with the caveat that they are not renormalizable. The $1 + 1$ dimensional chiral Gross-Neveu (GN) model [90] structurally resembles the NJL model and retains many of its properties while also being renormalizable. As such it is an important toy-model for the study of QCD. Its Hamiltonian density has the form

$$\mathcal{H}_{\mathrm{GN}} = \bar{\psi}(-i\gamma^1\partial_1 + m_0)\psi - G[(\bar{\psi}\psi)^2 + (\bar{\psi}i\gamma_5\vec{\tau}\psi)^2] \tag{11.1}$$

in terms of the $(1 + 1$ dimensional) Dirac matrices γ, see (7.2), the isospin SU(2) matrices $\vec{\tau}$, and the two-body coupling strength G. In this chapter the GN model is modified through the inclusion of non-Hermitian bilinear terms in the same way as the NJL model in Chapter 8 and Chapter 9.

Beyond their renormalizability these systems are of particular interest in the context of $\mathcal{PT}$ symmetry, because time reversal is an even operation in $1 + 1$ space-time dimensions: $\mathcal{T}^2 = +1$, see Chapter 7. The analysis of the modified GN model might therefore supplement the study of $\mathcal{PT}$ symmetry in the modified NJL model and clarify the role of $\mathcal{PT}$ symmetry in fermionic systems. This chapter is structured as follows.

In Section 11.1 the possible non-Hermitian bilinear extensions of the GN model are identified and their behavior under combined parity reflection and time reversal is established.

In Section 11.2 to Section 11.4 the gap equation for the modified GN models is derived following the same approach as in Chapter 9 for the NJL model. In addition, the systems are then renormalized.

Section 11.5 presents a comparison to the corresponding extensions of the NJL model and closing remarks.

11.1 Non-Hermitian Extension

The $1+1$ dimensional GN model is modified through the inclusion of various non-Hermitian bilinear terms $\bar{\psi}\,\Omega\,\psi$, containing a complex 2×2 matrix Ω, similar to the extension of the NJL model in Section 8.1. The Hamiltonian density of such a model has the form

$$\mathcal{H}_{\mathrm{GN}} = \bar{\psi}(-i\gamma^1\partial_1 + m_0 + g\,\Omega)\psi - G[(\bar{\psi}\psi)^2 + (\bar{\psi}i\gamma_5\vec{\tau}\psi)^2], \qquad (11.2)$$

where $g \in \mathbb{R}$ is the associated bilinear-coupling constant.

The complete set of complex 2×2 matrices can be written as a real superposition of the eight matrices that are generated by the $1+1$ dimensional Dirac matrices (7.2):

$$\mathbb{1}, \qquad \gamma_5, \qquad \gamma^\mu, \qquad i\mathbb{1}, \qquad i\gamma_5, \qquad i\gamma^\mu, \qquad (11.3)$$

where $\mu \in [0,1]$ denotes the spin indices. Based on these matrices, the following structurally distinct modifications are identified

$$\mathbb{1}, \qquad \gamma_5, \qquad A_\mu\gamma^\mu, \qquad i\mathbb{1}, \qquad i\gamma_5, \qquad iA_\mu\gamma^\mu, \qquad (11.4)$$

with A_μ being the elements of a real vector. Out of these, only the bilinears for which Ω has one of the forms

$$i\mathbb{1}, \qquad \gamma_5, \qquad iA_\mu\gamma^\mu, \qquad (11.5)$$

describe non-Hermitian extensions of the GN model.

Under the combined parity reflection $\mathcal{P}$ and time reversal $\mathcal{T}$, as given in (7.3), the bilinears $\bar{\psi}\,\Omega\,\psi$ with Ω being

$$\Omega_{aPT_1} = iA_\mu\gamma^\mu \qquad \text{or} \qquad \Omega_{aPT_2} = i\mathbb{1} \tag{11.6}$$

are anti-$\mathcal{PT}$-symmetric, that is $\{\mathcal{PT}, \Omega\} = 0$. The modified GN models based on these terms are therefore non-Hermitian and non-$\mathcal{PT}$-symmetric systems. Notice that the extension terms based on Ω_{aPT_1} and Ω_{aPT_2} have the same symmetry properties as their respective $3+1$ dimensional counterparts Γ_{aPT_1} and Γ_{aPT_3}, see (8.7).

The bilinear extension based on

$$\Omega_{PT_1} = \gamma_5, \tag{11.7}$$

on the other hand, is $\mathcal{PT}$ symmetric; that is $[\mathcal{PT}, \Omega_{PT_1}] = 0$. The associated modified GN model describes a $\mathcal{PT}$-symmetric theory. This is the exact opposite of the modified NJL model based on the $3+1$ dimensional counterpart Γ_{aPT_2}, see (8.7). The symmetry change from being a non-$\mathcal{PT}$-symmetric theory to being a $\mathcal{PT}$ theory was previously remarked upon for the modified Dirac fermion in [61], see also Chapter 7.

The behavior of the modified GN models under chiral symmetry remains unchanged from their $3+1$ dimensional counterparts. Namely, the model based on Ω_{aPT_1} is chirally symmetric, while the remaining models based on Ω_{PT_1} and Ω_{aPT_2} break chiral symmetry explicitly. In the latter cases the limit of vanishing bare mass m_0 is thus not a chiral limit.

A self-consistent approximation of the effective fermion mass in the modified GN models is obtained by following the same approach as described for the NJL model in Chapter 9. This mass m is determined by the gap equation of the form

$$m = m_0 + 2iGN_cN_f \int \frac{d^2p}{(2\pi)^2} \, \text{tr}[S(p)], \tag{11.8}$$

where m_0 denotes the bare mass term and $S(p)$ is the full fermion propagator, which has the general form

$$S(p) = (\not{p} - m - g\,\Omega)^{-1}. \tag{11.9}$$

For the standard GN model, obtained at $g = 0$, the propagator

$$S(p) = (\not{p} - m)^{-1} = \frac{\not{p} + m}{p^2 - m^2}, \quad \text{with} \quad \text{tr}[S(p)] = \frac{2m}{p^2 - m^2} \tag{11.10}$$

results in the gap equation of the form

$$1 = \frac{iGN_cN_f}{\pi^2} \int d^2p \, \frac{1}{p^2 - m^2} \tag{11.11}$$

in the chiral limit $m_0 \to 0$. By rewriting the momentum integral in Euclidean coordinates with $p_0 = ip_2$, so that $p_E^2 = p_1^2 + p_2^2 = -p^2$, and introducing a radial cutoff scale Λ, this reduces to

$$\frac{\pi}{GN_cN_f} = \ln\left(1 + \frac{\Lambda^2}{m^2}\right). \tag{11.12}$$

In the ultraviolet limit of large Λ, the divergence of the gap equation (11.12) can be absorbed into a renormalized two-body interaction strength G_R as follows. Rewriting the cutoff scale in terms of an arbitrarily chosen dimensional energy scale $c = 1$ MeV and a dimensionless parameter λ as $\Lambda = c\lambda$, the gap equation is expanded in the limit of large λ, yielding

$$\frac{\pi}{GN_cN_f} = 2\ln\lambda + \ln\left(\frac{c^2}{m^2}\right) + O\left(\frac{1}{\lambda^2}\right) \quad \text{as} \quad \lambda \to \infty. \tag{11.13}$$

The logarithmically divergent term is then absorbed into the renormalized two-body coupling as

$$\frac{1}{G_R} = \frac{1}{G} - \frac{2N_cN_f}{\pi}\ln\lambda. \tag{11.14}$$

The renormalized gap equation follows in the limit $\lambda \to \infty$ while keeping G_R fixed as

$$\frac{\pi}{G_RN_cN_f} = \ln\left(\frac{c^2}{m^2}\right), \tag{11.15}$$

with the solution for the renormalized mass being

$$m_{GN} = c\left[\exp\left(\frac{\pi}{G_RN_cN_f}\right)\right]^{-1/2}. \tag{11.16}$$

In the following sections the gap equation (11.8) is analyzed for the three non-Hermitian extensions of the GN model based on Ω in (11.6) and (11.7).

11.2 The Fermion Mass for $\Omega_{PT_1} = \gamma_5$

The analysis of the non-Hermitian GN model based on the $\mathcal{PT}$-symmetric, but chiral-symmetry-breaking extension term $\Omega_{PT_1} = \gamma_5$ has been published in [66] and the following discussion closely follows that presentation.

For the extension term $\Omega_{PT_1} = \gamma_5$ the fermion propagator (11.9) is formally given as

$$S(p) = (\not{p} - m - g\gamma_5)^{-1} \tag{11.17}$$

and can, similar to the discussion of the $3 + 1$ dimensional analogue discussed in Section 9.4, be rewritten as

$$S(p) = \frac{\not{p} + m - g\gamma_5}{p^2 - m^2 + g^2}, \quad \text{with} \quad \text{tr}[S(p)] = \frac{2m}{p^2 - m^2 + g^2}. \tag{11.18}$$

The general gap equation (11.8) thus takes the form

$$1 = \frac{iGN_cN_f}{\pi^2} \int d^2p \, \frac{1}{p^2 - m^2 + g^2} \tag{11.19}$$

in the limit of vanishing bare mass m_0. In Euclidean coordinates with $p_0 = ip_2$, so that $p_E^2 = p_1^2 + p_2^2 = -p^2$, and by introducing a radial cutoff scale Λ, this reduces to

$$\frac{\pi}{GN_cN_f} = \ln(1 + \frac{\Lambda^2}{m^2 - g^2}). \tag{11.20}$$

By rewriting $\Lambda = c\lambda$, with $c = 1$ MeV, the equation (11.20) behaves as

$$\frac{\pi}{GN_cN_f} = 2\ln\lambda + \ln(\frac{c^2}{m^2 - g^2}) + O(\frac{1}{\lambda^2}) \quad \text{as} \quad \lambda \to \infty. \tag{11.21}$$

The ultraviolet divergence can be absorbed into the renormalized two-body coupling

$$\frac{1}{G_R} = \frac{1}{G} - \frac{2N_cN_f}{\pi}\ln\lambda, \tag{11.22}$$

which has the same form as in the standard GN model, cf. (11.14). In the limit

of large λ, while keeping G_R fixed, the renormalized gap equation becomes

$$\frac{\pi}{G_R N_c N_f} = \ln\left(\frac{c^2}{m^2 - g^2}\right), \tag{11.23}$$

with the solution for the renormalized mass being

$$m = \sqrt{g^2 + c^2 \left[\exp\left(\frac{\pi}{G_R N_c N_f}\right)\right]^{-1}} = \sqrt{g^2 + m_{GN}^2}. \tag{11.24}$$

This effective mass solution parallels the solution found in the $3 + 1$ dimensional NJL model based on $\Gamma_{aPT_2} = \gamma_5$, cf. (9.64). In fact, when choosing $m_{GN} = m_{NJL}$ for comparison of the two systems, the mass solutions are identical.

In this the solution to the gap equation resembles the dispersion relation of the underlying modified Dirac fermion (obtained at $G = 0$) discussed in [61] and Chapter 7: Even though the behavior under $\mathcal{PT}$ symmetry changes between the $3+1$ dimensional system, in which time reversal is odd, and the $1+1$ dimensional system, where time reversal is even, the effective fermion-mass solution remains unchanged. Contrary to the modified Dirac fermion, the addition of two-body interactions has, however, restored the existence of *real* mass solutions even in the limit of vanishing bare mass m_0.

11.3 The Fermion Mass for $\Omega_{aPT_1} = iA_\mu\gamma^\mu$

In the non-Hermitian GN model based on the non-$\mathcal{PT}$-symmetric, but chirally symmetric extension term $\Omega_{aPT_1} = iA_\mu\gamma^\mu$ the fermion propagator (11.9) is formally given as

$$S(p) = (\not{p} - m - igA_\mu\gamma^\mu)^{-1} \tag{11.25}$$

and can, like the $3 + 1$ dimensional analogue in Section 9.3, be rewritten as

$$S(p) = \frac{\not{p} + m - iA_\mu\gamma^\mu}{p^2 - m^2 - g^2 A^2 - 2igA_\mu p^\mu}, \tag{11.26}$$

with the spinor trace

$$\mathrm{tr}[S(p)] = \frac{2m}{p^2 - m^2 - g^2 A^2 - 2igA_\mu p^\mu}. \tag{11.27}$$

In the limit of vanishing bare mass the gap equation (11.8) thus becomes

$$1 = \frac{iGN_cN_f}{\pi^2} \int d^2p \, \frac{1}{p^2 - m^2 - g^2A^2 - 2igA_\mu p^\mu}. \tag{11.28}$$

The momentum integral can now be evaluated in Euclidean coordinates with $p_0 = ip_2$ and $A_0 = iA_2$, so that $p^2 = -p_E^2$, $A^2 = -A_E^2$, and $A_\mu p^\mu = -A_E \cdot p_E$, by transforming into a polar coordinate system with $A_E \cdot p_E = |A_E| \, r \cos\theta$ and a radial cutoff Λ:

$$1 = \frac{GN_cN_f}{\pi^2} \int_0^\Lambda dr \int_0^{2\pi} d\theta \, \frac{r}{r^2 + m^2 - g^2A_E^2 - 2igA_E r \cos\theta}. \tag{11.29}$$

Both the angular integral and the resulting radial integral are standard integrals that can be found, for example, in [51]. Evaluating them yields the equation

$$\frac{\pi}{GN_cN_f} = \ln\left[\frac{1}{2\tilde{m}^2}\left(\sqrt{(1 + \tilde{m}^2 + \tilde{g}^2)^2 - 4\tilde{g}^2\tilde{m}^2} + 1 + \tilde{m}^2 + \tilde{g}^2\right)\right] \tag{11.30}$$

in terms of the rescaled quantities $\tilde{m} = m\Lambda^{-1}$ and $\tilde{g} = g|A_E|\Lambda^{-1}$.

When writing $\Lambda = c\lambda$, with $c = 1$ MeV, equation (11.30) behaves like

$$\frac{\pi}{GN_cN_f} = 2\ln\lambda + \ln\left(\frac{c^2}{m^2}\right) + \frac{m^2 + g^2}{c^2\lambda^2} + O\left(\frac{1}{\lambda^4}\right) \quad \text{as} \quad \lambda \to \infty. \tag{11.31}$$

Notably, the ultraviolet-divergent first term can be absorbed into the renormalized two-body coupling G_R in the same way as for the standard GN model (11.14),

$$\frac{1}{G_R} = \frac{1}{G} - \frac{2N_cN_f}{\pi}\ln\lambda. \tag{11.32}$$

Moreover, the remaining nonvanishing contribution does not depend on the bilinear-coupling constant g: the resulting renormalized gap equation

$$\frac{\pi}{G_RN_cN_f} = \ln\left(\frac{c^2}{m^2}\right) \tag{11.33}$$

is identical to the standard GN model, cf. (11.15), and as such has the mass solution m_{GN} given in (11.16). The renormalized mass remains unaffected by the inclusion of the non-$\mathcal{PT}$-symmetric bilinear extension term based on Ω_{aPT_1}.

11.4 The Fermion Mass for $\Omega_{aPT_2} = i\mathbb{1}$

The non-Hermitian, non-$\mathcal{PT}$-symmetric, and chiral-symmetry-breaking model based on the extension term $\Omega_{aPT_2} = i\mathbb{1}$ has the fermion propagator

$$S(p) = (\not{p} - m - ig)^{-1}, \tag{11.34}$$

which, in essence, corresponds to that of the standard GN model with the mass being shifted to $m + ig$. Accordingly, the trace of the propagator takes the form

$$\mathrm{tr}[S(p)] = \frac{2(m + ig)}{p^2 - (m + ig)^2}, \tag{11.35}$$

and after the introduction of a radial cutoff Λ the gap equation (11.8) becomes

$$\frac{\pi}{GN_cN_f} = \frac{m + ig}{m} \ln\left[1 + \frac{\Lambda^2}{(m + ig)^2}\right] \tag{11.36}$$

in the limit of vanishing bare mass m_0.

When writing $\Lambda = c\lambda$, with $c = 1$ MeV, equation (11.36) behaves like

$$\frac{\pi}{GN_cN_f} = 2\ln\lambda + \frac{2ig}{m}\ln\lambda + \frac{m + ig}{m}\ln\left[\frac{c^2}{(m + ig)^2}\right] + O(\tfrac{1}{\lambda^2}), \tag{11.37}$$

as $\lambda \to \infty$. Contrary to the cases discussed previously, the renormalization of the two-body coupling strength G according to (11.14),

$$\frac{1}{G_R} = \frac{1}{G} - \frac{2N_cN_f}{\pi}\ln\lambda, \tag{11.38}$$

does not rid the gap equation of its ultraviolet-divergent behavior:

$$\frac{\pi}{G_RN_cN_f} = \frac{2ig}{m}\ln\lambda + \frac{m + ig}{m}\ln\left[\frac{c^2}{(m + ig)^2}\right] + O(\tfrac{1}{\lambda^2}) \quad \text{as} \quad \lambda \to \infty. \tag{11.39}$$

This can be remedied by introducing the renormalized bilinear-coupling constant $g_R = g\ln\lambda$, resulting in the equation

$$\frac{\pi}{G_RN_cN_f} = \frac{2ig_R}{m} + \ln\left(\frac{c^2}{m^2}\right) \tag{11.40}$$

in the limit $\lambda \to \infty$ with G_R and g_R kept constant, which has the complex-valued solution

$$m = ig_R \left[W_0 \left(\pm \frac{ig_R}{m_{GN}} \right) \right]^{-1} \tag{11.41}$$

in terms of the Lambert W function [88] and the mass m_{GN} of the standard GN model, see (11.16). But already in (11.39) it is apparent that this model does not admit real-valued mass solutions. In this it parallels its $3 + 1$ dimensional counterpart, the modified NJL model based on $\Gamma_{aPT_3} = i\mathbb{1}$.

11.5 Summary

The effect of the three possible non-Hermitian bilinear extensions of the $1+1$ dimensional GN model on the generated renormalized fermion mass was investigated through the analysis of the self-consistent gap equation at vanishing bare mass. These three bilinear modifications, $\Omega_{PT_1} = \gamma_5$, $\Omega_{aPT_1} = iA_\mu \gamma^\mu$, and $\Omega_{aPT_2} = i\mathbb{1}$, form the counterparts to the three non-$\mathcal{PT}$-symmetric bilinears (8.7) of the $3 + 1$ dimensional NJL model. However, due to the change from odd time reversal in $3+1$ space-time dimensions to even time reversal in $1+1$ dimensions, the bilinear based on $\Omega_{PT_1} = \gamma_5$ is a $\mathcal{PT}$-symmetric extension of the GN model.

Notably, it is only this $\mathcal{PT}$-symmetric term which admits a real renormalized mass solution that depends on the bilinear-coupling strength g and generates mass dynamically. In fact, when choosing the standard GN model mass to coincide with the mass of the standard NJL model for comparison, $m_{GN} = m_{NJL}$, the mass solutions of both models coincide. When comparing the $\mathcal{PT}$-symmetric GN model based on Ω_{PT_1} to the $\mathcal{PT}$-symmetric extensions of the NJL model, one notices that in the GN model real mass solutions exist at all coupling values g, i.e. the system is always in an unbroken $\mathcal{PT}$-symmetry phase, while in the NJL model the unbroken $\mathcal{PT}$-symmetry phases were restricted to finite coupling regions.

Modifying the GN model through the inclusion of the bilinear based on $\Omega_{aPT_1} = iA_\mu \gamma^\mu$ remarkably does not affect the renormalized fermion mass, at least in the self-consistent first-order approximation that was investigated.

The modified GN model based on $\Omega_{aPT_2} = i\mathbb{1}$ does not admit real renormalized-mass solutions. In this it reflects the behavior of the corresponding NJL model.

Chapter 12

Conclusion and Remarks

Contrary to bosonic theories, the time reversal $\mathcal{T}$ is an odd operation in $3 + 1$ dimensional fermionic models. This has substantial implications when considering the role of $\mathcal{PT}$ symmetry in such systems.

In this second part of the thesis, the role of $\mathcal{PT}$ symmetry in fermionic quantum field theories was investigated through the analysis of non-Hermitian bilinear extensions to the NJL model. This was achieved in two ways: On one hand, the modified NJL models were investigated for a fixed two-body coupling-constant value G to relate these systems to the NJL model of QCD and study the fermion mass generation caused by the inclusion of the non-Hermitian bilinear terms. On the other hand, by varying the two-body coupling strength G, the modified NJL models were considered as extensions of the modified non-Hermitian Dirac fermions through two-body interactions. This allowed one to see whether an effective mass increase or loss is caused by the bilinear terms either modifying the interaction or rather by mimicking the inclusion of a bare mass term. In addition to the effective fermion mass, the scalar- and pseudoscalar-meson modes were studied to observe the interplay of $\mathcal{PT}$ symmetry and chiral symmetry in the modified NJL model.

Real-valued effective fermion mass solutions were found in four different non-Hermitian bilinear extension of the NJL model:

For the $\mathcal{PT}$-symmetric bilinear extension based on $\Gamma_{PT_1} = i\gamma_5 B_\mu \gamma^\mu$ real effective fermion masses were obtained in a finite region up to a critical bilinear-coupling strength g_{crit}, representing a phase of unbroken $\mathcal{PT}$ symmetry. This

region is split into two distinct parts: For $0 < g < g_{\text{dyn}}$ mass is dynamically generated. At both boundaries of this region, i.e. at $g = 0$ and $g = g_{\text{dyn}}$ the mass solution coincides with that of the standard NJL model. Therefore, the equivalent of a small current quark mass can be generated at small couplings near $g = 0$, or at "large" coupling values close to g_{dyn}. In the second region, $g_{\text{dyn}} < g < g_{\text{crit}}$, the bilinear extension results in an effective mass loss. While the generation of small current quark masses is possible at two distinct bilinear-coupling values, the variation of the two-body coupling constant reveals that this mass generation happens in two distinct ways. At coupling values near g_{dyn} the dynamical mass increase qualitatively results as a modification of the two-body interaction. But at small coupling values near $g = 0$ it resembles the inclusion of a small bare mass m_0. This latter case is especially noteworthy, because contrary to a bare mass term, Γ_{PT_1} does not explicitly break the chiral symmetry of the model. In particular, a massless pseudoscalar-meson mode that can be identified as the Nambu-Goldstone boson of the theory continues to be present in this model.

Similar to Γ_{PT_1} the second possible $\mathcal{PT}$-symmetric bilinear extension, based on $\Gamma_{PT_2} = F_{\mu\nu}\gamma^\mu\gamma^\nu$, admits real-valued mass solution in a finite region up to a critical bilinear-coupling constant g_{crit}, signifying an unbroken $\mathcal{PT}$-symmetry phase. But within this region the extension always results in an effective fermion mass loss. However, the variation of the two-body coupling strength G demonstrates that the inclusion of this bilinear extension resembles, in a way, the effect of a finite density on the NJL model. This similarity is the subject of ongoing investigations.

Moreover, the existence of real fermion mass solutions is not restricted to $\mathcal{PT}$-symmetric non-Hermitian bilinears. The extension based on $\Gamma_{aPT_1} = iA_\mu\gamma^\mu$ and the extension based on $\Gamma_{aPT_2} = \gamma_5$ admit real-valued fermion masses even though they are not $\mathcal{PT}$ symmetric. And contrary to the $\mathcal{PT}$-symmetric extensions, these solutions are not restricted to a finite region; the effective fermion mass remains real for all bilinear-coupling strengths g. Furthermore, in both models fermion mass is generated dynamically, increasing monotonically with g. A variation of the two-body coupling constant G shows that this mass generation is the result of the bilinear extensions modifying the effect of the two-body interaction rather than mimicking the inclusion of a bare mass term.

Γ	$\mathcal{PT}$ symmetry	real fermion mass	dynamical fermion mass generation	chiral symmetry
$i\gamma_5 B_\mu\gamma^\mu$	yes	$0 \le g \le g_{\mathrm{crit}}$ (unbroken $\mathcal{PT}$ symmetry)	$0 \le g \le g_{\mathrm{dyn}} < g_{\mathrm{crit}}$	yes (massless Goldstone boson)
$F_{\mu\nu}\gamma^\mu\gamma^\nu$	yes	$0 \le g \le g_{\mathrm{crit}}$ (unbroken $\mathcal{PT}$ symmetry)	no	no
$iA_\mu\gamma^\mu$	no	$\forall g$	$\forall g$	yes (massless Goldstone boson)
γ_5	no	$\forall g$	$\forall g$	no (tachyonic instability of the Goldstone boson)
$i\mathbb{1}$	no	no	–	no

Ω	$\mathcal{PT}$ symmetry	real fermion mass	dynamical fermion mass generation	chiral symmetry
γ_5	yes	$\forall g$ (unbroken $\mathcal{PT}$ symmetry)	$\forall g$	no
$iA_\mu\gamma^\mu$	no	$\forall g$ ($m = m_{GN}$)	no	yes
$i\mathbb{1}$	no	no	–	no

Table 12.1: Overview of the effects that various non-Hermitian bilinear extensions $\bar{\psi}\Gamma\psi$ or $\bar{\psi}\Omega\psi$ have on the 3+1 dimensional NJL model (top) or the renormalized $1+1$ dimensional GN model (bottom) respectively.

The modified NJL model based on Γ_{aPT_1} is, in addition, a chirally symmetric model. One finds this in particular reflected in a massless pseudoscalar-meson mode which is identified as the Nambu-Goldstone boson of this theory. Nevertheless, a study of the $1+1$ dimensional analogue of this system, the chiral GN model modified through the inclusion of a bilinear based on $\Omega_{aPT_1} = iA_\mu\gamma^\mu$, results in a renormalized fermion mass that is unaffected by the non-Hermitian bilinear. This might be a first indication that this non-$\mathcal{PT}$-symmetric extension of the NJL model is unphysical; but further investigation is necessary for conclusive statements.

The effective fermion mass of the modified NJL model based on $\Gamma_{aPT_2} = \gamma_5$, on the other hand, coincides with the renormalized fermion mass found in the $1+1$ dimensional analogue of the system. It is noteworthy in this context that the modified GN model based on $\Omega_{PT_1} = \gamma_5$ is symmetric under combined parity reflection and time reversal, even though the $3+1$ dimensional modified NJL model is not. The inclusion of the bilinear based on $\Gamma_{aPT_2} = \gamma_5$ (or $\Omega_{PT_1} = \gamma_5$) also breaks the chiral symmetry of the NJL (or GN) model explicitly. This leads in particular to a tachyonic instability of the Nambu-Goldstone boson.

An overview of the effects that the various non-Hermitian bilinear extensions have on the $3+1$ dimensional NJL model and the GN model is presented in Table 12.1.

Overall, this study of non-Hermitian extensions to the NJL model has demonstrated that the role of $\mathcal{PT}$ symmetry in fermionic quantum field theories is a very subtle one. The existence of real-valued mass solutions and even dynamical mass generation through the inclusion of non-Hermitian terms is a remarkable result, but this is markedly not immediately tied to the presence of $\mathcal{PT}$ symmetry in the system. Nevertheless, it is especially the $\mathcal{PT}$-symmetric model based on $\Gamma_{PT_1} = i\gamma_5 B_\mu\gamma^\mu$ which, in the dynamical mass generation that resembles the inclusion of a bare mass term but without breaking the chiral symmetry of the NJL model, displays remarkable behavior. Ongoing investigations studying the effect of non-Hermitian bilinears on the NJL model at finite temperature and density might reveal additional differences between the $\mathcal{PT}$-symmetric and the non-$\mathcal{PT}$-symmetric extensions and clarify the importance of $\mathcal{PT}$ symmetry in fermionic field theories further.

General Conclusion

Two problems in $\mathcal{PT}$-symmetric quantum field theory were discussed in this thesis: the analysis of the D-dimensional $\phi^2(i\phi)^\varepsilon$ quantum field theory and the extension of the Nambu–Jona-Lasinio model through non-Hermitian bilinear terms. These problems address important open questions of $\mathcal{PT}$ theory since it remains generally unclear how higher-dimensional non-Hermitian $\mathcal{PT}$ quantum field theories can be addressed, how renormalization works in such models, and how odd time reversal influences the role of $\mathcal{PT}$ symmetry in fermionic systems. As such they address questions that are essential for the development of a general framework of $\mathcal{PT}$-symmetric quantum field theories.

In the first part the perturbative techniques for the analysis of the $\phi^2(i\phi)^\varepsilon$ quantum field theory that were proposed in [1] were generalized beyond their first-order application and for a model including dimensional parameters. The general structure of the perturbation coefficients of the partition function and the Green's functions, as well as of the associated ground-state energy density and the effective mass, were derived. Closed-form solutions were obtained to second order in the nonlinearity parameter ε. Both the general coefficient structure and the closed-form solutions were furthermore used to perform the perturbative renormalization program proposed in [1] in two dimensions to second order and investigate the general asymptotic behavior of the theory. While the two-dimensional theory appears to be free to any finite order in ε, a multiple-scale analysis suggests that higher-order Green's functions might diverge beyond all orders in ε, requiring a more robust renormalization scheme.

The study of non-Hermitian bilinear extensions to the NJL model in the second part of this thesis has illustrated that the existence of real-valued effective mass solutions is, at least in the self-consistent first-order approximation considered,

not directly tied to the presence of $\mathcal{PT}$ symmetry. In fact, even the dynamical generation of fermion mass is possible through anti-$\mathcal{PT}$-symmetric extensions which result in non-$\mathcal{PT}$-symmetric models. The analysis of the effective fermion masses, as well as of the scalar- and pseudoscalar-meson masses, in various models has shown that non-Hermitian bilinear additions, $\mathcal{PT}$-symmetric or not, might give rise to feasible models, or that a more subtle property than the reality of the effective mass distinguishes the fermionic $\mathcal{PT}$ models from the fermionic non-$\mathcal{PT}$-symmetric models when time reversal is odd.

Moreover, this work has built a foundation for the investigation of $\mathcal{PT}$ symmetry in fermionic systems at finite temperature and density. Such investigations are, however, beyond the scope of this thesis and remain a part of ongoing investigations.

Acknowledgments

Appendix

A: The Free Propagator $\Delta_\lambda(x)$

The free propagator $\Delta_\lambda(x)$ obeys the D-dimensional Euclidean Klein-Gordon equation

$$(-\nabla^2 + \lambda^2)\,\Delta_\lambda(x) = \delta^{(D)}(x). \tag{A1}$$

Through Fourier transformation of this equation one finds that

$$(p^2 + \lambda^2)\,\tilde{\Delta}_\lambda(p) = 1, \qquad \text{i.e.} \qquad \tilde{\Delta}_\lambda(p) = 1/(p^2 + \lambda^2). \tag{A2}$$

The propagator $\Delta_\lambda(x)$ can thus be determined as the inverse Fourier transform:

$$
\begin{aligned}
\Delta_\lambda(x) &= \frac{1}{(2\pi)^D} \int d^D p\, e^{ipx} \frac{1}{p^2 + \lambda^2} \\
&= \frac{1}{(2\pi)^D} \int d^D p\, e^{ipx} \int_0^\infty ds\, e^{-(p^2 + \lambda^2)s} \\
&= \frac{1}{(2\pi)^D} \int_0^\infty ds\, e^{-\lambda^2 s} \int d^D p\, e^{-sp^2 + ipx}.
\end{aligned}
\tag{A3}
$$

After evaluating the D-dimensional Gaussian integral over p this becomes

$$
\begin{aligned}
\Delta_\lambda(x) &= \frac{1}{(2\pi)^D} \int_0^\infty ds\, e^{-\lambda^2 s} \left(\frac{\pi}{s}\right)^{D/2} e^{(ix)^2/4s} \\
&= \frac{1}{(4\pi)^{D/2}} \int_0^\infty ds\, s^{-D/2}\, e^{-\lambda^2 s - x^2/4s}.
\end{aligned}
\tag{A4}
$$

At $x = 0$, equation (A4) simplifies to the selfloop propagator in (2.30):

$$\Delta_\lambda(0) = \frac{\lambda^{D-2}}{(4\pi)^{D/2}} \int_0^\infty dr \, r^{-D/2} \, e^{-r} = \lambda^{D-2} \, (4\pi)^{-D/2} \, \Gamma\left(1 - \tfrac{D}{2}\right). \qquad (A5)$$

For general values of x, changing the variable of integration s in (A4) to $t = 2\lambda s/(i|x|)$ results in the expression

$$\Delta_\lambda(x) = -\frac{(i|x|)^{1-D/2}}{2\,(2\pi)^{D/2}\lambda^{1-D/2}} \int_{-i\infty}^0 dt \, t^{-D/2} \, \exp\left[-i\frac{|x|\lambda}{2}\left(t - \tfrac{1}{t}\right)\right]. \qquad (A6)$$

In this form the integral is identified as the Hankel function of the second kind [91],

$$\Delta_\lambda(x) = -\frac{(i|x|)^{1-D/2}}{2\,(2\pi)^{D/2}\lambda^{1-D/2}} \left[i\pi \, H^{(2)}_{D/2-1}(-i\lambda|x|)\right], \qquad (A7)$$

which can be rewritten [51] as

$$\Delta_\lambda(x) = -\frac{|x|^{1-D/2}}{(2\pi)^{D/2}\lambda^{1-D/2}} \frac{i^{D/2}\pi}{2} \, H^{(2)}_{1-D/2}(-i\lambda|x|) \qquad (A8)$$

and is then expressed in terms of the associated Bessel function [50], resulting in the form given in (2.28):

$$\Delta_\lambda(x) = (2\pi)^{-D/2} \, \lambda^{D/2-1} \, |x|^{1-D/2} \, K_{1-D/2}(\lambda|x|). \qquad (A9)$$

B: Evaluation of the Functional Integral

The functional integral

$$\frac{1}{Z(0)} \int \mathcal{D}\phi \, e^{-\int d^D x \, \mathcal{L}_0} \, \phi^{n_1}(z_1) \dots \phi^{n_k}(z_k) \tag{B1}$$

corresponds to the sum over all possible graphs on k vertices z_1 to z_k, with a total of n_1 to n_k lines ending at those respective vertices. That is, the summation over possible graphs extends over all possible arrangements of lines between the vertices such that all n_1 to n_k ends of the vertices z_1 to z_k are occupied.

Each line between two vertices z_i and z_j corresponds to a propagator $\Delta(z_i - z_j)$ of the free theory with Lagrangian density $\mathcal{L}_0$, including the possibility of selfloops $\Delta(0)$ when $i = j$.

The number of ends at a vertex z_i that are connected to another vertex z_j are labeled as l_{ij}. When z_i and z_j are distinct vertices, i.e. $i \neq j$, then z_i and z_j are connected by l_{ij} lines, meaning propagators $\Delta(z_i - z_j)$. However, in the case of selfloops, that is when $i = j$, both ends of each line are connected to the same vertex z_j, so that only $l_{jj}/2$ selfloops are formed, signifying only $l_{jj}/2$ propagators $\Delta(0)$.

Since the free propagator $\Delta(z_i - z_j)$ is symmetric in its argument, and therefore $l_{ij} = l_{ji}$, one can assume that $i \leq j$ without loss of generality. In this way, each possible graph is in particular proportional to the following propagators:

$$\prod_{\substack{i,j=1, \\ i<j}}^{k} \Delta(z_i - z_j)^{l_{ij}} \prod_{j=1}^{k} \Delta(0)^{l_{jj}/2}. \tag{B2}$$

The values of the numbers l_{ij} and l_{jj} in (B2) are, of course, restricted by the total numbers n_1 to n_k of available ends at the vertices z_1 to z_k. Together with the requirement that any number of selfloops occupies an even number of ends of a vertex, these constraints can be expressed as

$$\forall j \in [1, k]: \quad l_{jj} = n_j - L_j = n_j - \left(\sum_{r=1}^{j-1} l_{rj} + \sum_{r=j+1}^{k} l_{jr} \right) \stackrel{!}{=} \text{even}, \tag{B3}$$

where L_j denotes the number of ends of the vertex z_j at which it is connected

to any vertices other then itself, that is the number of ends which do not form selfloops. The constraint (B3) can be included algebraically using the factor

$$\prod_{j=1}^{k} \left(\frac{1 + e^{i\pi(n_j - L_j)}}{2} \right). \tag{B4}$$

Furthermore, for each specified graph, meaning an appropriately chosen set of numbers l_{ij}, one has to account for its symmetry factors. These account for the following considerations:

(i): All possible ways to choose l_{jr} ends at a vertex z_j, which connect it to another vertex z_r or itself, out of the total number of ends n_j that are available at that vertex, are interchangeable. Thus for each vertex z_j, the number of possible orderings of the ends give rise to a factor:

$$\forall j \in [1, k] : \quad \frac{n_j!}{(\prod_{r=1}^{j-1} l_{rj}!) \, l_{jj}! \, (\prod_{r=j+1}^{k} l_{jr}!)}. \tag{B5}$$

(These are the multinomial coefficients of the total number n_j of ends at the vertex and the numbers of ends connecting it to other vertices or itself.)

(ii): When two distinct vertices z_i and z_j are connected by l_{ij} lines, then these lines are indistinguishable. The different possible ways of interchanging them give rise to factors $l_{ij}!$ $(\forall i, j \in [1, k] : i < j)$.

(iii): Similar to (ii), the ways of interchanging the lines that connect a vertex z_j to itself give rise to factors $(l_{jj} - 1)!!$ $(\forall j \in [1, k])$.

When combining all symmetry factors from all vertices and connections, some simplifications can be made: In joining the factors in (i) for all k vertices, one notices, that every specific factor of $l_{ij}!$ with $i < j$ in the denominator occurs twice - once due to the contribution at the vertex z_i and once due to that at z_j. One of these two copies is canceled by the factors $l_{ij}!$ from (ii). Together with the remaining factors of $n_j!/l_{jj}!$ from (i) and the factors of $(l_{jj} - 1)!!$ from (iii), as well as the propagators in (B2) and the factors in (B4), each specified graph corresponds to the algebraic expression

$$\prod_{\substack{i,j=1, \\ i<j}}^{k} \frac{\Delta(z_i - z_j)^{l_{ij}}}{l_{ij}!} \prod_{j=1}^{k} n_j! \, \frac{(l_{jj} - 1)!!}{l_{jj}!} \Delta(0)^{l_{jj}/2} \left(\frac{1 + e^{i\pi(n_j - L_j)}}{2} \right). \tag{B6}$$

By rewriting the double factorial according to

$$(l_{jj} - 1)!! = l_{jj}! \left[2^{l_{jj}/2} \, \Gamma\left(\tfrac{l_{jj}}{2} + 1\right) \right]^{-1}, \tag{B7}$$

replacing l_{jj} as in (B3), and rewriting

$$n_j! = 2^{n_j} \, \pi^{-\frac{1}{2}} \, \Gamma\left(\tfrac{n_j}{2} + 1\right) \Gamma\left(\tfrac{n_j}{2} + \tfrac{1}{2}\right), \tag{B8}$$

the expression (B6) becomes

$$\left(\frac{1}{\sqrt{\pi}}\right)^k \prod_{j=1}^{k} \left[2\Delta(0)\right]^{\frac{n_j}{2}} \frac{\Gamma(\tfrac{n_j}{2} + 1)\Gamma(\tfrac{n_j}{2} + \tfrac{1}{2})}{\Gamma(\tfrac{n_j}{2} + 1 - \tfrac{1}{2}L_j)} \left(\frac{1 + e^{i\pi(n_j - L_j)}}{2}\right)$$
$$\times \prod_{\substack{i,j=1, \\ i<j}}^{k} \frac{1}{l_{ij}!} \left[\frac{2\Delta(z_i - z_j)}{\Delta(0)}\right]^{l_{ij}}. \tag{B9}$$

The summation over all graphs can now be taken to run over all integers $l_{ij} \in [0, \infty]$ with $i, j \in [1, k] : i < j$. Notice, in particular, the infinite upper limit of the summation: In general, the maximal number of connections l_{ij} is restricted by the number of ends at the vertices z_i and z_j, that is $l_{ij} \leq \min(n_i, n_j)$. However, having the limit of the summation depend on these variables is quite inconvenient. But, considering that the Γ functions in the denominator of (B9) result in vanishing contributions, when any l_{ij} exceeds these limits, one can extend the summation to infinity, obtaining independent summation limits. When denoting this summation over all integers l_{ij} with $i, j \in [1, k] : i < j$ as $\sum_l$, one thus finds that the functional integral (B1) can be evaluated in terms of the propagators as

$$\frac{1}{Z(0)} \int \mathcal{D}\phi \, e^{-\int d^D x \, \mathcal{L}_0} \, \phi^{n_1}(z_1) \dots \phi^{n_k}(z_k)$$
$$= \left(\frac{1}{\sqrt{\pi}}\right)^k \sum_l^{\infty} \prod_{\substack{i,j=1, \\ i<j}}^{k} \frac{1}{l_{ij}!} \left[\frac{2\Delta(z_i - z_j)}{\Delta(0)}\right]^{l_{ij}} \prod_{j=1}^{k} \left[2\Delta(0)\right]^{\frac{n_j}{2}}$$
$$\times \frac{\Gamma(\tfrac{n_j}{2} + 1)\Gamma(\tfrac{n_j}{2} + \tfrac{1}{2})}{\Gamma(\tfrac{n_j}{2} + 1 - \tfrac{1}{2}L_j)} \left(\frac{1 + e^{i\pi(n_j - L_j)}}{2}\right), \tag{B10}$$

where the numbers $L_j = \sum_{r=1}^{j-1} l_{rj} + \sum_{r=j+1}^{k} l_{jr}$, as defined in (B3).

In Section 2.1 the general integral (B10) is used for z_1 to z_k being the space-time points x_1 to x_k and with $n_j = 2(N_j + 1) + (2\omega_j + 1)m_j$, $\forall j \in [1, k]$. The propagators are of the form $\Delta_{m\mu_0}$ given in (2.28). In the multi-index notation introduced in Section 2.1, the result (B10) thus becomes:

$$\frac{1}{Z(0)} \int \mathcal{D}\phi \, e^{- \int d^D x \, \mathcal{L}_0} \left[\phi(x_\alpha) \right]^{2(N_\alpha + 1) + (2\omega_\alpha + 1)m_\alpha}$$

$$= \left(\frac{2\Delta_{m\mu_0}(0)}{\sqrt{\pi}} \right)^k \left[2\Delta_{m\mu_0}(0) \right]^{N_\alpha + m_\alpha(\omega_\alpha + \frac{1}{2})} \sum_l^\infty \prod_{\substack{i,j=1, \\ i<j}}^k \frac{1}{l_{ij}!} \left[\frac{2\Delta_{m\mu_0}(x_i - x_j)}{\Delta_{m\mu_0}(0)} \right]^{l_{ij}}$$

$$\times \frac{\Gamma[N_\alpha + 2 + m_\alpha(\omega_\alpha + \frac{1}{2})] \, \Gamma[N_\alpha + \frac{3}{2} + m_\alpha(\omega_\alpha + \frac{1}{2})]}{\Gamma[N_\alpha + 2 + m_\alpha(\omega_\alpha + \frac{1}{2}) - \frac{1}{2}L_\alpha]} \left(\frac{1 + e^{i\pi(m_\alpha - L_\alpha)}}{2} \right).$$

$$(B11)$$

In Section 4.1 the integral (B10) is evaluated for $k \to k + p$ space-time points: As before, z_1 to z_k are the space-time points x_1 to x_k with $n_j = 2(N_j + 1) + (2\omega_j + 1)m_j$, $\forall j \in [1, k]$. But in addition the p space-time points z_{k+1} to z_{k+p}, denoting y_1 to y_p are taken into account. For these latter points $n_j = 1$, $\forall j \in [k + 1, k + p]$, which simplifies the associated terms in (B10) significantly. The former contributions can be written in the multi-index notation as in (B11). Overall the functional integral becomes:

$$\frac{1}{Z(0)} \int \mathcal{D}\phi \, e^{- \int d^D x \, \mathcal{L}_0} \phi(y_1) \dots \phi(y_p) \left[\phi(x_\alpha) \right]^{2(N_\alpha + 1) + (2\omega_\alpha + 1)m_\alpha}$$

$$= \left[\tfrac{1}{2}\Delta_{m\mu_0}(0) \right]^{p/2} \left(\frac{2\Delta_{m\mu_0}(0)}{\sqrt{\pi}} \right)^k \left[2\Delta_{m\mu_0}(0) \right]^{N_\alpha + m_\alpha(\omega_\alpha + \frac{1}{2})} \sum_l^\infty \prod_{\substack{i,j=1, \\ i<j}}^{k+p} \frac{1}{l_{ij}!}$$

$$\times \left[\frac{2\Delta_{m\mu_0}(z_i - z_j)}{\Delta_{m\mu_0}(0)} \right]^{l_{ij}} \frac{\Gamma[N_\alpha + 2 + m_\alpha(\omega_\alpha + \frac{1}{2})] \, \Gamma[N_\alpha + \frac{3}{2} + m_\alpha(\omega_\alpha + \frac{1}{2})]}{\Gamma[N_\alpha + 2 + m_\alpha(\omega_\alpha + \frac{1}{2}) - \frac{1}{2}L_\alpha]}$$

$$\times \left(\frac{1 + e^{i\pi(m_\alpha - L_\alpha)}}{2} \right) \left\{ \prod_{r=1}^p \frac{1}{\Gamma(\frac{3}{2} - \frac{1}{2}L_{k+r})} \left(\frac{1 + e^{i\pi(1 - L_{k+r})}}{2} \right) \right\}.$$

$$(B12)$$

C: An Identity for Γ Functions

In the following it is demonstrated that

$$\int_0^\infty dt \sum_{\omega=0}^\infty \frac{2\,(-t^2)^\omega}{\pi\,(2\omega+1)!} \frac{\Gamma[a+m(\omega+\frac{1}{2})]\,\Gamma[b+m(\omega+\frac{1}{2})]}{\Gamma[c+m(\omega+\frac{1}{2})]}\, x^{m(\omega+\frac{1}{2})} = \frac{\Gamma(a)\,\Gamma(b)}{\Gamma(c)}. \tag{C1}$$

First, one rewrites $(2\omega+1)! = 2^{2\omega}\omega!\,(\frac{3}{2})^{(\omega)}$ in terms of the rising factorial (or Pochhammer symbol) [45], $(\frac{3}{2})^{(\omega)} = \Gamma(\frac{3}{2}+\omega)/\Gamma(\frac{3}{2})$, and expands the fraction of the Γ functions, so that they can be identified as rising factorials as well:

$$\int_0^\infty dt \sum_{\omega=0}^\infty \frac{2\,(-t^2)^\omega}{\pi\,(2\omega+1)!} \frac{\Gamma[a+m(\omega+\frac{1}{2})]\,\Gamma[b+m(\omega+\frac{1}{2})]}{\Gamma[c+m(\omega+\frac{1}{2})]}\, x^{m(\omega+\frac{1}{2})}$$
$$= \frac{2}{\pi} \frac{\Gamma(a+\frac{m}{2})\,\Gamma(b+\frac{m}{2})}{\Gamma(c+\frac{m}{2})}\, x^{\frac{m}{2}} \int_0^\infty dt \sum_{\omega=0}^\infty \frac{(-\frac{1}{4}x^m t^2)^\omega}{\omega!\,(\frac{3}{2})^{(\omega)}} \frac{(a+\frac{m}{2})^{(m\omega)}\,(b+\frac{m}{2})^{(m\omega)}}{(c+\frac{m}{2})^{(m\omega)}}. \tag{C2}$$

Then expanding the rising factorials according to their multiplication formula [92]

$$(z)^{(m\omega)} = m^{m\omega} \prod_{s=0}^{m-1} \left(\frac{z+s}{m}\right)^{(\omega)}, \tag{C3}$$

yields

$$\frac{2}{\pi} \frac{\Gamma(a+\frac{m}{2})\,\Gamma(b+\frac{m}{2})}{\Gamma(c+\frac{m}{2})}\, x^{\frac{m}{2}} \int_0^\infty dt \sum_{\omega=0}^\infty \frac{(-\frac{1}{4}m^m x^m t^2)^\omega}{\omega!\,(\frac{3}{2})^{(\omega)}} \left[\prod_{s=0}^{m-1} \left(\frac{a+\frac{m}{2}+s}{m}\right)^{(\omega)}\right]$$
$$\times \left[\prod_{p=0}^{m-1} \left(\frac{b+\frac{m}{2}+p}{m}\right)^{(\omega)}\right] \left[\prod_{q=0}^{m-1} \left(\frac{c+\frac{m}{2}+q}{m}\right)^{(\omega)}\right]^{-1}. \tag{C4}$$

The summation over ω can now be identified as the series expansion of the hypergeometric function

$$_{2m}F_{m+1}\left[\left(\frac{a+\frac{m}{2}}{m}\right), \ldots, \left(\frac{a+\frac{m}{2}+m-1}{m}\right), \left(\frac{b+\frac{m}{2}}{m}\right), \ldots, \left(\frac{b+\frac{m}{2}+m-1}{m}\right);\right.$$
$$\left.\left(\frac{c+\frac{m}{2}}{m}\right), \ldots, \left(\frac{c+\frac{m}{2}+m-1}{m}\right), \left(\frac{3}{2}\right); -\frac{1}{4}m^m x^m t^2\right], \tag{C5}$$

which is abbreviated as $_{2m}F_{m+1}(a, b, c, -\frac{1}{4}m^m x^m t^2)$ in the following. After rescaling the integration variable $t \to r = \frac{1}{4}m^m x^m t^2$ one thus obtains the expression

$$\frac{2}{\pi} \frac{\Gamma(a + \frac{m}{2})\,\Gamma(b + \frac{m}{2})}{\Gamma(c + \frac{m}{2})} \, m^{-m/2} \int_0^\infty dr \, r^{-\frac{1}{2}} {}_{2m}F_{m+1}(a, b, c, -r). \tag{C6}$$

The integral over the hypergeometric function is the Mellin transform of the Mellin-Barnes integral representation of the generalized hypergeometric function, see [93], which evaluates to

$$\int_0^\infty dr \, r^{-\frac{1}{2}} {}_{2m}F_{m+1}(a, b, c, -r)$$
$$= \frac{\pi}{2} \left[\prod_{s=0}^{m-1} \left(\frac{a + \frac{m}{2} + s}{m} \right)^{\left(-\frac{1}{2}\right)} \right] \left[\prod_{p=0}^{m-1} \left(\frac{b + \frac{m}{2} + p}{m} \right)^{\left(-\frac{1}{2}\right)} \right] \left[\prod_{q=0}^{m-1} \left(\frac{c + \frac{m}{2} + q}{m} \right)^{\left(-\frac{1}{2}\right)} \right]^{-1} \tag{C7}$$

in terms of rising factorials. Utilizing the multiplication formula (C3) once more thus leads to the result that

$$\int_0^\infty dt \sum_{\omega=0}^\infty \frac{2\,(-t^2)^\omega}{\pi\,(2\omega + 1)!} \frac{\Gamma[a + m(\omega + \frac{1}{2})]\,\Gamma[b + m(\omega + \frac{1}{2})]}{\Gamma[c + m(\omega + \frac{1}{2})]} \, x^{m(\omega + \frac{1}{2})}$$
$$= \frac{\Gamma(a + \frac{m}{2})\,\Gamma(b + \frac{m}{2})}{\Gamma(c + \frac{m}{2})} \frac{(a + \frac{m}{2})^{(-\frac{m}{2})}\,(b + \frac{m}{2})^{(-\frac{m}{2})}}{(c + \frac{m}{2})^{(-\frac{m}{2})}} = \frac{\Gamma(a)\,\Gamma(b)}{\Gamma(c)}. \tag{C8}$$

D: Evaluation of the Zero-Dimensional Model

In $D = 0$ dimensions the functional integral in the partition function, which is discussed in Section 2.1, can be evaluated directly as an ordinary integral over the (real) field. For $g = m = 1$, the partition function $\mathcal{Z}(\varepsilon)$ in (2.4) takes the explicit form

$$\mathcal{Z}(\varepsilon) = \frac{1}{Z(0)} \int_{-\infty}^{\infty} d\phi \, e^{-\mu_0^2 \phi^2/2} \, \exp\left[-\tfrac{1}{2}\mu_0^2 \sum_{n=1}^{\infty} \frac{\varepsilon^n}{n!} \phi^2 \, \ln^n(i\mu_0\phi)\right], \tag{D1}$$

with

$$Z(0) = \int_{-\infty}^{\infty} d\phi \, e^{-\mu_0^2 \phi^2/2} = \sqrt{2\pi\mu_0^{-2}}. \tag{D2}$$

The exponential factor in (D1) containing the summation is rewritten using the defining relation of the exponential complete Bell polynomials B_n, see [45],

$$\exp\left(\sum_{m=1}^{\infty} x_m \frac{t^m}{m!}\right) = 1 + \sum_{n=1}^{\infty} \frac{t^n}{n!} \mathrm{B}_n(x_1, \dots, x_n), \tag{D3}$$

so that

$$\mathcal{Z}(\varepsilon) = 1 + \sum_{n=1}^{\infty} \frac{\varepsilon^n}{n!} \frac{1}{Z(0)} \int_{-\infty}^{\infty} d\phi \, e^{-\mu_0^2 \phi^2/2} \, \mathrm{B}_n(I_1, \dots, I_n), \tag{D4}$$

with $I_n = -\tfrac{1}{2}\mu_0^2 \phi^2 \log^n(i\mu_0\phi)$. The partition-function coefficients $\mathcal{Z}_n$ in the non-linearity expansion (2.6) are thus identified as

$$\mathcal{Z}_n = \frac{1}{n! \, Z(0)} \int_{-\infty}^{\infty} d\phi \, e^{-\mu_0^2 \phi^2/2} \, \mathrm{B}_n(I_1, \dots, I_n). \tag{D5}$$

Because the field ϕ is not evaluated at different space-time points in the zero-dimensional model, the logarithmic terms can be factored out of the complete Bell polynomial

$$\mathcal{Z}_n = \frac{1}{n! \, Z(0)} \int_{-\infty}^{\infty} d\phi \, e^{-\mu_0^2 \phi^2/2} \, \log^n(i\mu_0\phi) \, \mathrm{B}_n\left(-\tfrac{1}{2}\mu_0^2 \phi^2, \dots, -\tfrac{1}{2}\,\mu_0^2 \phi^2\right), \tag{D6}$$

and the remaining Bell polynomial at all identical arguments is rewritten as the Touchard polynomial T_n, which is expressed in terms of Stirling numbers of the second kind as [45]:

$$\mathrm{B}_n(x, \dots, x) = \mathrm{T}_n(x) = \sum_{j=0}^{n} \left\{{n \atop j}\right\} x^j. \tag{D7}$$

Therefore, the partition-function coefficients have the form

$$
\mathcal{Z}_n = \frac{1}{n!\, Z(0)} \sum_{j=0}^{n} \begin{Bmatrix} n \\ j \end{Bmatrix} \left(-\tfrac{1}{2}\mu_0^2\right)^j \int_{-\infty}^{\infty} d\phi\, e^{-\mu_0^2\phi^2/2}\, \phi^{2j} \log^n(i\mu_0\phi). \tag{D8}
$$

Expanding the complex logarithm according to (2.21) and its power through the binomial theorem, keeping only even terms in the field ϕ, yields

$$
\mathcal{Z}_n = \sum_{j=0}^{n} \sum_{\substack{k=0 \\ \text{even}}}^{n} \begin{Bmatrix} n \\ j \end{Bmatrix} \binom{n}{k} \frac{(-\mu_0^2)^j (i\pi)^k}{2^{n+j}\, n!\, Z(0)} \int_{-\infty}^{\infty} d\phi\, e^{-\mu_0^2\phi^2/2}\, \phi^{2j} \log^{n-k}(\mu_0^2\phi^2). \tag{D9}
$$

The remaining real logarithm can be rewritten using the replica trick (2.25), resulting in the expression

$$
\mathcal{Z}_n = \lim_{N\to 0} \sum_{j=0}^{n} \sum_{\substack{k=0 \\ \text{even}}}^{n} \begin{Bmatrix} n \\ j \end{Bmatrix} \binom{n}{k} \frac{(-\mu_0^2)^j (i\pi)^k}{2^{n+j}\, n!\, Z(0)} \left(\frac{d}{dN}\right)^{n-k} \mu_0^{2N} \int_{-\infty}^{\infty} d\phi\, e^{-\mu_0^2\phi^2/2}\, \phi^{2(N+j)}. \tag{D10}
$$

Here the integral over the field is recognized as an integral representation of a Γ function, evaluating to

$$
\int_{-\infty}^{\infty} d\phi\, e^{-\mu_0^2\phi^2/2}\, \phi^{2(N+j)} = \left(2\mu_0^{-2}\right)^{N+j+\frac{1}{2}} \Gamma(N+j+\tfrac{1}{2}). \tag{D11}
$$

The partition-function coefficient thus simplifies to

$$
\mathcal{Z}_n = \lim_{N\to 0} \frac{1}{2^n\, n!\, \sqrt{2\pi}} \sum_{\substack{k=0 \\ \text{even}}}^{n} \binom{n}{k} (i\pi)^k \left(\frac{d}{dN}\right)^{n-k} 2^{N+\frac{1}{2}} \left[\sum_{j=0}^{n} \begin{Bmatrix} n \\ j \end{Bmatrix} (-1)^j \Gamma(N+j+\tfrac{1}{2})\right]. \tag{D12}
$$

The summation involving the Stirling numbers of the second kind can be evaluated according to

$$
\sum_{j=0}^{n} \begin{Bmatrix} n \\ j \end{Bmatrix} (-1)^j \Gamma(N+j+\tfrac{1}{2}) = (-1)^n (N+\tfrac{1}{2})^n\, \Gamma(N+\tfrac{1}{2}). \tag{D13}
$$

The remaining summation over only even values of k can then be evaluated in the

same way as in (2.43) and (2.44) using the general Leibniz rule [50], so that the partition-function coefficient becomes:

$$\mathcal{Z}_n = \lim_{N \to 0} \frac{(-1)^n}{2^n \, n! \, \sqrt{2\pi}} \left(\frac{d}{dN}\right)^n 2^{N + \frac{1}{2}} \cos(\pi N) \left(N + \tfrac{1}{2}\right)^n \Gamma(N + \tfrac{1}{2}). \tag{D14}$$

The evaluation for a chosen value of n is straightforward. In particular, the results for the first-order and second-order coefficients

$$\mathcal{Z}_1\big|_{D=0} = -\tfrac{1}{4} \left[\ln 2 + \psi(\tfrac{3}{2})\right], \tag{D15}$$

$$\mathcal{Z}_2\big|_{D=0} = \tfrac{1}{32} \left[\ln 2 + \psi(\tfrac{3}{2})\right]^2 + \tfrac{1}{8} \left[\ln 2 + \psi(\tfrac{3}{2})\right] + \tfrac{1}{32} \left[\psi^{(1)}(\tfrac{3}{2}) - \pi^2\right] \tag{D16}$$

confirm the result of the general solutions (2.42) and (2.62), when evaluated in $D = 0$ dimensions.

In order to find the exact solution $\mathcal{Z}(\varepsilon)$, one has to sum the coefficients (D14) to all orders in ε. After rescaling the variable $N \to -N/2$ the partition function can be written as

$$\mathcal{Z}(\varepsilon) = \lim_{N \to 0} \sum_{n=0}^{\infty} \frac{(\varepsilon/2)^n}{n! \, \sqrt{2\pi}} \left(\frac{d}{dN}\right)^n (1 - N)^n f(N), \tag{D17}$$

with $f(N) = 2^{(1-N)/2} \cos(-\frac{N\pi}{2}) \Gamma(\frac{1-N}{2})$. Using the general Leibniz rule to evaluate the derivative, this can be written as

$$\mathcal{Z}(\varepsilon) = \lim_{N \to 0} \sum_{n=0}^{\infty} \frac{(-\varepsilon/2)^n}{\sqrt{2\pi}} \sum_{k=0}^{n} \binom{n}{k} \frac{(-1)^k}{k!} \left(\frac{d}{dN}\right)^k f(N). \tag{D18}$$

Exchanging the order of summation then yields

$$\mathcal{Z}(\varepsilon) = \lim_{N \to 0} \sum_{k=0}^{\infty} \frac{(\varepsilon/2)^k}{\sqrt{2\pi} \, k!} \left(\frac{d}{dN}\right)^k f(N) \sum_{n=0}^{\infty} \binom{n+k}{k} (-\tfrac{1}{2}\varepsilon)^n. \tag{D19}$$

Here the summation over n can be evaluated according to

$$\sum_{n=0}^{\infty} \binom{n+k}{k} (-\tfrac{1}{2}\varepsilon)^n = (1 + \tfrac{1}{2}\varepsilon)^{-(1+k)}, \tag{D20}$$

so that

$$\mathcal{Z}(\varepsilon) = \frac{1}{\sqrt{2\pi}\,(1+\varepsilon/2)} \sum_{k=0}^{\infty} \frac{1}{k!} \left(\frac{\varepsilon}{\varepsilon+2}\right)^k \lim_{N\to 0} \left(\frac{d}{dN}\right)^k f(N). \qquad (D21)$$

In this form the summation is recognizable as the Taylor series of $f(\frac{\varepsilon}{\varepsilon+2})$ around 0. The partition function is therefore given by

$$\mathcal{Z}(\varepsilon) = \frac{1}{\sqrt{2\pi}\,(1+\varepsilon/2)}\, f\left(\frac{\varepsilon}{\varepsilon+2}\right) = \frac{2^{1/(\varepsilon+2)}}{\sqrt{2\pi}\,(1+\varepsilon/2)}\,\Gamma\left(\frac{1}{\varepsilon+2}\right)\cos\left(-\frac{\pi}{2}\,\frac{\varepsilon}{\varepsilon+2}\right). \qquad (D22)$$

Similarly, the integrals

$$N_p(\varepsilon) = \frac{1}{Z(0)} \int_{-\infty}^{\infty} d\phi\, e^{-\mu_0^2\phi^2/2}\, \phi^p\, \exp\left[-\tfrac{1}{2}\mu_0^2 \sum_{n=1}^{\infty} \frac{\varepsilon^n}{n!}\phi^2\,\ln^n(i\mu_0\phi)\right], \qquad (D23)$$

which arise in the numerator of the Green's functions $G_p(\varepsilon) = N_p(\varepsilon)/\mathcal{Z}(\varepsilon)$, can be evaluated, yielding the closed-form results

$$N_p^{\text{even}}(\varepsilon) = \frac{2^{(p+1)/(\varepsilon+2)}}{\sqrt{2\pi}(1+\varepsilon/2)}\Gamma\left(\frac{p+1}{\varepsilon+2}\right)\cos\left(-\frac{\pi}{2}\,\frac{(p+1)\varepsilon}{\varepsilon+2}\right) \qquad (D24)$$

for even values of p, and

$$N_p^{\text{odd}}(\varepsilon) = \frac{2^{(p+1)/(\varepsilon+2)}\,i}{\sqrt{2\pi}(1+\varepsilon/2)}\Gamma\left(\frac{p+1}{\varepsilon+2}\right)\sin\left(-\frac{\pi}{2}\,\frac{(p+1)\varepsilon}{\varepsilon+2}\right) \qquad (D25)$$

for odd values of p.

E: Rayleigh-Schrödinger Perturbation Theory

For the model in $D = 1$ dimension, it is possible to confirm the result of the energy-density coefficients using the Rayleigh-Schrödinger perturbation approach of quantum mechanics.

The ground-state wave function

$$\psi(\varepsilon) = \psi_0 + \varepsilon\,\psi_1 + \varepsilon^2\,\psi_2 + \varepsilon^3\,\psi_3 + O(\varepsilon^4) \tag{E1}$$

and the ground-state energy eigenvalue

$$\mathcal{E}(\varepsilon) = \mathcal{E}_0 + \varepsilon\,\mathcal{E}_1 + \varepsilon^2\,\mathcal{E}_2 + \varepsilon^3\,\mathcal{E}_3 + O(\varepsilon^4) \tag{E2}$$

satisfy the Schrödinger equation

$$H\psi(\varepsilon) = \mathcal{E}(\varepsilon)\,\psi(\varepsilon)\,, \tag{E3}$$

in which the Hamiltonian H is given to third order in ε as

$$H = -\frac{1}{2}\frac{d^2}{dx^2} + \frac{1}{2}x^2 + \frac{\varepsilon}{2}\,x^2\ln(i\,x) + \frac{\varepsilon^2}{4}\,x^2\ln^2(i\,x) + \frac{\varepsilon^3}{12}\,x^2\ln^3(i\,x) + O(\varepsilon^4). \tag{E4}$$

Expanding (E3) in orders of ε, one finds that at order $O(\varepsilon^0)$ the expected harmonic-oscillator equation is obtained:

$$-\tfrac{1}{2}\psi_0'' + \tfrac{1}{2}x^2\psi_0 - \mathcal{E}_0\,\psi_0 = 0, \tag{E5}$$

with eigenfunction $\psi_0 = \mathrm{e}^{-x^2/2}$ and ground-state eigenvalue $\mathcal{E}_0|_{D=1} = \tfrac{1}{2}$.

At order $O(\varepsilon^1)$, equation (E3) has the form

$$-\tfrac{1}{2}\psi_1'' + \tfrac{1}{2}x^2\psi_1 - \mathcal{E}_0\,\psi_1 = -\tfrac{1}{2}x^2\ln(i\,x)\psi_0 + \mathcal{E}_1\,\psi_0, \tag{E6}$$

which is an inhomogeneous version of (E5) for ψ_1. Since the eigenfunctions can be chosen orthogonally, the left-hand side vanishes under multiplication with ψ_0 and integration from $-\infty$ to ∞, so that

$$\mathcal{E}_1 = \int_{-\infty}^{\infty} ds\,\tfrac{1}{2}s^2\ln(i\,s)\,\mathrm{e}^{-s^2} \Big/ \int_{-\infty}^{\infty} ds\,\mathrm{e}^{-s^2} = \tfrac{1}{8}\,(2 - \gamma - 2\ln 2). \tag{E7}$$

Furthermore, following the discussion in [1], the eigenfunction is determined through a reduction of order of (E6) by substituting the ansatz $\psi_1 = f(x)\psi_0$, which yields

$$f''(x) - 2xf(x) = x^2 \ln(i\,x) - 2\mathcal{E}_1. \tag{E8}$$

After the introduction of an integrating factor e^{-x^2}, integration results in

$$f'(x)\,\mathrm{e}^{-x^2} = \int_{-\infty}^{x} ds\,[s^2 \ln(i\,s) - 2\mathcal{E}_1]\,\mathrm{e}^{-s^2}, \tag{E9}$$

which can then be integrated once more to find

$$f(x) = \int_{0}^{x} dt\,\mathrm{e}^{t^2} \int_{-\infty}^{t} ds\,[s^2 \ln(i\,s) - 2\mathcal{E}_1]\,\mathrm{e}^{-s^2}. \tag{E10}$$

At order $O(\varepsilon^2)$, equation (E3) has the form

$$-\tfrac{1}{2}\psi_2'' + \tfrac{1}{2}x^2\psi_2 - \mathcal{E}_0\,\psi_2 = [-\tfrac{1}{2}x^2 \ln(i\,x) + \mathcal{E}_1]\,\psi_1 + [-\tfrac{1}{4}x^2 \ln^2(i\,x) + \mathcal{E}_2]\,\psi_0. \tag{E11}$$

The calculation proceeds identically to that at first order: the energy eigenvalue has the form

$$\mathcal{E}_2 = \int_{-\infty}^{\infty} ds\,\{\,[\tfrac{1}{2}s^2 \ln(i\,s) - \mathcal{E}_1]f(s) + \tfrac{1}{4}s^2 \ln^2(i\,s)\,\}\,\mathrm{e}^{-s^2} \Big/ \int_{-\infty}^{\infty} ds\,\mathrm{e}^{-s^2} \tag{E12}$$

and for the ansatz $\psi_2 = g(x)\psi_0$, one finds that

$$g(x) = \int_{0}^{x} dt\,\mathrm{e}^{t^2} \int_{-\infty}^{t} ds\,\{\,[s^2 \ln(i\,s) - 2\mathcal{E}_1]f(s) + [\tfrac{1}{2}s^2 \ln^2(i\,s) - 2\mathcal{E}_2]\,\}\,\mathrm{e}^{-s^2}. \tag{E13}$$

With this second-order eigenfunction it is then also possible to determine the third-order energy eigenvalue: The Schrödinger equation at order $O(\varepsilon^3)$ has the form

$$-\tfrac{1}{2}\psi_3'' + \tfrac{1}{2}x^2\psi_3 - \mathcal{E}_0\,\psi_3 = [-\tfrac{1}{2}x^2 \ln(i\,x) + \mathcal{E}_1]\,\psi_2 + [-\tfrac{1}{4}x^2 \ln^2(i\,x) + \mathcal{E}_2]\,\psi_1$$
$$+ [-\tfrac{1}{12}x^2 \ln^3(i\,x) + \mathcal{E}_3]\,\psi_0, \tag{E14}$$

so that

$$\mathcal{E}_3 = \frac{\int_{-\infty}^{\infty} ds \left\{ \left[\frac{1}{2}s^2 \ln(i\,s) - \mathcal{E}_1\right]g(s) + \left[\frac{1}{4}s^2 \ln^2(i\,s) - \mathcal{E}_2\right]f(s) + \frac{1}{12}s^2 \ln^3(i\,s) \right\} e^{-s^2}}{\int_{-\infty}^{\infty} ds\, e^{-s^2}}.$$

(E15)

The ground-state energy coefficients $\mathcal{E}_2$ and $\mathcal{E}_3$ in (E12) and (E15) are quite difficult to evaluate analytically, because of the dependence on $f(x)$ and $g(x)$. But to confirm the results obtained using functional integral techniques it suffices to evaluate these expressions numerically:

$$\mathcal{E}_2\big|_{D=1} \approx 0.116445,$$ (E16)

$$\mathcal{E}_3\big|_{D=1} \approx -0.077952,$$ (E17)

which is in agreement with the results (3.20) in Section 3.3 and (3.27) in Section 3.5.

F: Two-Vertex Contributions of the Green's Function Coefficients

The general two-vertex contribution $G^c_{p,n}(y_1, \dots, y_p)\big|_{k=2}$ of the p-point Green's function at order $O(\varepsilon^n)$ is determined from the general coefficient (4.14) for $k = 2$, which specifies the multi-index $\alpha = (1, 2)$. Keeping the multi-index $\beta = (\beta_1, \beta_2)$ unspecified for now, it can be written as:

$$
G^c_{p,n}(y_1, \dots, y_p)\big|_{k=2} =
$$

$$
\frac{g^2 \Delta_m^2(0)}{2^n \pi} \left[\frac{2\mu_0^{D-2}}{\Delta_m(0)}\right]^{p/2} \sum_c \prod_{s=1}^{n-1} \frac{1}{c_s! \, (s!)^{c_s}} \int d^D x_1' \, d^D x_2' \lim_{N_1, N_2 \to 0} \sum_{q=0}^{p} \{\Sigma\Pi\Delta(p, q)\}
$$

$$
\times \sum_{m_1=0}^{\beta_1} \sum_{m_2=0}^{\beta_2} \binom{\beta_1}{m_1}\binom{\beta_2}{m_2}(i\pi)^{m_1+m_2}\left(\frac{d}{dN_1}\right)^{\beta_1-m_1}\left(\frac{d}{dN_2}\right)^{\beta_2-m_2}\left[2\Delta_m(0)\right]^{N_1+N_2}
$$

$$
\times \sum_{l_{12}=1}^{\infty} \frac{1}{l_{12}!}\left[\frac{2\Delta_m(x_1 - x_2)}{\Delta_m(0)}\right]^{l_{12}} \frac{\Gamma(N_1+2)\,\Gamma(N_1+\frac{3}{2})}{\Gamma(N_1+2-\frac{q}{2}-\frac{1}{2}l_{12})}\frac{\Gamma(N_2+2)\,\Gamma(N_2+\frac{3}{2})}{\Gamma(N_2+2-\frac{p-q}{2}-\frac{1}{2}l_{12})}
$$

$$
\times \left(\frac{1+e^{i\pi(m_1-q-l_{12})}}{2}\right)\left(\frac{1+e^{i\pi(m_2-(p-q)-l_{12})}}{2}\right),
$$

$$
\text{(F1)}
$$

where

$$
\{\Sigma\Pi\Delta(p, q)\} := \frac{1}{q! \, (p-q)!} \sum_\sigma \left[\prod_{i=1}^{q} \Delta_m(x_1' - y_{\sigma(i)}')\right]\left[\prod_{j=q+1}^{p} \Delta_m(x_2' - y_{\sigma(j)}')\right] \quad \text{(F2)}
$$

describes the possible ways in which the external points y_1 to y_p can be connected to the two internal points x_1 and x_2: $q \in [0, p]$ out of the p external points are connected to the internal point x_1 through a propagator Δ_m. The remaining $p - q$ external points are consequently connected to the internal point x_2. The summation $\sum_\sigma$ in (F2) is a sum over all permutations of the external points y_1 to y_p and thus accounts for all ways to choose the q points that are connected to x_1. A schematic visualization of these connections is shown in Figure F.1. The factorials $1/[q! \, (p - q!)]$ compensate for the fact that, once q such external points are chosen, they are interchangeable. This is, of course, a diagrammatic picture. Algebraically, the possible ways of connecting an external point y_j to either the internal point x_1 or x_2 enters in the general coefficient (4.14) through the different combinations of either the number $l_{1,2+j}$ of propagators connecting
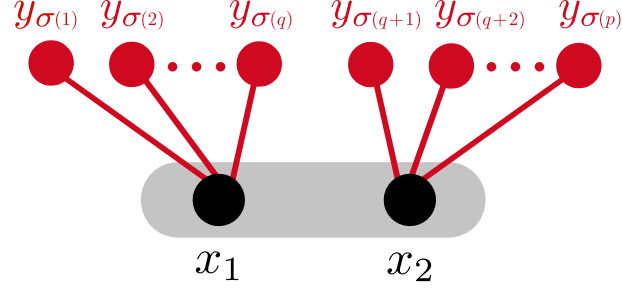
Figure F.1: Schematic visualization of the propagators in (F2). A total of q out of the p external points y_1 to y_p are connected to the internal point x_1, the remaining $p - q$ external points are connected to x_2. All choices of q out of p points are included, signified through the permutations σ of the indices. The points x_1 and x_2 are connected, shown by the grey obround shape.

y_j to x_1, or the number $l_{2,2+j}$ when connecting to x_2, being one, while the other vanishes. Note that when q external points are connected to x_1, the total number of propagators connected to x_1 is $L_1 = q + l_{12}$; accordingly the total number of propagators connected to x_2 is then $L_2 = (p - q) + l_{12}$.

The factors in (F1), which contain the exponential functions, imply that the summations over l_{12}, q, m_1, and m_2 split into different combinations of summing only even or odd instances. In particular, these combinations also depend on the evenness or oddness of p. For an even number p, (F1) takes the form:

$$G_{p,n}^c(y_1, \ldots, y_p)\big|_{k=2} =$$

$$\frac{g^2 \Delta_m^2(0)}{2^n \pi} \left[\frac{2\mu_0^{D-2}}{\Delta_m(0)} \right]^{p/2} \sum_c \prod_{s=1}^{n-1} \frac{1}{c_s! \, (s!)^{c_s}} \int d^D x_1' d^D x_2' \lim_{N_1, N_2 \to 0}$$

$$\times \left\{ \sum_{\substack{l_{12}=1 \\ \text{even}}}^{\infty} \frac{1}{l_{12}!} \left[\frac{2\Delta_m(x_1 - x_2)}{\Delta_m(0)} \right]^{l_{12}} \left(\sum_{\substack{q=0 \\ \text{even}}}^{p} \{\Sigma\Pi\Delta(p,q)\} \, M_1^{\text{even}} M_2^{\text{even}} \right. \right.$$

$$\left. + \sum_{\substack{q=0 \\ \text{odd}}}^{p} \{\Sigma\Pi\Delta(p,q)\} \, M_1^{\text{odd}} M_2^{\text{odd}} \right) \tag{F3}$$

$$+ \sum_{\substack{l_{12}=1 \\ \text{odd}}}^{\infty} \frac{1}{l_{12}!} \left[\frac{2\Delta_m(x_1 - x_2)}{\Delta_m(0)} \right]^{l_{12}} \left(\sum_{\substack{q=0 \\ \text{even}}}^{p} \{\Sigma\Pi\Delta(p,q)\} \, M_1^{\text{odd}} M_2^{\text{odd}} \right.$$

$$\left. \left. + \sum_{\substack{q=0 \\ \text{odd}}}^{p} \{\Sigma\Pi\Delta(p,q)\} \, M_1^{\text{even}} M_2^{\text{even}} \right) \right\},$$

where

$$M_1^{\text{even/odd}} = \sum_{\substack{m_1=0 \\ \text{even/odd}}}^{\beta_1} \binom{\beta_1}{m_1} (i\pi)^{m_1} \left(\frac{d}{dN_1}\right)^{\beta_1-m_1} [2\Delta_m(0)]^{N_1} \frac{\Gamma(N_1+2)\,\Gamma(N_1+\frac{3}{2})}{\Gamma(N_1+2-\frac{q}{2}-\frac{1}{2}l_{12})}$$

$$= \left(\frac{d}{dN_1}\right)^{\beta_1} [2\Delta_m(0)]^{N_1} \frac{\Gamma(N_1+2)\,\Gamma(N_1+\frac{3}{2})}{\Gamma(N_1+2-\frac{q}{2}-\frac{1}{2}l_{12})} \begin{cases} \cos(\pi N_1), & \text{when even} \\ i\,\sin(\pi N_1), & \text{when odd} \end{cases}$$

$$(F4)$$

and

$$M_2^{\text{even/odd}} = \sum_{\substack{m_2=0 \\ \text{even/odd}}}^{\beta_2} \binom{\beta_2}{m_2} (i\pi)^{m_2} \left(\frac{d}{dN_2}\right)^{\beta_2-m_2} [2\Delta_m(0)]^{N_2} \frac{\Gamma(N_2+2)\,\Gamma(N_2+\frac{3}{2})}{\Gamma(N_2+2-\frac{p-q}{2}-\frac{1}{2}l_{12})}$$

$$= \left(\frac{d}{dN_2}\right)^{\beta_2} [2\Delta_m(0)]^{N_2} \frac{\Gamma(N_2+2)\,\Gamma(N_2+\frac{3}{2})}{\Gamma(N_2+2-\frac{p-q}{2}-\frac{1}{2}l_{12})} \begin{cases} \cos(\pi N_2), & \text{when even} \\ i\,\sin(\pi N_2), & \text{when odd.} \end{cases}$$

$$(F5)$$

The summations in (F4) and (F5) were performed as variants of the Leibniz rule [50] in the same way as in Section 2.3, see (2.65) and (2.66).

Using the results for (F4) and (F5), the expression (F3) can be rewritten as

$$G_{p,n}^c(y_1,\dots,y_p)\big|_{k=2} =$$

$$\frac{g^2\Delta_m^2(0)}{2^n\pi} \left[\frac{2\mu_0^{D-2}}{\Delta_m(0)}\right]^{p/2} \sum_c \prod_{s=1}^{n-1} \frac{1}{c_s!\,(s!)^{c_s}} \int d^D x_1' d^D x_2' \lim_{N_1,N_2\to 0} \left(\frac{d}{dN_1}\right)^{\beta_1} \left(\frac{d}{dN_2}\right)^{\beta_2}$$

$$\times \Bigg\{ \cos(\pi N_1)\cos(\pi N_2)\Big(\sum_{\substack{q=0 \\ \text{even}}}^{p}\{\Sigma\Pi\Delta(p,q)\}L_{\text{even}}(N_1,N_2)$$

$$+ \sum_{\substack{q=0 \\ \text{odd}}}^{p}\{\Sigma\Pi\Delta(p,q)\}L_{\text{odd}}(N_1,N_2)\Big)$$

$$- \sin(\pi N_1)\sin(\pi N_2)\Big(\sum_{\substack{q=0 \\ \text{even}}}^{p}\{\Sigma\Pi\Delta(p,q)\}L_{\text{odd}}(N_1,N_2)$$

$$+ \sum_{\substack{q=0 \\ \text{odd}}}^{p}\{\Sigma\Pi\Delta(p,q)\}L_{\text{even}}(N_1,N_2)\Big)\Bigg\},$$

$$(F6)$$

where the summation over even or odd values of l_{12} is denoted as

$$
L_{\text{even/odd}}(N_1, N_2) = \left[2\Delta_m(0)\right]^{N_1+N_2} \sum_{\substack{l_{12}=1 \\ \text{even/odd}}}^{\infty} \frac{1}{l_{12}!} \left[\frac{2\Delta_m(x_1-x_2)}{\Delta_m(0)}\right]^{l_{12}}
$$
$$
\times \frac{\Gamma(N_1+2)\,\Gamma(N_1+\frac{3}{2})}{\Gamma(N_1+2-\frac{q}{2}-\frac{1}{2}l_{12})} \frac{\Gamma(N_2+2)\,\Gamma(N_2+\frac{3}{2})}{\Gamma(N_2+2-\frac{p-q}{2}-\frac{1}{2}l_{12})}.
$$

(F7)

The summation $\sum_c$ and the index β can now be specified following (2.69) to (2.73)

$$
G^c_{p,n}(y_1,\ldots,y_p)\big|_{k=2} =
$$
$$
\frac{g^2\Delta_m^2(0)}{2^{n+1}n!\,\pi}\left[\frac{2\mu_0^{D-2}}{\Delta_m(0)}\right]^{p/2} \int d^D x_1' d^D x_2' \lim_{N\to 0}\left(\frac{d}{dN}\right)^n
$$
$$
\times \Bigg\{ \cos^2(\pi N)\left[\sum_{\substack{q=0\\\text{even}}}^p \{\Sigma\Pi\Delta(p,q)\}\, L_{\text{even}}(N,N) + \sum_{\substack{q=0\\\text{odd}}}^p \{\Sigma\Pi\Delta(p,q)\}\, L_{\text{odd}}(N,N)\right]
$$
$$
-\sin^2(\pi N)\left[\sum_{\substack{q=0\\\text{even}}}^p \{\Sigma\Pi\Delta(p,q)\}\, L_{\text{odd}}(N,N) + \sum_{\substack{q=0\\\text{odd}}}^p \{\Sigma\Pi\Delta(p,q)\}\, L_{\text{even}}(N,N)\right]
$$
$$
-\cos(\pi N)\left[\sum_{\substack{q=0\\\text{even}}}^p \{\Sigma\Pi\Delta(p,q)\}\, L_{\text{even}}(N,0) + \sum_{\substack{q=0\\\text{odd}}}^p \{\Sigma\Pi\Delta(p,q)\}\, L_{\text{odd}}(N,0)\right]
$$
$$
-\cos(\pi N)\left[\sum_{\substack{q=0\\\text{even}}}^p \{\Sigma\Pi\Delta(p,q)\}\, L_{\text{even}}(0,N) + \sum_{\substack{q=0\\\text{odd}}}^p \{\Sigma\Pi\Delta(p,q)\}\, L_{\text{odd}}(0,N)\right]\Bigg\}.
$$

(F8)

By collecting summations over even or odd values of q one finds

$$
G^c_{p,n}(y_1,\ldots,y_p)\big|_{k=2} =
$$
$$
\frac{g^2\Delta_m^2(0)}{2^{n+1}n!\,\pi}\left[\frac{2\mu_0^{D-2}}{\Delta_m(0)}\right]^{p/2} \int d^D x_1' d^D x_2' \lim_{N\to 0}\left(\frac{d}{dN}\right)^n
$$
$$
\times \Bigg\{ \sum_{\substack{q=0\\\text{even}}}^p \{\Sigma\Pi\Delta(p,q)\} \left[\cos^2(\pi N)\, L_{\text{even}}(N,N) - \sin^2(\pi N)\, L_{\text{odd}}(N,N)\right.
$$
$$
\left. -\cos(\pi N)\, L_{\text{even}}(N,0) - \cos(\pi N)\, L_{\text{even}}(0,N)\right]
$$
$$
+\sum_{\substack{q=0\\\text{odd}}}^p \{\Sigma\Pi\Delta(p,q)\} \left[\cos^2(\pi N)\, L_{\text{odd}}(N,N) - \sin^2(\pi N)\, L_{\text{even}}(N,N)\right.
$$
$$
\left. -\cos(\pi N)\, L_{\text{odd}}(N,0) - \cos(\pi N)\, L_{\text{odd}}(0,N)\right]\Bigg\}.
$$

(F9)

Finally, notice that the functions $L_{\text{even/odd}}(N_1, N_2)$ in (F7) can be summed as Gaussian hypergeometric functions, similar to the discussion in (2.50) to (2.53):

$$L_{\text{even}}(N_1, N_2) =$$

$$\left[2\Delta_m(0)\right]^{N_1+N_2} \frac{\Gamma(N_1+2)\,\Gamma(N_1+\tfrac{3}{2})}{\Gamma(N_1+2-\tfrac{q}{2})} \frac{\Gamma(N_2+2)\,\Gamma(N_2+\tfrac{3}{2})}{\Gamma(N_2+2-\tfrac{p-q}{2})} \tag{F10}$$

$$\times \left\{-1 + {}_2F_1\left[-(N_1+1-\tfrac{q}{2}), -(N_2+1-\tfrac{p-q}{2}); \tfrac{1}{2}; \left(\tfrac{\Delta_m(x_1-x_2)}{\Delta_m(0)}\right)^2\right]\right\}$$

and

$$L_{\text{odd}}(N_1, N_2) =$$

$$\frac{2\Delta_m(x_1-x_2)}{\Delta_m(0)}\left[2\Delta_m(0)\right]^{N_1+N_2} \frac{\Gamma(N_1+2)\,\Gamma(N_1+\tfrac{3}{2})}{\Gamma(N_1+2-\tfrac{q}{2})} \frac{\Gamma(N_2+2)\,\Gamma(N_2+\tfrac{3}{2})}{\Gamma(N_2+2-\tfrac{p-q}{2})} \tag{F11}$$

$$\times {}_2F_1\left[-(N_1+\tfrac{1}{2}-\tfrac{q}{2}), -(N_2+\tfrac{1}{2}-\tfrac{p-q}{2}); \tfrac{3}{2}; \left(\tfrac{\Delta_m(x_1-x_2)}{\Delta_m(0)}\right)^2\right].$$

Overall, (F9) describes the two-vertex contribution of the general Green's function coefficient $G^c_{p,n}(y_1, \ldots, y_p)$ for unspecified values $n \geq 2$ and even numbers p.

For odd values of p, the calculation proceeds along the same lines as for even values of p, resulting analogously in the expression:

$$G^c_{p,n}(y_1, \ldots, y_p)\big|_{k=2} =$$

$$\frac{g^2 \Delta_m^2(0)}{2^{n+1} n!\,\pi}\left[\frac{2\mu_0^{D-2}}{\Delta_m(0)}\right]^{p/2} \int d^D x_1'\, d^D x_2'\, \lim_{N\to 0}\left(\frac{d}{dN}\right)^n \sum_{\substack{q=0 \\ \text{odd}}}^{p} \{\Sigma\Pi\Delta(p,q)\} \tag{F12}$$

$$\times \left[2i\,\sin(\pi N)\,\cos(\pi N)\,L_{\text{even}}(N,N) + 2i\,\sin(\pi N)\,\cos(\pi N)\,L_{\text{odd}}(N,N)\right.$$

$$\left. - 2i\,\sin(\pi N)\,L_{\text{even}}(N,0) - 2i\,\sin(\pi N)\,L_{\text{odd}}(0,N)\right].$$

List of Publications

Own Publications Included in this Thesis:

[i] *Towards perturbative renormalization of $\phi^2(i\phi)^\varepsilon$ quantum field theory*,
   A. Felski, C. M. Bender, S. P. Klevansky, and S. Sarkar, (submitted for publication), (2021), [arXiv: 2103.07577]

[ii] *$\mathcal{PT}$ Symmetry and Renormalisation in Quantum Field Theory*,
   C. M. Bender, A. Felski, S. P. Klevansky, and S. Sarkar, J. Phys.: Conf. Ser. (to be published), (2021), [arXiv: 2103.14864]

[iii] *Fermion and meson mass generation in non-Hermitian Nambu–Jona-Lasinio models*, A. Felski and S. P. Klevansky, Phys. Rev. D **103**, 056007 (2021), DOI: 10.1103/PhysRevD.103.056007

[iv] *Non-Hermitian extension of the Nambu–Jona-Lasinio model in $3 + 1$ and $1+1$ dimensions*, A. Felski, A. Beygi, and S. P. Klevansky, Phys. Rev. D **101**, 116001 (2020), DOI: 10.1103/PhysRevD.101.116001

Own Additional Publications:

[v] *Analytic eigenvalue structure of a coupled-oscillator system beyond the ground state*, A. Felski and S. P. Klevansky, Phys. Rev. A **98**, 012127 (2018), DOI: 10.1103/PhysRevA.98.012127

[vi] *Analytic structure of eigenvalues of coupled quantum systems*,
   C. M. Bender, A. Felski, N. Hassanpour, S. P. Klevansky, and A. Beygi, Phys. Scr. **92**, 015201 (2017), DOI: 10.1088/0031-8949/92/1/015201

Bibliography

[1] C. M. Bender, N. Hassanpour, S. P. Klevansky, and S. Sarkar, Phys. Rev. D **98**, 125003 (2018), DOI: 10.1103/PhysRevD.98.125003

[2] C. M. Bender, B. K. Berntson, D. Parker, and E. Samuel, Am. J. Phys. **81**, 173 (2013), DOI: 10.1119/1.4789549

[3] C. E. Rüter, K. G. Makris, R. El-Ganainy, D. N. Christodoulides, M. Segev, and D. Kip, Nat. Phys. **6**, 192–195 (2010), DOI: 10.1038/nphys1515

[4] K. G. Makris, R. El-Ganainy, D. N. Christodoulides, and Z. H. Musslimani, Phys. Rev. Lett. **100**, 103904 (2008), DOI: 10.1103/PhysRevLett.100.103904

[5] A. Guo, G. J. Salamo, D. Duchesne, R. Morandotti, M. Volatier-Ravat, V. Aimez, G. A. Siviloglou, and D. N. Christodoulides, Phys. Rev. Lett. **103**, 093902 (2009), DOI: 10.1103/PhysRevLett.103.093902

[6] Z. Lin, H. Ramezani, T. Eichelkraut, T. Kottos, H. Cao, and D. N. Christodoulides, Phys. Rev. Lett. **106**, 213901 (2011), DOI: 10.1103/PhysRevLett.106.213901

[7] J. Doppler, A. A. Mailybaev, J. Böhm, U. Kuhl, A. Girschik, F. Libisch, T. J. Milburn, P. Rabl, N. Moiseyev, and S. Rotter, Nature **537**, 76–79 (2016), DOI: 10.1038/nature18605

[8] X. Zhu, H. Ramezani, C. Shi, J. Zhu, and X. Zhang, Phys. Rev. X **4**, 031042 (2014), DOI: 10.1103/PhysRevX.4.031042

[9] R. Fleury, D. Sounas, and A. Alù, Nat. Commun. **6**, 5905 (2015), DOI: 10.1038/ncomms6905

[10] C. Shi, M. Dubois, Y. Chen, L. Cheng, H. Ramezani, Y. Wang, and X. Zhang, Nat. Comm. **7**, 11110 (2016), DOI: 10.1038/ncomms11110

[11] S. Bittner, B. Dietz, U. Günther, H. L. Harney, M. Miski-Oglu, A. Richter, and F. Schäfer, Phys. Rev. Lett. **108**, 024101 (2012), DOI: 10.1103/PhysRevLett.108.024101

[12] B. Peng, Ş. K. Özdemir, F. Lei, F. Monifi, M. Gianfreda, G. L. Long, S. Fan, F. Nori, C. M. Bender, and L. Yang, Nat. Phys. **10**, 394–398 (2014), DOI: 10.1038/nphys2927

[13] J. Schindler, A. Li, M. C. Zheng, F. M. Ellis, and T. Kottos, Phys. Rev. A **84**, 040101(R) (2011), DOI: 10.1103/PhysRevA.84.040101

[14] S. Assawaworrarit, X. Yu, and S. Fan, Nature **546**, 387–390 (2017), DOI: 10.1038/nature22404

[15] J. Rubinstein, P. Sternberg, and Q. Ma, Phys. Rev. Lett. **99**, 167003 (2007), DOI: 10.1103/PhysRevLett.99.167003

[16] N. M. Chtchelkatchev, A. A. Golubov, T. I. Baturina, and V. M. Vinokur, Phys. Rev. Lett. **109**, 150405 (2012), DOI: 10.1103/PhysRevLett.109.150405

[17] K. F. Zhao, M. Schaden, and Z. Wu, Phys. Rev. A **81**, 042903 (2010), DOI: 10.1103/PhysRevA.81.042903

[18] C. M. Bender, Rep. Prog. Phys. **70**, 947 (2007), DOI: 10.1088/0034-4885/70/6/R03

[19] C. M. Bender et al., *PT Symmetry in Quantum and Classical Physics* (World Scientific, Singapore, 2019)

[20] The proceedings of the international conference series on "Pseudo-Hermitian Hamiltonians in Quantum Physics" (PHHQP) are published in various journals, a list of which can be found on the PHHQP website: http://gemma.ujf.cas.cz/~znojil/conf/proceedphhqp.html

[21] C. M. Bender and S. Boettcher, Phys. Rev. Lett. **80**, 5243 (1998), DOI: 10.1103/PhysRevLett.80.5243

[22] P. Dorey, C. Dunning, and R. Tateo, J. Phys. A: Math. Gen. **34**, 5679 (2001), DOI: 10.1088/0305-4470/34/28/305

[23] C. M. Bender and D. W. Hook, J. Phys.: Conf. Ser. (to be published), (2021), [arXiv: 2103.04214]

[24] C. M. Bender, K. A. Milton, M. Moshe, S. S. Pinsky, and L. M. Simmons, Jr., Phys. Rev. Lett. **58**, 2615 (1987), DOI: 10.1103/PhysRevLett.58.2615

[25] C. M. Bender, K. A. Milton, M. Moshe, S. S. Pinsky, and L. M. Simmons, Jr., Phys. Rev. D **37**, 1472 (1988), DOI: 10.1103/PhysRevD.37.1472

[26] C. M. Bender, K. A. Milton, S. S. Pinsky, and L. M. Simmons, Jr., J. Math. Phys. **30**, 1447 (1989), DOI: 10.1063/1.528326

[27] D. Bessis and J. Zinn-Justin, private communication referenced in [19, 21]

[28] J. L. Cardy and G. Mussardo, Phys. Lett. B **225**, 275-278 (1989), DOI: 10.1016/0370-2693(89)90818-6

[29] B. C. Harms, S. T. Jones, and C.-I Tan, Nucl. Phys. B **171**, 392-412 (1980), DOI: 10.1016/0550-3213(80)90377-6

[30] B. C. Harms, S. T. Jones, and C.-I Tan, Phys. Lett. B **91**, 291-295 (1980), DOI: 10.1016/0370-2693(80)90452-9

[31] E. Caliceti, S. Graffi, and M. Maioli, Commun. Math. Phys. **75**, 51-66 (1980), DOI: 10.1007/BF01962591

[32] A. A. Andrianov, Ann. Phys. **140**, 82-100 (1982), DOI: 10.1016/0003-4916 (82)90336-0

[33] T. Hollowood, Nucl. Phys. B **384**, 523-540 (1992), DOI: 10.1016/0550-3213 (92)90579-Z

[34] F. G. Scholtz, H. B. Geyer, and F. J. W. Hahne, Ann. Phys. **213**, 74-101 (1992), DOI: 10.1016/0003-4916(92)90284-S

[35] C. M. Bender and K. A. Milton, J. Phys. A: Math. Gen. **32**, L87 (1999), DOI: 10.1088/0305-4470/32/7/001

[36] K. Symanzik, Lett. Nuovo Cimento **6**, 77–80 (1973), DOI: 10.1007/BF02788323

[37] R. A. Brandt, Phys. Rev. D **14**, 3381 (1976), DOI: 10.1103/PhysRevD.14.3381

[38] C. M. Bender, S. F. Brandt, J.-H. Chen, and Q. Wang, Phys. Rev. D **71**, 025014 (2005), DOI: 10.1103/PhysRevD.71.025014

[39] C. M. Bender and P. D. Mannheim, Phys. Rev. Lett. **100**, 110402 (2008), DOI: 10.1103/PhysRevLett.100.110402

[40] C. M. Bender, D. W. Hook, N. E. Mavromatos, and S. Sarkar, J. Phys. A: Math. Theor. **49**, 45LT01 (2016), DOI: 10.1088/1751-8113/49/45/45LT01

[41] C. M. Bender, M. Moshe, and S. Sarkar, J. Phys. A: Math. Theor. **46**, 102002 (2013), DOI: 10.1088/1751-8113/46/10/102002

[42] C. M. Bender, D. W. Hook, N. E. Mavromatos, and S. Sarkar, Phys. Rev. Lett. **113**, 231605 (2014), DOI: 10.1103/PhysRevLett.113.231605

[43] A. Felski, C. M. Bender, S. P. Klevansky, and S. Sarkar, (submitted for publication), (2021), [arXiv: 2103.07577]

[44] C. M. Bender, A. Felski, S. P. Klevansky, and S. Sarkar, J. Phys.: Conf. Ser. (to be published), (2021), [arXiv: 2103.14864]

[45] L. Comtet, *Advanced Combinatorics: The Art of Finite and Infinite Expansions* (Reidel, Dordrecht, 1974)

[46] M. Mezard, G. Parisi, and M. Virasoro, *Spin Glass Theory and Beyond: An Introduction to the Replica Method and Its Applications* (World Scientific, Singapore, 1986)

[47] G. E. Andrews, R. Askey, and R. Roy, *Special Functions* (Cambridge University Press, Cambridge, 1999)

[48] M. E. Peskin and D. V. Schroeder, *An Introduction To Quantum Field Theory* (Addison-Wesley, Reading, 1995)

[49] V. Branchina, A. Chiavetta, and F. Contino, (2020), [arXiv:2009.11846]

[50] M. Abramowitz and I. A. Stegun, *Handbook of Mathematical Functions* (Dover, New York, 1972)

[51] I. S. Gradshteyn and I. M. Ryzhik, *Table of Integrals, Series, and Products* (Academic Press, Amsterdam, 2007)

[52] R. P. Stanley, *Enumerative Combinatorics: Volume 2* (Cambridge University Press, Cambridge, 1999)

[53] J. Glimm and A. Jaffe, *Quantum Physics: A Functional Integral Point of View* (Springer, New York, 1987)

[54] C. M. Bender and S. A. Orzag, *Advanced Mathematical Methods for Scientists and Engineers I: Asymptotic Methods and Perturbation Theory* (Springer, New York, 1999)

[55] J. L. Gross, J. Yellen, and P. Zhang, *Handbook of Graph Theory, Second Edition* (CRC Press, Boca Raton, 2014)

[56] H. Cheng and T. T. Wu, Phys. Rev. D **1**, 2775 (1970), DOI: 10.1103/PhysRevD.1.2775

[57] K. Jones-Smith and H. Mathur, Phys. Rev. A **82**, 042101 (2010), DOI: 10.1103/PhysRevA.82.042101

[58] J. D. Bjorken and S. D. Drell, *Relativistic Quantum Mechanics* (McGraw-Hill, New York, 1964)

[59] A. Messiah, *Quantum Mechanics, Volume 2* (North-Holland, Amsterdam, 1965)

[60] C. M. Bender, H. F. Jones, and R. J. Rivers, Phys. Lett. B **625**, 333-340 (2005), DOI: 10.1016/j.physletb.2005.08.087

[61] A. Beygi, S. P. Klevansky, and C. M. Bender, Phys. Rev. A **99**, 062117 (2019), DOI: 10.1103/PhysRevA.99.062117

[62] C. M. Bender, D. C. Brody, J.-H. Chen, H. F. Jones, K. A. Milton, and M. C. Ogilvie, Phys. Rev. D **74**, 025016 (2006), DOI: 10.1103/PhysRevD.74.025016

[63] H. F. Jones and J. Mateo, Phys. Rev. D **73**, 085002 (2006), DOI: 10.1103/PhysRevD.73.085002

[64] Y. Nambu and G. Jona-Lasinio, Phys. Rev. **122**, 345 (1961), DOI: 10.1103/PhysRev.122.345

[65] Y. Nambu and G. Jona-Lasinio, Phys. Rev. **124**, 246 (1961), DOI: 10.1103/PhysRev.124.246

[66] A. Felski, A. Beygi, and S. P. Klevansky, Phys. Rev. D **101**, 116001 (2020), DOI: 10.1103/PhysRevD.101.116001

[67] A. Felski and S. P. Klevansky, Phys. Rev. D **103**, 056007 (2021), DOI: 10.1103/PhysRevD.103.056007

[68] C. M. Bender and S. P. Klevansky, Phys. Rev. A **84**, 024102 (2011), DOI: 10.1103/PhysRevA.84.024102

[69] O. Cherbal and D. A. Trifonov, Phys. Rev. A **85**, 052123 (2012), DOI: 10.1103/PhysRevA.85.052123

[70] A. Beygi, S. P. Klevansky, and C. M. Bender, Phys. Rev. A **97**, 032128 (2018), DOI: 10.1103/PhysRevA.97.032128

[71] A. Beygi and S. P. Klevansky, Phys. Rev. A **98**, 022105 (2018), DOI: 10.1103/PhysRevA.98.022105

[72] A. Mostafazadeh, J. Phys. A: Math. Gen. **37**, 10193 (2004), DOI: 10.1088/0305-4470/37/43/012

[73] K. Jones-Smith and H. Mathur, Phys. Rev. D **89**, 125014 (2014), DOI: 10.1103/PhysRevD.89.125014

[74] T. Ohlsson, Europhys. Lett. **113**, 61001 (2016), DOI: 10.1209/0295-5075/113/61001

[75] J. Alexandre, C. M. Bender, and P. Millington, J. High Energy Phys. **2015**, 111 (2015), DOI: 10.1007/JHEP11(2015)111

[76] J. Alexandre, N. E. Mavromatos, and A. Soto, Nucl. Phys. B **961**, 115212 (2020), DOI: 10.1016/j.nuclphysb.2020.115212

[77] N. E. Mavromatos and A. Soto, Nucl. Phys. B **962**, 115275 (2021), DOI: 10.1016/j.nuclphysb.2020.115275

[78] M. N. Chernodub, A. Cortijo, and M. Ruggieri, (2020), [hal-02940002]

[79] J. Bardeen, L. N. Cooper, and J. R. Schrieffer, Phys. Rev. **108**, 1175 (1957), DOI: 10.1103/PhysRev.108.1175

[80] S. P. Klevansky, Rev. Mod. Phys. **64**, 649 (1992), DOI: 10.1103/RevModPhys.64.649

[81] D. Colloday and V. A. Kostelecký, Phys. Rev. D **55**, 6760 (1997), DOI: 10.1103/PhysRevD.55.6760

[82] D. Colloday and V. A. Kostelecký, Phys. Rev. D **58**, 116002 (1998), DOI: 10.1103/PhysRevD.58.116002

[83] V. A. Kostelecký and R. Lehnert, Phys. Rev. D **63**, 065008 (2001), DOI: 10.1103/PhysRevD.63.065008

[84] R. D. Mattuck, *A Guide to Feynman Diagrams in the Many-body Problem* (McGraw-Hill, New York, 1976)

[85] G. 't Hooft, Phys. Rev. Lett. **37**, 8 (1976), DOI: 10.1103/PhysRevLett.37.8

[86] G. 't Hooft, Phys. Rev. D **14**, 3432 (1976), DOI: 10.1103/PhysRevD.14.3432

[87] A. H. Blin, B. Hiller, and M. Schaden, Z. Phys. A **331**, 75-82 (1988), DOI: 10.1007/BF01289433

[88] R. M. Corless, G. H. Gonnet, D. E. G. Hare, D. J. Jeffrey, and D. E. Knuth, Adv. Comput. Math. **5**, 329–359 (1996), DOI: 10.1007/BF02124750

[89] R. A. Horn and C. R. Johnson, *Matrix Analysis, Second Edition* (Cambridge University Press, Cambridge, 2012)

[90] D. J. Gross and A. Neveu, Phys. Rev. D **10**, 3235 (1974), DOI: 10.1103/ PhysRevD.10.3235

[91] G. B. Arfken, H. J. Weber, and F. E. Harris, *Mathematical Methods for Physicists, Seventh Edition* (Academic Press, New York, 2012)

[92] L. J. Slater, *Generalized Hypergeometric Functions* (Cambridge University Press, Cambridge, 1966)

[93] A. Erdélyi, W. Magnus, F. Oberhettinger, and F. G. Tricom, *Higher Transcendental Functions, Volume 1* (McGraw-Hill, New York, 1953)